UNIVERSITÀ DEGLI STUDI DI TRIESTE

XXXV CICLO DEL DOTTORATO DI RICERCA IN CHIMICA

Funded by PO FRIULI VENEZIA GIULIA - FONDO SOCIALE EUROPEO 2014/2020

Development of sensing strategies targeting bioactive phenols from olive oil and coffee

Settore scientifico-disciplinare: **CHIM/06**

Ph.D.STUDENT
VERONICA VIDA

Ph.D. PROGRAM DIRECTOR
PROF. ENZO ALESSIO

THESIS SUPERVISOR
PROF. FEDERICO BERTI

THESIS CO-SUPERVISOR
PROF. CRISTINA FORZATO

ANNO ACCADEMICO 2021/2022

UNIVERSITÀ DEGLI STUDI DI TRIESTE

XXXV CICLO DEL DOTTORATO DI RICERCA IN CHIMICA

Funded by PO FRIULI VENEZIA GIULIA - FONDO SOCIALE EUROPEO 2014/2020

Development of sensing strategies targeting bioactive phenols from olive oil and coffee

Settore scientifico-disciplinare: **CHIM/06**

Ph.D. STUDENT
VERONICA VIDA

Ph.D. PROGRAM DIRECTOR
PROF. ENZO ALESSIO

THESIS SUPERVISOR
PROF. FEDERICO BERTI

THESIS CO-SUPERVISOR
PROF. CRISTINA FORZATO

ANNO ACCADEMICO 2021/2022

TABLE OF CONTENTS

ABSTRACT

Coffee and olive oil are a huge source of secondary metabolites with many beneficial effects on human health. In particular, phenolic compounds exert an important antioxidant action, protecting cells from oxidative stress, but they also possess many other beneficial compound-specific properties.

Amongst the most important phenolic compounds present in olive oil there are hydroxytyrosol, tyrosol and oleuropein, the main polyphenols with beneficial properties. The identification and quantification of these polyphenols is usually performed by high performance liquid chromatography possibly coupled to mass spectrometry HPLC/ HPLC-MS. However, these HPLC-methods necessitate of very expensive laboratory instrumentation, are time consuming and must be performed by specialized personnel, also requesting sample pretreatment. Since the information on the content of these polyphenols could be very important for the producers to promote their products, an easy quantification of these compounds is desired. The development of biosensors to be applied in a portable device would help the producers in achieving this information quickly and in a simple manner.

Coffee is also rich in bioactive molecules and, apart from the well-known caffeine, polyphenols, such as chlorogenic acids, exert many beneficial effects on health, for example acting as antioxidant and anti-inflammatory agents. Moreover, during the process of coffee roasting, they undergo a series of reactions leading for example to the formation of quinides -which are chlorogenic acids lactones- responsible for the bitter taste of coffee. For this reason, chlorogenic acids are an important indicator for coffee quality monitoring, and the development of sensing methods for their easy quantification is very important due to the high commercial value of this product.

The present PhD project focuses on the development of different sensing strategies to identify an easy and convenient approach on the identification and quantification of these compounds in coffee and olive oil. In particular, covalent reactions were considered for target molecule recognition, using optical techniques, such as absorbance and fluorescence, for signal transduction. To provide complementary selectivity for the different target molecules, three covalent approaches have been developed.

1. Formation of green trihydroxybenzacridine (TBA) pigments from reaction of chlorogenic acid (CGA) with primary amino groups – this reaction usually occurs in the food industry leading to undesired products with green coloration called TBA pigments. They are formed from esters of caffeic acid- such as chlorogenic acid- and primary amino groups, and this reaction could be used for chlorogenic acid quantification for sensing purposes. As a first attempt *N*α-boc-lysine and chlorogenic acid were used, studying TBA pigment formation in excess of lysine both at the end point of reaction (24 hours) and in kinetic mode, monitoring the kinetics of reaction thanks to the presence of a linear range during the first 15 minutes, obtaining very promising results and LODs of 6 and 5 µM for the end point and kinetic measurements respectively. Then, the reaction has been applied to the synthesis of two peptides containing the amino acid lysine for covalent reaction with CGA and further amino acidic residues to favor interactions with the target molecule; for one of the two peptides, having the sequence Acetyl-Phe-Phe-Ala-Pro-Pro-Lys-Ala-Ser-Glu-NH_2 (**P1**), an improved performance could be obtained with respect to the starting amino acid. The reaction has been also applied to the synthesis of polymeric films containing aliphatic amino monomers capable of forming TBA pigments with CGA. After testing the reactivity of several polymeric compositions differing in the ratio between components and using two different amino-monomers -2-aminoethylmethacrylamide and *N*-(3-aminopropyl)methacrylamide - the best performing composition has been used to compare the performance in CGA quantification using a traditional multiwell plate reader and different portable devices. In particular, an optical fiber photometer and two in-lab built devices- an image reader and a pseudo differential reflection

spectrophotometer- have been tested, obtaining very promising results for CGA quantification especially with the in-lab built devices, with a LOD of 37.5 µM for the pseudo-differential portable device.

Moreover, new spectroscopic properties of the TBA pigment have been investigated, finding two fluorescence emissions, the first one at 426 nm when exciting at 318 nm, the second one, more interesting, at 700 nm when exciting between 620 and 660 nm, a range usually free from optical interferences.

As a proof-of-concept, the reaction has been also applied to protein labeling using bovine serum albumin BSA as a model protein, obtaining a very good linear range between 2.5-300 µM and a 28 nM calculated LOD, by monitoring the fluorescence emission at lower wavelengths.

2. Boronic esters formation between *ortho*-diphenols and boronic acid containing fluorophores – fluorescent boronic acids were used in the detection of *ortho*-diphenolic compounds such as chlorogenic acid, caffeic acid (CA) and hydroxytyrosol (HT), differentiating them from mono-phenols such as tyrosol that are not capable of forming stable cyclic boronic esters. Two fluorophores containing a boronic acid moiety and capable of modulating their fluorescence upon target molecules binding have been tested -the commercially available 2-(4-boronophenyl)quinoline-4-carboxylic acid **5** and a synthesized 1,8-naphthalimide derivative **20**. After evaluating the performance of the two fluorophores by fluorescence titrations with the target molecules CGA, CA, HT and catechol (CC), the naphthalimide fluorophore **20** resulted to be the best performing one and was used to synthesize three peptides: **P3** (**20**-succinyl-dPro-Pro-Trp-NH_2), **P4** (Acetyl-Arg-Gly-Glu(**20**)-Gly-NH_2) and **P5** (Acetyl-Arg-Gly-Glu(**20**)-dPro-Pro-Ala-His-Glu-NH_2). By comparing the performance of the peptides with respect to **20** alone in terms of the apparent dissociation constants K_d^{app} obtained from fluorescence titrations experiments, what emerged is that all the fluorescent probes exhibited the highest affinity for CGA, followed by CA, while showing reduced affinity for HT and CC. Comparing the affinities of the different probes for the same target molecule, **20** was the best performing one for CGA binding, followed by peptides **P4**, **P5** and finally **P3**, and the same order was maintained also for caffeic acid, with only a shift between **P5** and **P3**. The capability of the four fluorescent probes to discriminate between the different target molecules has been evaluated by using the obtained K_d^{app} values to calculate the cross reactivity with respect to CGA. What emerged is that all the tested recognition elements could discriminate quite well CGA from HT and CC, with cross reactivity values ranging between 5 and 13%. However, none of the probes was capable of distinguishing well between CGA and CA, the most structurally related compounds**:** only **P5** could provide a slightly better result, showing a cross reactivity value of 34%.

3. Diazo coupling reaction between phenols and the non-natural amino acid *p*-amino-phenylalanine, leading to formation of red-colored diazo coupling compounds- this reaction has been considered using peptides containing the non-natural amino acid *p*-amino-phenylalanine as reactive group. Two peptides have been synthesized, containing either fluorescein or EDANS as fluorophore, and the non-natural amino acid *p*-amino phenylalanine. The latter is capable of providing both π-π stacking interactions with phenols but also of reacting in covalent diazo-coupling reaction forming red-colored diazo-coupling derivatives upon reaction with tyrosol. The peptides have been tested in both the non-covalent approach -monitoring fluorescence changes induced in the fluorophores by the non-covalent interactions with tyrosol- and covalent approach -studying the fluorescence changes of the peptides upon diazo-coupling formation between *p*-amino-phenylalanine and tyrosol-. When testing the fluorescence of the two peptides in the presence of different concentrations of tyrosol by the non-covalent approach, both peptides exhibited a fluorescence enhancement, unfortunately without observing a linear trend. After assessing mild reaction conditions for the diazo-coupling reaction by using the amino acid *p*-amino-phenylalanine alone with tyrosol, the fluorescence of the peptides has been evaluated also after diazo-coupling reaction with tyrosol. Despite several attempts, no good results could be obtained with the synthesized peptides.

As a spin-off of the diazo-coupling approach, while studying the reactivity of different substituted cinnamic acids with aniline and *p*-amino-phenylalanine, an unexpected reaction leading to formation of novel diazadiene compounds has been discovered.

PUBLICATIONS

Forzato C.; Vida V.; Berti F. Biosensors and Sensing Systems for Rapid Analysis of Phenolic Compounds from Plants: A Comprehensive Review*, Biosensors*, **2020,** 10, 105.

Gutiérrez-Ortiz A.L.; Vida V.; Peterka M.; Tušar J.; Berti F.; Navarini L.; Forzato C. Fluorescent Imprinted Nanoparticles for Sensing of Chlorogenic Acid in Coffee Extracts, *Sensors*, **2022,** 22, 9874.

Vida V.; Minisini M.; Mardirossian M.; Brancolini C.; Scocchi M.; Forzato C.; Berti F. Novel Synthesis of 1, 2-Diaza-1, 3-Dienes with Potential Biological Activity from Cinnamic Acids and Diazonium Salts of Anilines, *RSC Advances*, **2023**, 13, 456-63.

1 INTRODUCTION

1.1 COFFEE

The coffee plant is an evergreen tropical tree species that belongs to the *Rubiaceae* family. Among more than 100 species of the *Coffea* genus, only two are broadly exploited for beverage production: *Coffea arabica* (*C. arabica*), commonly known as Arabica coffee, which accounts for around the 60% of traded coffee, and *Coffea canephora* (*C. canephora*), commonly known as Robusta coffee, which comprises the remaining 40% (Figure 1.1). Liberica coffee, a third species, is cultivated worldwide but is insignificant in terms of global trade.[1]

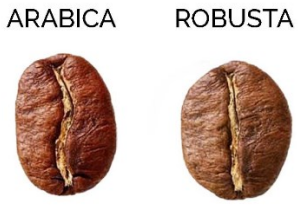

Figure 1.1- C. arabica and C. canephora roasted coffee beans.

C. arabica is the most valuable species, highly appreciated for the superior flavor and aroma of the beverage prepared from its beans. The Arabica trees can reach up to 6 m in height and are cultivated at places with high elevations and mild climates while Robusta trees can grow taller (up to 10 m), and most of their growing areas are at low elevations and warmer climates. Despite some desired agronomical features, such as higher resistance to diseases and higher productivity, *C. canephora* is less popular and far less valuable from the economical point of view due to the inferior quality.[2]

Coffee is one of the most consumed beverages in the world with a global production of 170 million of 60 kg bags in 2020, according to data from the International Coffee Organization (ICO).[3] Coffee is commercially cultivated throughout the geographic region between latitudes 30° N and 30° S, known as the "coffee belt", comprising Central and South America, Africa and the South-East area of Asia.[3,4] Brazil is the main producer and exporter of coffee in the world, being responsible for 37% of all coffee production in 2020, followed by Vietnam with 17% production and Colombia, with an estimated contribution of 8%.[3] However, due to climate changes, strong reductions in climate suitability for coffee cultivation are expected in most current growing regions, especially regarding the arabica species, with only few regions, mainly at higher elevations or latitudes, which might become suitable for coffee cultivation due to general increase in temperature.[5]

The word 'coffee' seems to derive from the ancient Kingdom of Kaffa (today part of Ethiopia), where coffee was first cultivated from around the fifth to the eighth century: a legend reports that an Ethiopian goatherd, discovered the coffee plant after seeing his goats energized by chewing it. The beverage was introduced into the Arab world through Egypt and Yemen, where it became widely consumed; it was in Yemen that coffee started to be cultivated commercially around the fourteenth century. The beverage became particularly common in the Ottoman Empire and it was then introduced into Europe through Venice around the 16th and the 17th century.[6] In the 18th century, Trieste became one of the most important commercial harbors in Europe, especially for the trade of coffee, since the city, at those times under the Austro-Hungary Empire, was declared a free port. Moreover, at the beginning of the 20th century, the first coffee Stock Market was created.[7]

1.1.1 From the coffee beans to roasted coffee

In the genus *Coffea*, the fruit development is highly variable (Figure 1.2), from few weeks (10 to 12), as in *C. racemosa* and *pseudozanguebariae*, to more than one year for *C. liberica.* Regarding the commercial species,

C. arabica requires 6 to 8 months to mature while *C. canephora* from 9 to 11 months.[8] Coffee fruits are classified as “drupes”, characterized by a pulpy mesocarp with lignified endocarp. Together with the exocarp (the peel), mesocarp and endocarp compose the pericarp (Figure 1.3-).[8]

Figure 1.2- Coffee flowers (left);[9] Coffee tree with fruits at different maturation stages (right).[10]

Fruit development comprises seven stages, divided into two main phases: growth (comprising the maternal phase and the endosperm development phase) and maturation (Figure 1.3-). During the initial maternal phase, the perisperm grows, causing the fruit to expand (stages 1 and 2), while the endosperm growth takes place during the endosperm development phase, arriving to fill almost the entire seed (thus corresponding to the bean) replacing the perisperm, which forms the outer layer, the so-called silver skin, (stages 3 and 4). Passing to the second maturation phase of the fruit, during stage 5 the exocarp appears green and the endosperm becomes thicker, and accumulation of cell wall polysaccharides as well as that of other components such as caffein and chlorogenic acids takes place. The final stages are associated with a change in the exocarp color, progressively becoming yellow (stage 6) and red (stage 7); also, the mesocarp (corresponding to the pulp) becomes thicker and the endocarp (the so-called parchment layer) becomes lignified, serving as a protection for the seed.[2]

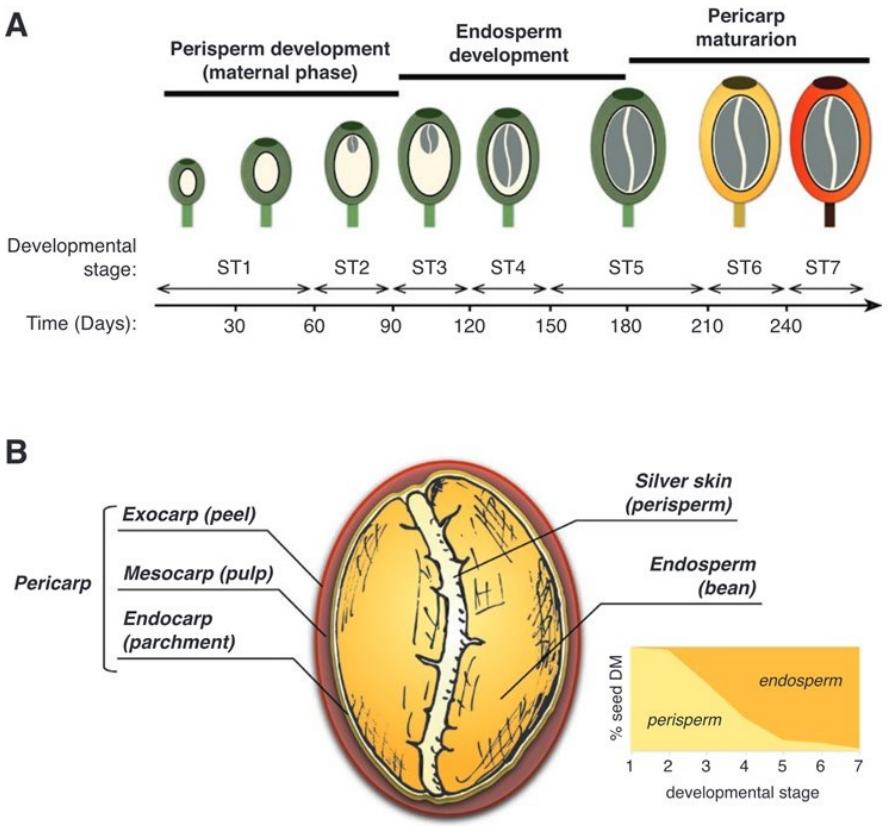

Figure 1.3- Coffee fruit development and coffee cherry composition. (A) Stages of coffee fruit development. (B) Schematic representation of coffee cherry composition, with contribution of perisperm and endosperm to coffee seed dry mass (DM) during developmental stages.[2]

At the end of the fruit development process, the raw fruits of the coffee plant, named coffee cherries, are obtained, which are composed of two coffee beans covered by a thin hull and further surrounded by pulp.[11]

Harvesting of coffee is usually performed by handpicking or by stripping the fruits onto sheets placed beneath the tree, even if the use of mechanical harvesters based on the vibration of tree branches has greatly increased all around the world. Due to the asynchronous development of coffee fruits, leading to the simultaneous presence of fruits at different maturation steps, the handpicking method is preferable allowing the exclusive selection of coffee cherries in their ideal stage of maturation. However, many producers choose between the simpler stripping or mechanical harvesting, removing immature coffee beans through a following sorting step.[4]

After harvesting, to obtain the green coffee beans, it is necessary to remove both the pulp and hull using either a wet or dry method. The dry method, commonly used for Robusta, is technologically simpler comparing with the wet method, generally used for Arabica. In the wet coffee process, the pulp and hull are removed while the cherry is still fresh: the procedure involves several stages using high amounts of water. A microbial fermentation step to remove any mucilage still attached to the beans is also necessary, but it provides the coffee with richer aroma quality thanks to the production of microbial volatile compounds during fermentation.[11]

The subsequent roasting process is of fundamental importance since specific organoleptic properties (flavor, aroma and color) greatly depend on this step thus influencing the quality of the coffee brew. This process is time–temperature dependent and leads to several changes in the chemical composition. Roasting of coffee results in pyrolysis reactions, structural carbohydrates are also degraded, and Maillard reaction takes place, leading to formation of several organic compounds.[12,13] Moreover, roasting process leads to moisture loss

and other major changes (color, volume, mass, form, pH, density, and volatile components), while CO_2 is generated.[11] The roasting process can be divided into three phases: drying, flavor and color development, and cooling. During the drying phase, which is generally the longest one of the roasting process, the moisture content of the beans is lowered, the bean's temperature rises rapidly, and swelling occurs. Then, during the next phase, flavor and color start to develop in the bean. Once the bean's temperature reaches nearly 200 °C, exothermic reactions such as Maillard reactions, take place, which are responsible for the color, flavor, and aromas typical of roasted beans. Additionally, carbon dioxide generated within the bean, causes the beans to further swell: at some point of this step, the so-called ''First Crack" is heard, characterized by a distinct popping sound. After First Crack, the bean's color continues to darken, and its aromas continue to enhance. Going on with time, a ''Second Crack" can then occur, when the bean becomes very dark in color. For industrially roasted coffee, it is important that the roasting process ends between First and Second Crack, which represents the maximum limit above which the bean is considered burnt. When the required period of roasting has occurred, to prevent further roasting, beans are transferred to a second chamber for the cooling phase, in which cooling can be obtained by adding liquid water or circulating cool air.[13]

1.1.2 Different types of coffee in the world

Coffee is consumed all over the world, and many different traditions have been developed in each country to consume this beverage. The preparation technique has a significant influence on the taste, aroma and composition of coffee brews. In general, three extraction methodologies are used: decoction, infusion and pressure methods. Each of these methods is related to specific granulation of coffee powder, water/coffee proportion, temperature and brewing time.[14]

For example, to prepare the so-called Turkish Coffee, diffused in Turkey but also in South-Eastern Europe countries, water is brought to the boil in a special long-handled pot made of copper or brass, called *cezve* in Turkey (*ibrik* in other countries): as soon as water starts to boil, the *cezve* is removed from the heat, coffee powder is added and the mixture is then put to boil twice (Figure 1.4, left).[15]

The infusion coffee preparation method is the most common way to prepare coffee, particularly diffused in northern Europe countries and America. According to the filtration/percolation method, ground coffee is placed on a specific support grid (filter paper, muslin, perforated plastic filter, sintered glass, etc.) and the coffee is extracted by slow gravity percolation.[11] As an alternative, it can be prepared using the French press, using a cylindrical pot with a plunger and built-in filter screen that presses hot water through ground coffee (Figure 1.4, right).[15]

In Italy, coffee is usually prepared by pressure methods, such as the espresso coffee machine or the Moka pot, consisting of a cylinder (bottom chamber), a filter funnel and a collector (top chamber) with a second removable filter, held in place by a rubber gasket (Figure 1.4, center). The mechanism of action is based on the heating of water in the bottom chamber: vapor pressure approaching two atmospheres pushes the water up through ground coffee in the filter, which collects in the upper chamber as liquid coffee.[15]

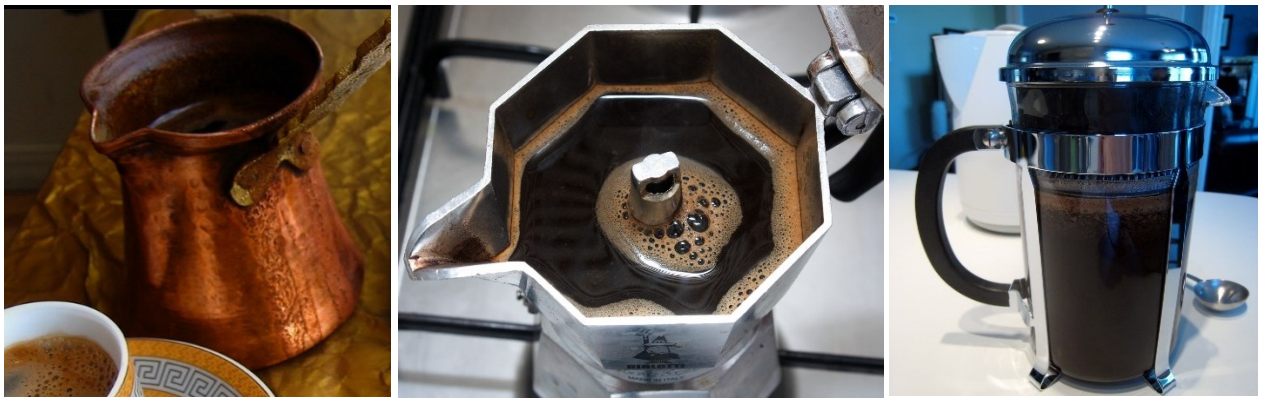

Figure 1.4- Different ways to prepare coffee: the cezve (left),[16] the Italian Moka (center),[17] the French press (right).[18]

1.1.3 Chemical composition

The chemical composition of green coffee beans is very complex, including more than 1000 substances with different chemical and physical properties.[4] The most known bioactive compound present in coffee is caffeine, which acts on the central nervous system, and its content is higher in the Robusta variety than in Arabica (1.7-4.0% vs 0.8-1.4% respectively). However, in terms of quantity, coffee is mainly composed by other classes of compounds, starting from carbohydrates, covering between 41-55% and 55-65% for Robusta and Arabica respectively on a dry-matter basis. Other very representative classes of compounds are chlorogenic acids (present in higher quantities in Robusta coffee), proteins and lipids. Very important are also minerals, vitamins, trigonelline and other acids (Table 1.1**Errore. L'origine riferimento non è stata trovata.**).[11]

Table 1.1- Chemical composition of Arabica and Robusta green coffee beans.[19]

Constituent	Arabica[a,b]		Robusta[a,b]	Components
Soluble carbohydrates	9–12.5		6–11.5	
Monosaccharides		0.2–0.5		Fructose, glucose, galactose, arabinose (traces)
Oligosaccharides	6–9		3–7	Sucrose (>90%), raffinose (0–0.9%), stachyose (0–0.13%)
Polysaccharides		3–4		Polymers of galactose (55–65%), mannose (10–20%), arabinose (20–35%), glucose (0–2%)
Insoluble polysaccharides	46–53		34–44	
Hemicelluloses	5–10		3–4	Polymers of galactose (65–75%), arabinose (25–30%), mannose (0–10%)
Cellulose, β(1–4)mannan	41–43		32–40	
Acids and phenols				
Volatile acids		0.1		
Nonvolatile aliphatic acids	2–2.9		1.3–2.2	Citric acid, malic acid, quinic acid
Chlorogenic acid[c]	6.7–9.2		7.1–12.1	Mono-, dicaffeoyl- and feruloylquinic acid
Lignin		1–3		
Lipids	15–18		8–12	
Wax		0.2–0.3		
Oil		7.7–17.7		Main fatty acids: 16:0 and 18:2 (9,12)
N Compounds		11–15		
Free amino acids		0.2–0.8		Main amino acids: Glu, Asp, Asp-NH_2
Proteins		8.5–12		
Caffeine	0.8–1.4		1.7–4.0	Traces of theobromine and theophylline
Trigonelline	0.6–1.2		0.3–0.9	
Minerals		3–5.4		

[a] Values in % of solids.
[b] Water content of raw coffee: 7–13%.
[c] Main components: 5-caffeoylquinic acid (chlorogenic acid: Arabica 3.0–5.6%; Robusta 4.4–6.6%).

Green coffee beans are characterized by an unpleasant taste, and development of the characteristic beverage flavor is achieved through thermal reactions that take place during roasting and partially also during preparation of coffee brews. In fact, green coffee beans have only a basic composition in terms of chemical

volatiles, containing an average of only 200 volatile compounds with respect to the more than 1000 that are generally detected in roasted coffee, comprising many heterocyclic compounds, which are fundamental in providing the distinctive flavor of roasted beans.[4] In particular, the volatiles exerting the greatest influence on sensory perception and determining roasted coffee aromatic profile are pyrazines, furans, esters, ketones, phenols and sulfur compounds, whose origin is related to different chemical pathways, the most important of which are the Strecker degradation and Maillard and pyrolysis reactions. The Maillard reaction comprises a complex series of chemical processes involving reducing sugars and amino acids, whereas the Strecker degradation causes the transformation of α-amino acids into aldehydes. Other important phenomena taking place during roasting are degradation of structural carbohydrates of the intercellular coffee matrix via the pyrolysis reaction, leading to increased internal porosity and carbon dioxide production, as well as other minor reactions comprising degradation of specific individual amino acids, aliphatic acids (particularly quinic acid) and lipids.[4]

1.1.3.1 Chlorogenic acids

Chlorogenic acids (CGAs) are secondary metabolites which can be found in many plants, and at particularly high concentrations in coffee. They are esters at the hydroxyl groups in positions 3, 4 or 5 of quinic acid with different hydroxycinnamic acids (caffeic acid, ferulic acid, *p*-coumaric acid and sinapic acid) to form mono-, di- and tri-esters (Figure 1.5). Existence of esters at position C-1 of the quinic acid core have also been documented in the plant kingdom but not in the *coffea* species.[20]

In the last few years, more than 80 chlorogenic acids have been isolated and identified in coffee. Caffeoylquinic acids (CQAs) monoesters, having the hydroxyl groups at C- 3, C-4 and C-5 positions of the quinic acid portion esterified with caffeic acid (Figure 1.5) are by far the most abundant, reaching together more than 80% of total chlorogenic acids. In addition to CQAs isomers, green coffee beans are particularly rich in dicaffeoylquinic acids (diCQAs), mono-feruloylquinic acids (FQAs) and mono-*p*-coumaroylquinic acids (*p*CoQAs).[21] The total content of chlorogenic acids in coffee can vary according to the coffee species, but also to the degree of roasting, the agriculture practices as well as the soil composition.[22]

During the roasting process, the non-bitter 5-*O*-caffeoylquinic acid (commonly known as chlorogenic acid CGA) present in the green coffee beans undergoes different transformations, such as transesterification, epimerization, and lactonization reactions, leading to a multiplicity of derivatives, including chlorogenic acid lactones, also known as quinides, which contribute to the bitterness of the beverage.[23] Chlorogenic acids can be used as indicators of coffee quality, since the final content of chlorogenic acids and their corresponding lactones formed after roasting are responsible for the acidity and bitterness of the beverage.[22]

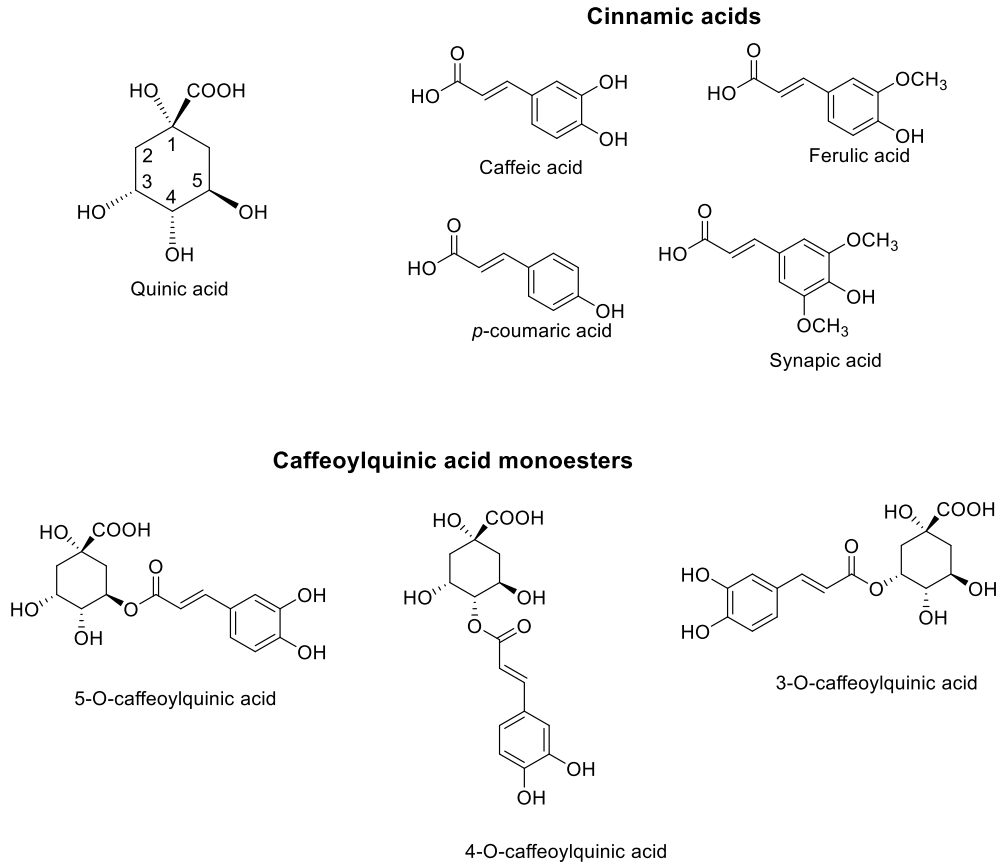

Figure 1.5- Structure of quinic acid and main hydroxycinnamic acids; structure of the main caffeoylquinic acid monoesters.

1.1.4 Effects of coffee on health

Thanks to the presence of many bioactive compounds, such as phenolic compounds (chlorogenic acids and hydroxycinnamic acids), alkaloids (caffeine and trigonelline), diterpenes (cafestol and kahweol) and other secondary metabolites, coffee has been demonstrated to have several effects on human health.[24]

The impact of coffee consumption on human health has been investigated in several research: moderate coffee intake seems to have positive health effects since most compounds possess antioxidant and anti-inflammatory properties, and it may protect from disorders including cardiovascular diseases, hepatic injury, cirrhosis, type 2 diabetes, obesity, depression and some types of cancer, also favoring gastrointestinal tract and gut microbiota establishment. Importantly, coffee consumption seems to be also correlated with a decreased risk of developing some neurodegenerative conditions such as Alzheimer's disease, Parkinson's disease, and dementia.[25, 24,26]

Several beneficial effects of coffee consumption can be attributed to chlorogenic acids, that several studies have demonstrated to relate to a series of health benefits, including antioxidant, anti-inflammatory, antispasmodic activities, and have also been proposed to have beneficial effects on type-2 diabetes, obesity, stroke, endothelial function as well as blood pressure. Other potential beneficial health effects include their anti-carcinogenic and anti-bacterial effects, and also reduction of the relative risk of cardiovascular and Alzheimer's diseases.[23, 27] They also exert antiviral activity, for example against RSV, HIV (by inhibiting the viral enzyme integrase), and hepatitis B virus.[28]

Caffeine is probably the most frequently ingested pharmacologically active substance in the world, since it is a central nervous system stimulant, and its effects upon consumption depend on the frequency of coffee consumption, daily coffee intake, metabolism rate and age/health state, with children[29] and pregnant women[30] that should avoid consuming this substance.[31] Caffeine exerts its effects by blocking the

neuromodulator adenosine receptors. At low (~40 mg or ~0.5 mg kg^{-1}) to moderate (~300 mg or 4 mg kg^{-1}) doses, it is capable of affecting cognitive functions, improving for example alertness, reaction time, vigilance and attention.[32] Other beneficial effects of caffeine are related to a likely reduced risk of Parkinson's disease and gallstones. It is also used as a treatment for apnea of prematurity in infants and contributes to pain relief when administered in association with common analgesic agents. Caffeine raises blood pressure levels in the short term, even if increased blood pressure has not been observed after caffeinated coffee intake, even in persons with hypertension, probably due to the counteracting action of compounds such as chlorogenic acid and to at least partial tolerance developing in the long term.[31] Caffeine regular use typically causes mild physical dependence, even if generally it is not considered particularly threatening; however, sustained abuse may in turn result in 'caffeinism', which refers to a syndrome characterized by a range of adverse reactions such as restlessness, anxiety, irritability, agitation, muscle tremor, insomnia, headache, diuresis, sensory disturbances, cardiovascular symptoms and gastrointestinal complaints. [29]

Other bioactive components responsible for some negative effects of coffee excessive consumption are diterpenes cafestol and kahweol, which cause total serum cholesterol raising. Their concentration largely depends on the brewing method: in fact, filtered coffee contains lower cholesterol-raising diterpenes levels.[33]

Besides the natural composition of green coffee beans, thermal reactions during the roasting processing allows the transformation of cell wall polysaccharides, soluble carbohydrates, nitrogen-containing compounds, lipids, and proteins into molecules with numerous biological activities.[25] For example, phenylidanes, products originated from hydroxylated cinnamates such as caffeic acid during roasting of coffee, show potent antioxidant effect and neuroprotective activity against the Alzheimer's disease pathology.[34] Melanoidins, high molecular weight compounds which are the final products of the Maillard reaction, exert antioxidant, antimicrobial, anticariogenic, anti-inflammatory, antihypertensive, and antiglycative activities, anticarcinogenic activity through inhibition of matrix metalloproteases, and antimicrobial action against both Gram-positive and -negative bacteria.[35]

1.2 OLIVE OIL

Olive oil is a liquid fat extracted from olives, the fruit of the olive plant *Olea europaea*: it is one of the main ingredients of the Mediterranean diet (MED) and it is considered amongst the key products responsible for the overall well-being of the Mediterranean populations.[36] Since its origins, olive cultivation and olive oil production is widely developed in the Mediterranean area, but it has now developed also in other regions with similar climate. According to the International Olive Council, in the 2020/2021 crop year, Spain has been the major olive oil producer with 1.3 millions of tons of olive oil produced, followed by Greece and Italy with a much lower production around 275.000 tons, Turkey with 210.000 and Morocco with 160.000 tons.[37]

There are around 2500 known varieties of olives, of which 250 are classified by the International Olive Oil Council as commercial cultivars, used to produce olive oil and/or table olives. The specific use of a cultivar mainly depends on its oil content and size: olive varieties poor in oil content (less than 12%) such as Ascolano, Calamata and Manzanillo are almost exclusively used for table olive production, while those enabling higher oil yield such as Hojiblanca, Verdial, Picual, Gemlik, Nychati, Kalamon and Arauco are usually preferred for olive oil production.[38]

Bianchera

Bianchera is an autochthonous cutivar typical of the area around Trieste, which has been selected during centuries in the area of San Dorligo della Valle – Dolina (Figure 1.6). The name of the cultivar probably comes from the fact that the change in the olive color takes place lately and is a progressive process, which usually does not reach completion even when fruits are completely mature. Bianchera plants live well on the hills surrounding the Trieste gulf, in the eastern part of northern Italy, but also in the Slovenian and Croatian peninsula of Istria, where it is named Belica (Slovenia) and Bjelica (Croatia). This variety is very resistant to cold weather and strong wind, which makes it suitable for climate typical of this northern Italy area.[39] It has a good production of oil (16%) whose quality is really excellent thanks to the high percentage of oleic acid and a very high content of polyphenols, and a naturally low oleic acid acidity.[39,40]

Figure 1.6 Flowering (left) and olives (right) of Bianchera cultivar.[40]

1.2.1 Origins of olive oil

The beginning of olive cultivation and olive oil production is very ancient, and it seems to date back to the early Bronze Age (3150 to 1200 B.C.), in the area of eastern Mediterranean coasts, corresponding to southern Turkey, Syria, Lebanon, Palestine and Israel based on written tablets, olive pits, and wood fragments found in ancient tombs. Then, cultivation of olive trees moved western, to Greece, Egypt and western Turkey, and then to Sicily, Sardinia, Italy, France, Spain, Portugal, Algeria, Tunisia, and Morocco. Olive oil in ancient times had many documented uses, apart for human consumption: it was used as lamp fuel, in rituals for religious anointing, to make offerings to the Gods, as pharmaceutical ointment to cure diseases, to make the skin and hair appear healthier, to prepare soap and to consecrate dead people.[41] There is also an Ancient Greece myth

testifying the importance of the olive plant and olive oil in that culture. Such myth attributes the creation of the olive plant to the goddess Athena. The story tells that Athena and Poseidon, competing for the patronage of Athens, offered gifts to the inhabitants of the city, so they could choose the best one to declare the protecting god. Poseidon offered the first horse, whereas Athena created the first olive plant: the olive oil was chosen, and Athena became protecting goddess of the city.

1.2.2 Classification of olive oils

Olive oil can be classified according to the method of extraction, as well as to the organoleptic properties.[42,43]

Virgin olive oils (VOOs) are the oils obtained from the fruit of the olive tree solely by mechanical or other physical means under conditions that do not lead to alterations in the oil, which are washing, decantation, centrifugation and filtration. Virgin olive oils can be classified based on their free acidity, expressed as quantity of free oleic acid per 100 g of olive oil: minor the acidity, higher the quality.

- **Extra virgin olive oil (EVOO)** is the highest quality olive oil, with an oleic acid content not higher than 0.8 (≤ 0.8%);
- **Virgin olive oil (VOO)** is characterized by an oleic acid acidity not higher than 2 (≤ 2%);
- **Lampante olive oil** is a virgin oil with organoleptic defects, characterized by an oleic acid acidity higher than 2 (>2%). It cannot be sold as it is.

Refined olive oil is obtained after the refining of a defective virgin olive oil (lampante olive oil for instance) which allows to reduce acidity and remove oxidized substances. At the end of the refining process, the acidity expressed as quantity of oleic acid/100 g of olive oil must not be higher than 0.3 (≤ 0.3%). This oil is not intended to be commercialized as it is, but it must be blended with virgin or extra-virgin olive oil conferring better sensory properties.

Olive oil results from the blend of refined olive oil and virgin olive oils (extra virgin and/or virgin). It has a degree of acidity up to 1%. The law does not establish the minimum percentage of virgin or extra virgin olive oil to be blended to the refined one: usually, the medium percentage of virgin oil ranges between 5 and 8%, but the best producers add up to 30% of extra virgin olive oils to obtain better quality and taste of the product.

Crude olive-pomace oil is the oil obtained from the olive-pomace, which is the solid residual mainly composed by skin, kernels and pulp, obtained after the oil is mechanically extracted from the olives, and which still contains some oil. The oil is extracted with a solvent, normally hexane, following the same technology adopted for seed oils. Then, oil is separated by distillation.

Refined olive-pomace oil is the oil obtained by refining of crude olive-pomace oil, obtaining a free oleic acid acidity not higher than 0.3 grams of oleic acid per 100 grams of oil.

Olive pomace oil is the oil obtained from the blend of refined olive-pomace oil and virgin olive oils. It has a free acidity not higher than 1 gram per 100 grams of oil.[42,43]

1.2.3 Production of virgin olive oil

The whole process of olive oil production is represented in Figure 1.7, and starts with picking up of olives, that can be done shaking the branches of the trees and collecting olives manually, or with specific machines. Olives are then defoliated and washed.[44]

Milling

During the milling process, olives are reduced to a homogeneous paste by breaking the pits, skin and pulp cells and the vacuoles containing tiny droplets of oil. The olive paste is a semiliquid mixture of two different types of solids (rigid pit fragments and soft fleshy parts from the pulp and skin) and two types of immiscible liquids (water and oil). Milling also breaks up the hard woody kernels, and the presence of pit fragments in the olive paste facilitates draining and separation of the liquid from the solid components. The milling process can be carried out in different ways: the modern ones, employing single/double-grid hammer mills or disc mills, and the traditional one, by stone milling, which employes huge stone mills.[44,45]

Melaxation

Melaxation is the process that allows to separate oil from the olive paste, recovering the liquid into bigger drops (coalescence process) thanks to a slow movement and heating of the mass. This is a key step in oil production, that influences quality, taste and quantity of produced oil: according to the temperature to which the process is carried out, the oil can be identified as "cold extracted" or not. "Cold-extracted" oil is obtained at a temperature ranging between 25 and 27°C, which allows to obtain oil with the highest quality. On the other side, between 27 and 30°C production increases in terms of quantity of produced oil, but the quality is affected, causing loss in taste and aroma and also of important substances such as polyphenols.[44,46]

Extraction, separation and filtration

Extraction is the process allowing to separate oil from the solid. Extraction can be done by using the pressure method, centrifugation (decanter) or by the Sinolea method. In the case of the pressure method, after separating the olive oil must from the pomace by means of mechanical or hydraulic presses, the obtained liquid consisting in a mixture of water and oil is separated exploiting the non-miscibility of the two phases using centrifugal separators working by rotating at very high speed.[44] The decanter method, based on centrifugation, is the most modern, and three-phases and two phases decanters are available.[47,48] Since obtained oil is turbid, it can be filtered to remove suspended particles.[49]

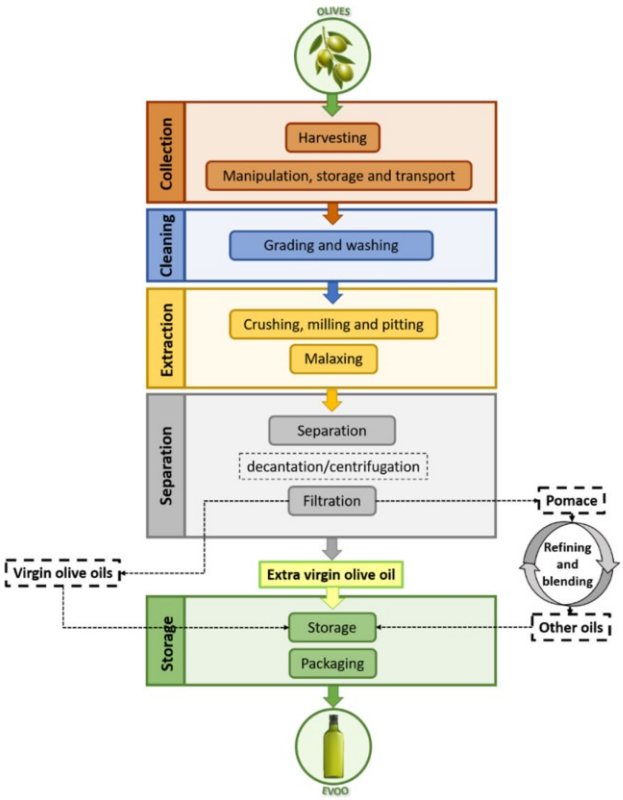

Figure 1.7- Olive oil production process.[50]

1.2.4 Olive oil composition

Olive oil mainly consists of two fractions, namely saponifiable and unsaponifiable. The saponifiable fraction, comprising triacylglycerols, partial glycerides, esters of fatty acids or free fatty acids, represents nearly the 98% of the oil chemical composition, while the unsaponifiable fraction, consisting of minor components such as phenolic compounds, tocopherols, phytosterols, coloring pigments and many other, contributes for around the 1–2%.[38]

The fatty acids present in olive oil are: oleic acid (C18:1, ω9), palmitic acid (C16:0), stearic acid (C18:0) and linoleic acid (C18:2) as the main components; palmitoleic acid (C16:1, ω7), linolenic acid (C18:3) and arachidic acid (C20:0) are present in small amounts, while behenic (C22:0), eicosanoic (C20:1), margaric (C17:0), myristic (C14:0), 11-*cis*-vaccenic (18:1, ω7) and lignoceric (C24:0) acids are present in trace amounts.[36,38] The most abundant constituent is always oleic acid, accounting for about the 55–75% of the total fatty acids, followed by palmitic, linoleic and stearic acid.[36] Some parameters such as the area of production, the latitude, the climate, the variety, and the stage of maturity of the fruit greatly affect the fatty acid composition of olive oil.[38]

Polyunsaturated fatty acids (PUFAs) with 18 carbon atoms such as linoleic (18:2, ω-6), and α-linolenic (18:3, ω-3), known as essential fatty acids (EFAs), are particularly important because, although indispensable for cell structure composition, they cannot be synthesized by the human body and must be assumed through the dietary intake.[38] The high content of mono-unsaturated fatty acids, the low content in saturated fatty acids and the considerable presence of essential fatty acids makes olive oil a very beneficial and precious product for human health.[38]

Fatty acids are mainly present in olive oil in the form of triacylglycerols: the most frequently found are oleic–oleic–oleic (OOO), representing about half of the total triacylglycerols portion found in EVOO, palmitic–oleic–oleic (POO), oleic–oleic–linoleic (OOL), palmitic–oleic–linoleic (POL) and stearic–oleic–oleic (SOO). Diacylglycerols and monoacylglycerols have been identified in VOO at concentrations of 1–2.8% and 0.25%, respectively.[50]

Apart from unsaturated fatty acids, compounds present in the minor fraction also exert important beneficial activities for human health and contribute mainly to the overall beneficial aspects of the olive oil consumption.

The unsaponifiable fraction of olive oil represents about the 2% of the total weight and comprises a high number of heterogeneous compounds (more than 230) such as hydrocarbons, tocopherols, hydroxyterpenic acids, sterols, carotenoids, volatiles and phenolic compounds.[51,52]

Phenolic compounds are amongst the most important considering the bioactive properties of olive oil. The phenolic composition of olives and olive oil is very complex and the concentration of the different compounds belonging to this category depends on several factors including maturation stage, part of the fruit, plant variety, season, climate conditions and oil production methods. In general, phenolic compounds are very powerful antioxidant compounds and participate to the organoleptic and nutritional properties of the extra virgin olive oil.[38]

The major phenolic compounds present in olive oil are:[38,50]

- phenolic alcohols such as, 3,4-dihydroxyphenyl-ethanol (3,4-DHPEA) and *p*-hydroxyphenyl-ethanol (*p*-HPEA);
- secoiridoids such as oleuropein, ligstroside, demethyloleuropein and their aglycones, the dialdehydic form of decarboxymethyl elenolic acid linked to 3,4-dihydroxyphenyl-ethanol (3,4-DHPEA-EDA) or *p*-hydroxyphenyl-ethanol (*p*-HPEA-EDA);

- phenolic acids and their derivatives such as vanillic acid, syringic acid, *p*-coumaric acid, *o*-coumaric acid, gallic acid, caffeic acid, protocatechuic acid, *p*-hydroxybenzoic acid, ferulic acid, cinnamic acid, 4-(acetoxyethyl)-1,2-dihydroxybenzene, benzoic acid;
- flavones, in particular luteolin, apigenin and their derivatives;
- lignans such as (+)-1-acetoxypinoresinol and (+)-pinoresinol;
- hydroxy-isocromans.

1.2.4.1 Oleuropein, hydroxytyrosol and tyrosol

The secoiridoid compound oleuropein (OL) and its derivatives hydroxytyrosol and tyrosol -also known as 3,4-dihydroxyphenyl-ethanol (3,4-DHPEA) and *p*-hydroxyphenyl-ethanol (*p*-HPEA) respectively- are amongst the molecules of major interest for their biological and pharmacological properties, resulting among the most investigated antioxidant natural compounds.[52] Iridoids and secoiridoids are compounds, usually glycosidically bound, produced from the secondary metabolism of terpenes as precursors of various indole alkaloids. The secoiridoids in *Oleaceae* are usually derived from the oleoside type of glucosides, characterized by an exocyclic 8,9-olefinic functionality, a combination of elenolic acid (EA) and a glucosidic residue. Oleuropein is an ester of hydroxytyrosol and the oleosidic skeleton whereas ligstroside is an ester of tyrosol and oleoside (Scheme 1.1).[53]

Considering the intact olive fruit, the most abundant secoiridoids are oleuropein, demethyloleuropein and ligstroside,[52] whose quantity generally decreases during maturation of olives, olive oil production and VOO storage due to their hydrolysis in hydroxytyrosol, tyrosol, and eleanolic acid (EA) and formation of oxidized phenols. The concentration of secoiridoids is largely affected by agronomic factors (cultivar, ripening stage, geographic origin of olive fruit, and olive trees irrigation) and by oil extraction conditions during crushing, malaxation, and VOO separation.[52]

At the beginning, during olives growing, accumulation of oleuropein occurs, whereas its concentration diminishes during fruits maturation, with particularly rapid decline in black cultivars. The first degradation process of OL takes place during maturation of olives and is accompanied by accumulation of demethyloleuropein and EA glucosides, produced by the action of endogenous esterases present in mature fruits. The second degradation pathway includes activation of β-glucosidases during crushing and malaxation of olives, and originates aglycone derivatives, known as VOO secoiridoids.[52] Then, aglycones of OL (and also ligstroside) are furtherly transformed by enzymatic and chemical reactions, leading to the opening of the secoiridoidic ring, resulting in the formation of the dialdehydic form of decarboxymethyl EA linked to HT or tyrosol, termed 3,4-DHPEA-EDA and *p*-HPEA-EDA respectively (also known as oleacin and oleocanthal), and to the monoaldehydic isomers of OL aglycone (3,4-DHPEA-EA) and ligstroside aglycone (*p*-HPEA-EA) (Scheme 1.1).[52,54]

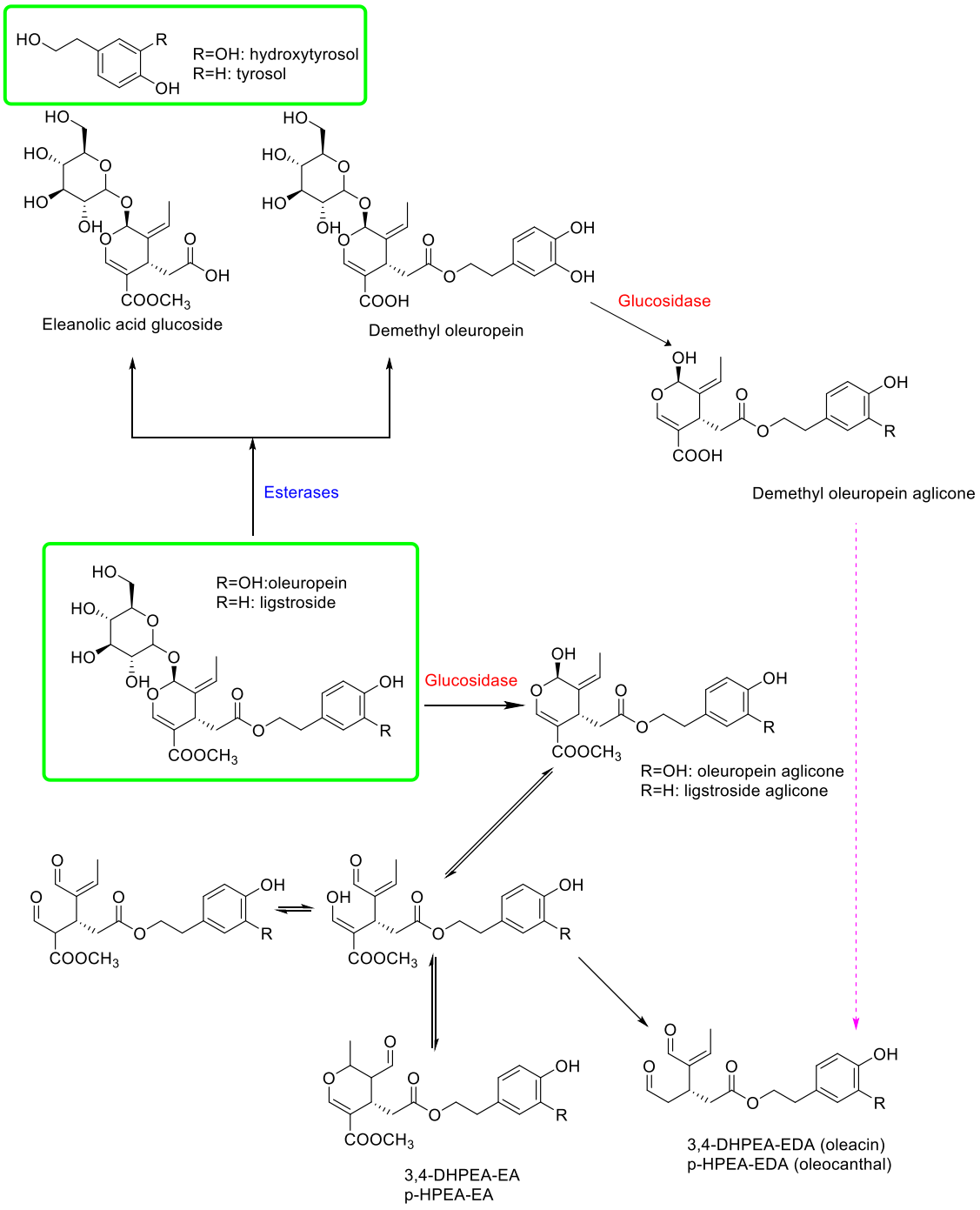

Scheme 1.1- Possible degradation pathways for oleuropein and ligstroside. Adapted from [52,55 56].

1.2.5 Beneficial effects of olive oil on health

Olive oil is a key ingredient component of the Mediterranean diet (MED),[50] consisting of a balanced consumption of fruit, vegetables, legumes and cereals, associated with a large assumption of bluefish and EVOO, reduced consumption of red meat and dairy products, and moderate intake of alcohol. The MED has many beneficial effects contributing in maintaining health and increasing longevity, as stated by the United Nations Educational Scientific and Cultural Organization (UNESCO) in 2010 (Figure 1.8).[57]

The health benefits of olive oil are mainly ascribed to the presence of high content of monounsaturated fatty acids and functional bioactive compounds. The latter -whose composition varies in relation to various factors, in particular cultivar, ripeness and harvesting regime, agroclimatic conditions as well as the processing

techniques employed to produce oil- not only contribute to the unique flavor and taste of olive oil but also confer multiple biological activities.[38]

Amongst the most beneficial substances present in olive oil there are phenolic compounds, in particular oleuropein, hydroxytyrosol and tyrosol, as attested also by the presence of a dedicated health claim from EFSA, the European Food Safety Authority. Health claims are nutritional and health indications approved by the European Commission to help consumers to be more aware of the beneficial properties and high quality of certain products, avoiding the risk of misleading indications. The claims must therefore be easily understandable to the consumer and must demonstrate, based on scientific evidence, that the nutrient has a nutritional or beneficial effect.[54] There are four health claims that can be applied to olive oil, and one in particular is specific for this product, and regards the presence of olive oil polyphenols. The health claim says "olive oil polyphenols contribute to the protection of blood lipids from oxidative stress", and it can be applied only for olive oils containing at least 5mg of hydroxytyrosol and its derivatives (i.e. oleuropein complex and tyrosol) per 20 g of olive oil, which is the daily intake to have the beneficial effect.[58]

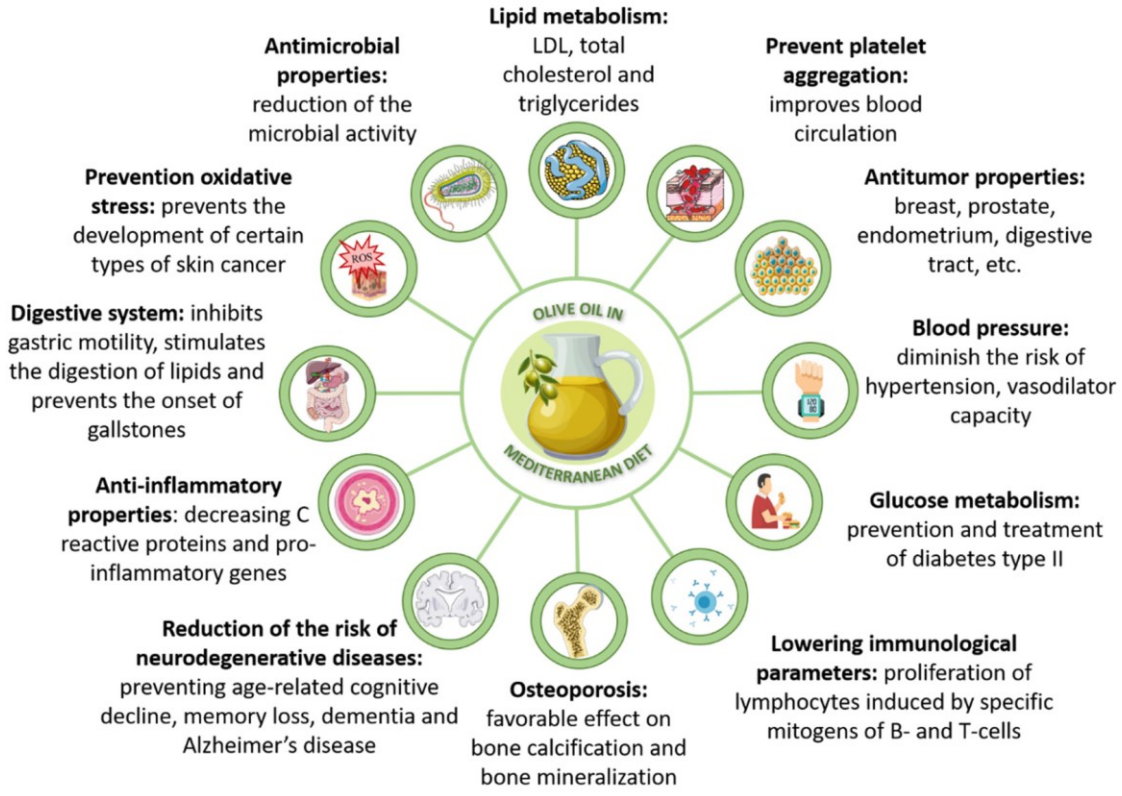

Figure 1.8- Overview of the beneficial effects of olive oil inclusion in the Mediterranean diet.[50]

Oleuropein exerts its antioxidant activity on different levels. In fact, oxidation is defined as a general degenerative process taking place in biological systems due to the presence of endogenous reactive oxygen species (ROS), which are produced as the result of normal metabolic processes and can damage different cellular components such as proteins or DNA, possibly leading to the development of degenerative diseases.[52] Protection from negative action of ROS relies on the presence of several endogenous defense systems, comprising protective enzymes such as superoxide dismutase, catalase and glutathione peroxidase. However, when these defensive mechanisms are not effective in neutralizing all the free radicals, cellular damages caused by ROS contribute to the pathogenesis of various diseases, such as atherosclerosis and cardiovascular diseases, diabetes mellitus and metabolic syndrome, skin and neurodegenerative diseases

and also onset of cancer.[52] Antioxidants can exert their function according to different neutralization mechanisms, acting as free radical scavengers, anti-oxygen radicals, and metal chelators. Oleuropein and hydroxytyrosol can cover all these roles thanks to the presence of the catecholic moiety allowing them to act as free radicals and peroxyl radicals scavengers due to the stabilizing effect that the presence of the *ortho*-hydroxyl group has on the phenolic radical, which can form intramolecular hydrogen bonds with the second hydroxyl moiety (Scheme 1.2). Moreover, the ability of the catecholic structure to strongly chelate metals such as iron and copper, reduces the formation of ROS derived from reactions associated with these metals.[52] As previously reported, oleuropein also inhibits oxidation of low-density lipoproteins and has both the ability to scavenge nitric oxide and to cause an increase in the inducible nitric oxide synthase expression in the cell.[59]

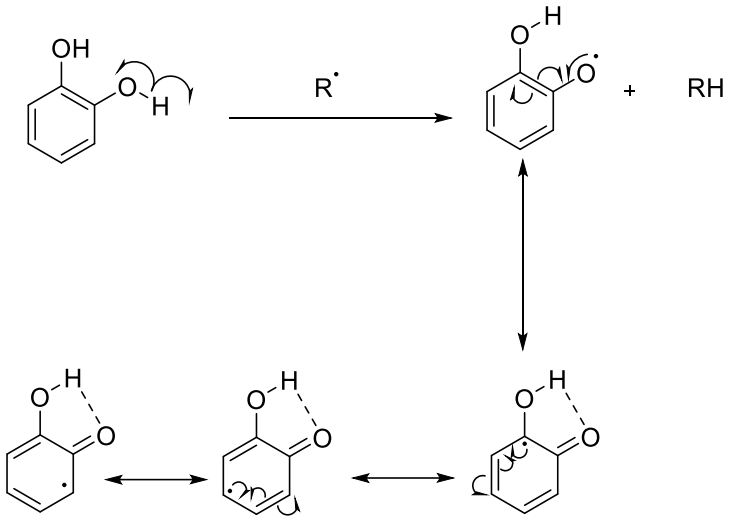

Scheme 1.2- Resonance structures of a phenolic radical in a catecholic structure (adapted from [52]).

Other very important beneficial effects of olive oil derive from its anti-inflammatory and cardioprotective properties, anti-tumor activity, positive modulation of the gut microbiota, antimicrobial and antiviral activity, skin protection, anti-ageing effect, neuroprotective and anti-platelet aggregation action, hypotensive and antidiabetic effects.[52,59]

1.3 SENSORS AND BIOSENSORS

A chemical sensor is a device that transforms chemical information, ranging from the concentration of a specific sample component to total composition analysis, into an analytically useful signal. Biosensors are a particular type of chemical sensor in which the recognition element utilizes a biochemical mechanism, and might be of biological origin or bioinspired.[60] The essential components in biosensors are a bioreceptor, capable of selectively recognizing the target analyte, a transducer, which converts the recognition event into a measurable signal, and a signal processing system (Figure 1.9).[61,62,63]

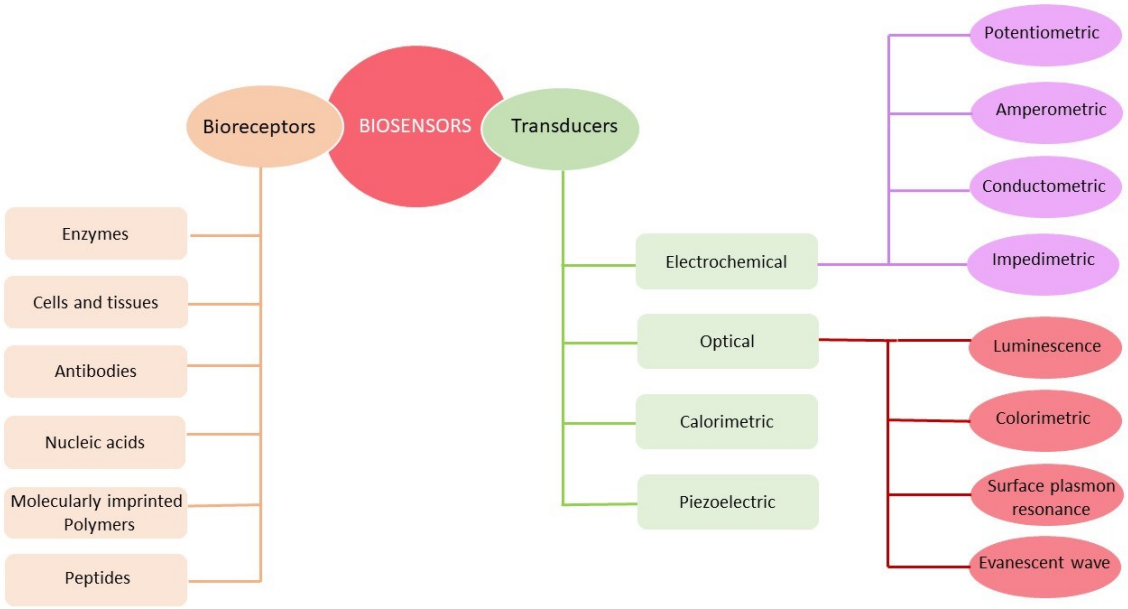

Figure 1.9- General scheme for a biosensor (adapted from [63]).

Clark and Lyons, who proposed the initial concept of glucose enzyme electrodes in 1962, first started the era of "biosensing research and development". Clark's technology was then transferred to Yellow Spring Instrument Company which launched in 1975 the first dedicated glucose biosensor.[64,65] Since then, research has made huge improvements, and biosensors have now found application in a wide range of fields, including environmental and water quality monitoring, health monitoring, food and beverage security analysis, agriculture, drug development and monitoring.[61]

In order to work well, a biosensor should possess several qualities. First of all, it should be selective for the target analyte (the bio-receptor can recognize a specific analyte element in a sample consisting of a mixture of species and unwanted contaminants) and stable under normal storage conditions.[61] Secondly, the recognition should be as independent as possible with respect to physical parameters such as stirring, pH and temperature, and the response should be accurate, precise, reproducible and linear over the concentration range of interest. Last, but not least, the complete biosensor should be cheap, small, portable and capable of being used by semi-skilled operators.[64]

All these features make biosensors convenient alternatives to standard laboratory techniques requesting expensive laboratory equipment, time-demanding sample pretreatment procedures and analysis, and skilled personnel to perform the entire process.

Biosensors may be classified according to the biosensing element, or to the mode of signal transduction.[60,62]

Based on the transducer, the biosensors can be mainly classified into electrochemical, optical, mass-based and thermal.[61,66] Considering optical transduction, it is based on the variation of an optical property such as

absorption, fluorescence, phosphorescence, chemiluminescence, surface plasmon resonance and evanescent wave, when the recognition element of the biosensor binds to the target molecule.[62,67]

The working mechanism of optical biosensors can be based on two main principles: the first exploits changes in the intrinsic optical properties of the bioreceptor resulting from the interaction with the target analyte, but application of this type of sensors is limited due to their low sensitivity and also because the spectral range usually involved is the deep UV, which cannot be easily applied to the analysis of complex real samples.[68] The second type of biosensors exploits optical labels and probes that must be conjugated to the receptor and can be chosen to have the most appropriate working wavelengths to generate the analytical signal.[68]

Considering electrochemical transducers, they can sense produced or consumed ions or electrons as a result of a reaction between the target analyte and the bioreceptor.[66] Typically in (bio-)electrochemistry, signal transduction can rely on amperometric methods -which measure a current-, potentiometric methods -which measure a potential or charge accumulation- or conductometric methods -measuring the conductometric properties of the medium-. Other detection techniques measure electrical impedance and field-effect, which uses transistor technology to measure current as a result of a potentiometric effect at a gate electrode.[64]

Passing to mass-based biosensors, the transduction mechanism is based on a change in the oscillating frequency, related to an increase in the mass of the sensor after target molecule binding. These sensors are divided into four major categories: piezoelectric quartz, surface acoustic, magnetoelastic biosensors, and microcantilevers.[61]

1.3.1 Recognition elements

The recognition element is the portion of the biosensor responsible for selective binding of the target analyte, which can be of natural origin but also artificially designed based on recognition mechanisms present in nature. Amongst the most common biosensing elements there are enzymes, antibodies, nucleic acids, cells and tissues, aptamers, peptides and molecularly imprinted polymers (MIPs).[61] Considering the recognition mechanisms, they can be classified as biocatalytic or bioaffinity-based.[60,68]

1.3.1.1 Enzymes

The working mechanism of enzymatic biosensors is based on the catalytic action and binding capability of the enzymatic recognition element for specific detection of target analyte.[62] There are two main mechanisms that can be exploited according to the analyte of interest: substrate detection and enzymatic inhibition. Substrate detection mechanisms are based on the conversion of the substrate into the reaction product(s) by the enzymatic recognition element. On the other hand, inhibition based enzymatic biosensors rely on the ability of the target analyte to reduce enzymatic activity, so they are based on the determination of enzyme activity in the presence and absence of inhibitor compounds, that can work in a reversible or irreversible manner: the decrease in product concentration provides the detection of inhibitory targets (Figure 1.10).[66]

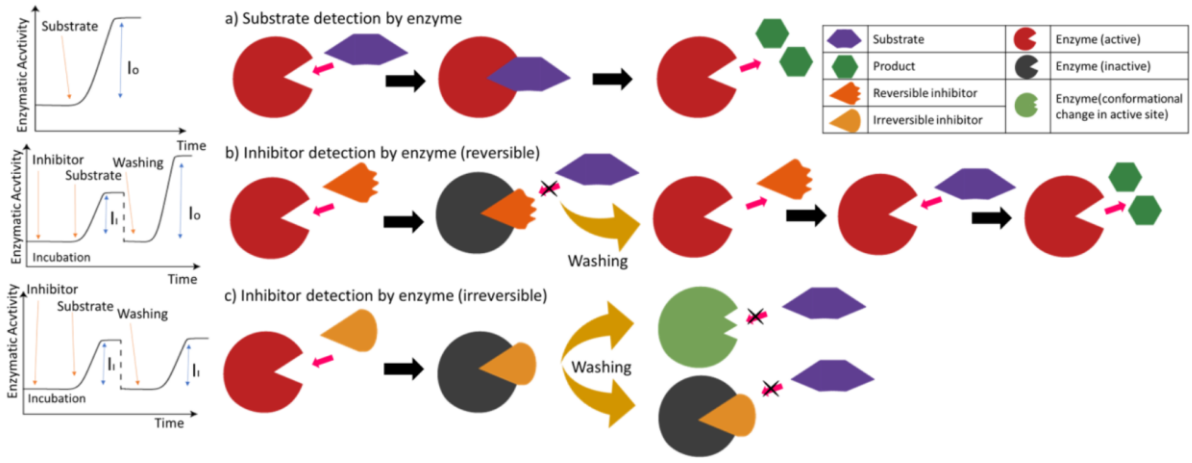

Figure 1.10- Scheme of enzymatic biosensors based on substrate detection (a), reversible enzymatic inhibition (b), irreversible enzymatic inhibition (c).[66]

1.3.1.2 Whole cells and tissues

In cell-based sensors the living cell acts as the sensing element exploiting its capability to detect the intracellular and extracellular microenvironment conditions, producing a response upon interaction.[62] Microorganisms such as bacteria and fungi can be used as biosensors to detect the overall ''state'' of the surrounding environment but they can be used also to sense specific molecules thanks to proteins that are present in cells. Cells as recognition elements have both positive and negative aspects. The major limitations of cell-based biosensors are the stability of the cells -which depends on various conditions such as sterilization, lifetime, biocompatibility-, the selectivity -due to their multireceptor nature-, and it must also be considered that the detection limit is mainly determined by the natural environmental conditions in which the cell can stay alive for a long period. Considering positive aspects, cell-based biosensors are less sensitive to inhibition by solutes and are more tolerant of suboptimal pH and temperature values than enzyme based biosensors; they also have a longer lifetime and are much cheaper because the active cells do not need to be isolated.[62] Despite some limitations of cell-based biosensors with respect to molecular ones such as a reduced sensitivity to environmental changes, an important opportunity is the possibility of modifying them by means of genetic engineering methods, using them for monitoring complex phenomena inside the living, providing important information related to the pharmacology, cell physiology, toxicology of a sample, data that cannot be obtained from molecular biosensors. To develop a cell-based sensor specific for a target analyte, the main issues are the selection of a reporter gene, as well as the selectivity and sensitivity deriving from binding of the regulator proteins to their target analytes. The mechanism of a whole cell-based biosensor is typically based on the recognition of the target analyte from the regulator protein, and the amplification of the recognition event into an electrical and optical signal via a processor (Figure 1.11).[69]

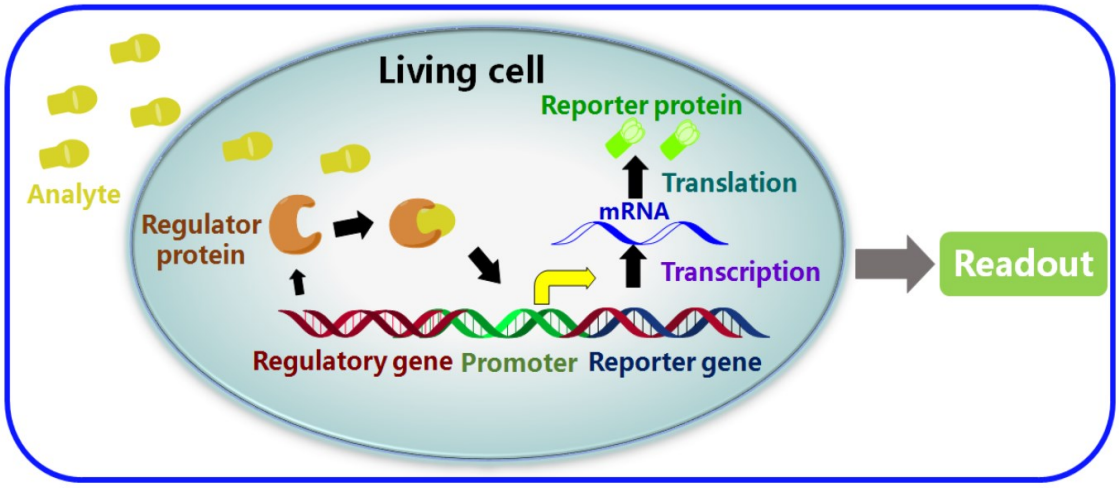

Figure 1.11- Schematic diagram of a typical whole cell-based sensor.[69]

1.3.1.3 Antibodies

Antibodies are the most popular affinity-recognition elements used in biosensors, which have found application in many different fields comprising food safety, environmental monitoring, clinical analysis, and medical diagnosis.[70] An antibody is composed by four polypeptide chains, two heavy (H) chains with molecular weights of 50 kDa and two light (L) chains (25 kDa molecular weight) linked by disulphide bonds. The chains have both constant (C) and variable (V) regions.[71] Antibodies can be classified as polyclonal and monoclonal. Polyclonal antibodies are generated from a range of immune cells, and may bind to the antigen at different locations or with different binding affinities; on the other hand, monoclonal antibodies are generated from identical clones of a single parent cell: since they bind to the same target region, named the epitope, with equivalent affinity, they are more selective than polyclonal antibodies.[70]

The most widely used formats for antibody-based biosensors are illustrated in Figure 1.12.[68]

a) Direct assay is the easiest assay format, in which an unlabeled antigen binds to an unlabeled antibody, and this allows signal generation.
b) Competitive assay in which an unlabeled antigen (the analyte) and its labeled form compete for a limited number of binding sites of the immobilized antibody.
c) Sandwich-type assay, widely used in common ELISA tests for example, which requires relatively large antigens that contain at least two epitopes to allow binding to the immobilized capture antibody and to the labeled second antibody.
d) Displacement assay, which requires an initial saturation of all the antibody binding sites with a labeled antigen, that upon introduction of the unlabeled target antigen is displaced.
e) Binding Inhibition assay, which requires immobilization of an unlabeled analyte derivative on the surface of a waveguide: in the absence of the antigen, the labeled antibody can bind to the surface, whereas in the presence of the analyte in solution binding to the immobilized antigen is inhibited because binding site of the antibody is already occupied.[68]

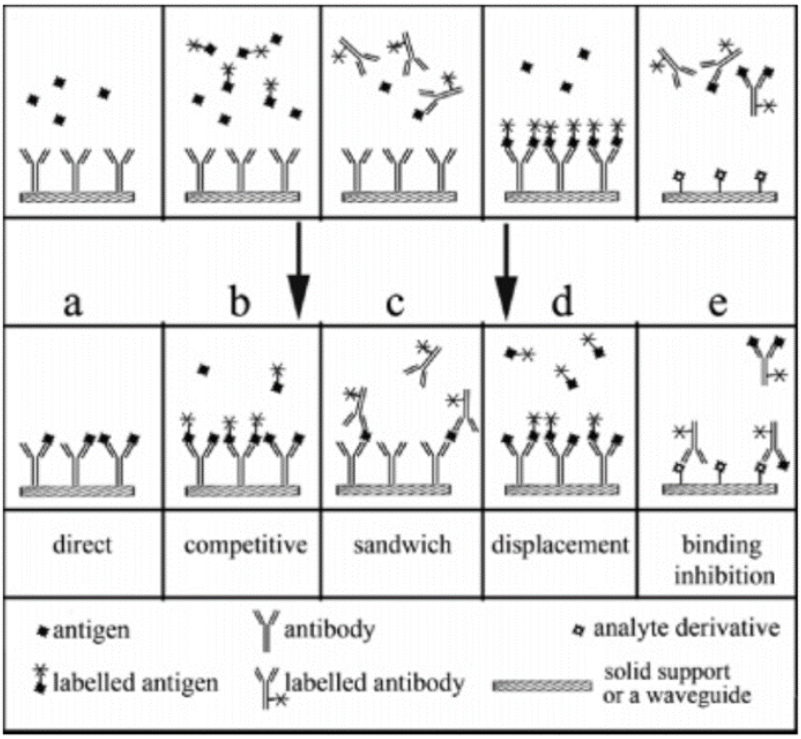

Figure 1.12- Different formats of antibody-based assays.[68]

More recently, advancements in recombinant DNA technology and protein engineering paved the way to antibody structure modification and development of recombinant antibodies, retaining the antigen specificity of the native antibody, while having the advantage of smaller size and easier production.[71] The best known antibody fragments are the fragment antigen-binding Fab (55 kDa) and the smaller single chain fragment variable scFv (25 kDa), which consists only of the VH and VL domains, joined by a synthetic polypeptide linker.[71] The use of small recombinant antibody fragments has several advantages with respect to entire antibodies, first of all the possibility to obtain them from bacteria, avoiding the need to immunize animals and significantly decreasing costs of production. Moreover, due to their reduced dimensions, they can be immobilized at higher density and, by means of antibody engineering, they can be further modified to improve affinity or stability, eliminate unwanted cross-reactivities, or add tags for purification or immobilization.[71]

An alternative to traditional antibodies is represented by nanobodies, antibodies naturally produced by camelids and sharks composed only by the heavy chain, without light chains: with a size of only 15 kDa, nanobodies represent the smallest existing antigen-binding fragments, possessing many favorable properties such as their high stability to a wide range of conditions, including high temperatures and denaturing conditions.[71]

1.3.1.4 Nucleic acids

The most common type of nucleic acid-based recognition element is composed of single-strand (ss) DNA which can hybridize with the complementary strand, thus allowing efficient and specific detection of the target strand of DNA or RNA.[72] Nucleic acids-based biosensors can find application for example in inspecting individual genomic or genetic details of a patient, but also to identify sequences from pathogens infection,[72] taking advantage of the exceptional long-term stability of nucleic acids, their high selectivity for the complementary chains and the ease of synthesis.[68]

A particular type of nucleic acid-based sensing elements, first described by Tyagi and Kramer, are molecular beacons (MBs), which have become an important tool for studies in genetics, disease mechanisms, and molecular interactions. MBs represent a single-stranded type of oligonucleotide probes that possess a stem-and-loop structure. The stem is formed by the annealing of two complementary arm sequences that are on either side of the probe sequence, complementary to the target one, positioned in the loop portion. The mechanism is based on the presence of a fluorophore and a quencher attached to one and the other end of the stem respectively, so that little or no fluorescence is observed in the native conformation. Hybridization of the complementary sequence to the loop portion results in conformational reorganization that brings the stem apart so that fluorescence is enhanced.[68,73]

Another type of nucleic acid-based recognition elements is aptamers, ssDNA or RNA molecules, typically containing less than 100 nucleotides, which have the ability to bind to other molecules with high affinity and specificity. Aptamers are selected from random oligonucleotide pools by a process called Systematic Evolution of Ligands by EXponential enrichment (SELEX), based on the ability of these small oligonucleotides to fold into unique three-dimensional (3D) structures which can specifically interact with a target exploiting non-covalent interactions such as van der Waals interactions, hydrogen bonding and π-π stacking interactions. Examples of aptamers for the detection of a variety of target molecules have been reported, ranging from small molecules -including metal ions, organic dyes, amino acids, antibiotics and peptides- as well as proteins, whole cells, viruses and bacteria.[74] Aptamers properties such as their high specificity, small size, versatility of modification and immobilization, regenerability or conformational change induced by the target binding, have been successfully exploited to optimize a variety of biosensing formats, including clinical diagnostics to detect pathogens, viruses and infectious diseases.[62]

Finally, Deoxyribozymes (DNAzymes) are functional oligonucleotides having enzymatic properties that allow them to mediate various chemical reactions such as DNA and RNA cleavage, ligation, and phosphorylation. The activity of some DNAzymes is dependent on the presence of specific compounds, such as metal ions and proteins: because of this property, these catalytic oligonucleotides can be used to develop biosensors capable of detecting such compounds. DNAzymes have already found application for the detection of food contaminants, pathogens, metal ions, as well as nucleic acids, proteins and in cancer detection.[75]

1.3.1.5 Molecularly imprinted polymers (MIPs)

Molecularly imprinted polymers (MIPs) are a synthetic class of biomimetic recognition elements designed to selectively recognize target molecules that fit the shape and size of the imprinted molecular cavities. Such cavities are obtained during the synthesis of the MIPs that involves three main steps (Figure 1.13). The first step consists in the prearrangement of functional monomers around the template molecule in solution, promoted by self-assembling exploiting non-covalent or covalent interactions. Then, polymerization of the pre-arranged complex is achieved by adding cross linkers and porogens (such as suitable solvents or ionic liquids); finally template is removed thus obtaining cavities complementary in shape that can host the target molecule for sensing purposes.[76] MIPs have attracted much attention due to several unique properties, such as simplicity, low cost, facile preparation, high selectivity and sensitivity.[77]

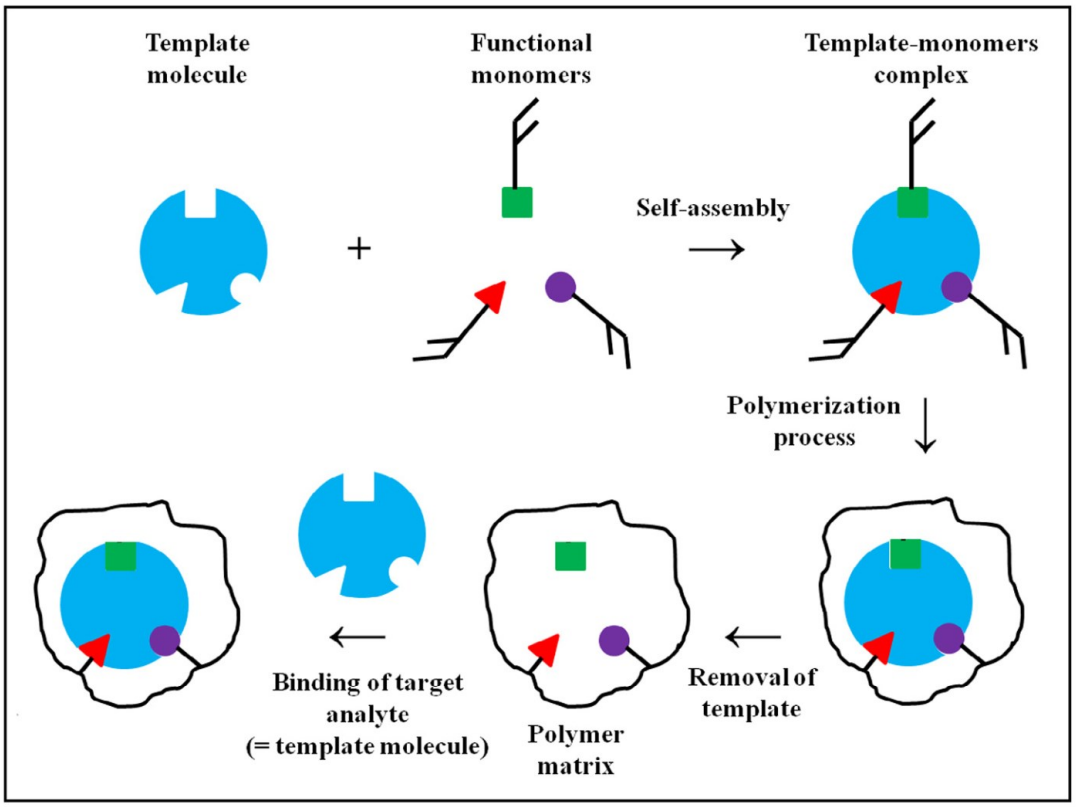

Figure 1.13- General scheme for the synthesis of MIPs.[70]

1.3.1.6 Peptides

Peptides are very important synthetic bioinspired recognition elements, that will be extensively discussed in section 1.4 of the Introduction.

1.3.2 Optical detection based on colorimetric/fluorimetric reactions

Plenty of optical sensors are reported in the literature, the majority of which is based on non-covalent interactions between recognition element and target molecule leading to change in the spectroscopic properties of the sensor.

However, several colorimetric reactions are commonly used in the laboratory practice to monitor chemical reactions as well as the presence of specific functional groups. One of the most widely used examples in this sense is the ninhydrin test, based on the reaction of the indicator dye ninhydrin with primary amino groups leading to the formation of the purple dye known as Ruhemann's purple (RP), first discovered in 1910 by Siegfrid Ruhemann.[78] Such method, introduced for quantification of amino acids in 1948, has undergone several improvements during the past decades, and is nowadays widely used both in the peptide and protein field and for the determination of amino-containing compounds in food and other matrices as well as in pharmaceutical products, for the evaluation of polysaccharides such as chitosan, and it has also found application in forensic science.[78,79]

A very important field in which colorimetric assays are frequently used is biology, in which they are often applied to monitor cells conditions and activity. Some assays are simply based on the capability of the different dyes to permeate specific cells regions or to differentiate between live/dead cells. However, there are also several assays based on reactions catalyzed by specific enzymes, leading to changes in the spectroscopic properties of the probes. A very interesting example in this sense is the use of the water-soluble

tetrazolium salt MTT, (3-[4,5-dimethylthiazol-2-yl]-2,5- diphenyltetrazolium bromide; thiazolyl blue), for cell viability, proliferation, and cytotoxicity monitoring. The MTT assay is based on the reduction of the yellow water-soluble MTT dye to the purple formazan product (*Scheme 1.3*). Such reaction is catalyzed by dehydrogenases in the presence of nicotinamide-adenine-dinucleotide (NAD(P)H) coenzyme, present in metabolically active cells. Purple formazan, insoluble in water, is then solubilized in an organic solvent, and the dissolved material can be analyzed spectrophotometrically, correlating absorbance (proportional to the quantity of converted dye) to the quantity of NAD(P)H-dependent cellular dehydrogenases, which reflects the number of viable cells present.[80]

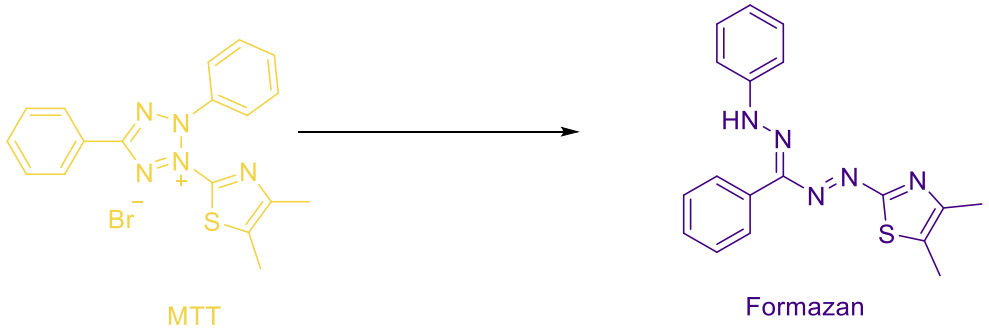

Scheme 1.3- Conversion of MTT tetrazolium salt to formazan.

Another interesting example of enzymatic reaction applied in the biological field is quantification of ATP based on the bio-luminescent luciferin–luciferase reaction. Such assay is based on the oxidation of D-luciferin to oxyluciferin catalyzed by the enzyme firefly luciferase, requesting consumption of ATP in the presence of oxygen and magnesium ions. Enzymatic oxidation of D-luciferin results in the emission of a luminescent signal that can be correlated to the quantity of ATP present (*Scheme 1.4*).[81]

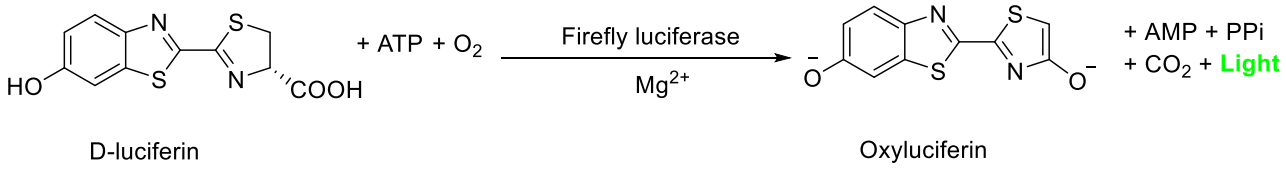

Scheme 1.4- Enzymatic conversion of D-luciferin to oxyluciferin catalyzed by firefly luciferase in the presence of ATM, oxygen and Mg^{2+} ions.

Besides enzymatic transformations, several examples have been reported regarding molecules reactive to specific functional groups/molecules undergoing changes in the spectroscopic signals upon specific chemical reactions. Chromogenic of fluorogenic dyes based on reversible covalent reactions are usually referred to as reactands, whereas dyes based on irreversible binding are usually referred to as chemodosimeters.[82]

Several examples have been reported by Mohr and colleagues regarding stilbene and azobenzene derivatives containing a reactive trifluoroacetyl group sensitive to several nucleophilic functional groups such as amines, alcohols, humidity (few examples are reported in Figure 1.14). Reaction of the trifluoroacetyl group leads to the formation of hemiaminals, zwitterions, hemiacetals or diols according to the nucleophile. This causes a change in the degree of delocalization within the dye molecule, thus causing significant changes in absorbance or fluorescence properties of the dye, resulting in a shift in the absorbance or emission spectrum. The dyes have been embedded in different polymeric materials, and methacrylate derivatives have also been synthesized to allow covalent incorporation into polymeric matrices.[82,83,84]

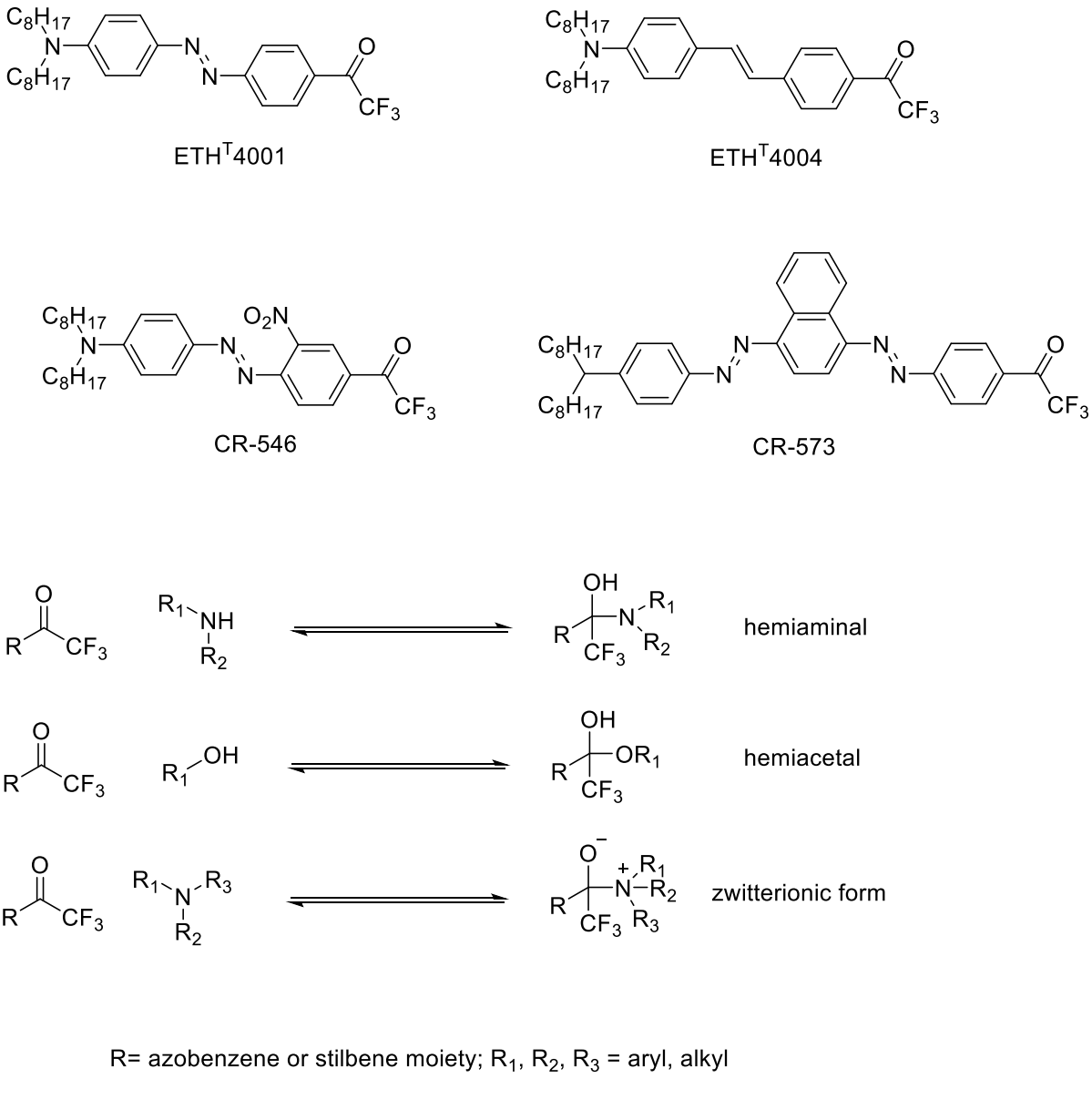

Figure 1.14- Different stilbene and azobenzene derivatives containing the reactive trifluoroacetyl moiety and examples of reactivity with amines and alcohols (adapted from [84,83]).

Based on a different chemical reaction, a very interesting example of sensing system based on a colorimetric reaction has been proposed in 2022 by Darder and colleagues, who developed a fiberoptic colorimetric sensor for *in situ* measurements of airborne formaldehyde, based on the acid catalyzed reaction between formaldehyde and the dye Leuco Fuchsin (LF), leading to conversion of the pale yellow LF reagent (absorbance at 455 nm) into the violet product VP upon reaction with formaldehyde (absorbance at 575 nm). Poly(methyl methacrylate) 3D printed filaments coated with a LF-doped Nafion® perfluorosulfonated cladding have been used as optical waveguides, monitoring the reaction using a custom-built optoelectronic device using dedicated software (*Scheme 1.5*).[85]

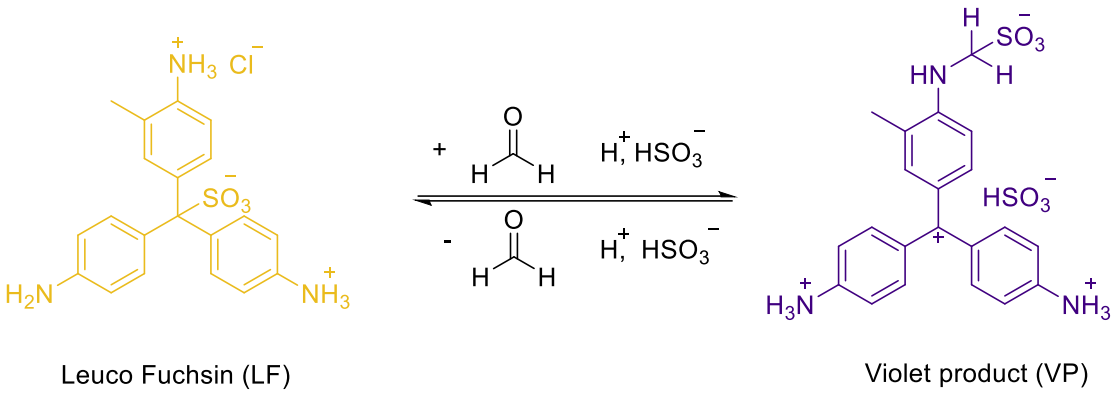

Scheme 1.5- Reversible reaction of Leuco Fuchsin LF with formaldehyde in acidic media leading to formation of the violet product VP (adapted from [85]).

Gojon and colleagues proposed a system in which two molecules of on-colored 4-*N*,*N*-dimethylaminobenzaldehyde (*p*DMAB) react with target molecule hydrazine leading to the formation of a colored benzalazine moiety, exhibiting an absorbance at 460 nm (*Scheme 1.6*). The aldehyde *p*DMAB was both physically entrapped and covalently immobilized in sol-gel glass, and regeneration of the system could be achieved by heating the system at 50°C in 1 M nitric acid.[86]

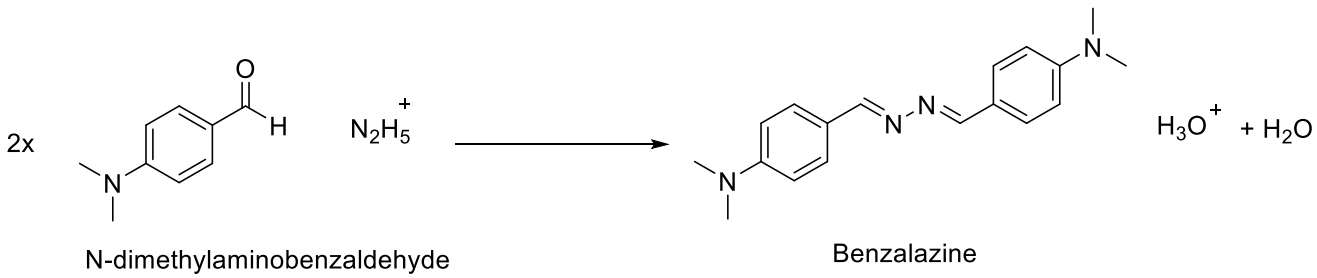

Scheme 1.6- Reaction of 4-N,N-dimethylaminobenzaldehyde with hydrazine leading to the colored benzalazine derivative (adapted from [86]).

Another example of colorimetric detection, in which the colored dye forms upon reaction of the analyte with the sensing system, has been proposed for furfural determination by Rico-Yuste and colleagues. In particular, the group applied the Stenhouse reaction to polymeric films containing reactive aromatic amines capable of reacting in acidic conditions with the target molecule furfural, leading to the formation of the pink Stenhouse adduct (*Scheme 1.7***Errore. L'origine riferimento non è stata trovata.**). Furfural quantification by measuring the colorimetric signal could thus be performed by either using a portable fiberoptic spectrophotometer or the built-in camera of a smartphone.[87]

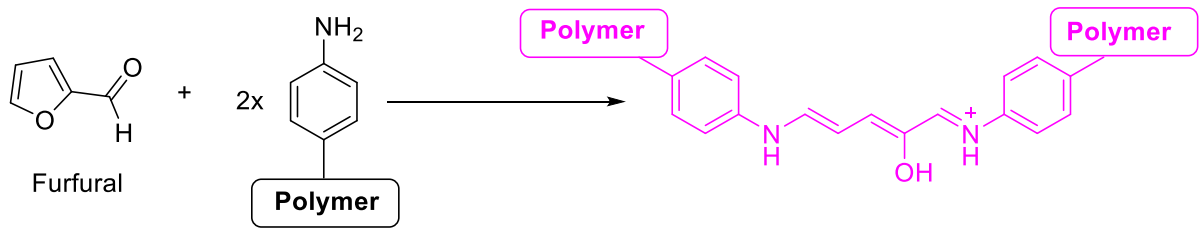

Scheme 1.7- Stenhouse reaction of aniline-containing polymeric film and furfural (adapted from [87]).

A commonly used transduction mechanism is based on the presence of a functional group that quenches luminescence due to photoinduced electron transfer (PET). As a consequence of the reaction between the

quenching group and the analyte, PET from the functional group to the fluorophore is modulated and an increase in luminescence is observed.[83]

An example is the fluorophore *N*-amino-*N*'-(1-hexylheptyl)-perylene- 3,4:9,10-tetracarboxylbisimide, in which the fluorescence of the perylene unit, initially quenched by PET with the amino group, is restored upon Schiff base formation with aldehydes and ketones (*Scheme 1.8*).[88]

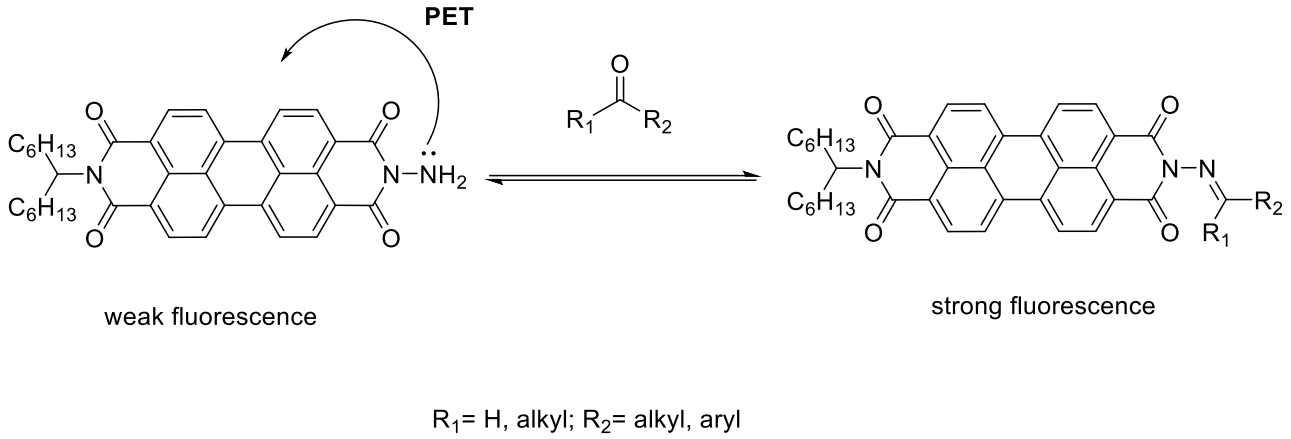

Scheme 1.8- Mechanism of fluorescence enhancement of N-amino-N'-(1-hexylheptyl)-perylene- 3,4:9,10-tetracarboxylbisimide upon reaction with carbonyl compounds (adapted from [88]).

Based on a similar principle, Hampe and Rudkevich developed the interesting chemosensors 1-aminomethylnaphthalene and 1-aminomethylpyrene, exhibiting poor fluorescence in the native state, due to PET effect from the lone pair of the free amino group, but exhibiting fluorescence enhancement upon reaction with CO_2, obtaining the corresponding carbamic acids. Bubbling nitrogen through the carbamic acids solutions resulted in loss of CO_2, even at room temperature, with a consequent decrease in fluorescence emission. Upon addition of the free amino fluorophores, carbamic acids can also be converted into the corresponding fluorescent carbamate salts, which could be converted back to the free amino compounds upon heating (*Scheme 1.9*).[89]

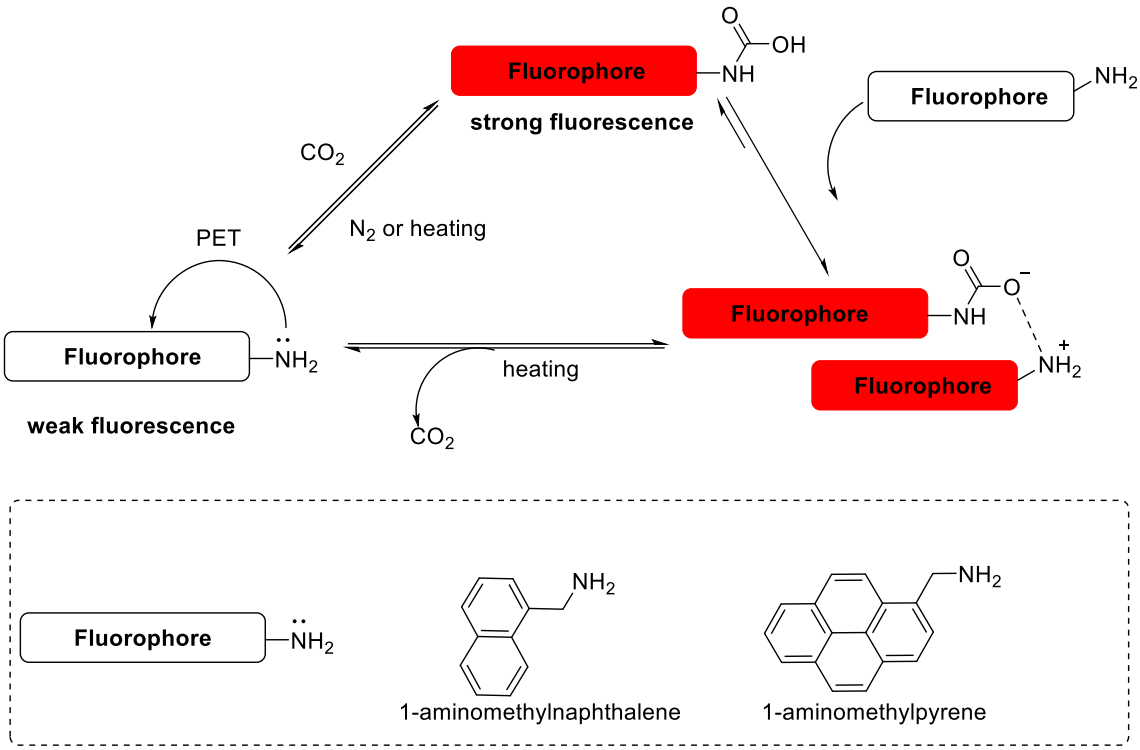

Scheme 1.9- General scheme of covalent reversible binding of CO_2 and fluorescence transduction (adapted from [89]).

Regarding thiols detection by means of a non-reversible reaction, de Silva and colleagues proposed a method based on a naphthalimide derivative functionalized with a maleimide group, observing a PET effect from the excited state of the fluorophore to the electron deficient alkene. Upon Michael reaction of a thiol with the maleimide portion, a succinimide derivative forms, the photoinduced electron transfer becomes unfavorable and fluorescence enhancement is observed.[90]

Very importantly, and relevant for this thesis, one of the best-known examples of covalent reactions leading to change in spectroscopic properties is the application of boronic acid fluorescent probes, undergoing changes in fluorescence upon boronic esters formation. This application will be discussed in more details in chapter 4 of the present thesis.

Considering chemodosimeters, the analyte can directly react with the dosimeter, producing a product having different spectroscopic properties with respect to the starting material. However, another possibility is that the analyte acts as the catalyst and the chemodosimeter acts as the substrate of the catalyzed reaction. According to the second mechanism, the turnover is much greater, allowing to obtain lower detection limits.[91] Very commonly chemodosimeters are employed for metal cations and anions sensing. Some of the reactions that can be catalyzed by the analytes are “de-reactions” -meaning reactions in which there is the loss of a portion, such as desulfurization, deselenation and deprotection-, cyclization, hydrolysis, rearrangements and fluoride-triggered Si-O bond cleavage.[91] Just to cite one example, since the subject has been widely reviewed,[91,92] in 2005 Ros-Lis and colleagues developed a Hg^{2+} chemodosimeter based on the desulfurization capability of Hg^{2+} ions.[93] The assay is based on the indicator dye, which is initially “switched-off” by the addition of a thiol- which acts as a “spectroscopic inhibitor”. The target ion Hg^{2+} then reacts with the inhibitor thiol due to its thiophilicity, causing a dramatic change of color due to the appearance of a new and intense absorption band at 642 nm that is typical for a squaraine dye, and a fluorescence emission at 670 nm when exciting at 642 nm (*Scheme 1.10*).[93]

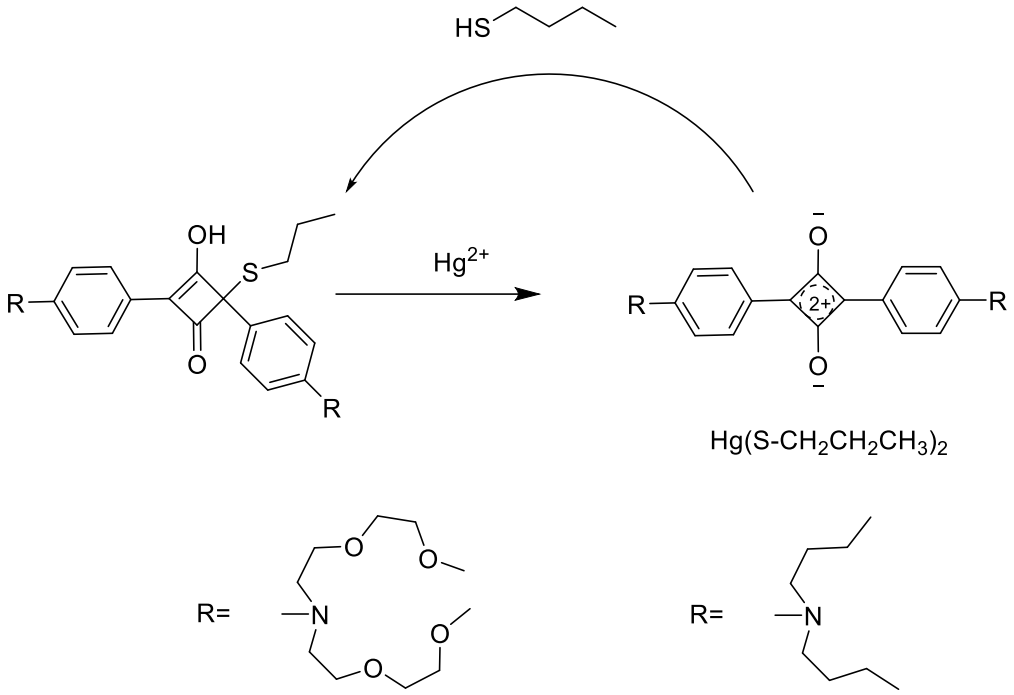

Scheme 1.10- Hg^{2+} chemodosimeter based on the desulfurization capability of Hg^{2+} ions (adapted from [93]).

A further development in optical sensing based on covalent reactions comes from the concept of simultaneous multi-analyte detection using "reactive" luminescent probes able to produce an optical signal only in response to multiple (bio)chemical inputs and through covalent chemical reactions with target (bio)analytes, capable of working in complex media and with high selectivity.[94] Hettie and colleagues developed four three-input AND gates to monitor the simultaneous presence of glutamate, zinc ions and pH, designed for directly imaging the co-release of glutamate and the zinc(II) cation from glutamatergic secretory vesicles. This aim has been achieved thanks to the presence of an aldehyde at the 3-position of the coumarin core, capable of forming a Shiff base with the amino group of glutamate. In this way, the glutamate creates together with the lactone carbonyl group a multiple-point binding site for zinc ions. The presence of the hydroxyl position in the 7-position of the coumarin core grants pH sensitivity, switching on fluorescence and red-shifting absorbance of about 45 nm (*Scheme 1.11*).[95]

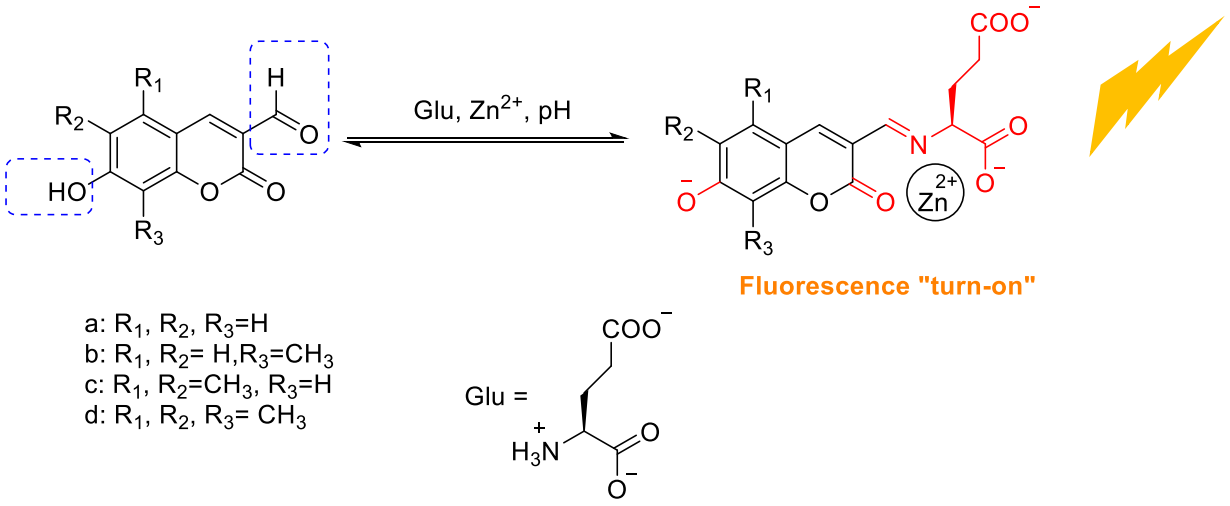

Scheme 1.11- Three-input AND gates to monitor glutamate, zinc ions and pH (adapted from [95]).

1.4 PEPTIDE BIOSENSORS

Peptides are a very interesting option to mimic recognition mechanisms occurring in complex macromolecules such as enzymes, antibodies, drug receptors and transmembrane proteins.[96] In particular, short peptides represent an excellent opportunity for the design of artificial receptors because of (1) the ideally infinite number of different peptide sequences that can be obtained by combining both natural and non-natural amino acids, (2) the availability of both molecular biology and chemical techniques for the fast screening of peptide libraries, (3) the possibility of automated and low-cost synthesis of relatively large amounts of purified peptides, (4) the ease of modification to further enhance target molecule binding or to attach labels, and (5) relatively easy modeling.[96]

Many peptide-based sensing systems have been reported in recent literature, targeting a wide range of different analytes including whole cells, proteins, but also small organic molecules such as drugs, hormones, pollutants, and ions.[96] There are plenty of peptide sequences known to be specific binding partners for important biomolecules;[97] however, very important tools to develop peptide-based sensors are also *in silico* design and the use of random phage display to select suitable aminoacidic sequences.[96]

Since in the present thesis work different peptide structures have been synthesized for sensing purposes, in this section, some illustrative examples of peptide-based biosensors will be reviewed, with particular attention to works published after 2012, year in which our group published a review on peptide based biosensor transducers.[96] Selected peptides will be classified according to how the sequence has been developed into:

- Small sequences based on the interactions of few amino acids with small target molecules, in particular metal ions;
- Phage displayed peptides;
- Peptides based on *in silico* design;
- Peptides based on knowledge of specific sequences which are known to be recognized by/recognize the target molecule;
- Peptide Nucleic Acids (PNAs)

1.4.1 Small peptide sequences for metal binding

Peptides contain a great number of potential donor atoms both through the amino acidic backbone and amino acid side chains. Based on the strong interactions of single amino acids and peptide structures with some metal ions, several examples have been reported in literature since long ago of peptides which can very effectively, and often specifically, act as ligands for a variety of metal ions.[98]

One of the most typical examples is the tripeptide sequence GlyGlyHis, capable of selectively binding copper ions without cross-reactivity with zinc, whereas the isomer GlyHisGly does not. The GlyGlyHis sequence has been used to realize field-effect transistors[99] and polypirrole nanowire electrode for Cu(II) detection,[100] and was also immobilized on the surface of a microcantilever.[101]

Another possibility is that of taking inspiration from binding motives present in nature, as it has been done by Godwin and Berg who developed a FRET (Förster Resonance Energy Transfer)-based peptide modifying the zinc finger consensus peptide with two fluorescent dyes, fluorescein as the FRET donor and lissamine as the FRET acceptor, to reveal zinc binding, thanks to the target-promoted conformational change of the peptide, resulting in an increased amount of intramolecular energy transfer due to spatial proximity of the two fluorophores.[102]

Instead of exploiting sequences taken from natural binding domains, Imperiali and Walkup reported two other peptides targeting zinc, based on the combination of different useful elements contributing to efficient

and selective Zn(II) binding, in particular the 8-hydroxyquinoline fluorophore -capable of forming fluorescent complexes upon bidentate metal binding- and a cysteine residue -favoring Zn(II) binding with respect to hard ions such as Ca(II) and Mg(II) thanks to its soft character-, both inserted at the edges of the reverse-turn promoting motif Val-Pro-D-Ser-Phe, to grant spatial proximity of the metal-binding elements.[103]

1.4.2 Phage display

Bacteriophages, or phages, are viruses that infect bacteria. Generally, the genome of each phage particle, called virion, is enclosed into a protein coat, the capsid: phage display refers to the expression of peptides or protein variants on the surface of the phage virion by cloning the corresponding encoding gene as a fusion with one of the phage coat proteins. Phage-displayed libraries are composed by a huge number of phage clones, each one displaying a unique peptide or protein sequence on its surface due to the different foreign DNA insert, which can be derived from a natural source or can be artificially designed. Phage-displayed libraries thus offer a unique opportunity to screen peptides/proteins for target binding and select specific binders, exploiting the biopanning process.[104] The process of *in vitro* affinity selection, generally includes: (I) the construction of protein or peptide libraries consisting of a huge number of variants; (II) the display method that allows to relate the expressed protein variant to the gene coding for it; (III) the application of selective pressure to screen for target-specific binders, and, finally, (IV) the amplification of the selected variants.[104] The screening process of phage-displayed libraries starts with exposure of the library to the target immobilized onto a solid surface. A successive washing phase allows removal of unbound and nonspecifically bound phages, thus granting that only selectively bound phages remain attached to the immobilized target. Then, high affinity phages are eluted from the target, and are amplified through bacterial infection. The selection process is repeated several times, and finally provides a mixture of clones with different target-binding properties (Figure 1.15A). Screening of individual clones, typically by phage-based immunoassays, such as enzyme-linked immunosorbent assay (ELISA), is usually performed, thus allowing the selection of the clones exhibiting the best target-binging capabilities, whose DNA is finally sequenced (Figure 1.15B).[104]

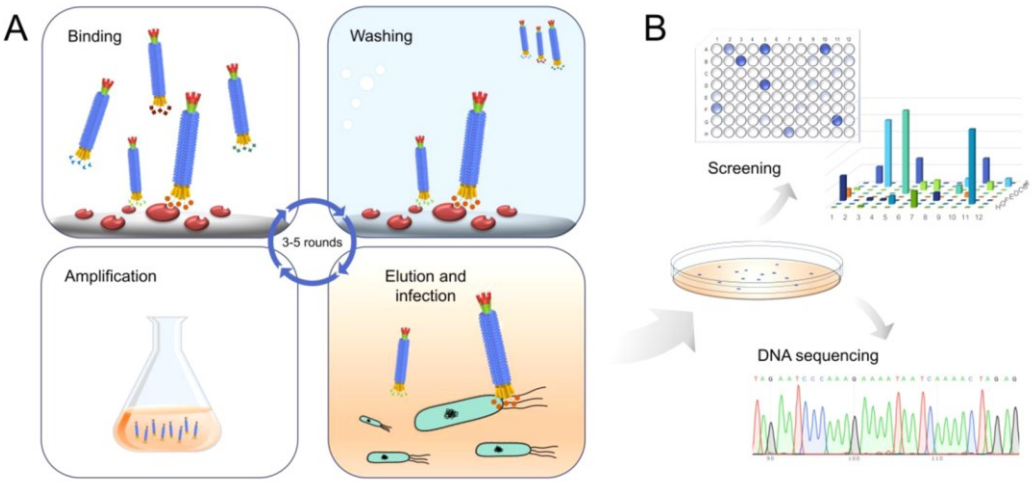

Figure 1.15- Selection of affinity binders from a phage-displayed library. (A) Selection process consisting of binding, washing, elution, and amplification steps, usually repeated few times. (B) Screening of target specificity of individual clones in ELISA assays and identification of the positive clones by DNA sequencing.[104]

Phage display is a highly versatile tool, which can be applied to different approaches, such as finding an amino acidic sequence capable of target molecule recognition -for example it is often used for screening of affibodies-[105] but it can also be employed for discovering a target molecule analogue useful in the case of a competitive assay (this is the case of anti-mimotope peptides).

Regarding competitive immunoassays, it must be considered that obtaining the labelled competitor of low molecular weight molecules requires conjugation of the target to a label or a carrier molecule, which can be a very difficult and time-consuming step in some cases. To overcome all the drawbacks that might arise from this step, a possible alternative is the development of protein or peptide substitutes that mimic the target and serve as the competitor in the competitive immunoassay, the so-called anti-mimotope peptides. Such epitope mimics bind to the same antibody paratope as the target, eliciting an antibody response similar to that of the analyte, and can be easily selected by phage-display and further modified. Analytical applications of epitope-mimics have been reported especially in the field of mycotoxins detection.[71]

For example, in 2018, Peltomaa and colleagues developed a homogeneous fluorescence quenching competitive immunoassay based on gold nanoparticles (AuNPs) and a recombinant epitope-mimicking fusion protein for the detection of mycotoxin fumonisin B1 (FB1), exploiting a previously identified epitope-mimicking peptide. The fumonisin mimotope was cloned as a fusion protein with a yellow fluorescent protein (YFP). The recognition principle of the homogeneous assay is based on fluorescence quenching by FRET of the mimotope-YFP emission when the mimotope binds to the antibody immobilized on gold nanoparticles. In the presence of the target FB1, competition between the natural target and the mimotope prevents the fusion protein binding to the antibody, and fluorescence is recovered due to the larger distance of the fluorescent mimic from the AuNP (Figure 1.16).[106]

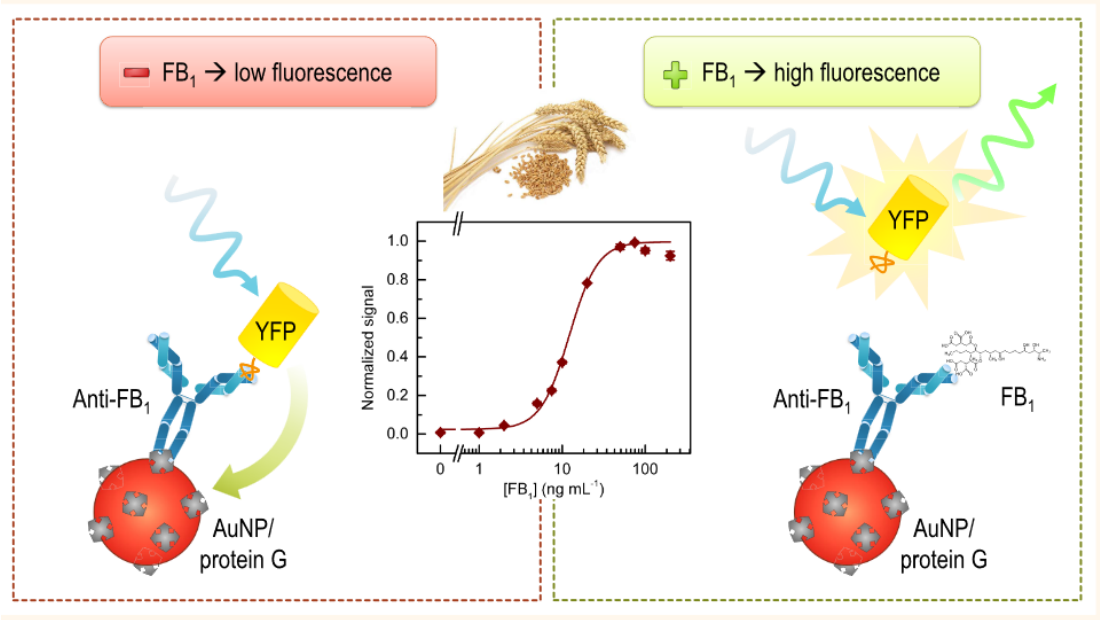

Figure 1.16- working mechanism of the fumonisin B1 competitive assay based on the recombinant fluorescent mimic of FB1.[106]

1.4.3 *In-silico* designed peptides

Another possibility to obtain peptide sequences capable of target molecules recognition is that of designing peptides *ex novo*, exploiting complex algorithms to find the best aminoacidic sequences. For example, our group proposed an innovative algorithm capable of designing short cyclic peptides with high binding affinity toward a target organic molecule.[107] The approach is based on a stochastic search in the peptide sequence space driven by a series of single point mutations. At each mutation step, a conformational sampling is performed by molecular dynamics simulation in an explicit solvent environment and the mutation is accepted or rejected according to a Monte Carlo scheme targeted at improving the estimated stability of the complex.[107,108]

This computational approach has been applied by our group for the *in-silico* design of peptides targeting the anti-cancer drug irinotecan. Three peptides have been designed in vacuum, whereas two peptides have been designed in methanol, and their ability to bind irinotecan has been assessed by surface plasmon resonance

and fluorescence spectroscopy, obtaining binding affinity results in good agreement with those predicted by initial molecular dynamics simulation, with peptides designed in methanol showing the highest affinity. Selectivity of peptides between irinotecan and a structurally related active metabolite has also been considered, and peptides designed in methanol resulted capable of discriminating between the two molecules, thus highlighting the need of designing the peptides in an explicit solvent environment.[108]

Another example proposed in 2016 by our group is that of the cyclic peptide CWWEVITFFKEC, designed for the recognition of the phenolic compound chlorogenic acid and related molecules. The study of the interactions of the peptide with two *ortho*-diphenols -chlorogenic acid (CGA) and caffeic acid (CA)- and two mono-phenols -*p*-coumaric acid (*p*CA) and ferulic acid (FA)- by using the fluorescence emission of the two tryptophan residues, confirmed peptide selectivity toward its target CGA, with association constants for the other tested ligands at least ten times less favorable. Benefiting from the electroactive nature of phenolic species, the binding ability of the peptide has been evaluated also by differential pulse voltammetry: only the two diphenols CGA and CA showed a significant decrease of the anodic current, and this behavior can be attributed to the binding ability of the peptide that reduces the electrochemical availability of the phenolic groups of the two *ortho*-diphenolic molecules.[109]

1.4.4 Peptide based on target-specific binding sequences present in nature

Very often, peptide sequences can be derived from binding motives present in nature. One possibility is that of making use of naturally existing receptors, extrapolating reduced functional sequences to obtain simpler recognition elements for target molecule recognition.[96] However, one of the most common approaches is that of using peptides for recognizing their receptors, mainly enzymes, but also other types of proteins, cells and bacteria.

1.4.4.1 Peptides targeting enzymes

Since many proteins and peptides are the natural substrate for enzymes such as kinases or proteases, many peptide-based biosensors have been developed based on specific aminoacidic sequences recognized by target enzymes whose presence/activity should be monitored.

A very important class of enzymes are protein kinases, which catalyze the transfer of the γ-phosphoryl group of ATP to the hydroxyl groups of amino acid residues in peptides and proteins. Generally, protein kinases are divided into two subfamilies based on their ability to phosphorylate the aromatic side chain of tyrosine or the aliphatic side chain of serine or threonine. The activity of these enzymes is crucial for normal cellular communication and physiology, and aberrant action is associated with numerous disease states. For this reason, monitoring their activity is of pivotal importance. For this purpose, many fluorescent sensors based on different fluorescence-tuning strategies have been developed: generally, creating a library to make a screening to select the best fluorophore and position in the peptide chain is highly recommended.[110]

One strategy to obtain fluorescent protein kinase sensors in that of appending an environmentally-sensitive fluorophore on the peptide, provided the peptide experiences some form of phosphorylation dependent solvent change which is what might happen if, working in aqueous environment, the peptide is embedded in a hydrophobic environment after phosphorylation -normally, there is fluorescence enhancement once inserted into the hydrophobic domain- (Figure 1.17 left).[111]

Another very interesting strategy is deep-quenching, using a kinase substrate peptide sequence functionalized with a fluorophore which, in the presence of a quencher, exhibits little or no fluorescence emission but, after phosphorylation, is recognized by a specific binding domain, which breaks the interaction with the quencher, thus causing fluorescence restoring (Figure 1.17 center). [112]

Finally, self-reporting fluorescence substrates have also been developed, which benefit from the ability of tyrosine aryl side chain to engage π-π stacking interactions with other aromatic species, including

fluorophores, thus reducing their fluorescence quantum yields. In this type of sensors, phosphorylation of tyrosine alters its interactions with the fluorophore, thus leading to restoring of fluorescence of the emitting species (Figure 1.17 right).[113]

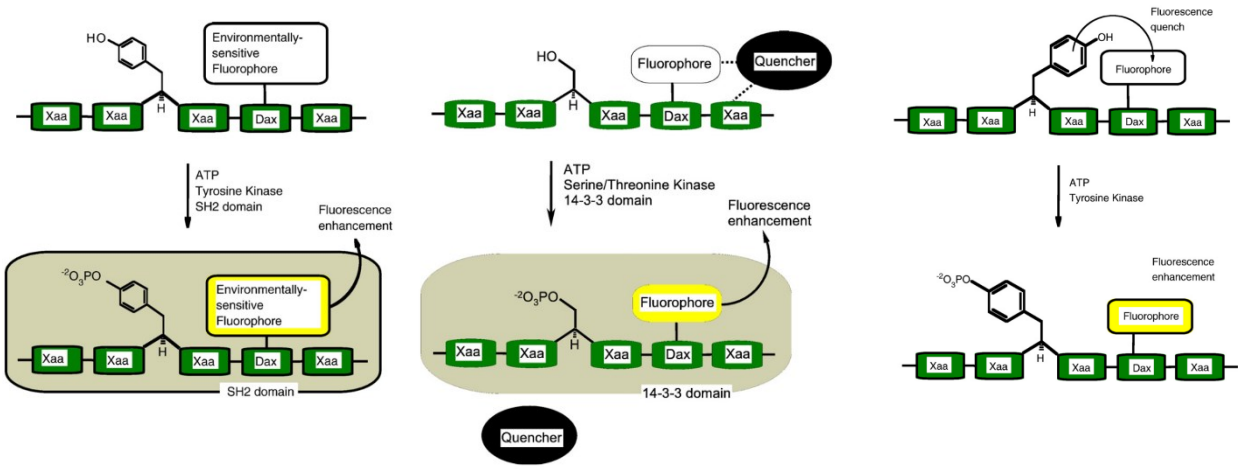

Figure 1.17- Different types of fluorescent protein kinase probes based on environmentally sensitive fluorophores (left), deep quenching (center) and self-reporting probes (right).[110]

Apart from directly targeting kinases, since kinase complexes (kCDKs) are formed by the association of cyclin-dependent kinases (CDK) and a regulatory cyclin unit, another possibility is that of monitoring cyclin A: in this perspective, a particularly convenient strategy is that of targeting its substrate recruitment element, called the cyclin binding groove (CBG).[114] According to this strategy, in 2008 Pazos and colleagues developed a very interesting approach for cyclin A detection based on peptide sequences capable of selectively binding to the cyclin binding groove. For signal transduction, peptides were provided with a Tb^{3+} chelating macrocycle: in fact, Tb^{3+} fluorescence emission can be achieved by excitation through intra/inter molecular energy transfer from aromatic residues in spatial proximity, and a tryptophan residue is present in the CBG which might act as an antenna to sensitize the lanthanide ion. One of the synthesized peptides in particular showed very efficient fluorescence emission upon cyclin addition, thus demonstrating the feasibility of this approach.[114] Based on the same CBG-binding peptide sequence, the same group also developed a peptide library to investigate the effect of two environment-sensitive fluorophores in different positions of the sequence, identifying two peptides capable of greatly enhancing their fluorescence upon cyclin A binding.[115]

Another very important class of enzymes whose presence is often monitored by using peptide sensors are proteases. Probably the most common strategy in this case is the introduction of a fluorescent unit and a quencher at opposite ends of protease sensitive peptide sequences: fluorescence emission intensity of the fluorophore, initially quenched (or shifted), is restored by specific degradation of the probe by the target protease, resulting in removal of the quenching portion. This allows to correlate fluorescence enhancement with the presence and activity of the enzymes.[97,116] There are numerous variations of this basic design motif relying on alternative photophysical effects like FRET, quenching by photoinduced electron transfer, or dimerization, and even using quantum dot conjugates.[97]

Changing to electrochemical transduction mechanisms, in 2019 Meng and colleagues developed a novel electrochemical biosensor for sensitive analysis of prostate specific antigen (PSA), a serine protease with chymotrypsin-like enzymatic activity, whose increased production has long been identified as the best available biomarker for the screening of prostate cancer. The assay is based on the immobilization on a gold electrode of a specific peptide sequence (CGGHSSKLQFWYFWY) which is a PSA substrate for cleavage. In the absence of PSA, graphene oxide (GO) can be immobilized on the peptide modified electrode, triggering the aggregation of silver ions and their subsequent reduction reaction to form silver nanoparticles (AgNPs) which

can be electrochemically detected. On the other side, in the presence of PSA, the peptide is specifically recognized and cleaved, and this causes no immobilization of GO and subsequent no formation of AgNPs, and this makes the electrochemical response decrease remarkably, which can be correlated to the concentration of PSA (Figure 1.18).[117]

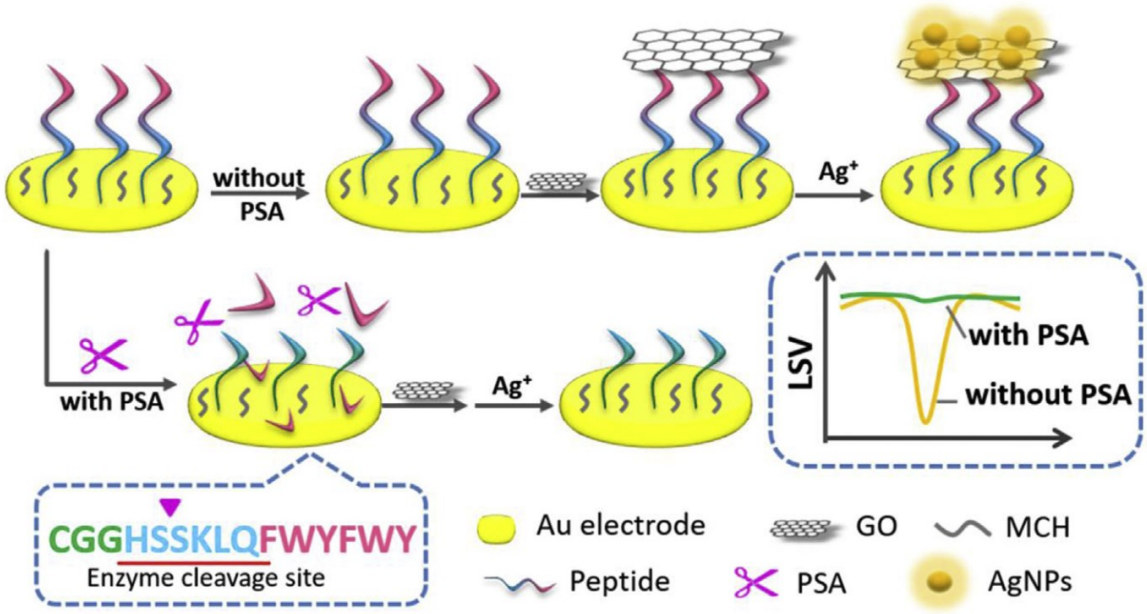

Figure 1.18- Working principle of the electrochemical cleavage-based biosensor for PSA detection.[117]

Even if the majority of available proteases sensors are based on the hydrolytic cleavage of peptide substrate sequences, another possibility is that of exploiting other detection mechanisms, for example targeting the catalytic site of the enzymes.

Based on this principle, a very interesting example of protease sensor was proposed by Wang and colleagues in 2021 for detection of Covid-19 by targeting its main protease. In this case the assay is based on the covalent binding of the catalytic cysteine of the enzyme -a papain-like cysteine protease- to the Michael-acceptor portion of a substrate peptide capable of targeting its catalytic site. The transduction and signal amplification systems are quite innovative and are based on dityrosine-crosslinking between nonspecific interfering proteins in the sample, reaction that can be triggered by the presence at the end of the peptide of a complexed Ruthenium ion, which acts as photocatalyst for such reaction. The dityrosine reaction leads to formation of a hydrogel with a distinct fluorescence signal: the reaction can take place in any circumstance, but only in the presence of the target SARS-Cov-2 protease the hydrogel is anchored to the peptide (which does not contain tyrosine residues), immobilized on a fiber optic, and this allows washing treatments to remove nonspecific interferents (Figure 1.19). [118]

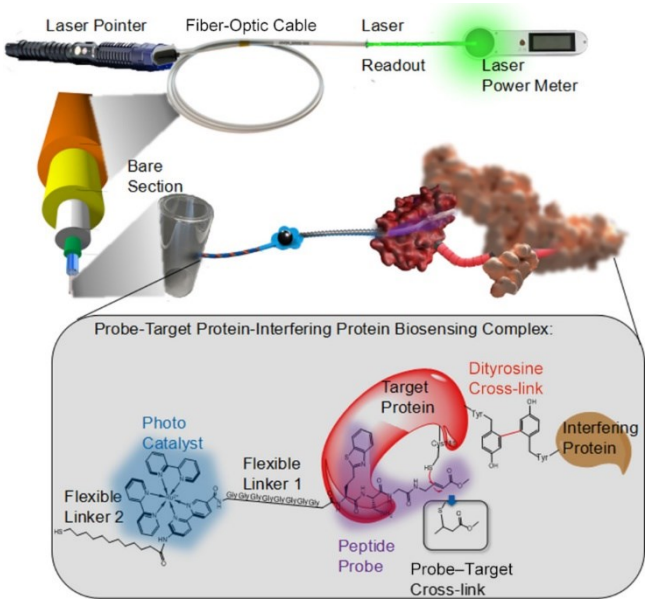

Figure 1.19- Scheme of detection for SARS-Cov-2.[118]

1.4.4.2 Antibodies

Another class of macromolecules that can be targeted by peptides are antibodies. For example, Puiu and coworkers realized an interesting electrochemical peptide-based sensor for the detection of anti-deamidated gliadin peptide (DGP) monoclonal antibodies, diagnostic of celiac disease. The approach is based on the immobilization on the surface of a gold electrode of a short helical support peptide (SP). The SP peptide, having the sequence α-lipoic acid-YAAAHAEAR-NH_2, can fold in a regular α-or 3_{10}-helical structure which can significantly increase the electron transfer rate of the Methylene Blue (MB) electrochemical tag coupled to it. The SP peptide is also coupled with the recognition peptide, the alpha-2 deamidated gliadin peptide (DGP), a 33-mer peptide containing the 56–88 residues of alpha gliadin from gluten. The binding of the target anti-DGP IgG monoclonal antibody to the recognition peptide reduces the efficiency of electrons transfer through the SP to the gold surface, thus causing a signal decrease, allowing antibody detection in the nanomolar range.[119]

1.4.4.3 Antimicrobial peptides

Antimicrobial peptides (AMPs) are natural compounds isolated from a wide variety of organisms including microorganisms, insects, amphibians, plants, and humans. In general, AMPs are mainly cationic small peptide sequences composed of 10–50 amino acid residues, with molecular masses ranging from 1 to 5 kDa. Due to their capability of selectively interacting with cell membrane components of a wide range of pathogenic agents possessing a lipoprotein envelope -including bacteria, fungi, toxins, and viruses-, AMPs can be exploited to target such pathogens for sensing purposes. The main factors influencing the thermodynamics of the recognition event between AMPs and target pathogen are lipid membrane composition and peptide properties such as hydrophobicity, amphipathicity and molecular charge, since the selective binding is mainly based on non-covalent interactions such as hydrogen bonds, hydrophobic and electrostatic interactions.[120]

In 2017 Quiao and colleagues developed an AMP-based colorimetric bioassay for rapid and sensitive detection of *E. coli O157:H7*. The AMP magainin I was conjugated with horseradish peroxidase (AMP-HRP) via biotin-streptavidin conjugation, to develop a signal reporter. AMP–HRP could anchor on the surface of target bacteria rapidly through electrostatic and hydrophobic interactions. After removal of unbound probes by filtration, HRP catalyzed 3,3',5,5' tetramethylbenzidine (TMB) transformation to a colored derivative, whose absorbance was measured by UV-vis spectroscopy to quantify *E. coli O157:H7*. Due to the abundant

AMP-binding sites on the surface of target bacteria, the bioassay could detect the target at a very low concentration and it was also applied for its sensitive and selective detection in food samples previously treated by an immunomagnetic capture-release procedure to selectively extract pathogens from the real matrix (Figure 1.20).[121]

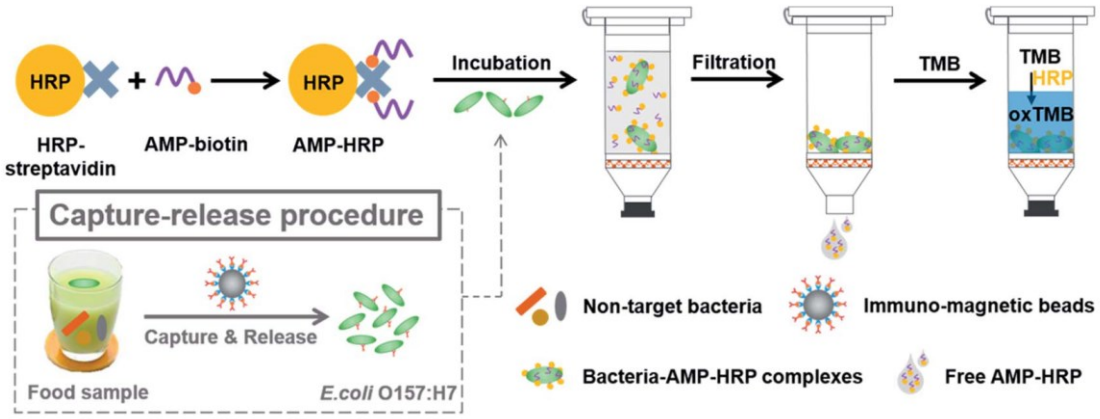

Figure 1.20- Illustration of the AMP-based colorimetric assay for the detection of E. coli O157:H7.[121]

Changing to a different transduction mechanism**,** Li and coworkers developed two electrogenerated chemiluminescence (ECL) biosensors for selective and sensitive detection of *E. coli* O157:H7, working in a direct and sandwich format (Figure 1.21). Both assays were based on the AMP magainin I and the ruthenium complex Ru1 as the ECL probe. In a direct format, the biosensor (I) was fabricated by self-assembling a Ru1-labeled magainin peptide directly onto the gold electrode surface: in this case, binding of target pathogen resulted in a decreased ECL signal. In the sandwich format, the biosensor (II), Magainin I was immobilized onto the gold electrode surface and, only after incubation with target pathogen, the system was incubated with the Ru1-labeled magainin I peptide as the signal probe, leading in this case to ECL signal increase.[122]

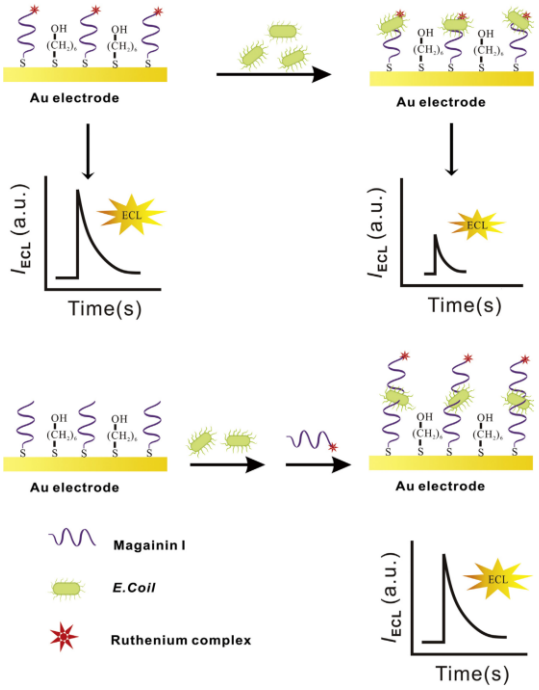

Figure 1.21- Schematic diagram of ECL determination of E. coli O157:H7 in direct and sandwich-type assay.[122]

1.4.5 Peptide nucleic acids (PNAs)

Considering nucleic acid sensing, apart from nucleic acid based probes, a very convenient strategy is that of using a particular type of peptide-like material, peptide nucleic acids (PNAs), firstly reported by Nielsen and colleagues in 1991, which are DNA/RNA analogues with a neutral peptide backbone modified with nucleobases instead of negatively charged sugar-phosphate units.[123] Due to the structure similarity of PNA with DNA, it is able to bind to its complementary nucleic acid sequence obeying the Watson–Crick base-pairing rules. PNA has an achiral backbone containing repeated units of *N*-(2-aminoethyl)-glycine linked by peptide bonds: each of the four bases adenine, cytosine, guanine and thymine is attached to the backbone by methylenecarbonyl linkages (Figure 1.22). PNA has an amine-terminus (or *N*-terminus) and a carboxy terminus (or *C*-terminus), corresponding to the 5'- and 3'-ends of DNA oligonucleotides, respectively.[124] PNA has several differences over DNA, that make it a very appealing tool in many applications: (1) PNA oligomers can be easily synthesized using peptide chemistry tools, in particular solid phase peptide synthesis; (2) the *C*- and *N*-terminals, as well as lateral chains that might be present in the backbone, offer convenient sites for covalent modification; (3) since PNA is achiral, all enantiomeric purity problems are avoided; (4) unlike DNA backbone which is negatively charged, PNA peptide backbone is neutral, and the lack of electrostatic repulsion upon hybridization with another PNA or DNA oligomer can partially account for the higher thermal stability of PNA-PNA duplexes with respect to DNA-PNA and DNA-DNA duplexes; 5) PNAs and chemically resistant to strong acids and weak bases and, since they are not susceptible to nucleases and peptidases degradation, they are highly stable in biological environment. All these properties make PNAs very appealing candidates for many applications, especially as molecular probes for diagnostics and detection, in which their high sensitivity even to single mismatches in duplex formation, makes them ideal candidates for replacing DNA in the detection of target nucleic acids sequences.[125]

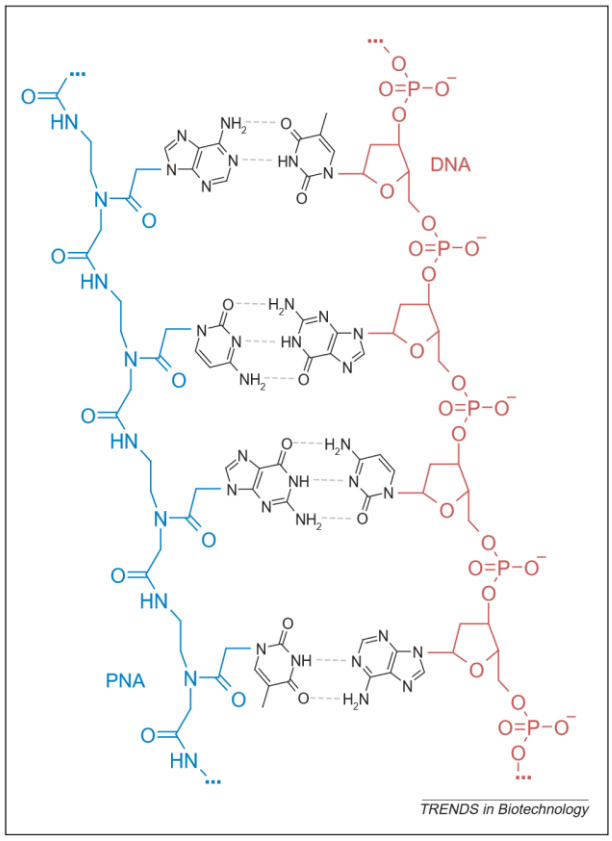

Figure 1.22- Comparison of the structures of PNA (in blue) and DNA (in red), forming a double strand by base pairing (nucleobases are in black).[126]

To cite an interesting example, in 2020 Fu and colleagues developed a sophisticated electrochemical method for simultaneous detection of miRNA21 and miRNA155, overexpressed in cancer cells, using a PNAs-modified gold electrode coupled with the target-catalyzed hairpin assembly (CHA) strategy. Four hairpin probes (H1-H2 and H3-H4, two by two complementary), two of which containing electroactive labels (ferrocene (Fc)-H2 and methylene blue (MB)-H4) were designed for the CHA reaction. Target miRNAs were first incubated with H1, Fc-H2, H3 and MB-H4 probes, and then the resulting products containing CHA21 and CHA155 were selectively captured by PNA21 and PNA155 for signal amplification on the surface of a gold electrode, thus bringing the Fc and MB labels into close proximity to generate apparently enhanced electrochemical signals for sensitive, selective and simultaneous detecting of low amount miRNA21 and miRNA155 in cancer cells at fM levels (Figure 1.23).[127]

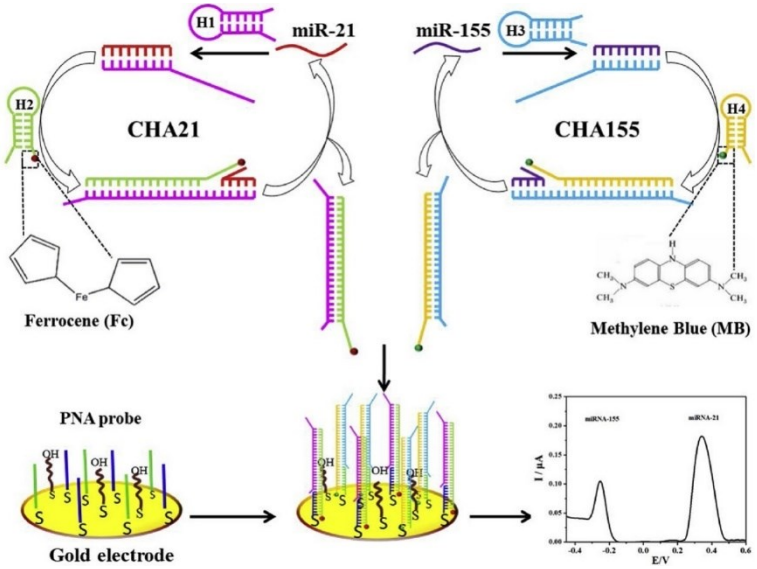

Figure 1.23- Schematic illustration of electrochemical and simultaneous detection of miRNA21 and miRNA155 by coupling the E-PNA biosensor with target-triggered CHA amplifications.[127]

1.5 BIBLIOGRAPHY

(1) Davis, A. P.; Chadburn, H.; Moat, J.; O'Sullivan, R.; Hargreaves, S.; Nic Lughadha, E. High extinction risk for wild coffee species and implications for coffee sector sustainability. *Sci. Adv.*, **2019**, 5(1), eaav3473.

(2) Li, Z.; Zhang, C.; Zhang, Y.; Zeng, W.; Cesarino, I. Coffee Cell Walls—Composition, Influence on Cup Quality and Opportunities for Coffee Improvements. *Food Quality and Safety,* **2021**, 5, 1-21, fyab012.

(3) International Coffee Organization (ICO) (2020) Coffee Production by Exporting Countries. https://Ico.Org/Prices/Po-Production.Pdf. Accessed 30 Apr 2023.

(4) de Melo Pereira, G. V.; de Carvalho Neto, D. P.; Magalhães Júnior, A. I.; Vásquez, Z. S.; Medeiros, A. B. P.; Vandenberghe, L. P. S.; Soccol, C. R. Exploring the Impacts of Postharvest Processing on the Aroma Formation of Coffee Beans – A Review. *Food Chem.,* **2019**, 272, 441–452.

(5) Grüter, R.; Trachsel, T.; Laube, P.; Jaisli, I. Expected Global Suitability of Coffee, Cashew and Avocado Due to Climate Change. *PLoS ONE,* **2022**, 17 (1), e0261976.

(6) Vieira, H. D. Coffee: The Plant and Its Cultivation. In: Souza, R. M. (eds) Plant-Parasitic Nematodes of Coffee, Springer, Netherlands: Dordrecht, **2008**, 3–18.

(7) Vetrano, A. Dalle politiche di Maria Teresa d'Austria ai capolavori di grandi letterati: la storia del caffè a Trieste. Trieste Prima, https://www.triesteprima.it/social/storia-caffe-trieste.html.

(8) De Castro, R. D.; Marraccini, P. Cytology, Biochemistry and Molecular Changes during Coffee Fruit Development. *Braz. J. Plant Physiol*. **2006**, 18 (1), 175–199.

(9) "Coffee Flowers in Spring, Puerto Rico" by USFWS/Southeast Is Licensed under CC BY 2.0.

(10) "Coffee Tree" by Yeahbouyee Is Licensed under CC BY 2.0.

(11) Mussatto, S. I.; Machado, E. M. S.; Martins, S.; Teixeira, J. A. Production, Composition, and Application of Coffee and Its Industrial Residues. *Food Bioprocess Tech.,* **2011**, 4 (5), 661–672.

(12) Cardoso, W. S.; Dias, S. R.; Coelho, V. S.; Pereira, L. L.; Fioresi, D. B.; Pinheiro, F. de A. Maillard Reaction Precursors and Arabica Coffee (*Coffea Arabica L.*) Beverage Quality. *Food and Humanity,* **2023**, 1, 1–7.

(13) Fadai, N. T.; Melrose, J.; Please, C. P.; Schulman, A.; Van Gorder, R. A. A Heat and Mass Transfer Study of Coffee Bean Roasting. *Int. J. Heat Mass Tran.,* **2017**, 104, 787–799.

(14) Niseteo, T.; Komes, D.; Belščak-Cvitanović, A.; Horžić, D.; Budeč, M. Bioactive Composition and Antioxidant Potential of Different Commonly Consumed Coffee Brews Affected by Their Preparation Technique and Milk Addition. *Food Chem.,* **2012**, 134 (4), 1870–1877.

(15) Illy Website, https://Www.Illy.Com/En-Us/Coffee/Coffee-Preparation.

(16) "turkish Coffee and Tiramisu" by Blhphotography Is Licensed under CC BY 2.0.

(17) "moka Coffee" by Penguincakes Is Licensed under CC BY-NC-SA 2.0.

(18) "French Press Coffee" by Fritish Is Licensed under CC BY-NC-SA 2.0.

(19) Belitz, H.D.; Grosch, W.; Schieberle, P. Coffee, Tea, Cocoa. In Food Chemistry, Springer, Berlin, Heidelberg, **2009**, 938-970.

(20) Gutiérrez Ortiz, A. L.; Berti, F.; Navarini, L.; Crisafulli, P.; Colomban, S.; Forzato, C. Aqueous Extracts of Walnut (*Juglans Regia L*.) Leaves: Quantitative Analyses of Hydroxycinnamic and Chlorogenic Acids. *J. Chromatogr. Sci.,* **2018**, 56 (8), 753–760.

(21) Gutiérrez Ortiz, A. L.; Berti, F.; Solano Sánchez, W.; Navarini, L.; Colomban, S.; Crisafulli, P.; Forzato, C. Distribution of *p*-Coumaroylquinic Acids in Commercial Coffea Spp. of Different Geographical Origin and in Other Wild Coffee Species. *Food Chem.,* **2019**, 286, 459–466.

(22) Gutiérrez Ortiz, A. L.; Berti, F.; Navarini, L.; Monteiro, A.; Resmini, M.; Forzato, C. Synthesis of *p* -Coumaroylquinic Acids and Analysis of Their Interconversion. *Tetrahedron: Asymmetr.,* **2017**, 28 (3), 419–427.

(23) Sinisi, V.; Boronová, K.; Colomban, S.; Navarini, L.; Berti, F.; Forzato, C. Synthesis of Mono-, Di-, and Tri-3,4-Dimethoxycinnamoyl-1,5-γ-Quinides: Synthesis of Mono-, Di-, and Tri-3,4-Dimethoxycinnamoyl-1,5-γ-Quinides. *Eur. J. Org. Chem*., **2014**, 2014 (6), 1321–1326.

(24) Socała, K.; Szopa, A.; Serefko, A.; Poleszak, E.; Wlaź, P. Neuroprotective Effects of Coffee Bioactive Compounds: A Review. *Int. J. Mol. Sci.,* **2021**, 22 (1), 107.

(25) de Melo Pereira, G. V.; de Carvalho Neto, D. P.; Magalhães Júnior, A. I.; do Prado, F. G.; Pagnoncelli, M. G. B.; Karp, S. G.; Soccol, C. R. Chemical Composition and Health Properties of Coffee and Coffee By-Products. In Advances in Food and Nutrition Research; Elsevier, **2020**, 91, 65–96.

(26) O'Keefe, J. H.; Bhatti, S. K.; Patil, H. R.; DiNicolantonio, J. J.; Lucan, S. C.; Lavie, C. J. Effects of Habitual Coffee Consumption on Cardiometabolic Disease, Cardiovascular Health, and All-Cause Mortality. *J. Am. Coll. Cardiol.,* **2013**, 62 (12), 1043–1051.

(27) Tajik, N.; Tajik, M.; Mack, I.; Enck, P. The Potential Effects of Chlorogenic Acid, the Main Phenolic Components in Coffee, on Health: A Comprehensive Review of the Literature. *Eur. J. Nutr.,* **2017**, 56 (7), 2215–2244.

(28) Sinisi, V.; Stevaert, A.; Berti, F.; Forzato, C.; Benedetti, F.; Navarini, L.; Camps, A.; Persoons, L.; Vermeire, K. Chlorogenic Compounds from Coffee Beans Exert Activity against Respiratory Viruses. *Planta Med.,* **2017**, 83 (07), 615–623.

(29) Nawrot, P.; Jordan, S.; Eastwood, J.; Rotstein, J.; Hugenholtz, A.; Feeley, M. Effects of Caffeine on Human Health. *Food Addit. Contam.,* **2003**, 20 (1), 1–30.

(30) James, J. E. Maternal Caffeine Consumption and Pregnancy Outcomes: A Narrative Review with Implications for Advice to Mothers and Mothers-to-Be. *BMJ Evid. Based Med.,* **2021**, 26 (3), 114–115.

(31) van Dam, R. M.; Hu, F. B.; Willett, W. C. Coffee, Caffeine, and Health. *N. Engl. J. Med.,* **2020**, 383 (4), 369–378.

(32) McLellan, T. M.; Caldwell, J. A.; Lieberman, H. R. A Review of Caffeine's Effects on Cognitive, Physical and Occupational Performance. *Neurosci. Biobehav. R.,* **2016**, 71, 294–312.

(33) Svatun, Å. L.; Løchen, M.-L.; Thelle, D. S.; Wilsgaard, T. Association between Espresso Coffee and Serum Total Cholesterol: The Tromsø Study 2015–2016. *Open Heart,* **2022**, 9 (1), e001946.

(34) Mancini, R. S.; Wang, Y.; Weaver, D. F. Phenylindanes in Brewed Coffee Inhibit Amyloid-Beta and Tau Aggregation. *Front. Neurosci*.-Switz., **2018**, 12, 735.

(35) Moreira, A. S. P.; Nunes, F. M.; Domingues, M. R.; Coimbra, M. A. Coffee Melanoidins: Structures, Mechanisms of Formation and Potential Health Impacts. *Food Funct*., **2012**, 3 (9), 903.

(36) Wani, T. A.; Masoodi, F. A.; Gani, A.; Baba, W. N.; Rahmanian, N.; Akhter, R.; Wani, I. A.; Ahmad, M. Olive Oil and Its Principal Bioactive Compound: Hydroxytyrosol – A Review of the Recent Literature. *Trends Food Sci. Technol.,* **2018**, 77, 77–90.

(37) International Olive Council (IOC) https://www.Internationaloliveoil.Org/the-World-of-Olive-Oil/ Accessed 28 Apr 2023.

(38) Ghanbari, R.; Anwar, F.; Alkharfy, K. M.; Gilani, A.-H.; Saari, N. Valuable Nutrients and Functional Bioactives in Different Parts of Olive (*Olea Europaea L.*)—A Review. *Int. J. Mol. Sci.,* **2012**, 13 (3), 3291–3340.

(39) Starec, M.; Calabretti, A.; Berti, F.; Forzato, C. Oleocanthal Quantification Using ^{1}H NMR Spectroscopy and Polyphenols HPLC Analysis of Olive Oil from the Bianchera/Belica Cultivar. *Molecules,* **2021**, 26 (1), 242.

(40) Parovel Website, https://Www.Parovel.Com/Index.Php/It/Oli-Extravergini/Bianchera-Cultivar-Autoctona.

(41) Vossen, P. Olive Oil: History, Production, and Characteristics of the World's Classic Oils. *Hortscience* **2007**, 42 (5), 1093–1100.

(42) Council of the European Union. Council Regulation (EC) No 1234/2007 of 22 October 2007 Establishing a Common Organisation of Agricultural Markets and on Specific Provisions for Certain Agricultural Products (Single CMO Regulation). *Off. J. Eur. Union,* **2007**, 299, 1–149.

(43) Olio Carli Website, https://Www.Oliocarli.It/Magazine/Conoscere-Olio/Classificazione-Olio.

(44) Frantoio San Martino Website, https://Www.Frantoiosanmartino.Com/Fasi-Produzione-Olio/.

(45) Leone, A. Olive Milling and Pitting. In The Extra-Virgin Olive Oil Handbook; Peri, C., Ed.; John Wiley & Sons, Ltd: Chichester, UK, **2014**; 117–126.

(46) Tamborrino, A. Olive Paste Malaxation. In The Extra-Virgin Olive Oil Handbook; Peri, C., Ed.; John Wiley & Sons, Ltd: Chichester, UK, 2014; 127–137.

(47) Baccioni, L.; Peri, C. Centrifugal Separation. In The Extra-Virgin Olive Oil Handbook; Peri, C., Ed.; John Wiley & Sons, Ltd: Chichester, UK, 2014; 139–154.

(48) Olio Cristofaro Website, https://Oliocristofaro.It/Olivo-Olio-Evo-Ecco-Come-Avviene-Estrazione/.

(49) Peri, C. Filtration of Extra-Virgin Olive Oil. In The Extra-Virgin Olive Oil Handbook; Peri, C., Ed.; John Wiley & Sons, Ltd: Chichester, UK, 2014; 155–164.

(50) Jimenez-Lopez, C.; Carpena, M.; Lourenço-Lopes, C.; Gallardo-Gomez, M.; Lorenzo, J. M.; Barba, F. J.; Prieto, M. A.; Simal-Gandara, J. Bioactive Compounds and Quality of Extra Virgin Olive Oil. *Foods,* **2020**, 9 (8), 1014.

(51) Boskou, D. Olive Fruit, Table Olives, and Olive Oil Bioactive Constituents. In Olive and Olive Oil Bioactive Constituents; Elsevier, **2015**; 1–30.

(52) Bulotta, S.; Oliverio, M.; Russo, D.; Procopio, A. Biological Activity of Oleuropein and Its Derivatives. In Natural Products; Ramawat, K. G., Mérillon, J.-M., Eds.; Springer Berlin Heidelberg, **2013**; 3605–3638.

(53) Soler-Rivas, C.; Espín, J. C.; Wichers, H. J. Oleuropein and related compounds. *J. Sci. Food Agr.*, **2000**, 80(7), 1013-1023.

(54) Bellumori, M.; Cecchi, L.; Innocenti, M.; Clodoveo, M. L.; Corbo, F.; Mulinacci, N. The EFSA Health Claim on Olive Oil Polyphenols: Acid Hydrolysis Validation and Total Hydroxytyrosol and Tyrosol Determination in Italian Virgin Olive Oils. *Molecules,* **2019**, 24 (11), 2179.

(55) Obied, H. K.; Prenzler, P. D.; Ryan, D.; Servili, M.; Taticchi, A.; Esposto, S.; Robards, K. Biosynthesis and Biotransformations of Phenol-Conjugated Oleosidic Secoiridoids from *Olea Europaea L*. *Nat. Prod. Rep.,* **2008**, 25 (6), 1167-1179.

(56) Diamantakos, P.; Giannara, T.; Skarkou, M.; Melliou, E.; Magiatis, P. Influence of Harvest Time and Malaxation Conditions on the Concentration of Individual Phenols in Extra Virgin Olive Oil Related to Its Healthy Properties. *Molecules,* **2020**, 25 (10), 2449.

(57) Romani, A.; Ieri, F.; Urciuoli, S.; Noce, A.; Marrone, G.; Nediani, C.; Bernini, R. Health Effects of Phenolic Compounds Found in Extra-Virgin Olive Oil, By-Products, and Leaf of *Olea Europaea L*. *Nutrients,* **2019**, 11 (8), 1776.

(58) Commission Regulation (EU) No 432/2012 of 16 May 2012 Establishing a List of Permitted Health Claims Made on Foods, Other than Those Referring to the Reduction of Disease Risk and to Children's Development and HealthText with EEA Relevance.

(59) Omar, S.H. Oleuropein in Olive and Its Pharmacological Effects. *Sci. Pharm.,* **2010**, 78 (2), 133–154.

(60) Thevenot, D. R.; Toth, K.; Durst, R. A.; Wilson, G. S. Electrochemical Biosensors: Recommended Definitions and Classification*. Biosens. Bioeletron.*, **2001**, 16 (1-2), 121-131.

(61) Chadha, U.; Bhardwaj, P.; Agarwal, R.; Rawat, P.; Agarwal, R.; Gupta, I.; Panjwani, M.; Singh, S.; Ahuja, C.; Selvaraj, S. K.; Banavoth, M.; Sonar, P.; Badoni, B.; Chakravorty, A. Recent Progress and Growth in Biosensors Technology: A Critical Review*. J. Ind. Eng. Chem.,* **2022**, 109, 21–51.

(62) Perumal, V.; Hashim, U. Advances in Biosensors: Principle, Architecture and Applications. *J. Appl. Biomed.,* **2014**, 12 (1), 1–15.

(63) Wu, Q.; Zhang, Y.; Yang, Q.; Yuan, N.; Zhang, W. Review of Electrochemical DNA Biosensors for Detecting Food Borne Pathogens. *Sensors,* **2019**, 19 (22), 4916.

(64) Grieshaber, D.; MacKenzie, R.; Vörös, J.; Reimhult, E. Electrochemical Biosensors - Sensor Principles and Architectures, *Sensors*, **2008**, 8(3), 1400-1458.

(65) Wang, J. Glucose Biosensors: 40 Years of Advances and Challenges. *Electroanal.,* **2001**, 13 (12), 983–988.

(66) Asal, M.; Özen, Ö.; Şahinler, M.; Polatoğlu, İ. Recent Developments in Enzyme, DNA and Immuno-Based Biosensors. *Sensors,* **2018**, 18 (6), 1924.

(67) Choi, M. M. F. Progress in Enzyme-Based Biosensors Using Optical Transducers. *Microchim. Acta,* **2004**, 148 (3–4), 107–132.

(68) Borisov, S. M.; Wolfbeis, O. S. Optical Biosensors. *Chem. Rev.,* **2008**, 108 (2), 423–461.

(69) Gui, Q.; Lawson, T.; Shan, S.; Yan, L.; Liu, Y. The Application of Whole Cell-Based Biosensors for Use in Environmental Analysis and in Medical Diagnostics. *Sensors,* **2017**, 17 (7), 1623.

(70) Justino, C. I. L.; Freitas, A. C.; Pereira, R.; Duarte, A. C.; Rocha Santos, T. A. P. Recent Developments in Recognition Elements for Chemical Sensors and Biosensors. *Trends Analyt. Chem.,* **2015**, 68, 2–17.

(71) Peltomaa, R.; Benito-Peña, E.; Moreno-Bondi, M. C. Bioinspired Recognition Elements for Mycotoxin Sensors. *Anal. Bioanal. Chem.,* **2018**, 410 (3), 747–771.

(72) Du, Y.; Dong, S. Nucleic Acid Biosensors: Recent Advances and Perspectives*. Anal. Chem.,* **2017**, 89 (1), 189–215.

(73) Tyagi, S.; Kramer, F. R. Molecular beacons: probes that fluoresce upon hybridization. *Nat. biotechnol.*, **1996**, 14(3), 303-308.

(74) Sefah, K.; Phillips, J. A.; Xiong, X.; Meng, L.; Van Simaeys, D.; Chen, H.; Martin, J.; Tan, W. Nucleic Acid Aptamers for Biosensors and Bio-Analytical Applications. *Analyst,* **2009**, 134 (9), 1765-1777.

(75) Khan, S.; Burciu, B.; Filipe, C. D. M.; Li, Y.; Dellinger, K.; Didar, T. F. DNAzyme-Based Biosensors: Immobilization Strategies, Applications, and Future Prospective. *ACS Nano,* **2021**, 15 (9), 13943–13969.

(76) Cieplak, M.; Kutner, W. Artificial Biosensors: How Can Molecular Imprinting Mimic Biorecognition? *Trends Biotechnol.,* **2016**, 34 (11), 922–941.

(77) Gui, R.; Jin, H.; Guo, H.; Wang, Z. Recent Advances and Future Prospects in Molecularly Imprinted Polymers-Based Electrochemical Biosensors. *Biosens. Bioelectron.,* **2018**, 100, 56–70.

(78) Sun, S.-W.; Lin, Y.-C.; Weng, Y.-M.; Chen, M.-J. Efficiency Improvements on Ninhydrin Method for Amino Acid Quantification. *J. Food Compos. Anal.*, **2006**, 19 (2–3), 112–117.

(79) Friedman, M. Applications of the Ninhydrin Reaction for Analysis of Amino Acids, Peptides, and Proteins to Agricultural and Biomedical Sciences. *J. Agric. Food Chem*., **2004**, 52 (3), 385–406.

(80) Stockert, J. C.; Horobin, R. W.; Colombo, L. L.; Blázquez-Castro, A. Tetrazolium Salts and Formazan Products in Cell Biology: Viability Assessment, Fluorescence Imaging, and Labeling Perspectives. *Acta Histochem*., **2018**, 120 (3), 159–167.

(81) Morciano, G.; Sarti, A. C.; Marchi, S.; Missiroli, S.; Falzoni, S.; Raffaghello, L.; Pistoia, V.; Giorgi, C.; Di Virgilio, F.; Pinton, P. Use of Luciferase Probes to Measure ATP in Living Cells and Animals. *Nat. Protoc.*, **2017**, 12 (8), 1542–1562.

(82) Mohr, G. J. New Chromogenic and Fluorogenic Reagents and Sensors for Neutral and Ionic Analytes Based on Covalent Bond Formation–a Review of Recent Developments. *Anal. Bioanal. Chem.,* **2006**, 386 (5), 1201–1214.

(83) Mohr, G. J. Covalent Bond Formation as an Analytical Tool to Optically Detect Neutral and Anionic Analytes. *Sensor Actuat. B-Chem.,* **2005**, 107 (1), 2–13.

(84) Mohr, G. J.; Citterio, D.; Demuth, C.; Fehlmann, M.; Jenny, L.; Lohse, C.; Moradian, A.; Nezel, T.; Rothmaier, M.; Spichiger, U. E. Reversible Chemical Reactions as the Basis for Optical Sensors Used to Detect Amines, Alcohols and Humidity. *J. Mater. Chem*., **1999**, 9 (9), 2259–2264.

(85) Darder, M. del M.; Bedoya, M.; Serrano, L. A.; Alba, M. Á.; Orellana, G. Fiberoptic Colorimetric Sensor for in Situ Measurements of Airborne Formaldehyde in Workplace Environments. *Sensor Actuat. B-Chem.*, **2022**, 353, 131099.

(86) Gojon, C.; Dureault, B.; Hovnanian, N.; Guizard, C. A Comparison of Immobilization Sol-Gel Methods for an Optical Chemical Hydrazine Sensor. *Sensor Actuat. B-Chem.*, **1997**, 38 (1–3), 154–162.

(87) Rico-Yuste, A.; González-Vallejo, V.; Benito-Peña, E.; de las Casas Engel, T.; Orellana, G.; Moreno-Bondi, M. C. Furfural Determination with Disposable Polymer Films and Smartphone-Based Colorimetry for Beer Freshness Assessment. *Anal. Chem.,* **2016**, 88 (7), 3959–3966.

(88) Langhals, H.; Jona, W. The Identification of Carbonyl Compounds by Fluorescence: A Novel Carbonyl-Derivatizing Reagent. *Chem. Eur. J*., **1998**, 4 (11), 2110–2116.

(89) Hampe, E. M.; Rudkevich, D. M. Reversible Covalent Chemistry of CO_2. *Chem. Commun*., **2002**, 14, 1450–1451.

(90) Prasanna de Silva, A.; Nimal Gunaratne, H. Q.; Gunnlaugsson, T. Fluorescent PET (Photoinduced Electron Transfer) Reagents for Thiols. *Tetrahedron Lett.*, **1998**, 39 (28), 5077–5080.

(91) Du, J.; Hu, M.; Fan, J.; Peng, X. Fluorescent Chemodosimeters Using "Mild" Chemical Events for the Detection of Small Anions and Cations in Biological and Environmental Media. *Chem. Soc. Rev.,* **2012**, 41 (12), 4511-4535.

(92) Kaur, K.; Saini, R.; Kumar, A.; Luxami, V.; Kaur, N.; Singh, P.; Kumar, S. Chemodosimeters: An Approach for Detection and Estimation of Biologically and Medically Relevant Metal Ions, Anions and Thiols. *Coordin. Chem. Rev.*, **2012**, 256 (17–18), 1992–2028.

(93) Ros-Lis, J. V.; Marcos, M. D.; Mártinez-Máñez, R.; Rurack, K.; Soto, J. A Regenerative Chemodosimeter Based on Metal-Induced Dye Formation for the Highly Selective and Sensitive Optical Determination of Hg^{2+} Ions. *Angew. Chem. Int. Ed*., **2005**, 44 (28), 4405–4407.

(94) Romieu, A. "AND" Luminescent "Reactive" Molecular Logic Gates: A Gateway to Multi-Analyte Bioimaging and Biosensing. *Org. Biomol. Chem*., **2015**, 13 (5), 1294–1306.

(95) Hettie, K. S.; Klockow, J. L.; Glass, T. E. Three-Input Logic Gates with Potential Applications for Neuronal Imaging. *J. Am. Chem. Soc*., **2014**, 136 (13), 4877–4880.

(96) Pavan, S.; Berti, F. Short Peptides as Biosensor Transducers. *Anal. Bioanal. Chem.,* **2012**, 402 (10), 3055–3070.

(97) Pazos, E.; Vázquez, O.; Mascareñas, J. L.; Vázquez, M.E. Peptide-Based Fluorescent Biosensors. *Chem. Soc. Rev.,* **2009**, 38 (12), 3348-3359.

(98) Gooding, J.J.; Hibbert, D.B; Yang, W. Electrochemical Metal Ion Sensors. Exploiting Amino Acids and Peptides as Recognition Elements. *Sensors,* **2001**, 1 (3), 75–90.

(99) Bi, X.; Agarwal, A.; Balasubramanian, N.; Yang, K.-L. Tripeptide-Modified Silicon Nanowire Based Field-Effect Transistors as Real-Time Copper Ion Sensors. *Electrochem. Commun.,* **2008**, 10 (12), 1868–1871.

(100) Lin, M.; Cho, M.; Choe, W.-S.; Yoo, J.-B.; Lee, Y. Polypyrrole Nanowire Modified with Gly-Gly-His Tripeptide for Electrochemical Detection of Copper Ion. *Biosens. Bioelectron.*, **2010**, 26 (2), 940–945.

(101) Xu, Y.-M.; Pan, H.-Q.; Wu, S.-H.; Zhang, B.-L. Interaction Between Tripeptide Gly-Gly-His and Cu2+ Probed by Microcantilevers. *Chinese J. Anal. Chem.*, **2009**, 37 (6), 783–787.

(102) Godwin, H. A.; Berg, J. M. A Fluorescent Zinc Probe Based on Metal-Induced Peptide Folding. *J. Am. Chem. Soc.,* **1996**, 118 (27), 6514–6515.

(103) Walkup, G. K.; Imperiali, B. Stereoselective synthesis of fluorescent α-amino acids containing oxine (8-hydroxyquinoline) and their peptide incorporation in chemosensors for divalent zinc. *J. Org. Chem*., **1998**, 63(19), 6727-6731.

(104) Peltomaa, R.; Benito-Peña, E.; Barderas, R.; Moreno-Bondi, M. C. Phage Display in the Quest for New Selective Recognition Elements for Biosensors. *ACS Omega,* **2019**, 4 (7), 11569–11580.

(105) Justino, C. I. L.; Duarte, A. C.; Rocha-Santos, T. A. P. Analytical Applications of Affibodies. *Trends Analyt. Chem.,* **2015**, 65, 73–82.

(106) Peltomaa, R.; Amaro-Torres, F.; Carrasco, S.; Orellana, G.; Benito-Peña, E.; Moreno-Bondi, M. C. Homogeneous Quenching Immunoassay for Fumonisin B 1 Based on Gold Nanoparticles and an Epitope-Mimicking Yellow Fluorescent Protein. *ACS Nano,* **2018**, 12 (11), 11333–11342.

(107) Gladich, I.; Rodriguez, A.; Hong Enriquez, R. P.; Guida, F.; Berti, F.; Laio, A. Designing High-Affinity Peptides for Organic Molecules by Explicit Solvent Molecular Dynamics. *J. Phys. Chem. B,* **2015**, 119 (41), 12963–12969.

(108) Guida, F.; Battisti, A.; Gladich, I.; Buzzo, M.; Marangon, E.; Giodini, L.; Toffoli, G.; Laio, A.; Berti, F. Peptide Biosensors for Anticancer Drugs: Design in Silico to Work in Denaturizing Environment. *Biosens. Bioelectron.* **2018**, 100, 298–303.

(109) Del Carlo, M.; Capoferri, D.; Gladich, I.; Guida, F.; Forzato, C.; Navarini, L.; Compagnone, D.; Laio, A.; Berti, F. In Silico Design of Short Peptides as Sensing Elements for Phenolic Compounds. *ACS Sens*., **2016**, 1 (3), 279–286.

(110) Sharma, V.; Wang, Q.; Lawrence, D. S. Peptide-Based Fluorescent Sensors of Protein Kinase Activity: Design and Applications. *BBA-Proteins Proteom.,* **2008**, 1784 (1), 94–99.

(111) Wang, Q.; Lawrence, D. S. Phosphorylation-Driven Protein−Protein Interactions: A Protein Kinase Sensing System. *J. Am. Chem. Soc*., **2005**, 127 (21), 7684–7685.

(112) Sharma, V.; Agnes, R. S.; Lawrence, D. S. Deep Quench: An Expanded Dynamic Range for Protein Kinase Sensors. *J. Am. Chem. Soc*., **2007**, 129 (10), 2742–2743.

(113) Wang, Q.; Cahill, S. M.; Blumenstein, M.; Lawrence, D. S. Self-Reporting Fluorescent Substrates of Protein Tyrosine Kinases. *J. Am. Chem. Soc*., **2006**, 128 (6), 1808–1809.

(114) Pazos, E.; Torrecilla, D.; Vázquez López, M.; Castedo, L.; Mascareñas, J. L.; Vidal, A.; Vázquez, M. E. Cyclin A Probes by Means of Intermolecular Sensitization of Terbium-Chelating Peptides. *J. Am. Chem. Soc*., **2008**, 130 (30), 9652–9653.

(115) Pazos, E.; Pérez, M.; Gutiérrez-de-Terán, H.; Orzáez, M.; Guevara, T.; Mascareñas, J. L.; Vázquez, M. E. Rational Design of a Cyclin A Fluorescent Peptide Sensor. *Org. Biomol. Chem*., **2011**, 9 (22), 7629-7632.

(116) Chen, G.; Song, F.; Xiong, X.; Peng, X. Fluorescent Nanosensors Based on Fluorescence Resonance Energy Transfer (FRET). *Ind. Eng. Chem. Res*., **2013**, 52 (33), 11228–11245.

(117) Meng, F.; Sun, H.; Huang, Y.; Tang, Y.; Chen, Q.; Miao, P. Peptide Cleavage-Based Electrochemical Biosensor Coupling Graphene Oxide and Silver Nanoparticles. *Anal. Chim. Acta,* **2019**, 1047, 45–51.

(118) Wang, J.; Lv, M.; Xia, H.; Du, J.; Zhao, Y.; Li, H.; Zhang, Z. Minimalist Design for a Hand-Held SARS-Cov-2 Sensor: Peptide-Induced Covalent Assembly of Hydrogel Enabling Facile Fiber-Optic Detection of a Virus Marker Protein. *ACS Sens*., **2021**, 6 (6), 2465–2471.

(119) Puiu, M.; Idili, A.; Moscone, D.; Ricci, F.; Bala, C. A Modular Electrochemical Peptide-Based Sensor for Antibody Detection. *Chem. Commun*., **2014**, 50 (64), 8962-8965.

(120) Silva, R. R.; Avelino, K. Y. P. S.; Ribeiro, K. L.; Franco, O. L.; Oliveira, M. D. L.; Andrade, C. A. S. Optical and Dielectric Sensors Based on Antimicrobial Peptides for Microorganism Diagnosis. *Front. Microbiol.,* **2014**, 5, 443.

(121) Qiao, Z.; Lei, C.; Fu, Y.; Li, Y. An Antimicrobial Peptide-Based Colorimetric Bioassay for Rapid and Sensitive Detection of *E. Coli* O157:H7. *RSC Adv.,* **2017**, 7 (26), 15769–15775.

(122) Li, Z.; Yang, H.; Sun, L.; Qi, H.; Gao, Q.; Zhang, C. Electrogenerated Chemiluminescence Biosensors for the Detection of Pathogenic Bacteria Using Antimicrobial Peptides as Capture/Signal Probes. *Sensor Actuat. B: Chem.,* **2015**, 210, 468–474.

(123) Nielsen, P. E.; Egholm, M.; Berg, R. H.; Buchardt, O. Sequence-Selective Recognition of DNA by Strand Displacement with a Thymine-Substituted Polyamide. *Science,* **1991**, 254 (5037), 1497–1500.

(124) Singh, R. P.; Oh, B.-K.; Choi, J.-W. Application of Peptide Nucleic Acid towards Development of Nanobiosensor Arrays. *Bioelectrochemistry,* **2010**, 79 (2), 153–161.

(125) Bonifazi, D.; Carloni, L.-E.; Corvaglia, V.; Delforge, A. Peptide Nucleic Acids in Materials Science. *Artif. DNA PNA XNA,* **2012**, 3 (3), 112–122.

(126) Brandt, O.; Hoheisel, J. D. Peptide Nucleic Acids on Microarrays and Other Biosensors. *Trends Biotechnol.,* **2004**, 22 (12), 617–622.

(127) Fu, P.; Xing, S.; Xu, M.; Zhao, Y.; Zhao, C. Peptide Nucleic Acid-Based Electrochemical Biosensor for Simultaneous Detection of Multiple MicroRNAs from Cancer Cells with Catalytic Hairpin Assembly Amplification. *Sensor Actuat. B: Chem.,* **2020**, 305, 127545.

2 AIM OF THE PROJECT

The aim of this PhD project is the development of sensing strategies for targeting bioactive phenolic compounds from olive oil and coffee - chlorogenic acid (CGA) and caffeic acid in coffee, tyrosol and hydroxytyrosol in olive oil- for quality monitoring purposes. The focus is on investigating different covalent recognition strategies to provide complementary selectivity for the targets of interest according to their structural differences, leading to changes in optical signals –absorbance and fluorescence- to monitor the recognition event. Moreover, a second focus is on short peptides, to be used as scaffolds for the reactive and sensing molecules/functional groups. Such natural or biomimetic structures allow in principle to establish further interactions with the targets, besides their covalent capture, and on the other side allow immobilization on many kinds of surfaces on optical devices. For these reasons, the main focus will be exploring potential covalent reactions that could take place on natural or non-natural amino acid side chains, as well as on sensing moieties that can be incorporated into a peptide sequence.

This will be a preliminary, broad-range investigation, aiming at finding new reactions for target molecule recognition rather than at the development of a complete analytical method.

After preliminary studies, three reactions have been selected, and the exploration of their suitability to our aims is reported in this thesis (Scheme 2.1):

1. Formation of green trihydroxybenzacridine (TBA) pigments from reaction of CGA with primary amino groups as the ε-amino group of lysine or those of designed biomimetic reactive materials;
2. Boronic esters formation between *ortho*-diphenols and boronic acids labeled with fluorophores that could be easily linked to a peptide;
3. Diazo coupling reaction between phenols and the non-natural amino acid *p*-amino-phenylalanine, leading to formation of red-colored diazo coupling compounds.

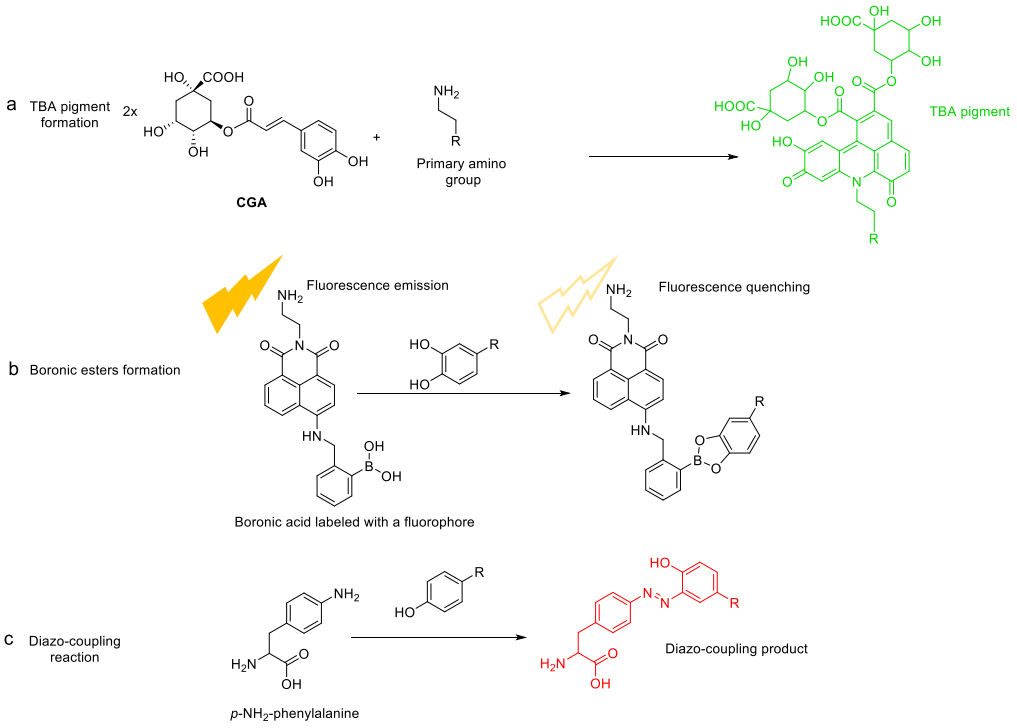

Scheme 2.1- General reaction schemes for the three investigated reactions: TBA-pigment formation (a), boronic esters formation (b) and diazo-coupling reaction (c).

The reason of focusing mainly on covalent reactions for target molecule (TM) binding comes from the idea of adding a mechanism for specific recognition of TMs possessing the required functional groups in addition to non-covalent interactions that might be provided by other types of recognition elements, thus facilitating the differentiation between structurally related molecules. For example, cyclic boronic esters formed upon reaction with *ortho*-diphenols are much more stable with respect to the mono-phenolic counterpart, and this is expected to allow differentiation even between very similar molecules such as hydroxytyrosol -a *ortho*-diphenol- and tyrosol -the related monophenol. Moreover, in the case of the TBA pigment formation and diazo-coupling reaction, it is the covalent reaction itself that leads to formation of green and red compounds respectively, thus providing the transduction mechanism. Whereas, in the case of boronic acids, formation of boronic esters is responsible for the modulation of the fluorophore providing the signal transduction mechanism.

The development of the project will involve:

- Synthesis of the colored pigments in the case of TBA and diazo-coupling reactions, and synthesis of the reactive fluorophore in the case of boronic esters reaction.
- Characterization and evaluation of the spectroscopic properties of the colored/fluorescent compounds.
- Design, synthesis and characterization of several peptides for each approach, incorporating into the peptide the moiety responsible for covalent molecular recognition.
- Design, synthesis and characterization of sensing polymeric films in the case of the TBA pigment.

3 RESULTS AND DISCUSSION - GREEN TRIHYDROXYBENZACRIDINE PIGMENT

3.1 STATE OF THE ART

3.1.1 The discovery of green trihydroxybenzacridine pigments

Since years, it is well documented that chlorogenic acid and, in general, esters of caffeic acid, can react with primary amines leading to the formation of green pigments, called trihydroxybenzacridine (TBA) pigments. Such reaction takes place in conditions favoring the oxidation of the *ortho*-diphenolic portion of caffeic acid, i.e. in basic environment or in the presence of oxidizing enzymes, such as polyphenol oxidases.[1] This reaction has been at first observed in food products containing sunflower kernels, sweet potatoes or fried burdock, causing an unexpected green color formation.[2]

From a practical point of view, this reaction has been documented as an unwanted process in the food industry, taking place for example in sunflower meal (SFM), the secondary product obtained during the extraction of sunflower oil, which is composed by proteins (27% to 62%), fibers, minerals and polyphenols, the most important of which is chlorogenic acid.[3] Sunflower meal is used almost only in animal feed as an important source of non-animal proteins at low cost. Since green pigmentation appears during its processing, which is considered as a negative aspect in the food industry, recent studies are developing some methods to avoid pigment formation and promote a larger use of this material. Such green pigmentation can be observed also by using sunflower seeds butter in the preparation of bakery products containing also baking soda for example (Figure 3.1).[3]

Figure 3.1- Progress in green color formation of cookies containing sunflower seed butter and baking soda.[3]

3.1.2 TBA pigments characterization and isolation

Since their discovery, the isolation and structure elucidation of these pigments has been quite difficult, as well as the understanding of the mechanism of reaction. In fact, even if the greening reaction has been known since a lot of time, the TBA pigments are very difficult to isolate due to their high polymerizing character, and this made very difficult to unveil their structure.[2] A first attempt of isolating the TBA pigment has been done by Matsui in 1981, who performed the reaction between ethyl caffeate and methylamine in order to study the reaction on a slightly simpler system with respect to chlorogenic acid and amino acids.[2] He first performed the reaction by mixing ethyl caffeate and methylamine in Menzel buffer under weakly alkaline conditions in an equimolar ratio. He performed a first purification by size exclusion chromatography using a G10 stationary phase, then separating three main fractions by thin layer chromatography. However, despite the attempt, in this article the author was not able to elucidate the correct structure of the green pigments.[2]

Years later, in 1996, Yabuta and coworkers were the first to isolate a pigment derivative. Also in this case they first tried to isolate the pigment by thin layer chromatography, but due to the reactivity of the pigment that was changing color during analysis, they understood that the key was that of converting it into a stable crystalline form by first acidifying the reaction mixture, then treating it with ascorbic acid to reduce it, finally acetylating the hydroxyl groups. In this way, thanks to NMR spectroscopy and crystallographic measurements that allowed to elucidate the structure of the reduced and acetylated derivative of the pigment (yellow in these conditions), Yabuta and colleagues could finally hypothesize the structure of the green TBA pigment, which is a precursor of the yellow product isolated, probably in an oxidized form (Scheme 3.1).[1]

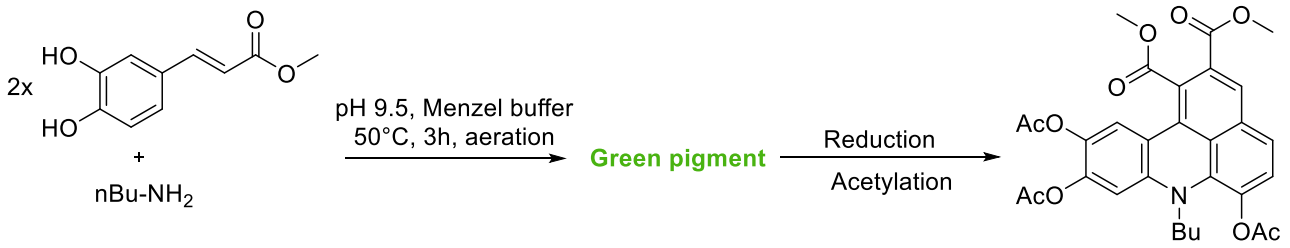

Scheme 3.1- Formation of the reduced acetylated form of the TBA pigment (adapted form [1]).

After isolating and characterizing with many efforts the TBA pigment derivative, some attempts have been done to try to elucidate the reaction mechanism. In 2001, Yabuta and colleagues proposed a mechanism involving as the first step the oxidation of one molecule of chlorogenic acid. One quinone molecule then reacts with the primary amine forming an imine, which then acts as a nucleophile toward another quinone molecule in a Michael reaction. After the oxidation of the dimeric intermediate, a Diels-Alder reaction takes place. Then, after some rearrangements, the green TBA pigment forms (Scheme 3.2). Yabuta also demonstrated that the green TBA pigment can be obtained by oxidation of the reduced yellow product previously isolated.[4]

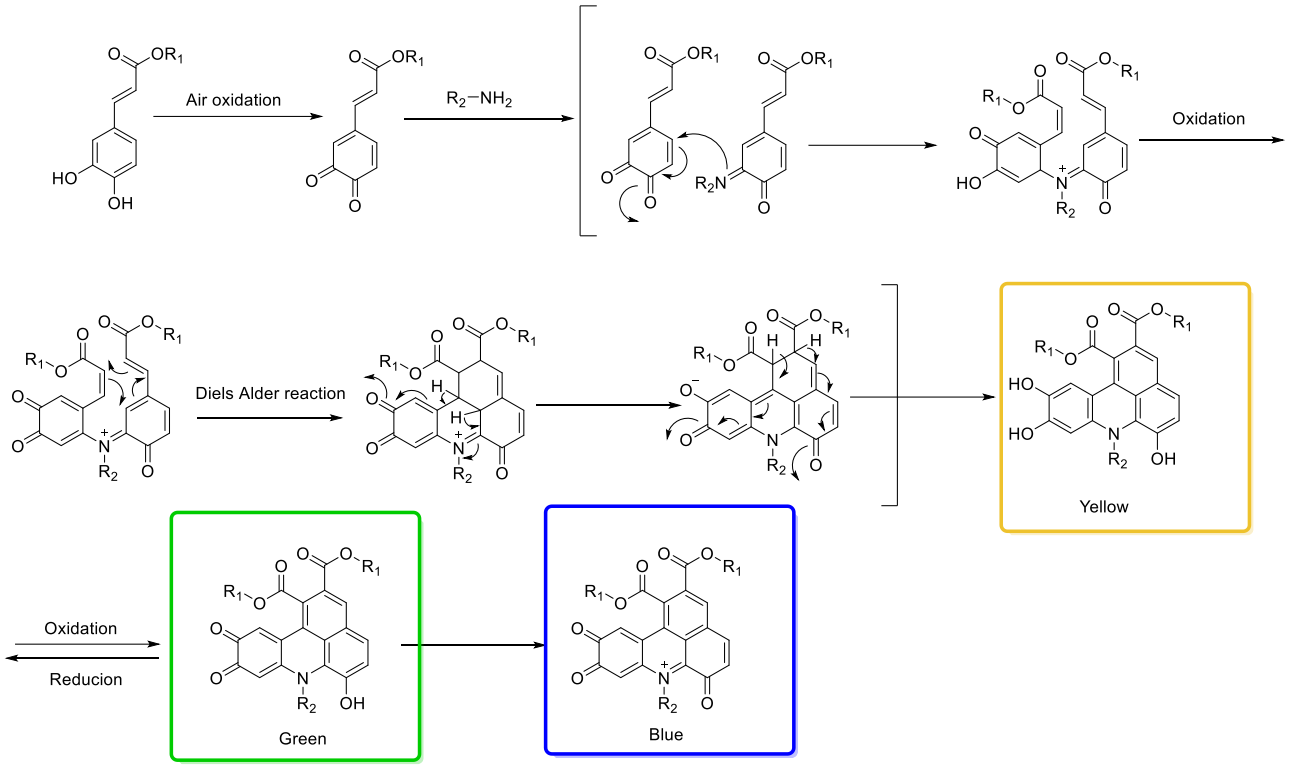

Scheme 3.2 – Proposed mechanism of TBA pigment formation from caffeic acid esters and an amino compound (adapted from [4]).

Another mechanism proposed by the same group based on Electron Spin Resonance (ESR) experiments results, involves the formation in the first step of a caffeic acid ester radical, which then dimerizes with another ester molecule. After some proton rearrangements and subsequent oxidations, cyclization and Michael addition on the quinonic form take place, followed by nitrogen cyclization leading to formation of the nitrogen containing six-membered cycle (Scheme 3.3).[5]

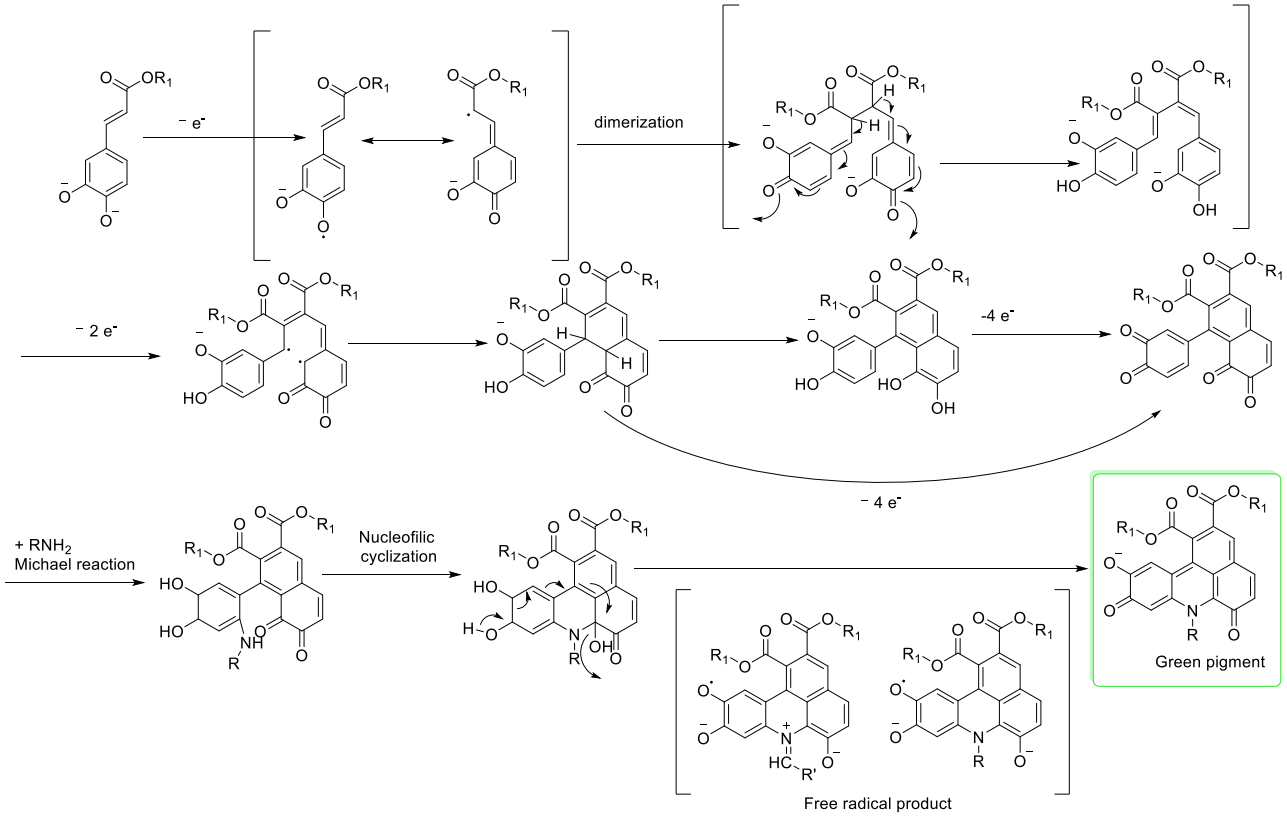

Scheme 3.3- Mechanism proposed for TBA pigment formation involving free radical intermediate (adapted from [5]).

The structure of the TBA pigments has then been confirmed some years later by LC-MS where signals corresponding to the green TBA pigments formed by reaction of lysine with CGA were detected.[6,7,8] However, it was elucidated that there are two different reaction pathways depending on which amino group of lysine is involved in the reaction: if lysine (or other α amino acid) reacts through its α amino group, this results in the loss of the amino acid side chain, and only the nitrogen atom of the α amino group is incorporated into the pigment structure (Scheme 3.4, path a); on the other side, if reaction involves the amino group which is not in α position with respect to the carboxylic group, this results in the formation of the TBA pigment with retention of the amino acid lateral side chain (Scheme 3.4, path b).[8]

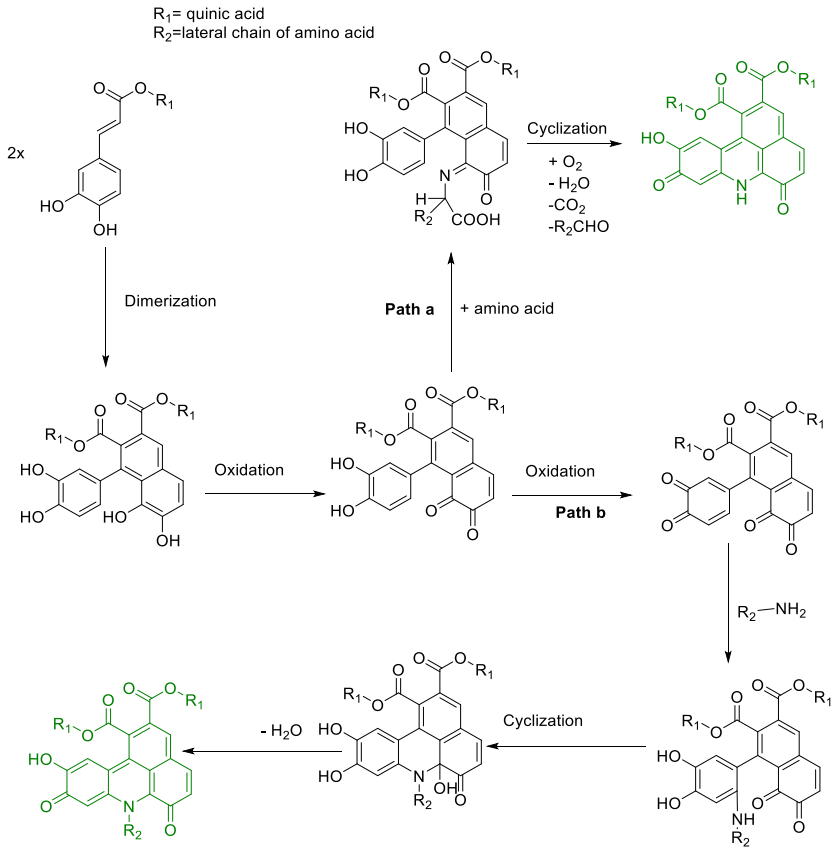

Scheme 3.4- Proposed reaction mechanism between chlorogenic acid and individual amino acids. Path a) Reaction involving an α-amino group; Path b) Reaction involving a non-α amino group (adapted from [8]).

Moreover, also lateral side chains of amino acids different from lysine can react with CGA. Considering cysteine, it reacts through its highly nucleophilic thiol moiety on the monomeric quinone form of chlorogenic acid (not the dimer), and adducts with addition of one or two cysteine molecules have been observed, which are non-colored.[6] Other amino acids have also been reported to react through their lateral side chain when the α amino group is protected: histidine, tyrosine and tryptophan.[7] Moreover, tryptophan having the free α amino group, can react with chlorogenic acid in the same basic environment requested for the synthesis of the TBA pigments, leading to the formation of very interesting red cyanin type chromophores.[9]

Colors obtained by reaction of CGA with the different free amino acids in basic conditions can be observed in Figure 3.2.[8] CGA alone in basic environment leads to the formation of a brown solution due to its oxidation products. It can be observed that proline does not react with CGA due to the absence of a primary amino group, thus leading to the formation of the same brown solution of CGA alone. Ammonia as well does not lead to the formation of green coloring. As already mentioned, cysteine leads to a colorless product because it reacts with the quinone of CGA thus avoiding the formation of TBA pigments but also of the brown oxidation products, whereas tryptophan, thanks to the formation of the cyanine-type pigments leads to a red color.[8]

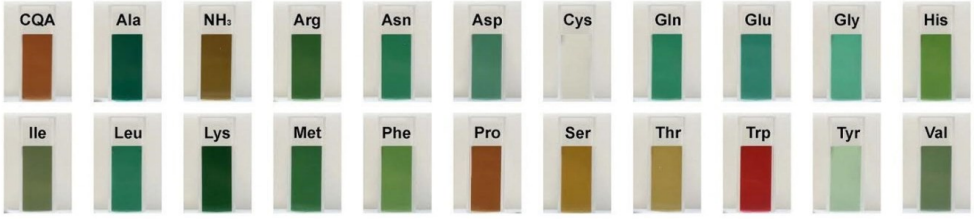

Figure 3.2- Color development in model systems containing chlorogenic acid and individual amino acids at pH 9.[8]

Considering the spectroscopic properties of the TBA pigments, another very important feature is their capability to change their VIS spectrum according to the protonation form. In fact, the pigments can exist in 3 prototropic forms: the anionic one, which is the most important at pH between 7 and 9 and has a maximum absorbance at 680 nm; the neutral form, predominant at pH 4, showing a maximum absorbance at 620nm; the cationic form, which exists at pH lower than 2, having a typical absorbance at 500nm (Scheme 3.5).[10]

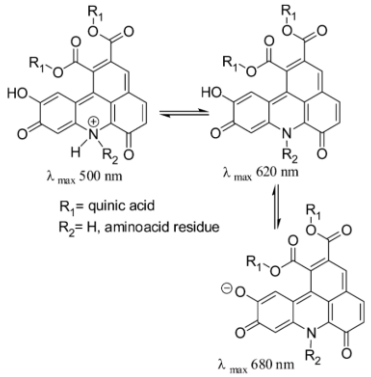

Scheme 3.5- Proposed prototropic forms of TBA pigment responsible for different absorbance maxima at different pHs.[10]

3.1.3 Other possible applications of the green TBA pigment

Despite the negative aspect of greening in foods, the formation of green TBA pigments might be considered also as an opportunity to exploit. For example, a group in Naples thought about the possibility of using the TBA pigments for food coloring applications.[10] In fact, the presence of natural green coloring agents is very rare, with only chlorophylls and semisynthetic chlorofillins (natural green 3, 141) available, whereas the synthetic agent triarylmethanegreen (E142) is permitted in Europe only for few preparations.[10] In particular, Iacomino and colleagues made some tests on alginate beads colored with the TBA pigments, as well as on reaction of CGA with bovine serum albumin and chicken egg white. Pigments never showed cytotoxic effects at doses comparable with those required for food coloring, and thermal stability resulted to be satisfactory up to 90°C.[10]

The same group also exploited the pH-dependent color properties of the pigment to detect the generation of volatile amines such as ammonia and trimethylamine from microbial spoilage of food. By exposing filter paper sheets, silica plates and alginate films loaded with the acidic solution of the TBA pigment to vapors from decomposing fish, it was observed that the color of all the test supports shifted from the red form at acidic pH to the green anionic form after 24 hours exposure to volatile amines.[10]

3.2 STUDY OF THE REACTION BETWEEN CHLOROGENIC ACID AND LYSINE

3.2.1 Synthesis and purification of the pigment

In the perspective of applying TBA pigment formation for sensing purposes, the first step has been that of studying the reactivity of a system already reported in literature, composed by chlorogenic acid (5-*O*-caffeoylquinic acid, CGA) and lysine. Since the final aim is that of obtaining a peptide-based sensing element, the choice of the amino acid lysine is very suitable, due to the presence of two different amino groups, the α one -useful for future peptide bond formation in peptides- and the ε one on the lateral side chain - available for TBA pigment formation-. Compound **1**, a lysine protected at the α amino group with a *tert*-butoxycarbonyl group, has been used to avoid unwanted reactivity of the α-amino group since, according to the literature, a not protected α amino group would form TBA pigments with loss of lateral side chain as already explained in the introducing part of this section. Several of the experiments of chapter 3 of the present thesis regarding the study of TBA pigment in solution have been done in collaboration with the master student Cristian Verona, during his Master thesis internship.[11]

As a starting point, the reaction conditions proposed by Iacomino and colleagues have been reproduced, in order to isolate the pure TBA pigment **2** to be used as a reference in the study of the reaction for sensing purposes.[10] A solution of *N*α-boc lysine **1** and CGA in carbonate buffer at pH 9, has been left to react for 48 hours at room temperature, under stirring, keeping the vial open to allow a continuous supply of oxygen, essential for the reaction to take place (Scheme 3.6): very soon green color development has been observed, starting from the yellowish color of CGA alone in its deprotonated form, to a dark green color with the passing of time (Figure 3.3).

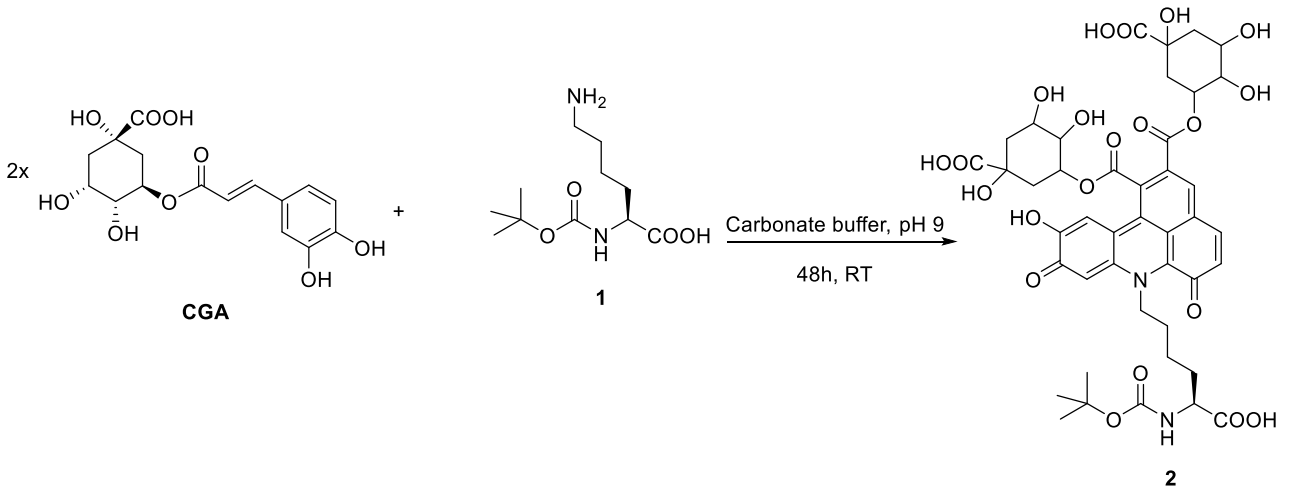

*Scheme 3.6 – Reaction scheme of CGA with Nα-boc-lysine **1** leading to formation of product TBA pigment **2**.*

*Figure 3.3 – Green color development upon formation of compound **2**.*

After obtaining the green reaction mixture, TBA pigment **2** has been purified by size exclusion chromatography (SEC) as suggested by Iacomino's group.[10] For this purpose, a polyacrylamide gel with a fractionating interval between 800 and 4000 Da has been used. The first eluted fractions resulted in a yellow-brownish color corresponding to oxidation and polymerization byproducts from CGA alone. Then, green fractions started to be eluted, reaching a maximum green color intensity that finally shifted to a more blueish

shade. This is in accordance with the literature and the shift to a more blueish color might be attributed to a change in the oxidation state of the pigment.[2,4]

Fractions collected by SEC have then been analyzed by UV-Visible spectroscopy, to detect the presence of the pigment according to its typical absorbance at 680 nm, as well as to identify the presence of chlorogenic acid byproducts thanks to their absorbance at 325 nm. Only fractions having a ratio between absorbances at 680 nm and 325 nm lower than 0.3 were collected and lyophilized (Figure 3.4): this allowed to discriminate the purest fractions having a less amount of chlorogenic acid byproducts[10] (identified as fractions **a** and **b**, Figure 3.5).

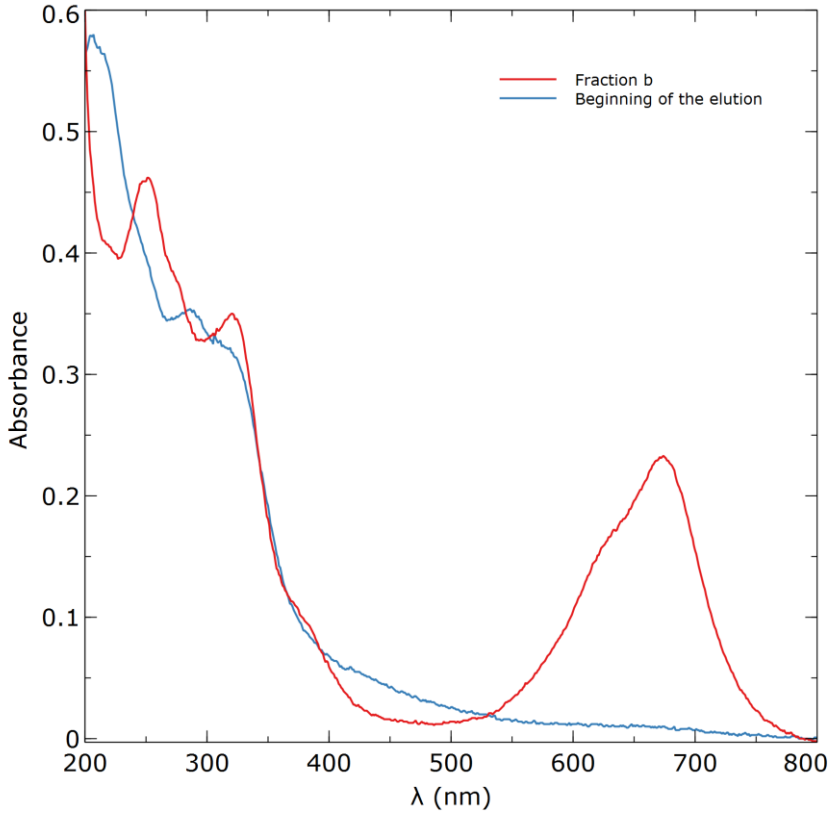

*Figure 3.4- Absorbance spectra of the first eluted fraction (only CGA byproducts, blue spectrum) and of fraction **b** containing pigment **2** (red spectrum).*

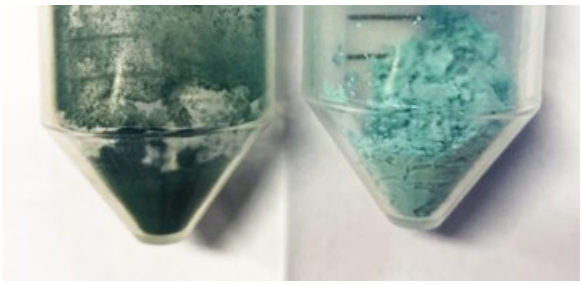

*Figure 3.5 – Lyophilized fractions **a** (on the left) and **b** (on the right).*

The isolated fractions **a** and **b** have then been analyzed by High Performance Liquid Chromatography coupled to diode-array detector and mass spectrometry (HPLC-DAD-MS), using an elution gradient of water and acetonitrile containing 0.1% of formic acid. Considering chromatograms monitoring by DAD, it is important to highlight that at the acidic pH used for elution, the prevalent prototropic form of the pigment is the acidic one, which is pink and absorbs at 510 nm. Therefore, the chosen wavelengths for monitoring the composition were 214 nm (standard wavelength to monitor almost every kind of substance), 330 nm (wavelength for

monitoring the presence of CGA byproducts), 670 nm (secondary absorption of the pigment at acidic pH) and 510 nm (main absorbance peak of the pigment at acidic pH).

Looking at the chromatograms at 510 and 670 nm, at retention times ranging between 29 and 40 minutes, both the analyzed fractions **a** and **b** (Figure 3.6) showed signals diagnostic for the pigment **2**, corresponding to signals in the mass spectra with a mass/charge ratio (m/z) of 929 in positive mode and 927 in negative mode (Figure 3.7), consistent with the protonated and deprotonated form of the TBA pigment **2** respectively. In the same range of retention times, analysis of fraction **a** also revealed the presence of impurities absorbing at 330 nm, probably due to the presence of CGA byproducts. To verify this hypothesis, a CGA solution in carbonate buffer reacted in the presence of air for 36 hours was also analyzed by HPLC-DAD-MS: in this way, it was possible to detect the presence of many peaks with retention times between 20 and 40 minutes absorbing at 330 nm, but showing no absorbance at 510 or 670 nm, thus confirming that the absorbances in the visible come only from the reaction products with lysine. However, looking at the chromatograms of fraction **b** (Figure 3.6), the cleanest one, in correspondence of the peaks at 510 nm, there are still signals absorbing at 330 nm, thus indicating that also the pigment itself absorbs at 330 nm.

The presence of a set of peaks absorbing at 510 nm and having the same MS signals is in accordance with the literature[10] and this is due to the isomerization of chlorogenic acid in alkaline environment. In fact, 5-*O*-caffeoylquinic acid (that in the text has been simply called chlorogenic acid CGA) can isomerize to 4-*O*-caffeoylquinic acid in basic environment; the same type of reactivity can lead to isomerization of 4-*O*-caffeoylquinic acid to 3-*O*-caffeoylquinic acid (Scheme 3.7).[12] Considering that TBA pigment **2** forms from two CGA molecules and that each of them can isomerize to the other 2 positional isomers, there are a total of 9 possible isomers, and this can explain the presence of multiple peaks with the TBA pigment m/z ratio. Nevertheless, in the text pigment **2** will be mentioned in the singular form comprising all the possible isomeric forms.

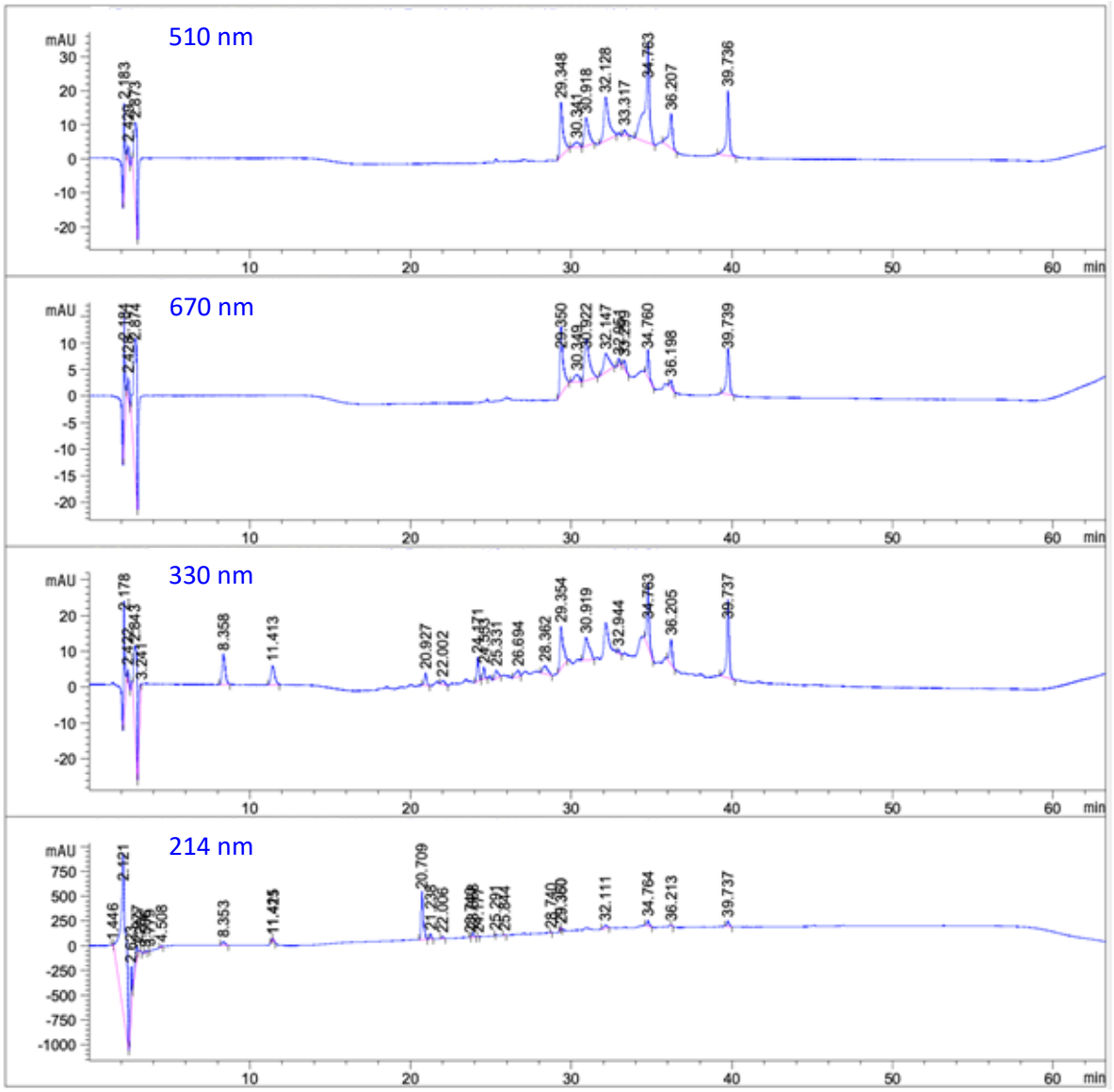

*Figure 3.6 – HPLC Chromatograms of fraction **b** registered at the specified wavelengths (510 nm, 670 nm, 330 nm, 214 nm).*

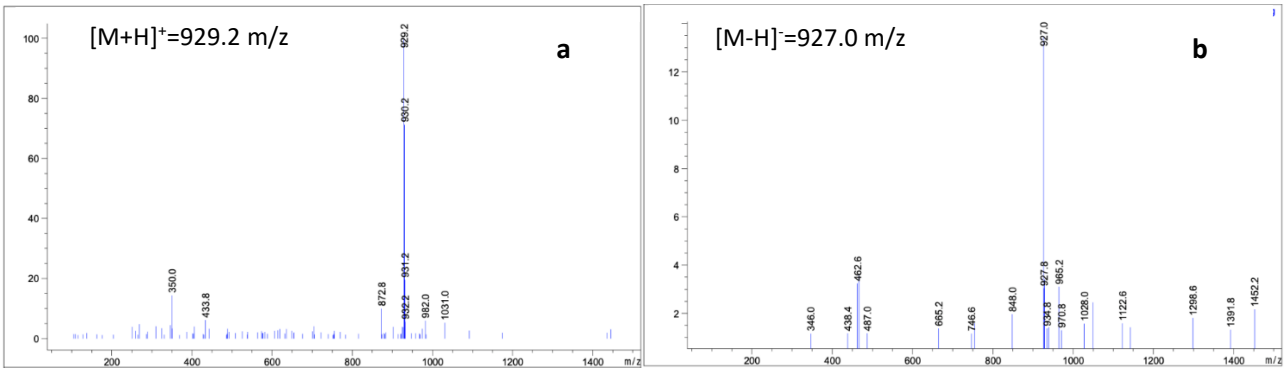

*Figure 3.7 – Mass spectra of **2** in positive (a) and negative (b) mode.*

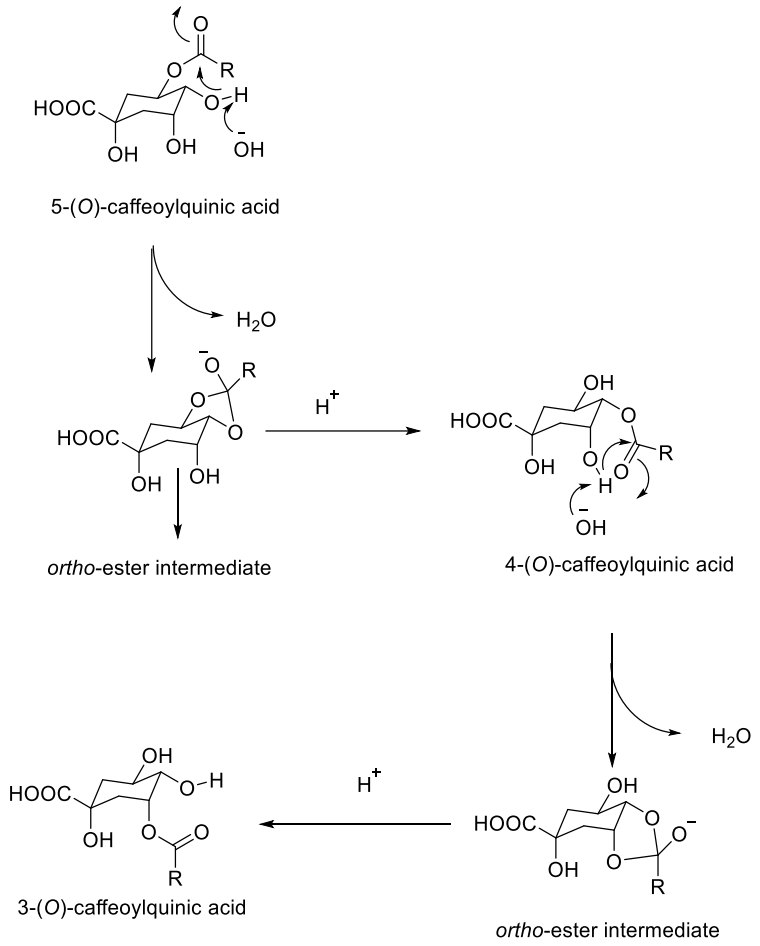

Scheme 3.7 - Proposed acyl migration pathways of 5-O-caffeoylquinic acid (adapted from [12]).

3.2.2 Study of the reaction kinetics

After isolating and characterizing **2**, the next step was that of studying the kinetics of reaction to explore the possibility of using the reaction to quantify CGA from the absorbance of the pigment, either at the end point of the reaction or by measuring the initial rate of color formation. The first option should be available if one works in the presence of an excess amount of lysine with respect to the expected concentration of CGA, while the second option requires also that the initial rate depends on the concentration of CGA.

A first measurement was performed over 24 hours, following the increase of absorbance at 680 nm in carbonate buffer 180 mM (pH 9) with *N*α-boc-lysine (18 mM) in a 10-fold excess with respect to chlorogenic acid (1.18 mM). Looking at the kinetic profile (Figure 3.8 a), it is possible to observe that the process ends in about 24 hours, with an almost linear increase of absorbance during the first three hours. Actually, a more detailed study of the initial rate shows that a first linear burst occurs in the first 15 min, followed by a knee and a second, slower, linear increase (Figure 3.8 b). The occurrence of an initial burst is usually regarded as a suggestion for a change in the rate determining step after the accumulation of a key intermediate. However, more detailed studies would be necessary to rationalize this, which go far beyond the aim of this work, whose purpose was that of trying to find a practical application of this reaction for sensing purposes, without investigating the reaction mechanism in full details.

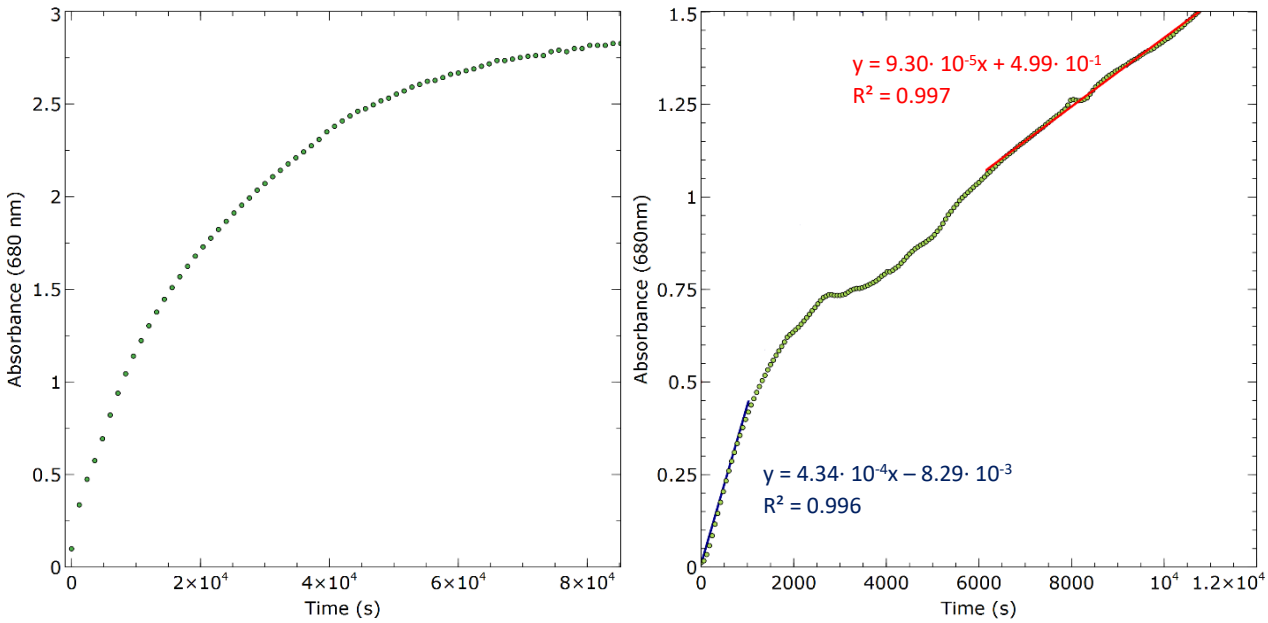

*Figure 3.8- (a) Kinetics of pigment **2** formation during the first 24 hours of reaction; (b) kinetics of pigment **2** formation during the first 3 hours of reaction.*

Nevertheless, to gain some further insight in the behavior of the system, a second experiment has been performed, reverting the conditions to an excess of CGA (17.5 mM) in defect of *N*α-boc lysine **1** (1 mM, 500 µM and 250 µM), again working in carbonate buffer at pH 9. In this case, the behavior is more complicated (Figure 3.9). For all the tested lysine concentrations, it is possible to observe a latency time between 0 and 200 s. Then, in all three cases, the absorbance at 680 nm increases: at 250 µM and 500 µM lysine absorbance reaches a plateau within 15 min whereas at 1 mM the plateau is not observed. It is difficult to rationalize this behavior, due to the presence of a complex reaction mechanism: the absence of a correlation between rate of color formation and lysine concentration seems to suggest that the rate determining step must be anterior to lysine nucleophilic attack.

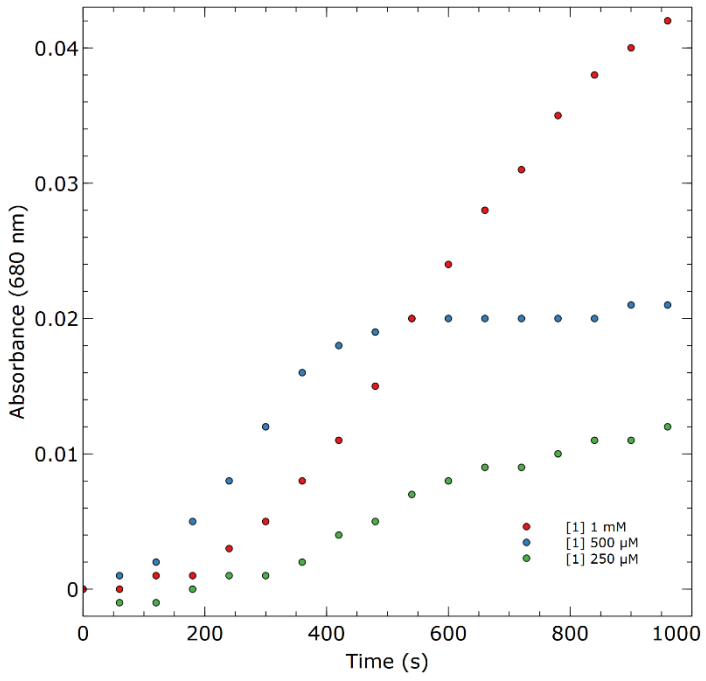

*Figure 3.9- Study of pigment **2** formation in excess of CGA at different Nα-boc lysine concentrations.*

3.2.2.1 Effect of the buffer

After performing the previously described experiments to evaluate the applicability of the TBA pigment reaction for sensing purposes, the influence of the type of buffer has been studied. Carbonate buffer (already used for all previous experiments), phosphate buffer and borate buffer, all at pH 9, have been considered.

After assessing that pigment **2** formation does not take place at all in borate buffer, measurements at different buffer concentrations have been carried out with carbonate and phosphate buffer, to determine if basic catalysis is involved in the reaction. Both carbonate buffer and phosphate buffer have been tested at different concentrations (259 mM, 175 mM and 86 mM), at 1.7 mM CGA and 17 mM *N*α-boc-lysine. Looking at the graphs in Figure 3.10 a and Figure 3.10 b, it is possible to observe that the color development is faster in carbonate buffer (Figure 3.10 a) than in phosphate (Figure 3.10 b). In both cases there is a latency time before reaction starts, but this time is longer for phosphate buffer (300 seconds with respect to the 60 seconds for carbonate buffer). By plotting the initial rates vs. the buffer concentrations, linear correlations have been obtained, with a much higher slope in the case of carbonate buffer (0.00116 $s^{-1}\cdot$ L $\cdot mol^{-1}$ for carbonate, 0.0003 $s^{-1}\cdot$ L $\cdot mol^{-1}$ for phosphate) (Figure 3.11). All these data suggest that general base catalysis occurs in the rate determining step, and therefore this is most likely a bi-electronic step rather than a radical one. As general catalysis is observed if a change of hybridization is involved in a rate determining step with protons transfer, this result seems in favor of the Michael addition as the slow step of the reaction, or of an ionic reaction not identified in the currently proposed mechanisms. However, from our practical point of view, carbonate is the best option to speed up the reaction.

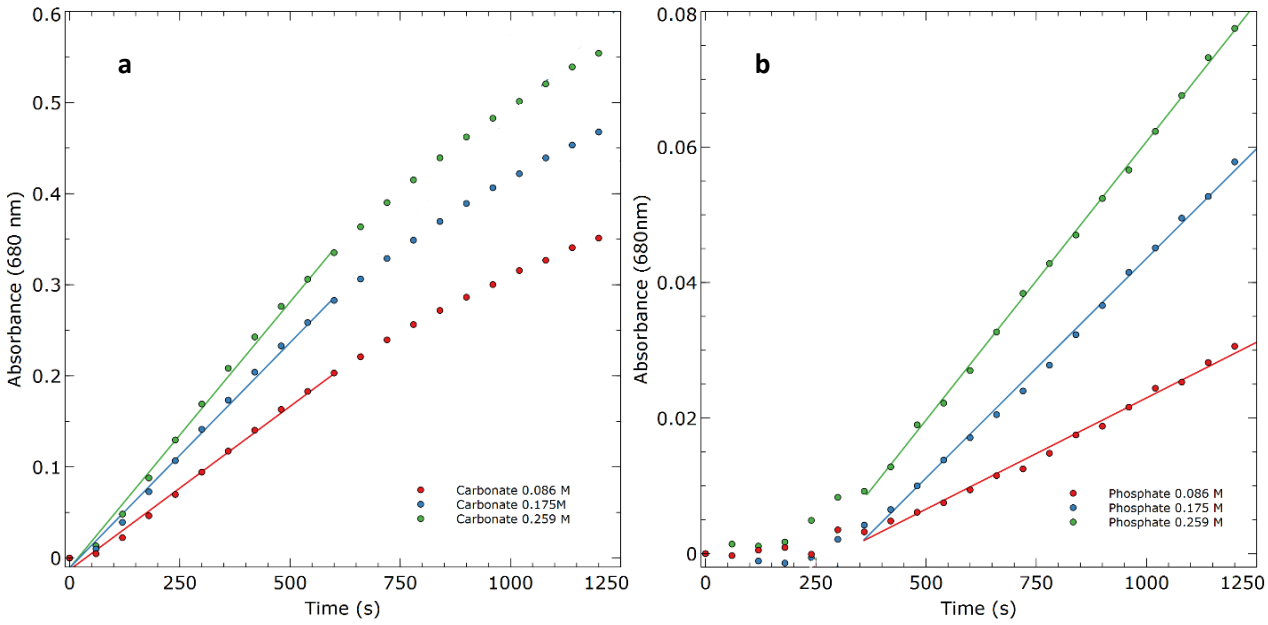

*Figure 3.10 – Kinetics of pigment **2** formation at different carbonate (a) and phosphate (b) concentrations.*

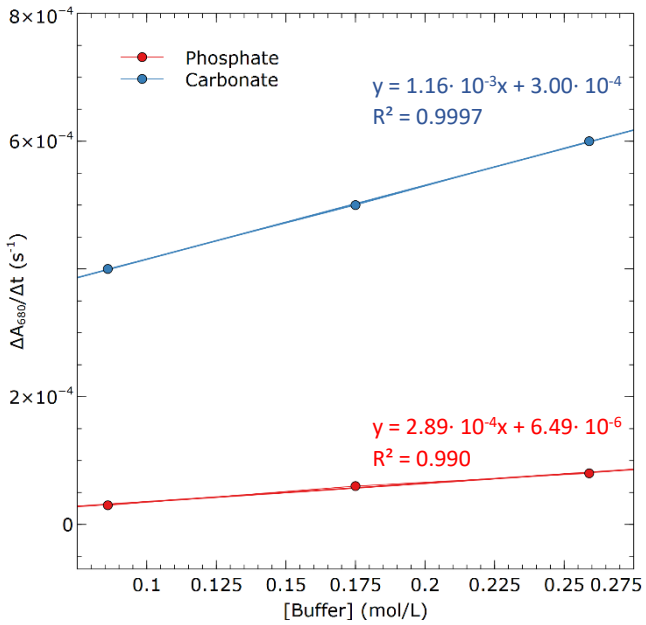

*Figure 3.11 – Comparison between kinetics of reaction of pigment **2** formation in carbonate and phosphate buffer.*

3.2.3 CGA quantification in absorbance mode

3.2.3.1 Assay at the endpoint of reaction

A first CGA quantification experiment has been done at the endpoint, after 24 hours of reaction. To do so, different reaction mixtures containing the same quantity of lysine **1** in excess (5.8 mM) and different CGA concentrations (ranging between 1.1 mM and 22 µM) in 56 mM carbonate buffer at pH 9, have been prepared in triplicate and have been left to react in an open system under stirring for 24 hours. The reaction mixtures have then been analyzed by measuring the absorption spectra between 500 and 800 nm (Figure 3.12).

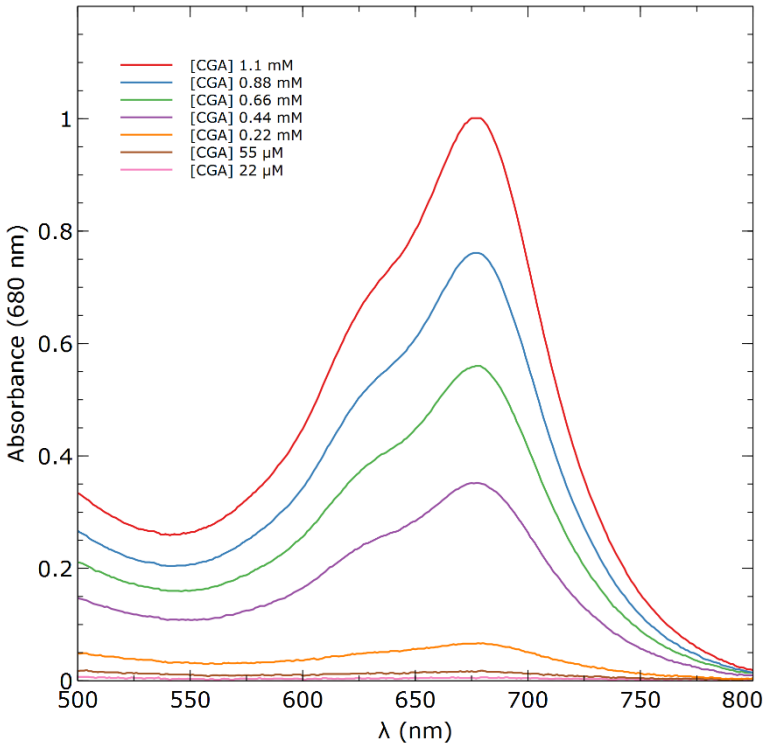

Figure 3.12- Absorbance spectra after 24 hours of reaction of solutions containing Nα-boc-lysine in excess and CGA at different concentrations.

By plotting the absorbance maxima at 680 nm against the concentration of CGA, it is possible to observe a linear relationship (Figure 3.13).

The occurrence of the linear relation allows in principle to exploit the end-point absorbance to quantify CGA, and the best fitting equation (Eq 3.1)

$$A_{680} = 8.47 \cdot 10^{2}[CGA] - 2.01 \cdot 10^{-2} \ (\mathrm{R}^2 = 0.993) \quad (Eq\ 3.1)$$

can be regarded as a potential calibration curve for such analytical methodology.

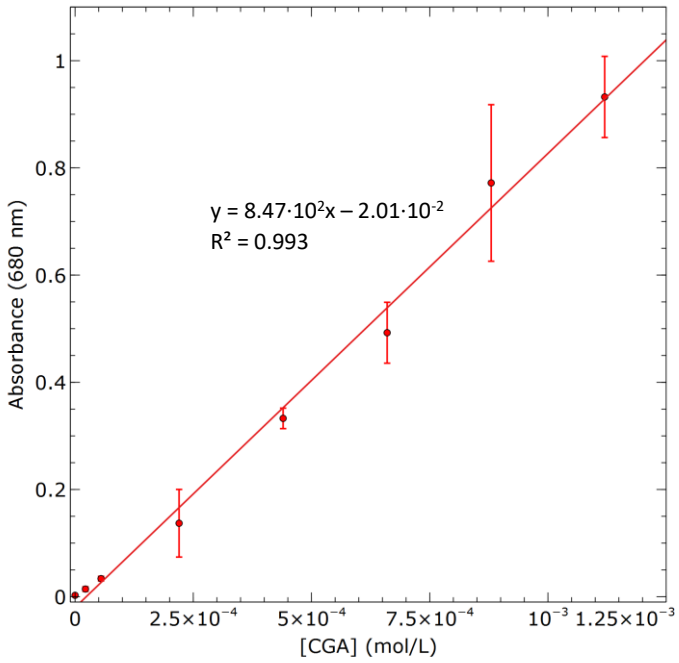

Figure 3.13- Linear correlation between absorbance at 680 nm measured after 24 hours of reaction and initial CGA concentration working in excess of Nα-boc-lysine.

Thanks to this linear relationship, it was possible to calculate the limit of detection (LOD) (Eq. 3.2) and limit of quantification (LOQ) (Eq. 3.3) according to the International Council for Harmonisation of Technical Requirements for Pharmaceuticals for Human Use (ICH) guidelines.[13]

$$LOD = \frac{3.3\sigma}{m} = \frac{3.3 \times 1.54 \cdot 10^{-3}}{847} = 6.00 \cdot 10^{-6}\ mol/L \qquad (Eq.\ 3.2)^{i}$$

$$LOQ = \frac{10\sigma}{m} = \frac{10 \times 1.54 \cdot 10^{-3}}{847} = 1.82 \cdot 10^{-5}\ mol/L \qquad (Eq.\ 3.3)^{i}$$

The found values of LOD and LOQ are quite good, even if they are above those reported for electrochemical and optical sensors for CGA detection present in literature.[14] However, the system is sensitive enough and would allow to quantify CGA present in extracts of coffee with sufficient sample dilution to reduce matrix effects, since the expected quantity of monocaffeoylquinic acids CQAs (of which 5-*O*-caffeoylquinic acid CGA is the most abundant) in espresso coffee for example is approximatively in the 1-30 mM range. However, it must be considered that the concentration of CQAa greatly depends on the arabica/robusta blending, on roasting and grinding procedures, but mainly on the quantity of coffee used.[15] Moreover, the great advantage of this system is that despite its high simplicity, it is expected to be highly selective for chlorogenic acid (and related caffeic acid esters), since the reaction does not take place for caffeic acid alone nor with other

[i] Where *m* is the slope of the curve and σ is the standard deviation calculated on 3 blank samples.

cinnamic acids such as *p*-coumaric acid, ferulic acid, isoferulic acid and corresponding esters, as well as hydrocaffeic acid esters and protocatechic acid esters, thus meaning that both the *ortho*-diphenolic moiety and the conjugated double bond are necessary, as well as the esterification of the carboxyl group.[4] However, considering the sensing application, waiting 24 hours to have a result is far too much and this type of method would never have a real possibility of application. For this reason, the choice was that of trying to decrease reaction times, by using the linear response in the first 16 minutes of reaction, far from the end point of the reaction.

3.2.3.2 Assay in kinetic mode far from the endpoint

A new quantification experiment has been thus set up, this time working in kinetic mode, exploiting the linear relationship of increase of color during the first 15 min. Again, excess lysine (17.5 mM) has been reacted with different concentrations of CGA (ranging between 1.8 mM and 60 µM). In this case, both the reactants were dissolved in water, and concentrated sodium carbonate was added directly in the cuvettes to start the reactions after mixing the reagents (final concentration 180 mM). For all the tested CGA concentrations, a linear kinetics has been observed during the first 15 min (Figure 3.14). To understand the order of reaction with respect to CGA, the initial rates measured as slopes of the curves $\Delta A_{680}/\Delta t$ have been plotted against the concentration of CGA, obtaining a linear correlation (Figure 3.15): this is the proof that the reaction is of pseudo first order with respect to CGA concentration. Considering that the relationship between the rate of reaction and lysine concentration is quite complex -there seems to be no linear correlation-, and that the kinetics is of first order with respect to CGA, it is possible to hypothesize that the rate determining step might be correlated with the processes leading to the formation of the reactive *ortho*-quinone from chlorogenic acid. However, the lucky occurrence of the linear relation allows to exploit the reaction to quantify CGA by measuring the initial rate, and also in this case the best fitting equation (3.4):

$$\frac{\Delta A_{680}}{\Delta t} = 2.90 \cdot 10^{-1}[CGA] - 4.11 \cdot 10^{-6} (\mathrm{R}^2 = 1.00) \qquad \textit{(Eq. 3.4)}$$

can be used as a calibration equation to obtain the concentration of CGA from the measured rate.

Also in this case it has been possible to calculate the LOD (Eq. 3.5) and LOQ (Eq. 3.6) according to the ICH guidelines.[13]

$$LOD = \frac{3.3\sigma}{m} = \frac{3.3 \times 4.40 \cdot 10^{-7}}{0.290} = 5.0 \cdot 10^{-6}\ mol/L \qquad (\textit{Eq. 3.5})^{ii}$$

$$LOQ = \frac{10\sigma}{m} = \frac{10 \times 4.40 \cdot 10^{-7}}{0.290} = 1.5 \cdot 10^{-5}\ mol/L \qquad (\textit{Eq. 3.6})^{ii}$$

By comparing these values with those obtained with the endpoint method, it is possible to see that they are very similar (LOD and LOQ of $6.0 \cdot 10^{-6}$ mol/L and $1.8 \cdot 10^{-5}$ mol/L respectively with the end point method), even if working in kinetic mode has the great advantage of obtaining the same results waiting only 15 minutes instead of 24 hours. However, for both the end point and kinetic method, it should be noted that the LOD and LOQ values previously discussed are only calculated. Actually, by measuring the kinetics of reaction for a 10 µM solution of CGA, it was not possible to detect any signal. So, the experimental LOD is higher with respect to the one calculated using the kinetic method (5 µM).

[ii] Where *m* is the slope of the curve and σ is the standard deviation calculated on 3 blank samples.

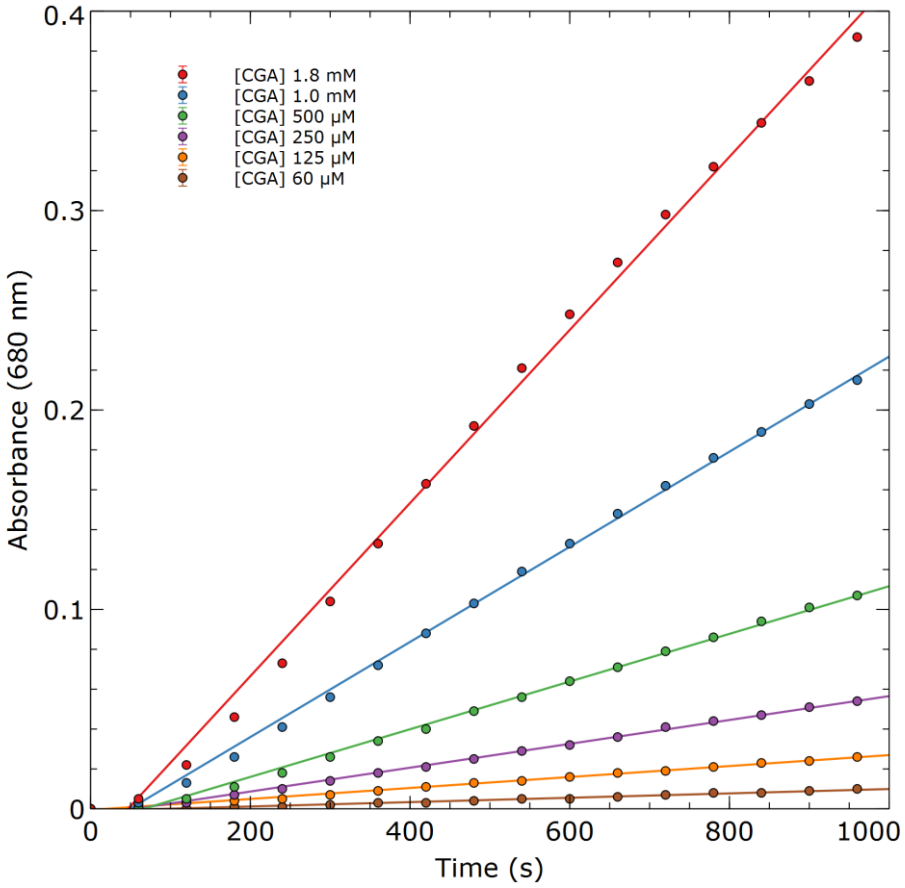

*Figure 3.14- Kinetics of pigment **2** formation working in excess of Nα-boc-lysine at different CGA concentrations over the first 960s of reaction.*

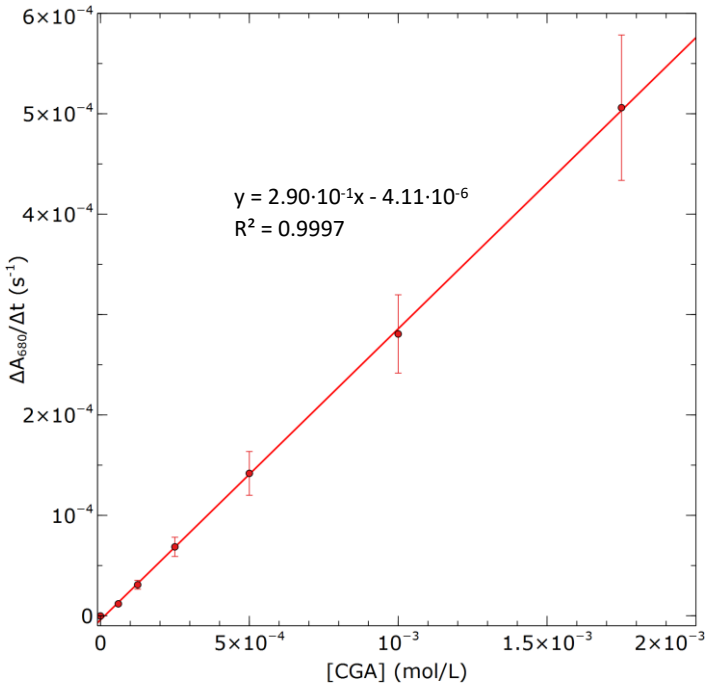

Figure 3.15- Linear correlation between $\Delta A_{680}/\Delta t$ (s^{-1}) and initial CGA concentration working in excess of Nα-boc-lysine.

3.2.3.3 Measurements with a portable photometer

In the perspective of trying to obtain better sensitivity and to pass to a more portable device, some preliminary experiments have been done using an in-lab built photometer (Figure 3.16).[iii] Such device is capable of measuring the absorbance of a sample in a cuvette with respect to a reference. Differently from a spectrophotometer, in this case the light source is a LED (light emitting diode), and this allows measurements only at a fixed wavelength. However, even if this might seem a disadvantage in terms of measurement flexibility, the advantages are the low cost of LED sources and the fact that they do not need expensive systems for light diffraction such as monochromators or filters. These features make them suitable for specific applications in which there is no need to use different wavelengths and the portability of the instrument for performing analyses "on field" is an added value.

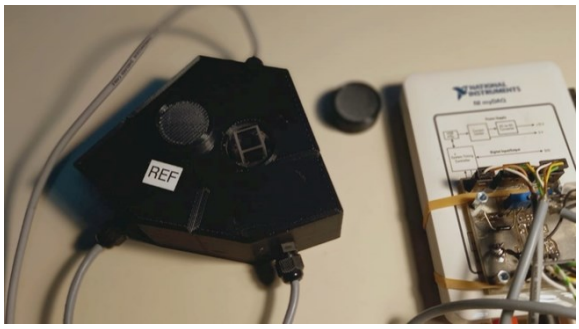

Figure 3.16- In-lab built photometer to perform analysis in cuvette.

To try to compare performances obtained with the developed portable device with the ones obtained with the laboratory spectrophotometer, a preliminary test has been performed measuring the kinetics of few solutions containing *N*α-boc lysine in excess (17.5 mM) and different CGA concentrations in carbonate buffer 175 mM at pH 9. A sample of distilled water has been used as the blank in this case, representing the noise associated with the scattering during measurement. For the 100 µM, 10 µM and 5 µM CGA concentrations it has been possible to observe a good linear range of the $\Delta A_{680}/\Delta t$ signal emerging from the noise; only for the 1 µM solution the sample signal was not distinguishable from the blank one (Figure 3.17). It is important to make two considerations: first, with the portable photometer, it is possible to observe oscillations from the linear plot approximating the kinetic measurements, and this is due to the higher sensitivity of the photometer with respect to the laboratory instrument, since the photometer can appreciate variations in the order of 10^{-9} absorbance units. Such oscillations might be attributed to scattering phenomena due to the presence of particles in solutions, but also to the movements in solution due to the addition of reagents right before the analysis. The second consideration is that with the photometer it was possible to significantly lower the detectability of the target CGA: in fact, the lowest concentration measured with the benchtop spectrophotometer was 60 µM, whereas with this device it was possible to go one order of magnitude lower. By comparing linear ranges obtained with the two systems, it is possible to see that results compare quite well, with slope and intercept in the same order of magnitude: such difference is perfectly in line with the use of different instrumentations (Figure 3.18). However, in the case of the spectrometer, only measurements at few CGA concentrations have been done, with no replicates, so these must be considered as very preliminary results to demonstrate that the proposed portable device is suitable for on field applications and might be used in the future for further tests.

[iii] The instrument was realized by a team of engineers, composed by Prof. Antonio Boscolo and Prof. Agostino Accardo of the Department of Engineering and Architecture of the University of Trieste, and Dott. Giuseppe Boscolo of the Company GRUPPO TECNICHE AVANZATE.

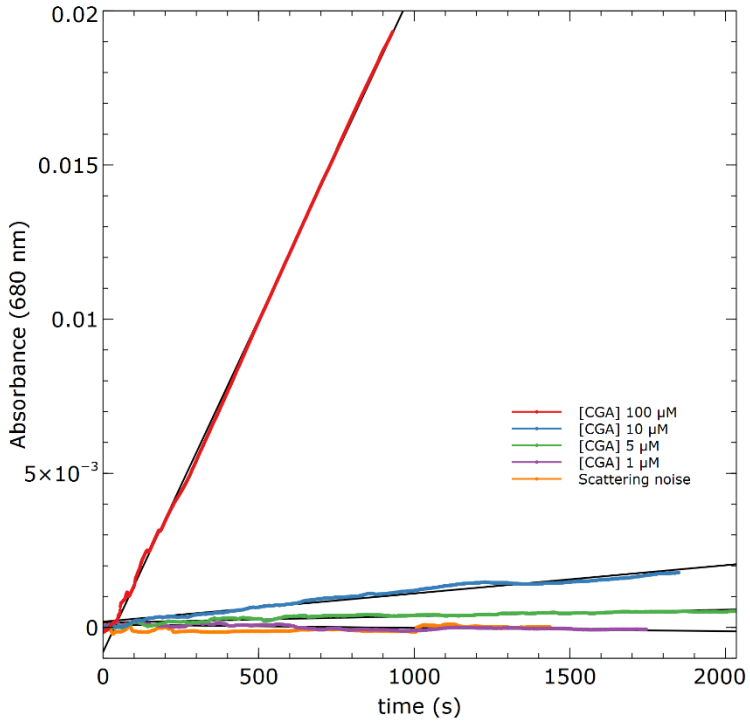

Figure 3.17- Kinetics obtained with the photometer working in excess of Nα-boc lysine and different CGA concentrations.

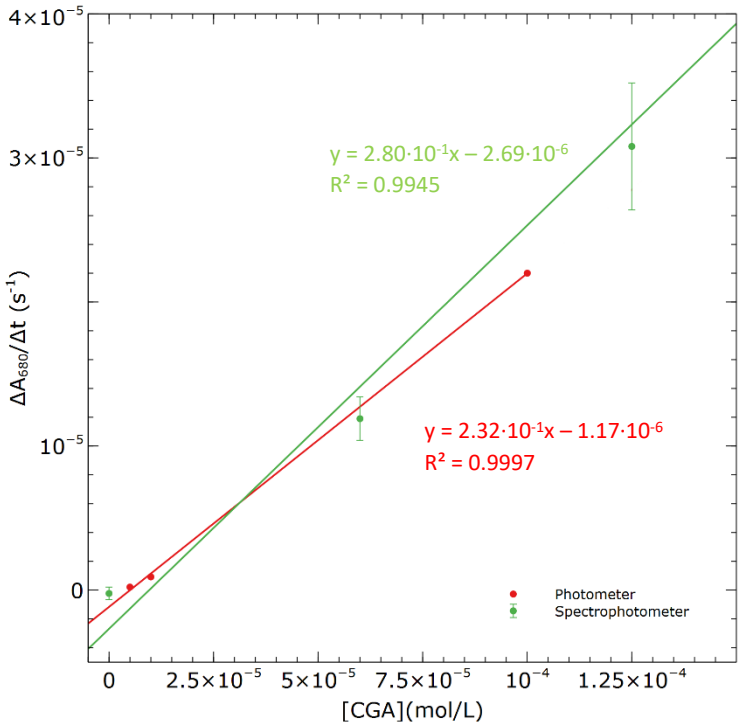

Figure 3.18- Comparison between linear correlation of in-lab built photometer and spectrophotometer.

3.3 PEPTIDES

After studying the spectrophotometric properties of pigment **2** obtained from *N*α-boc lysine and CGA, the next step was that of inserting the reactive lysine residue inside a peptide structure. The first reason for applying the reaction to peptides was that of identifying, at least preliminarily, an amino acidic sequence capable of interacting with CGA or with the CGA-derived intermediates and providing some selectivity. The other reason was that, by using a peptide scaffold, it would also be possible to introduce functionalities suitable for immobilizing the sensing unit on a surface, which would be very advantageous in a biosensing perspective because it would allow to eliminate interferents by simply washing the functionalized support after reaction.

3.3.1 Design of the peptides

As a starting point, four peptide sequences have been selected:[iv]

1st sequence: **Phe-Phe-Ala**-Pro-Pro-**Lys**-Ala-Glu
2nd sequence: **Phe-Phe-Ala**-Glu-Ser-**Lys**-Ala-Ser-Glu
3rd sequence: **Phe-Phe-Ala**-Val-Pro-Asp-Ser-**Lys**-Ser
4th sequence: **Phe-Phe-Ala**-Val-D(Pro)-Asp-Ser-**Lys**-Ser

The four sequences share the starting tripeptide portion **Phe-Phe-Ala**, taken from the β-amyloid peptide, responsible for the formation of proteic extracellular plaques in people affected by the Alzheimer's disease: this motif should have aggregating properties,[16] possibly useful in the perspective of immobilizing peptides inside polystyrene wells, since many examples of application of sequences containing amyloid-derived motives, but also the **Phe-Phe** diad alone, have been reported in material sciences exploiting their self-assembling abilty.[17] Another reason for inserting this tripeptide, is that it should interact by π-π stacking with CGA. Looking at the first proposed sequence, there is a proline diad that should provide a turn secondary structure, whereas the presence of hydrophilic residues common to all the four proposed structures such as glutamic acid, aspartic acid and serine should favor water solubility of the peptides, which is very important considering that the TBA pigments formation takes place in aqueous environment. Obviously, all the proposed sequences contain the lysine residue necessary for reaction with CGA.

Once establishing the starting peptide structures, the algorithm "PEP-FOLD", an online resource capable of making conformational predictions on peptides has been used to calculate the most stable conformation of each of the selected peptides.[18] The search was further refined on the *N*-acetylated, *C*-amidated peptides by optimizing their geometries with the Amber* force field,[19] with explicit treatment of the solvent water. Finally, conformational searches have been conducted using a "Monte Carlo" method implemented in the MacroModel module of the Schrödinger suite.[20] In the resulting models, the 1st peptide sequence Acetyl-Phe-Phe-Ala-Pro-Pro-Lys-Ala-Glu-NH_2 contains a loop conformation formed by the two prolines and closed on one end by the amino group of lysine (Figure 3.19). In the case of the 2nd peptide sequence Acetyl-Phe-Phe-Ala-Glu-Ser-Lys-Ala-Ser-Glu-NH_2, the structure is that of an anti-parallel β-sheet, with the turn forming in correspondence of the amino acids Glu-Ser, and the lateral side chain of lysin is external to the loop (Figure 3.20). The 3rd and 4th sequences show a conformational simulation result very similar to that of the 2nd one (Figure 3.21 and Figure 3.22).

[iv] Peptides sequences have been designed in collaboration with Dott. Andrea Caporale of the Department of Life Sciences of the University of Trieste.

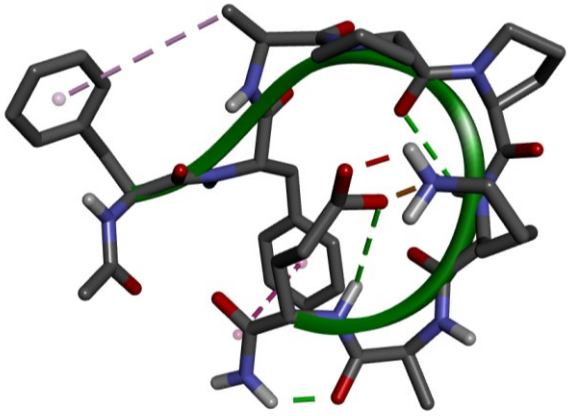

Figure 3.19 - Conformational minimum of the 1st peptide N-Acetyl-Phe-Phe-Ala-Pro-Pro-Lys-Ala-Glu-NH_2 simulated by molecular dynamic study.

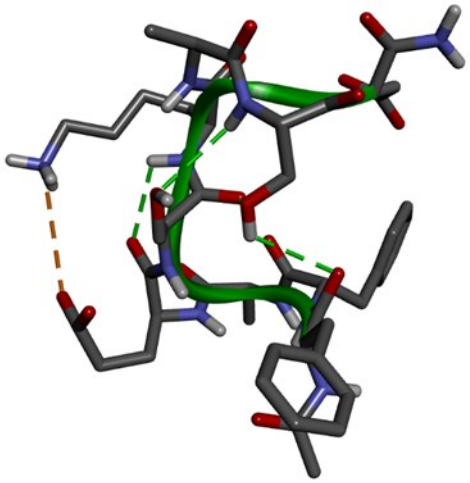

Figure 3.20- Conformational minimum of the 2nd peptide N-Acetyl-Phe-Phe-Ala-Glu-Ser-Lys-Ala-Ser-Glu -NH_2 simulated by molecular dynamic study.

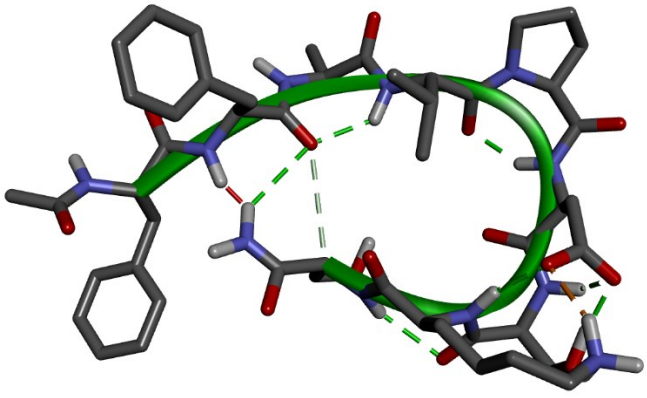

.

Figure 3.21 -Conformational minimum of the 3rd peptide N-Acetyl-Phe-Phe-Ala-Val-Pro-Asp-Ser-Lys-Ser -NH_2 simulated by molecular dynamic study.

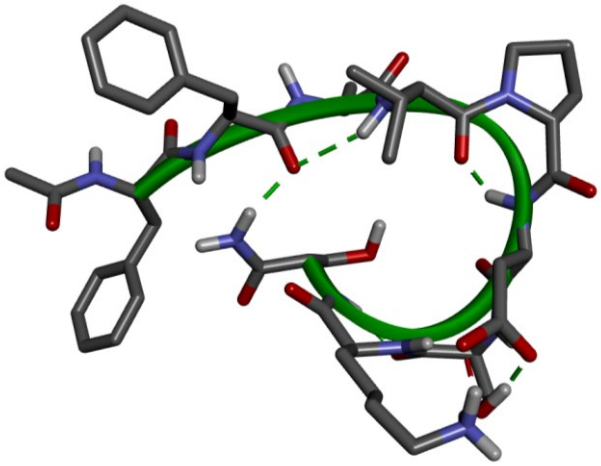

Figure 3.22- Conformational minimum of the 4th peptide N-Acetyl-Phe-Phe-Ala-Val-D(Pro)-Asp-Ser-Lys-Ser -NH_2 simulated by molecular dynamic study.

Based on computational results, it has been decided to synthesize only the 1st and 2nd peptide sequences due to their differing conformations -the 3rd and 4th sequences have not been synthesized since their conformation is quite similar to that of the 2nd one-. As far as the first sequence is concerned, it was changed to Ac-Phe-Phe-Ala-Pro-Pro-Lys-Ala-Ser-Glu-NH_2, thus inserting a serine between alanine and the *C*-terminal glutamic acid residue, in order to have a higher distance between lysine and aspartate, thus diminishing the possibilities of ionic bond formation, but also to create a more symmetric structure with respect to the loop position. Moreover, the presence of a further polar hydrophilic amino acid should favor water solubility of the peptide.

3.3.2 Synthesis of the peptides

Both selected peptides Ac-Phe-Phe-Ala-Pro-Pro-Lys-Ala-Ser-Glu-NH_2 (**P1**) and Acetyl-Phe-Phe-Ala-Glu-Ser-Lys-Ala-Ser-Glu-NH_2 (**P2**) have been synthesized by solid phase synthesis using an automatic microwave synthesizer.[v] Syntheses have been carried out adopting the traditional fluorenyl metoxycarbonyl (FMOC) approach. All the amino acids have been used having the free carboxy-terminal, the α-amino terminal protected as FMOC -which can be deprotected under basic conditions- and lateral side chains protected, when necessary, with acid-labile protecting groups, removable during the acidic cleavage of the peptide from the resin. By using Rink amide resin MBHA, after the cleavage, it is possible to obtain the peptides with the carboxy-terminal amidated. The coupling has been carried out using 2-(1H-Benzotriazole-1-yl)-1,1,3,3-tetramethylaminium tetrafluoroborate (TBTU), 1-Hydroxybenzotriazole hydrate (HOBT) as nucleophilic catalyst and diisopropylethylamine (DIPEA) as base.

Cycles of FMOC-deprotection with 20% piperidine, washing cycles with DMF, double coupling with the FMOC-amino acids (FMOC-AA-OH) under microwave irradiation and washing cycles were repeated for each amino acid residue to be added to the peptide sequences until the amino terminal. After adding the last amino acid, the amino terminals have been acetylated with acetic anhydride. Then, peptides have been cleaved from the resin using 95% trifluoroacetic acid (TFA) with 2.5% water and 2.5% triisopropylsilane (TIS) as scavengers. Then, TFA has been removed under a flux of argon almost to dryness, and the peptides have been precipitated with *tert*-butyl-methyl ether. The crude peptides have been analyzed by MS to verify the presence of the desired peptide. Then, purification has been done by preparative HPLC, using a gradient of water (+ 0.05% TFA) and acetonitrile (+ 0.05% TFA). After purification, the fractions of interest have been lyophilized and analyzed by MS and NMR spectroscopy.

[v] Peptides have been synthesized at the Department of Life Sciences of the University of Trieste, under the supervision of Dott. Andrea Caporale.

3.3.2.1 Peptide Ac-Phe-Phe-Ala-Pro-Pro-Lys-Ala-Ser-Glu-NH₂ (P1)

Looking at the mass spectrum of **P1**, it is possible to distinguish the most intense peak at m/z 1034.7, corresponding to the $[M+H]^+$ adduct, together with a minor signal at m/z 1072.6 corresponding to the $[M+K]^+$ adduct (Figure 3.23).

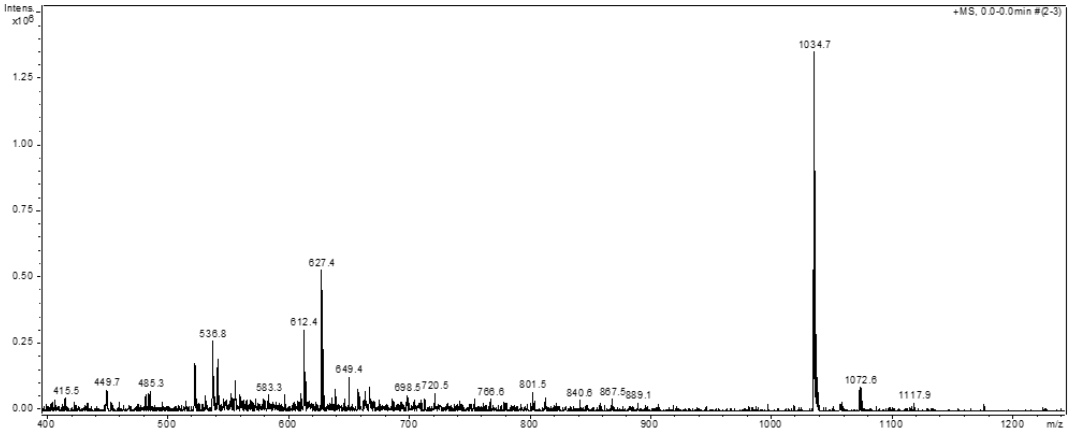

*Figure 3.23- Mass spectrum of **P1.***

NMR characterization has been performed by registering ^1H, ^1H-^1H-COSY and ^1H-^1H-TOCSY spectra. The solvent used for the analysis is water plus 10% of deuterium oxide, by operating suppression of the water peak. This choice can be explained considering that by registering spectra in pure deuterium oxide, information about the exchangeable protons, such as the amide ones, would be lost due to exchange with deuterium; on the other side, registering the spectrum in water with only a 10% of deuterated solvent (suppressing the water signal that would otherwise cover everything), all the diagnostic peptide signals can be seen.[21] By using the TOCSY spectrum, that allows to distinguish protons belonging to the same spin system, and the COSY spectrum, correlating protons directly coupled one to each other, it has been possible to assign the signals of all the amino acid residues of the peptide. In the ^1H-NMR spectrum (Figure 3.24), the signals of amide protons are found between 8.5 and 8.1 ppm, whereas the aromatic protons of the two phenylalanine residues resonate between 7.4 and 7 ppm. The region of α-protons lies between 4.6 and 4.2 ppm, whereas all the other side chains signals resonate at higher fields. The general procedure adopted for the assignments has been that of trying to correlate the amide protons to the corresponding α-protons, exploiting specific signals of the side chains. For example, the two doublets diagnostic for the methyl groups of the side chain of the alanine residues A and A' are found at 1.42 and 1.30 ppm. Thanks to their correlations in the TOCSY and COSY spectra, it is possible to identify the α protons (at 4.33 and 4.57 ppm respectively) and the amide protons (at 8.42 and 8.08 ppm respectively) of each alanine, even if with this type of NMR experiments it is not possible to determine which spin system belongs to which alanine, but only to distinguish the two series of signals.

The signals of lysine are recognizable thanks to the high number of signals (seven) of the protons of its side chain. At 8.37 ppm there is the amide proton, which correlates with the α one at 4.26 ppm. The β protons are splitted into two different signals at 1.81 and 1.76 ppm because they are diastereotopic, and the γ, δ and ε signals can be distinguished thanks to the COSY spectrum at 1.47, 1.70 and 3.02 ppm respectively.

Glutamic acid has the amide bond resonating at 8.33 ppm, and it couples with the α proton at 4.39 ppm, that correlates with the two diastereotopic β protons at 2.01 and 2.18 ppm, whereas the γ ones are at 2.49 ppm.

As for serine and the two phenylalanine residues, the distinction has been made based on the expected chemical shift values reported in literature, because the three systems have the same correlation pattern: in fact the aromatic protons of phenylalanine that can be observed between 7.40 and 7.17 ppm are part of a distinct spin system with respect to the amide, α and β signals, because they do not correlate with the protons

in the principal peptide backbone. Some hint in the assignment comes also from the fact that phenylalanine residues are two, and they are expected to have similar chemical shifts in this type of simple peptide structure. In fact, it is possible to attribute to the two phenylalanine residues the two amide protons at 8.12 and 8.08 ppm, the two α protons at 4.50 ppm and the two couples of β protons at 2.95 and 2.94 ppm. Whereas, as far as serine is concerned, it is possible to distinguish the amide, α and β protons at 8.33, 4.43 and 3.88 ppm respectively. Finally, the proline signals can be recognized thanks to the absence of any amide bond protons, since in the peptide sequence their secondary amino group forms a tertiary amide, and assignments could be done based on COSY spectrum (see Table 3.1).

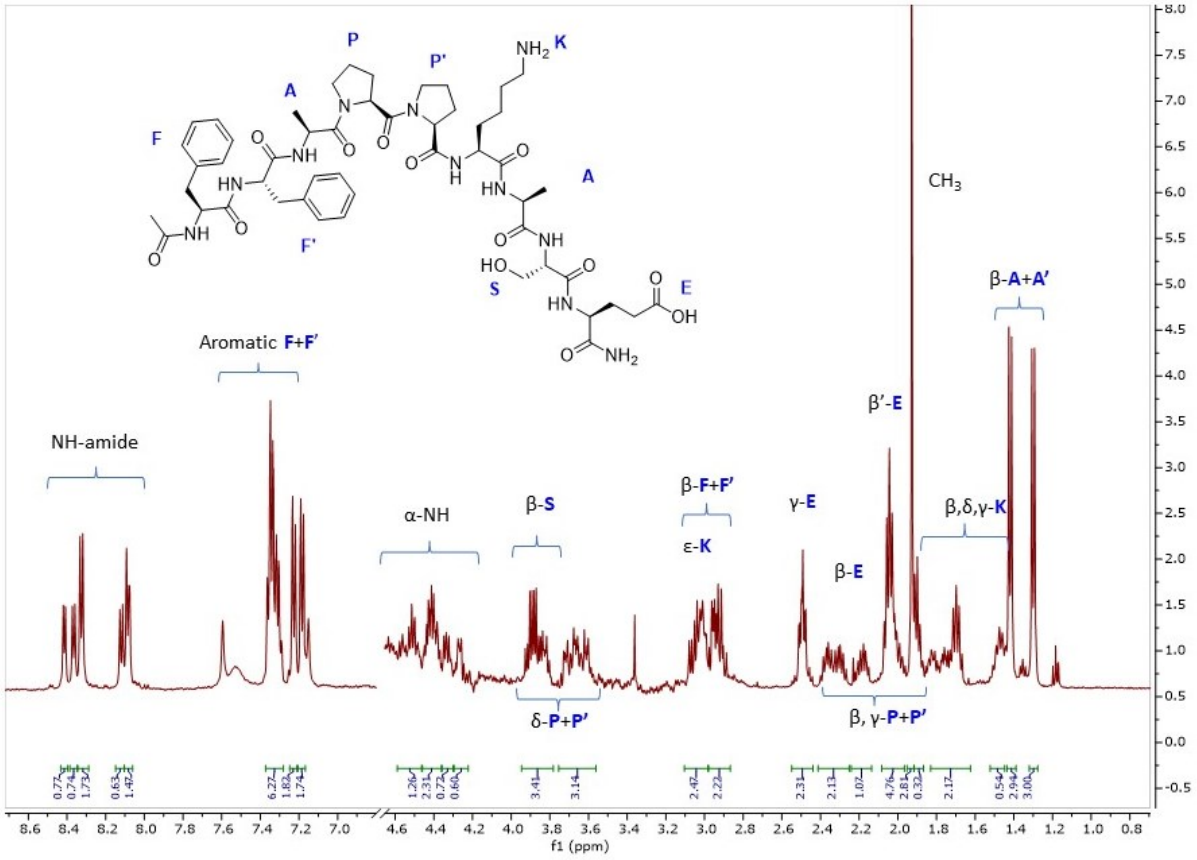

*Figure 3.24-^{1}H-NMR spectrum of **P1** (water + 10% D_2O).*

*Table 3.1- ^{1}H-NMR signals of **P1***

Amino acid	N-H ammide (δ)	α-NH (δ)	β-NH (δ)	γ-NH (δ)	δ-NH (δ)	ε-NH (δ)
A	8.08	4.57	1.30			
A'	8.42	4.33	1.42			
K	8.37	4.26	1.76, 1.81	1.47	1.70	3.02
E	8.33	4.39	2.01 2.18	2.49		
S	8.33	4.43	3.88			
F	8.12	4.50	2.95			
F'	8.08	4.50	2.94, 3.02			
P		4.42	2.30	1.91 2.04	3.67	
P'		4.42	2.30	1.91 2.04	3.82	

3.3.2.2 Peptide Ac-Phe-Phe-Ala-Glu-Ser-Lys-Ala-Ser-Glu-NH_2 (P2)

Looking at the mass spectrum of the purified peptide **P2** Ac-Phe-Phe-Ala-Glu-Ser-Lys-Ala-Ser-Glu-NH_2, it is clearly possible to observe the peak at the m/z ratio of 1054.6, corresponding to the $[M-H]^-$ adduct in negative mode (Figure 3.25), whereas in positive mode there is a signal at 1056.6 corresponding to the $[M+H]^+$ adduct.

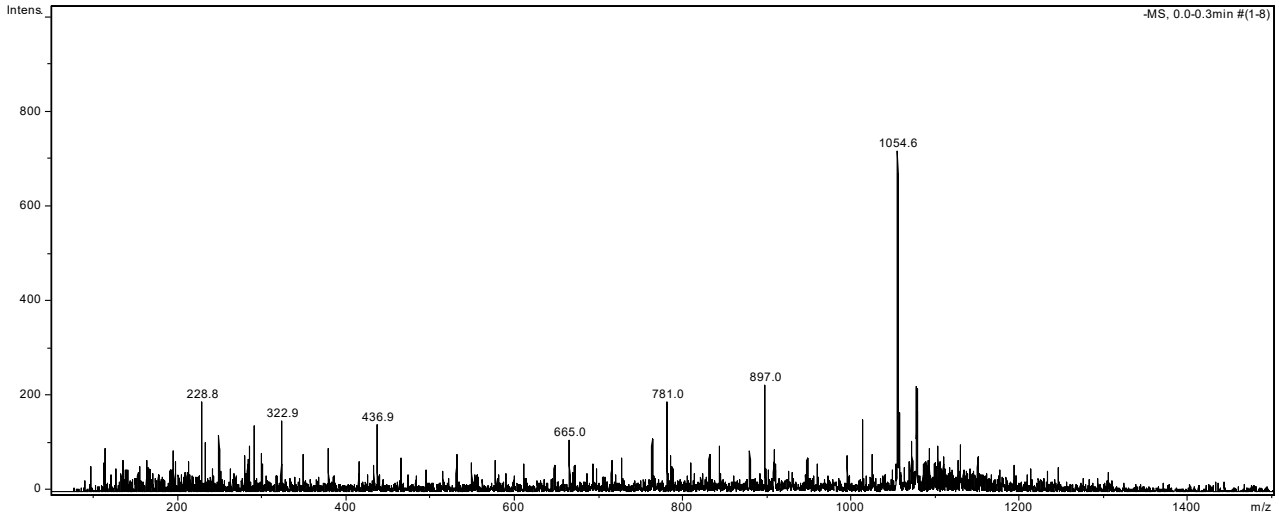

*Figure 3.25 -MS spectrum in negative mode of **P2.***

Also in this case, the NMR characterization of the peptide has been done by ^1H, ^1H-^1H COSY and ^1H-^1H TOCSY spectra, preparing the sample in water with 10% of deuterium oxide suppressing the water peak, as explained for **P1**. Signal assignments of the ^1H-NMR spectrum (Figure 3.26) have been done as explained for **P1** and are reported in Table 3.2.

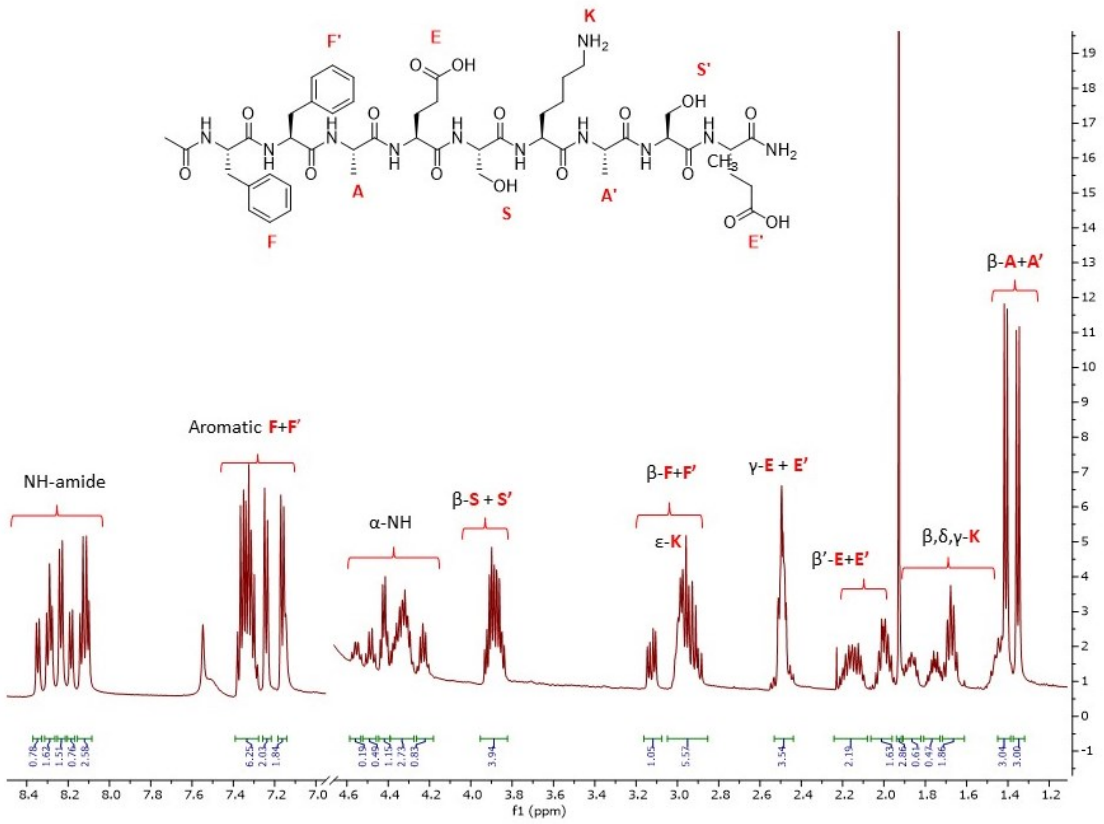

*Figure 3.26- ^1H-NMR spectrum of **P2** (water + 10% D_2O).*

*Table 3.2- ^{1}H NMR signals of **P2***

Amino acid	N-H ammide (δ)	α-NH (δ)	β-NH (δ)	γ-NH (δ)	δ-NH (δ)	ε-NH (δ)
A	8.10	4.23	1.35			
A'	8.28	4.31	1.41			
K	8.35	4.32	1.76 1.86	1.43	1.68	2.99
E	8.19	4.34	2.00 2.16	2.49		
E'	8.24	4.37	2.00 2.17	2.49		
F	8.12	4.55	3.12			
F'	8.13	4.48	2.95			
S	8.24	4.37	3.89			
S'	8.30	4.42	3.87			

3.3.3 Reactivity of the peptides towards CGA

Peptides reactivity in TBA pigment formation has been tested with CGA, to see if there is any structural effect on the reactivity of the peptides. A kinetic measurement has been made, reacting 0.19 mM CGA with a ten-fold excess of each peptide (1.9 mM) in 19 mM carbonate buffer at pH 9. In the case of **P1**, it is possible to distinguish a linear range over the first 960 s of reaction, while a plateau is reached in around 1 hour and a half. (Figure 3.27 a) Also the kinetics of **P2** presents a linear range in the first 960 seconds of reaction, but in this case the absorbance continues to increase without reaching a plateau in the time explored (Figure 3.27 b).

By taking the slopes of the first 960 seconds of reaction, linear correlations in equations 3.7 and 3.8 have been obtained:

P1: $Abs_{680nm} = 3.18 \cdot 10^{-5}\, t + 1.96 \cdot 10^{-2}$ (R^2=0.973) (Eq. 3.7)

P2: $Abs_{680nm} = 1.03 \cdot 10^{-5}\, t + 1.25 \cdot 10^{-2}$ (R^2=0.951) (Eq. 3.8)

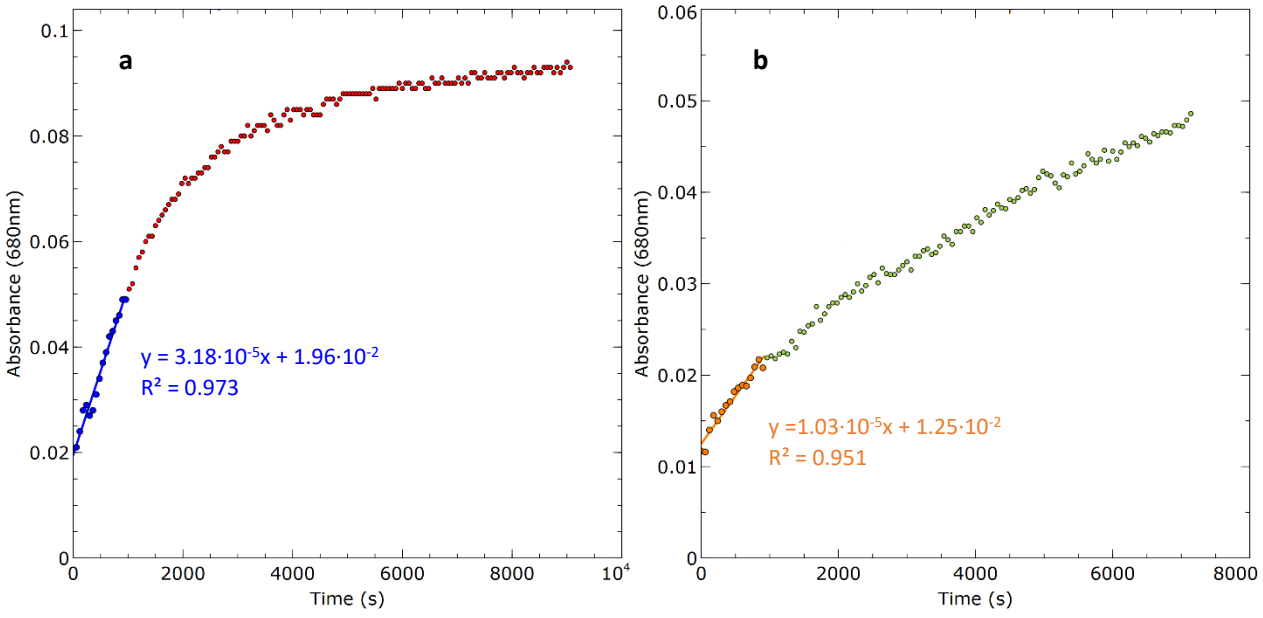

*Figure 3.27- Kinetics of reaction with CGA 0.19 mM of **P1** (a) and **P2** (b) at a 1.9 mM concentration in carbonate buffer 19 mM (pH 9).*

The reaction of **P1** is about 3 times faster than that of **P2**. Since the rates cannot be directly compared with that previously measured with lysine, as in this experiment the concentration of peptides is ten times lower, a kinetic measurements using lysine at the same concentration (1.9 mM) revealed that the structure of **P1** (Figure 3.27 a) slightly increases the initial reaction rate with respect to *N*α-boc-lysine alone (Figure 3.28), whereas **P2** makes the reaction somewhat slower (Figure 3.27 b).

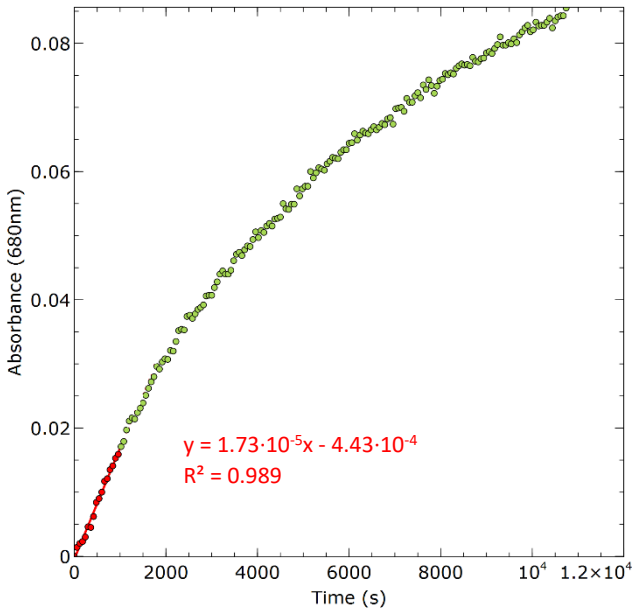

Figure 3.28- Kinetics of reaction with CGA 0.19mM of Nα-boc-lysine at a 1.9 mM concentration in carbonate buffer 19 mM (pH 9).

In order to establish if there is the possibility to discriminate between CGA and another caffeic acid ester, kinetic measurements were performed by reacting **P1** and *N*α-boc-lysine on both CGA and ethyl caffeate (EtCA). As it can be seen in Figure 3.29, for both lysine and **P1** the kinetic rates with EtCA are faster with respect to CGA, and no substantial difference in the performance of the two receptors can be distinguished.

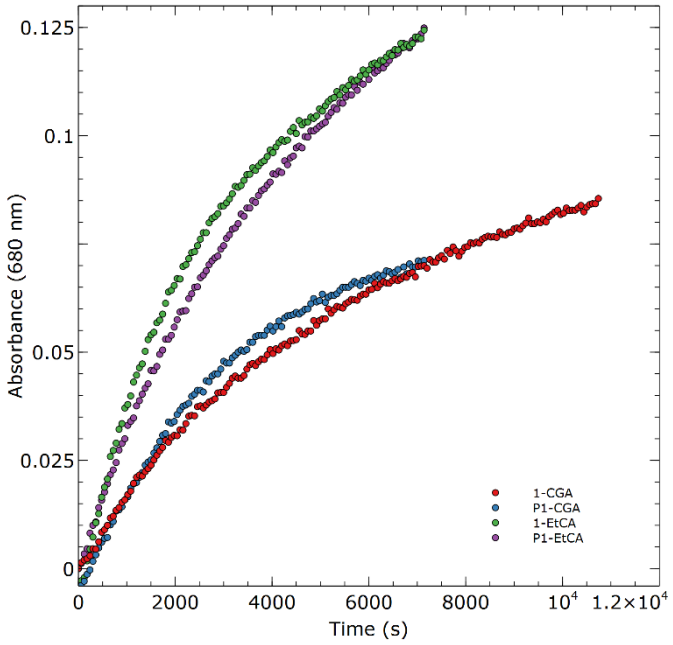

*Figure 3.29- Comparison between kinetics of reaction of **P1** and Nα-boc-lysine **1** with CGA and EtCA.*

To make a final evaluation of performance of **P1** and *N*α-boc-lysine, kinetics of reaction has been measured at different CGA concentrations during the first 20 minutes of reaction, with *N*α-boc-lysine and **P1** in a 10-fold excess with respect to CGA, having concentrations ranging between 24 µM and 190 µM, using carbonate buffer at a 19 mM concentration, pH 9. By making a plot of the slopes of the kinetics $\Delta A_{680}/\Delta t$ with respect to initial CGA concentration, it is possible to observe a linear correlation in both cases (Figure 3.30 a and b), with **P1** having the highest slope, even if correlation is worse. However, these are only preliminary results, and replicates would be necessary to evaluate and compare the two performances.

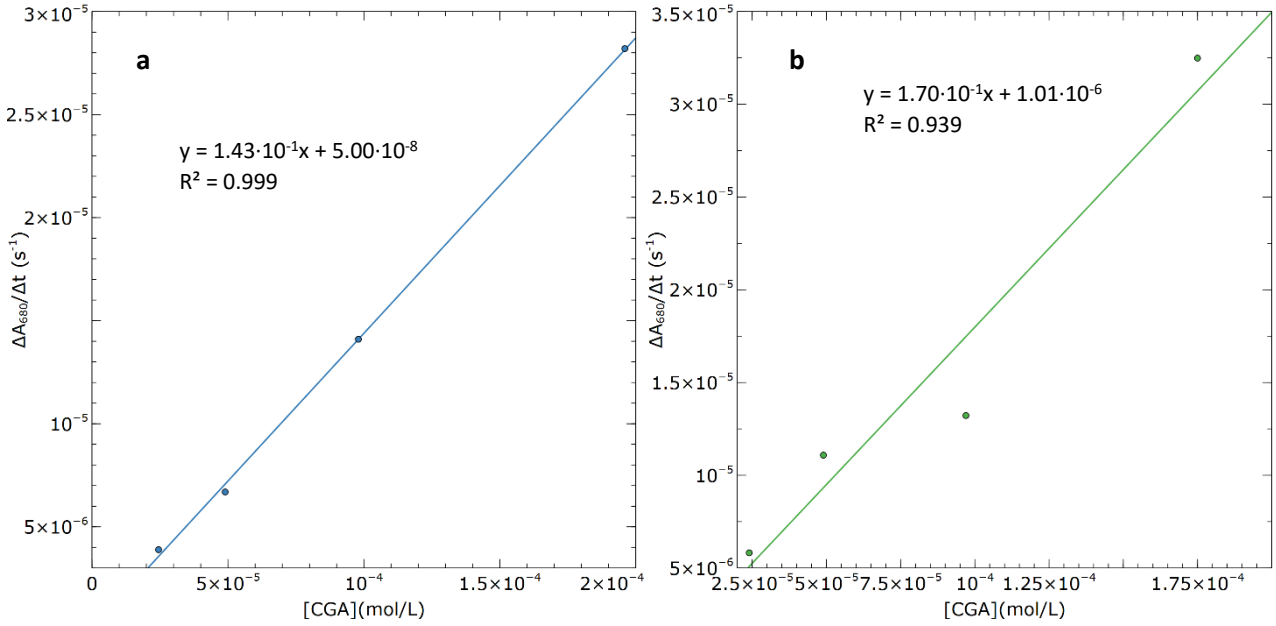

*Figure 3.30- Comparison of the kinetics of reaction of Nα-boc-lysine (a) and **P1** (b) at 1.9 mM concentration with CGA in carbonate buffer 19 mM.*

In conclusion, after testing the performance of the *N*α-boc-lysine system and verifying that the reaction is of pseudo-first order with respect to CGA concentration, two peptides containing a lysine residue have been developed, **P1** and **P2**: the reaction takes place with both peptides, but whereas **P2** seems to have a worse performance with respect to lysine alone, **P1** seems to work a bit better. After these preliminary tests, to fully explore the possibilities of using the formation of TBA pigments for CGA quantification purposes, the idea was that of applying it to polymeric films containing primary amino monomers.

3.4 DESIGN AND SYNTHESIS OF POLYMERIC FILMS

Another important application of the TBA pigment formation reaction, developed during the six-months period at Complutense University of Madrid at the Chemical Optosensors and Applied Photochemistry Group (GSOLFA),[vi] was the synthesis of polymeric films containing primary amino groups capable of reacting with CGA, taking inspiration from previous experience of the group. In fact, in 2016 the group developed polymeric films for detection of furfural in beer. In that case, polymers were prepared containing 2-hydroxyethyl methacrylate (HEMA) as a comonomer to increase the polymer hydrophilicity, ethylene glycol dimethacrylate (EGDMA) as crosslinker and 4-vinylaniline as reactive monomer capable of reacting with furfural by the Stenhouse reaction, resulting in red-pink coloration of the films due to the formation of covalent adducts with the target molecule. Quantification could be performed both with a portable optical fiber spectrometer or exploiting an app capable of analyzing pictures of the reacted membranes.[22] In the case of the TBA pigment, after assessing that the reaction does not take place with aromatic amines such as 4-vinylaniline employed in the above mentioned films for furfural sensing, the composition of the polymers had to be changed to contain aliphatic amino monomers. To do so, a new recipe has been tested taken from the article by Alvarez-Rivera and colleagues, in which the authors realized hydrogel contact lenses containing viral vectors to heal eye.[23] Despite the difference in the scope with respect to the original films, used for biomedical applications, such recipe has been chosen due to the presence in the composition of the amino-containing monomer *N*-(3-aminopropyl)methacrylamide (APMA), together with HEMA and the crosslinker EGDMA, using 2,2'-Azobis(2-methylpropionitrile) (AIBN) as radical initiator (Figure 3.31). The authors tested different polymer compositions, by changing the quantity of the amino monomer (see Table 3.3)

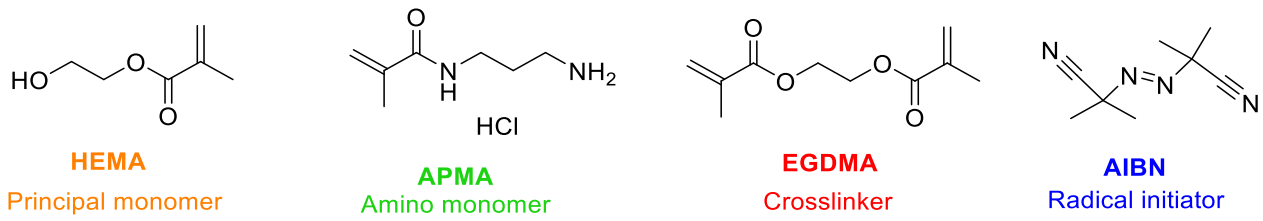

Figure 3.31- Components of the polymers prepared for CGA sensing.

Table 3.3-Compositions of the polymers synthesized by Alvarez-Rivera and colleagues [23]

Hydrogel	HEMA (mL)	EGDMA (µL/mM)	AIBN (mg/mL)	APMA (mg/mM)
H_C	3	45.20/80	4.93/10	0/0
H_1	3	45.20/80	4.93/10	21.40/40
H_2	3	45.20/80	4.93/10	42.80/80

A first test has been done starting from the composition containing the highest APMA concentration (composition H_2, APMA 80 mM) to test the performance of the films in CGA sensing. For synthesizing the films, the amino monomer APMA was first dissolved in 2 mL of HEMA, the principal monomer of the polymer, which also acts as the dissolving medium. Then, the radical initiator AIBN was dissolved in the crosslinker EGDMA and in the remaining volume of HEMA. The EGDMA-containing mixture was then added to the APMA-containing one, and the mixture was vortexed to obtain a homogeneous mixture. Then, the mixture has been flushed with nitrogen for 5 minutes, and it has then been injected with a syringe between two glass slides 10x10 cm separated by a 0.5 mm thick silicone frame. The mold has been put to polymerize in the oven at 70°C for 24 hours (Figure 3.32).

[vi] A six-months period has been spent at the GSOLFA group, under supervision of Prof. María Cruz Moreno Bondi, Prof. Elena Benito Peña and Prof. Guillermo Orellana Moraleda.

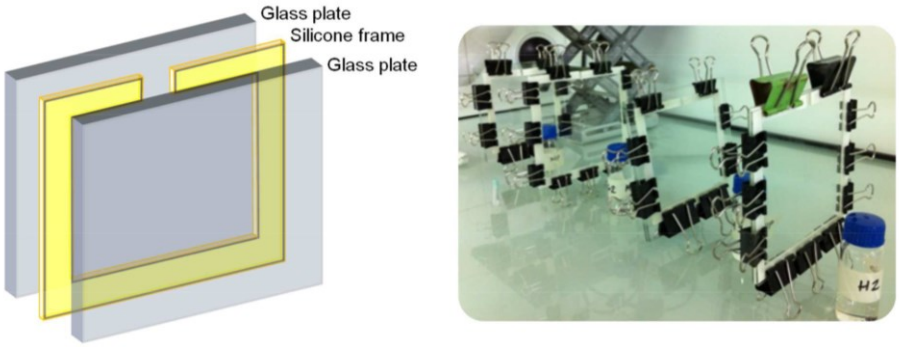

Figure 3.32- Schematic representation of the molds to obtain polymers (on the left) and picture of the sealed glass slides to be filled with the prepolymerization mixture.[22]

At the end of the polymerization process, the polymer has been removed from the glass slides and it has been submerged for 15 minutes in hot water to wash away all residual unreacted monomers. Then, it has been cut into discs (approximatively of the diameter of 5.5 mm) with a metal puncher.

To test the reactivity of the synthesized film, few discs have been submerged into a 2 mM CGA solution prepared in carbonate buffer at pH 9.5 and they have been left to incubate overnight. The day after, it was possible to observe a pale green coloring of the films, suggesting that the approach might be applied for CGA detection after increasing the amino-monomer content of the membrane to improve the response.

3.4.1 APMA polymers

The main problem to increase APMA concentration in the polymers is the fact that it is poorly soluble in HEMA (which is the diluent monomer but can also be considered as the solvent of the reaction), so different strategies have been evaluated to overcome this problem. The first idea was that of obtaining APMA, which is solid in the commercially available hydrochloride salt form, in the liquid deprotonated form. Unfortunately, several attempts to obtain APMA in the deprotonated form have been done, but they all failed: this was probably due to immediate Michael reaction occurring between the deprotected amino group of APMA and its conjugated double bond.

So, two other strategies have been considered:

-using succinimidyl methacrylate, which is more soluble in HEMA, instead of APMA, and then reacting the activated succinimidyl esters with ethylene diamine to obtain reactive primary amino groups;

- using DMSO as solvent to help solubilization of APMA hydrochloride.

The last strategy of using DMSO as co-solvent resulted to be successful and several polymer compositions have been tested (Table 3.4, Figure 3.33).

Table 3.4- APMA polymers compositions

Membrane	HEMA (mL)	DMSO (mL)	APMA (mg/mM*)	EGDMA (µL/mM*)	AIBN (mg/mM*)
Mp1	1.5	0.250	63.39/236	23/81.3	4.27/17
Mp2	1.5	0.500	216.6/808	23/81.3	4.3/17
Mp3	0.750	0.375	53.7/401	11.3/79.9	2.39/19.4
Mp4	1.0	0.167	42.8/240	150.7/799	4.85/30.0
Mp5	1.0	0.333	143.4/803	150.7/799	5/30.5
Mp6	0.750	0.375	53.87/402	56.5/399	2.3/18.7
Mp7	0.750	0.375	107.28/801	33.9/240	2.55/20.7

*All the concentration values are calculated with respect to HEMA volume only

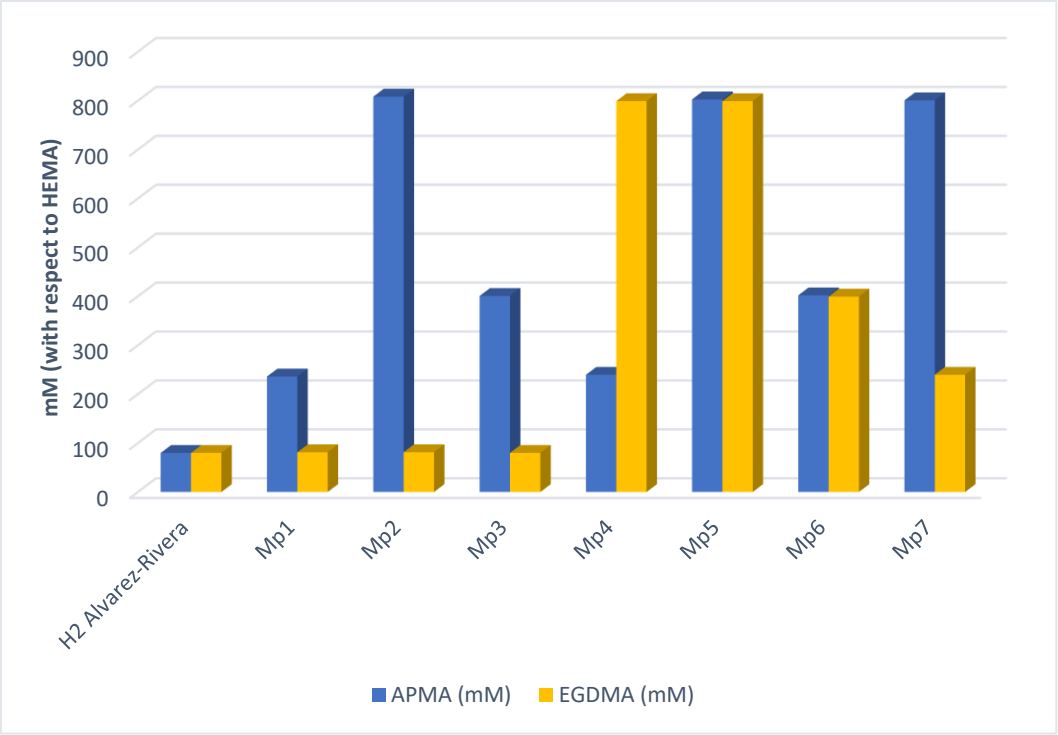

Figure 3.33- Comparison between APMA polymers compositions in terms of mM concentrations (calculated with respect to HEMA volume only).

The obtained discs (preserved in water to keep them hydrated) have been used in a preliminary kinetic experiment to test their reactivity with CGA. Three discs for each composition have been put in three wells of a multiwell plate (measurement has been done in triplicate) and to each well 200 µL of a 2 mM CGA solution in carbonate buffer (pH 9.5) have been added. A multiwell plate reader has been used to measure at regular timepoints the absorbance at 680 nm of the green TBA pigments that form upon reaction of the primary amino groups of the discs with CGA present in solution (Figure 3.34). The wells have been scanned using a "map mode", taking a 15x15 points-grid at 680 nm for each well: this is the best option to analyze solid samples. A measurement has been taken at time 0 (t_0), immediately after adding CGA to the discs, and then the kinetics of the reaction has been monitored, observing a progressive increase in green color formation (and thus increased absorbances at 680 nm). Since discs have a diameter smaller than that of the wells, the map-mode of monitoring has the advantage of allowing to distinguish exactly the position of the discs, so that only the area of each well in which the disc is present can be considered. Selected points have then been processed removing outliers by using Box-Plot analysis method,[24] finally obtaining the mean absorbance value for each disc at a certain time point. Polymers giving the best results working in kinetic mode (2 mM CGA) have been evaluated also at different CGA concentrations. To do so, also in this case discs have been placed in the wells of a multiwell plate and solutions at different CGA concentrations (2 mM, 1 mM, 0.5 mM and 0.25 mM always working in carbonate buffer at pH 9.5) have been added: a measurement has been taken immediately after CGA addition to the wells (t_0), then measurements have been repeated after a certain time of incubation (usually 60 or 90 minutes), correlating absorbance at 680 nm with CGA concentration. After data processing carried out as previously explained, absorbance values at a certain time point (t_x) were corrected subtracting to each replicate for each concentration (c_x) the absorbance at the corresponding t_0, considering that it can be a bit different amongst replicates and for the different CGA concentrations considered. Corrected absorbance values have then been averaged (see equation 3.9)

$$\text{Average corrected absorbance } (t_x, C_x) = \text{Average } [\text{Abs } (t_x, C_x)_{\text{replicate x}} - \text{Abs } (t_0, C_x)_{\text{replicate x}}] \quad \text{(eq. 3.9)}$$

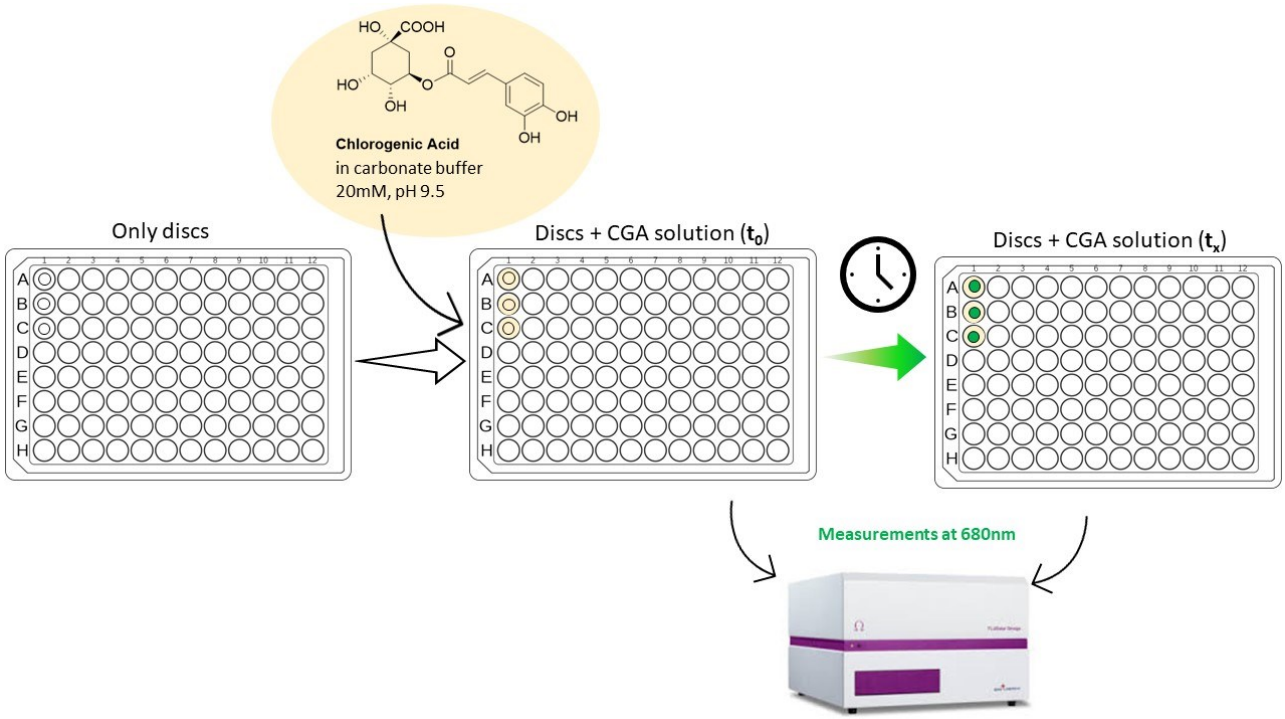

Figure 3.34- Scheme of the multiwell plate assay to monitor change in absorbance of the polymeric discs.

Considering composition **Mp1**, containing a 3-fold excess of APMA monomer with respect to the starting composition H_2,[23] from the kinetics point of view as it can be seen in Figure 3.35 a, the color increases following a linear trend in the first 90 min, whereas for longer times there is a change in the slope and the kinetics of reaction slows down. Considering analyses at different CGA concentrations, a very good linear relationship was obtained after 60 minutes of reaction (Figure 3.35 b).

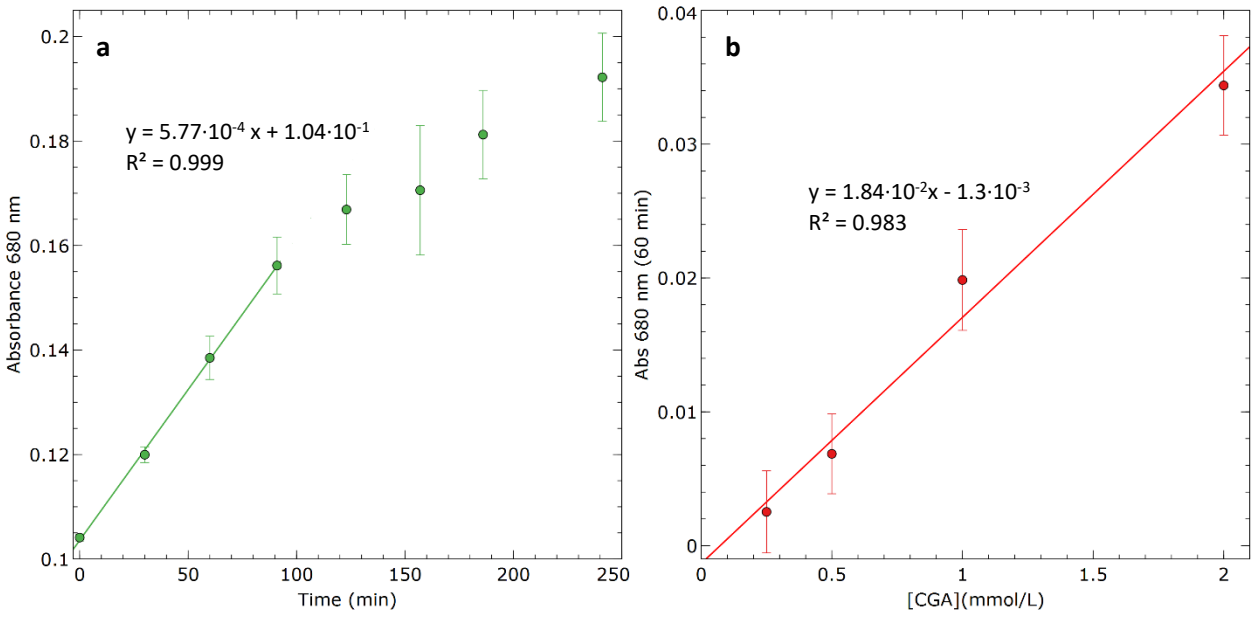

*Figure 3.35- (a) Kinetics of **Mp1** at 2 mM CGA; (b) correlation between absorbance at 680 nm (60 min) of **Mp1** and CGA concentration.*

Considering composition **Mp2**, having a ten-fold excess of APMA monomer with respect to the original recipe H_2 while having the other reagents in the same quantity, due to the high amino-monomer content, it was observed that after polymerization some white crystal formed on the surface of the membrane when

removing it from the glass slides. However, such crystals were removed by simply scratching the membrane surface with a spatula. Then, discs were cut as usual. With the new composition the discs resulted much less rigid and tended to largely swell when preserved in water: for this reason, they had to be cut a second time to fit the wells dimensions before proceeding with the spectrophotometric experiments. Probably, this is due to the fact that the amino monomer content was increased, while leaving crosslinker concentration unchanged: in this way, the crosslinking degree diminished, and softer polymers were obtained. The kinetic study performed with 2 mM CGA concentration allowed to observe a good linearity that extends all over the time points analyzed. In addition, the slope of the curve is higher with respect to results obtained with the **Mp1** composition, and this is consistent with the higher amino monomer content (Figure 3.36). However, when testing the performance of **Mp2** discs at 2 mM, 1 mM, 0.5 mM and 0.25 mM, increasing incubation to 90 minutes to try to increase sensitivity, no good linear correlation could be observed, as well as a huge variability amongst replicates. Moreover, the biggest issue of this composition is the fact that, despite the use of DMSO as solvent, APMA has solubility problems at high concentrations, and this causes irreproducibility of the membranes (with formation of crystals for example). The second big issue is the fact that these discs are very soft, and this is a negative aspect because they are much more fragile and tend to break.

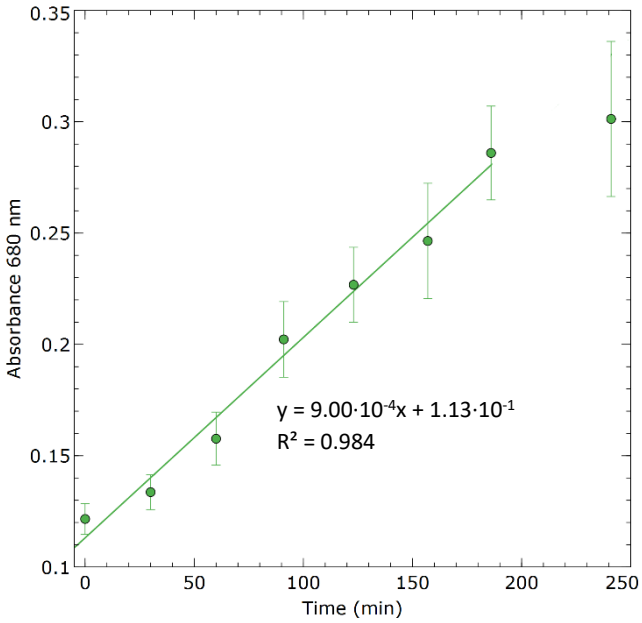

*Figure 3.36- Kinetics of **Mp2** at 2 mM CGA.*

Considering the intermediate composition **Mp3**, containing a 5-fold excess of APMA with respect to the starting composition, measuring the kinetics with 2 mM CGA concentration, it seems that performance is quite similar to the one obtained with **Mp1**, but with a linear range extending until 200 minutes of reaction (Figure 3.37). However, making the experiment at the different CGA concentrations after 90 minutes of reaction, differently from **Mp1**, no good correlations could be found, with very high variability between replicates.

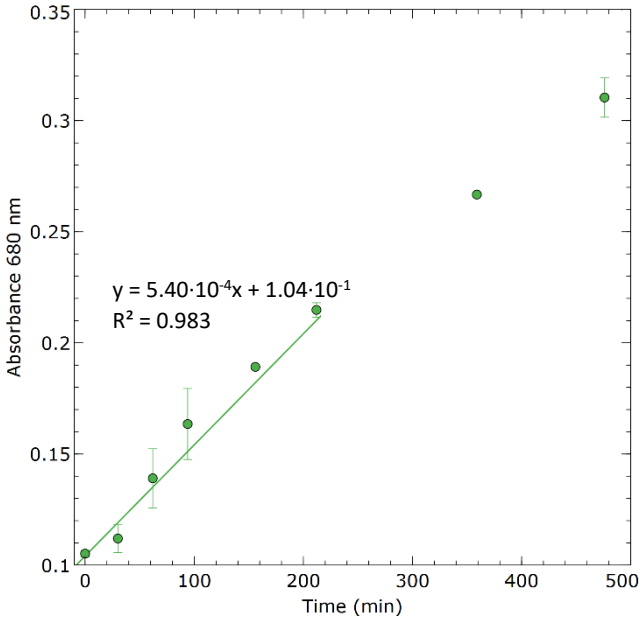

*Figure 3.37- Kinetics of **Mp3** at 2 mM CGA.*

After testing compositions in which only APMA monomer content has been changed while maintaining the same crosslinker amount (calculated with respect to the HEMA content), other polymers have been synthesized increasing the crosslinker content, to try to improve rigidity of the polymers and to investigate if this can have positive effects on performance and mechanical properties of the membranes.

Polymer **Mp4** (3-fold APMA, 10-fold EGDMA with respect to H_2 composition) seemed to be very rigid when it was removed from the glass slides and when performing the kinetics at 2mM CGA concentration, results were not very good, with a very little slope.

For polymer **Mp5** (10-fold APMA, 10-fold EGDMA with respect to H_2 composition) some solubility problems with APMA have been encountered, it was not possible to dissolve it completely, and this is a problem because in this way the composition is not reproducible. After the 24 hours of polymerization white crystals were clearly visible on the surface of the polymer, which could be removed by gently scratching the surface of the film (as it happened for **Mp2**). In this case, the polymer resulted to be flexible but resistant: after washing and cutting into discs, a kinetics experiment has been done but with no satisfactory results.

As for polymeric film **Mp6** (5-fold APMA, 5-fold EGDMA with respect to H_2 composition), while the wet film was quite flexible, it became more rigid when getting dry. Also, the color was quite strange, it appeared sort of opaque white (not only crystals as it happened in other cases). Slope in kinetics was not satisfactory, and the discs were discarded also because they were not transparent.

Considering composition **Mp7** (10-fold APMA, 3-fold EGDMA with respect to H_2), when film was removed from the glass slides, it was possible to observe the presence of white crystals as for **Mp2** and **Mp5**, but this time they could not be removed simply scratching the surface because they were embedded into the polymer: due to this inhomogeneity, also this composition was discarded.

3.4.2 AEM polymers

After synthesizing different polymers with the amino monomer APMA, with non-completely satisfactory results, the choice was that of investigating the performance of another amino monomer, 2-aminoethyl methacrylamide (AEM), with a shorter carbon chain (Figure 3.38).

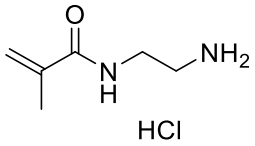

AEM

Figure 3.38- Structure of the amino-monomer 2-aminoethyl methacrylamide (AEM).

From previous results of the APMA polymers, compositions **Me1** and **Me2** were analogue to **Mp1** and **Mp3** respectively, those performing better (**Mp2** was discarded because the consistence is too soft). Moreover, **Me3** composition has been added, quite similar to **Me2** but containing more crosslinker (Figure 3.39, Table 3.5).

Table 3.5 Composition of AEM polymers

Membrane	HEMA (mL)	DMSO (mL)	AEM (mg/mM)*	EGDMA (µL/mM)*	AIBN (mg/mM)*
Me1	1.5	0.250	59.37/237	23/80.0	4.41/17.6
Me2	1.5	0.750	98.85/394	23/78.7	3.5/14.0
Me3	1.5	0.750	98.84/394	67.8/236	3.39/13.6

*All the concentration values are calculated with respect to HEMA volume only

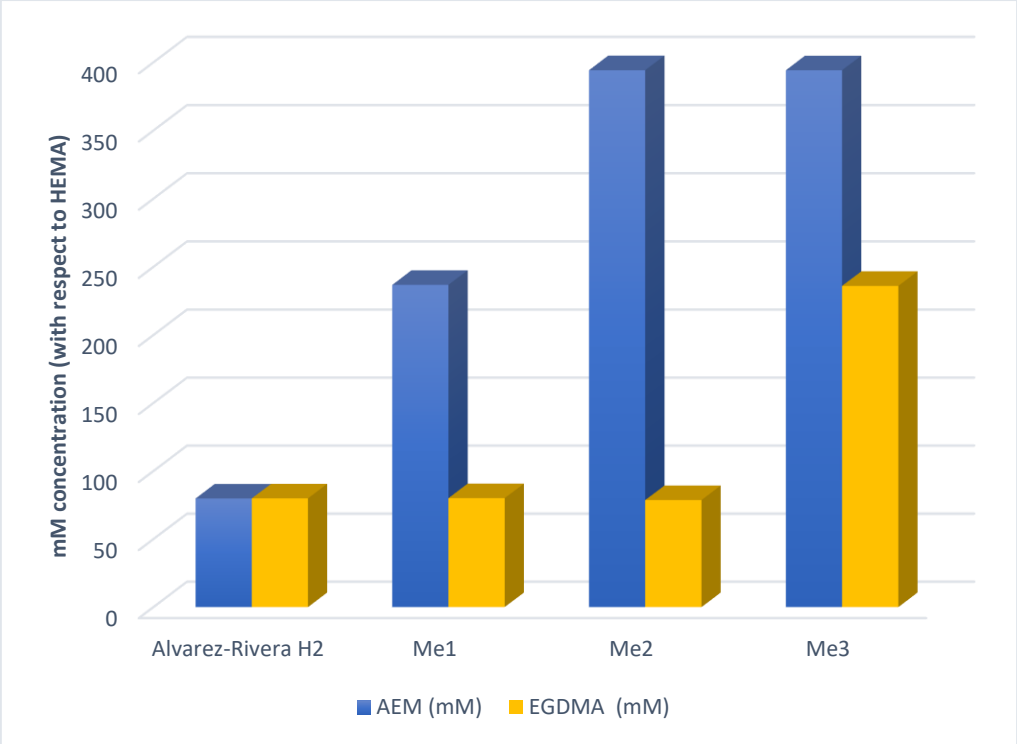

Figure 3.39- Comparison between AEM polymers compositions in terms of mM concentrations (calculated with respect to HEMA volume only).

Measuring kinetics of **Me1** discs with 2 mM CGA, there is a good linear relationship (Figure 3.40 a), but the slope is halved with respect to the one obtained with **Mp1**. Considering measurements at different CGA concentrations after 90 minutes of incubation, after correction for t_0, a slope slightly lower with respect to the one obtained with **Mp1** has been obtained, with a bit worse correlation in terms of reproducibility of results (even if R^2 is better) (Figure 3.40 b).

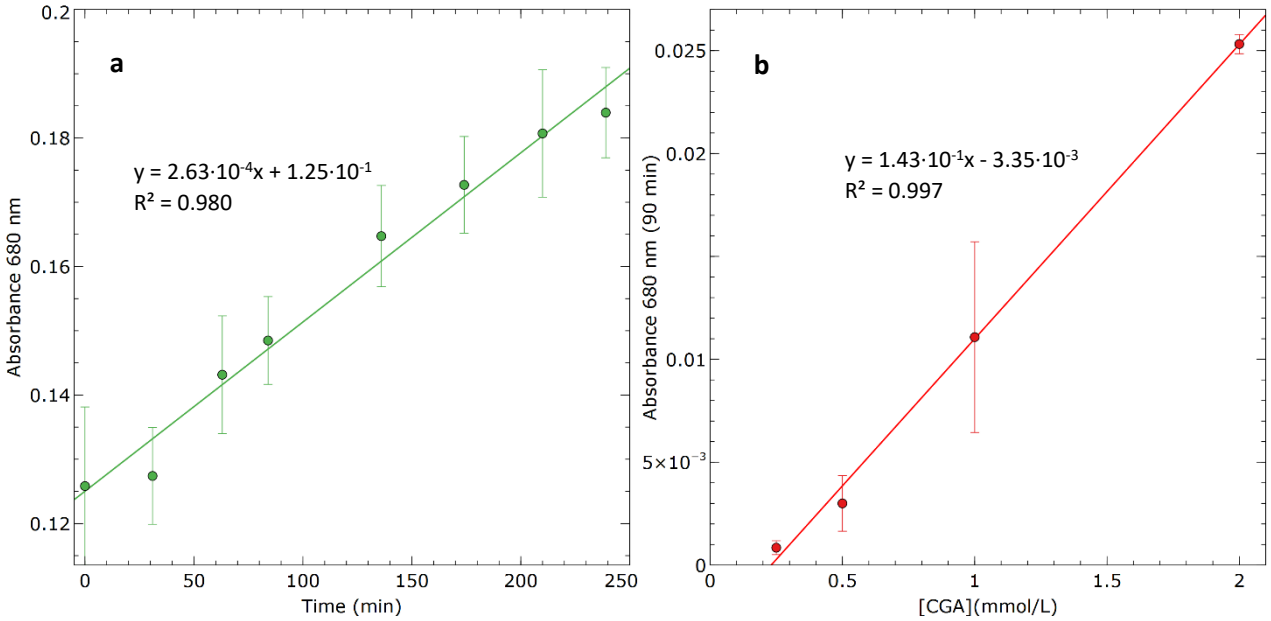

*Figure 3.40 (a) Kinetics of reaction of **Me1** with 2 mM CGA; (b) Absorbance at 680 nm (90 min) vs. CGA concentration of **Me1**.*

Moving to the **Me2** composition, it is the counterpart of **Mp3** having the ethyl monomer, thus allowing to compare performances of the APMA and AEM monomers with a different polymer composition with respect to the **Mp1**/**Me1** couple.

Considering **Me2** discs, the 2 mM kinetics is very good, comparable to the one from **Mp1** and **Mp3** in terms of reproducibility and slope (Figure 3.41 a). Considering the analyses in non-kinetic mode at different CGA concentrations, good correlations could be obtained taking corrected absorbance values after 90 minutes of reaction (Figure 3.41 b). The 2 mM concentration deviates from linearity, but taking into account only the three lower concentrations, there seems to be the perspective of a good linear correlation, even if more points should be taken into account, at concentrations lower than 1 mM. This composition seemed to be quite promising.

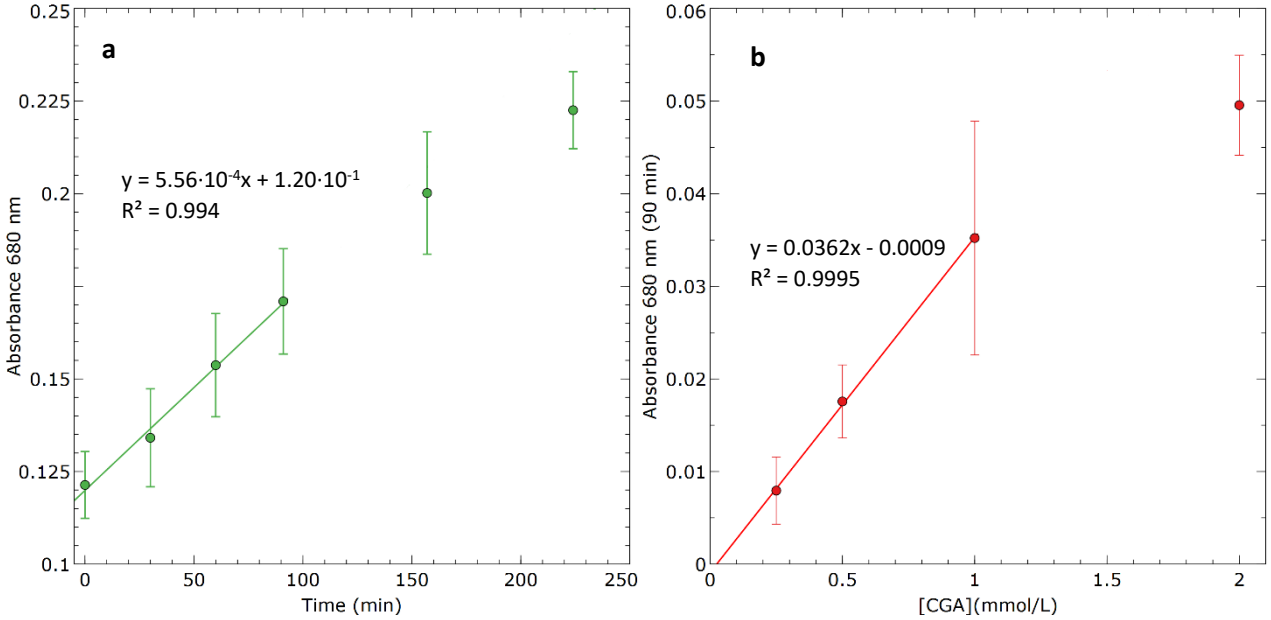

*Figure 3.41(a) Kinetics of reaction of **Me2** with 2 mM CGA; (b) Absorbance at 680 nm (90 min) vs. CGA concentration of **Me2**.*

As a last attempt, a new polymer composition has been tested, similar to **Me2** but with slightly more crosslinker (5-fold APMA, 3-fold EGDMA with respect to H_2 composition). The kinetics results of this new composition are quite good, with good linear range for the 2 mM CGA concentration (Figure 3.42 a). Also the non-kinetic measurements are quite good (Figure 3.42 b), but not as much as the **Me2** ones, so the **Me2** composition has been selected for further analyses.

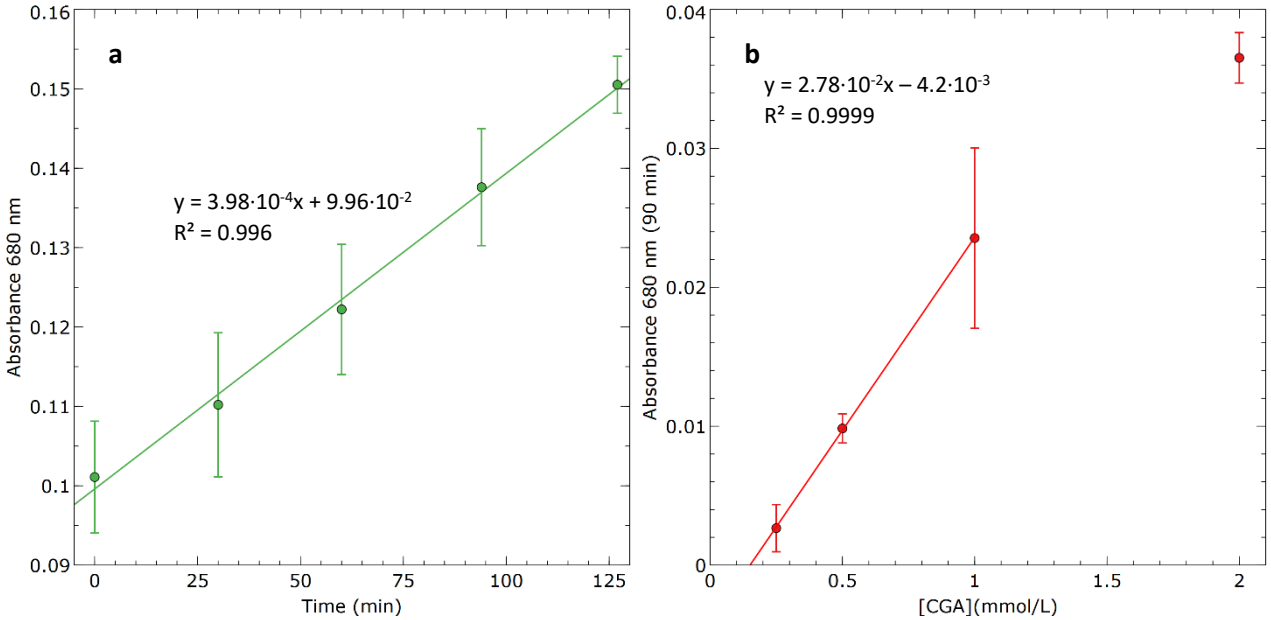

*Figure 3.42-(a) Kinetics of reaction of **Me3** with 2 mM CGA; (b) Absorbance at 680 nm (90 min) vs. CGA concentration of **Me3**.*

Experiments on **Me2** have been repeated also on discs dried in vacuum oven, because drying the membranes might be a good way to preserve them for longer times, and starting from a dry material might also increase the capability of reaction with the target. Kinetics results at 2, 1, 0.5 and 0.25 mM CGA concentrations were quite good, even better than those of the wet membranes, provided that a 10 min rehydration time is allowed before starting the measurements (Figure 3.43 a). Considering the non-kinetic measurements, they seemed to be good, with good linear correlations taking into account both the 60 and 90 minutes incubation times. In this case, also the 2 mM concentration is in the linear range (Figure 3.43 b).

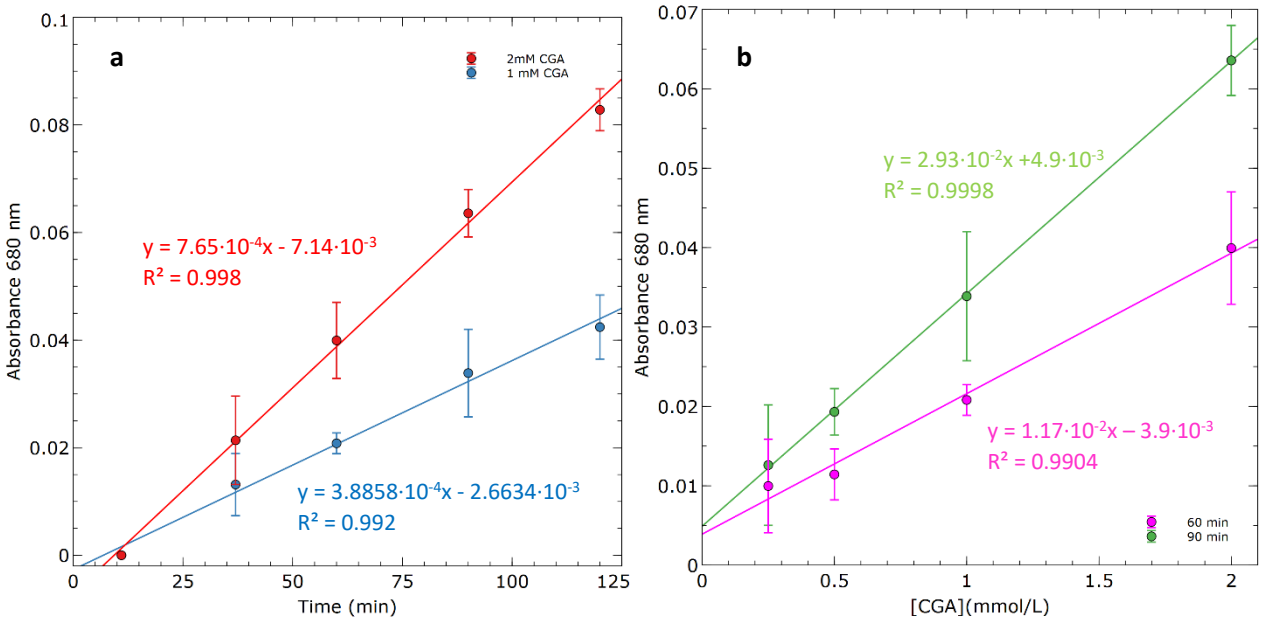

*Figure 3.43- (a) Kinetics of reaction of **Me2** dried in vacuum oven at 2 mM and 1 mM CGA concentration; (b) Absorbance at 680 nm (60 and 90 min) vs. CGA concentration of **Me2** dried in vacuum oven.*

3.4.3 Tests on portable devices

The performance of polymeric discs **Me2** has been tested also on portable devices.

First of all, discs were analyzed using an optical fiber spectrometer[vii] (Figure 3.44). The instrument is composed by a LED illuminator as a light source, a bifurcated optical fiber with randomly distributed fibers and a portable spectrometer for detection. Discs cut with a 10 mm puncher, larger than those used for the multiwell plate reader measurements, seemed to be more suitable for this type of measurement, so that the edge of the optical fiber, directly placed on the membrane can completely cover it. Since the optical fiber must completely adhere on the discs surface that must be pressed, it is important that membranes are left to dry after incubation in CGA so they become more resistant to avoid they can smash under the fiber. In all the cases, a white sheet of paper has been used as a background on which putting the membranes for measurements with optical fiber.

[vii] Experiments were carried out at the GSOLFA group, at Complutense University, Madrid.

Figure 3.44 -General scheme of the optical fiber spectrometer.[25]

A test has been done by incubating membranes **Me2** cut with the 10 mm puncher in solutions of CGA at concentrations 1 mM, 0.5 mM, 0.4 mM, 0.3 mM, 0.2 mM, 0.1 mM in carbonate buffer 20 mM at pH 9.5. Three membranes were incubated for 1 hour in 10 mL of each CGA solution at the different concentrations. Three membranes have also been incubated in 10 mL of carbonate buffer without CGA to be used as the reference. After incubation, membranes were dried for around 10 minutes and then were analyzed with the optical fiber. As the blank the membranes incubated in only carbonate buffer, with no CGA, have been used. Since spectra taken with the optical fiber are not aligned, correction has been done taking for all the spectra the absorbance value at 590 nm, where there is an isosbestic point, and subtracting it to absorbance values at all the wavelengths of the corresponding spectrum, to report all the spectra at the same baseline level (Figure 3.45 a). Then, corrected absorbance values at 691 nm have been taken and correlation with CGA concentration has been extrapolated (Figure 3.45 b). In this case it seems that linear correlation is good (Eq. 3.10), even if reproducibility amongst replicates is non optimal and spectra are very noisy.

$$Abs_{680} = 51.8[CGA] + 0.0032 \ (\mathrm{R}^2 = 0.9961) \qquad \textit{(Eq. 3.10)}$$

Also in this case it has been possible to calculate the LOD (Eq. 3.11) and LOQ (Eq. 3.12) according to the ICH guidelines.[13]

$$LOD = \frac{3.3\sigma}{m} = \frac{3.3\times0.004041}{51.8} = 2.58 \cdot 10^{-4}\ mol/L \qquad (\textit{Eq. 3.11})^{viii}$$

$$LOQ = \frac{10\sigma}{m} = \frac{10\times0.004041}{51.8} = 7.81 \cdot 10^{-4}\ mol/L \qquad (\textit{Eq. 3.12})^{viii}$$

[viii] Where *m* is the slope of the curve and σ is the standard deviation calculated on 3 blank samples.

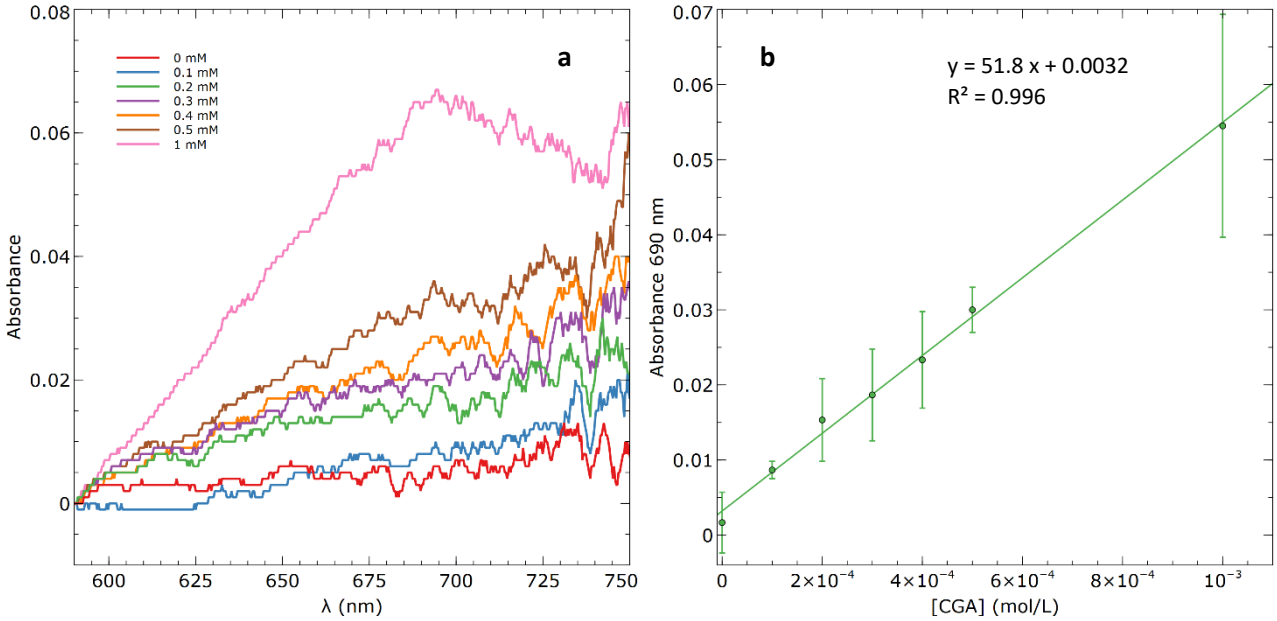

*Figure 3.45 – (a) Spectra of **Me2** discs incubated at different CGA concentrations taken with the optical fiber spectrometer; (b) Correlation between absorbance at 680 nm of **Me2** and CGA concentrations.*

After obtaining promising preliminary results with the optical fiber device, some further experiments have been carried out exploiting two portable in-lab built devices.[ix]

The image reader instrument is composed by a high-resolution USB camera positioned on the top of a 3D-printed white box with a central holder to place membranes and red (λ = 675 nm) and green (λ = 520 nm) LEDs all around to illuminate the inner part of the closed box. The images from the camera are analyzed by using the software "JustColorPicker", which is capable of identifying the Red-Green-Blue components of an image (Figure 3.46).

Figure 3.46- Image reader in-lab built device.

The second device is a pseudo differential reflection spectrophotometer, composed by two LED sources operating at the wavelengths of interest at λ =675 nm and λ=860 nm (also serving as the reference), and an optical fiber mixer collimating the two sources on a white diffusive surface of reference. The two optical

[ix] The in-lab built devices have been developed by a team of engineers, composed by Prof. Antonio Boscolo and Prof. Agostino Accardo of the Department of Engineering and Architecture of the University of Trieste, and Dott. Giuseppe Boscolo of the Company GRUPPO TECNICHE AVANZATE.

sensors are positioned so that the light emitted by the light sources (sensor 1) and light retro diffused by the sample (sensor 2) can be measured. The sample slot is white, whereas all the rest of the surfaces are black (Figure 3.47).

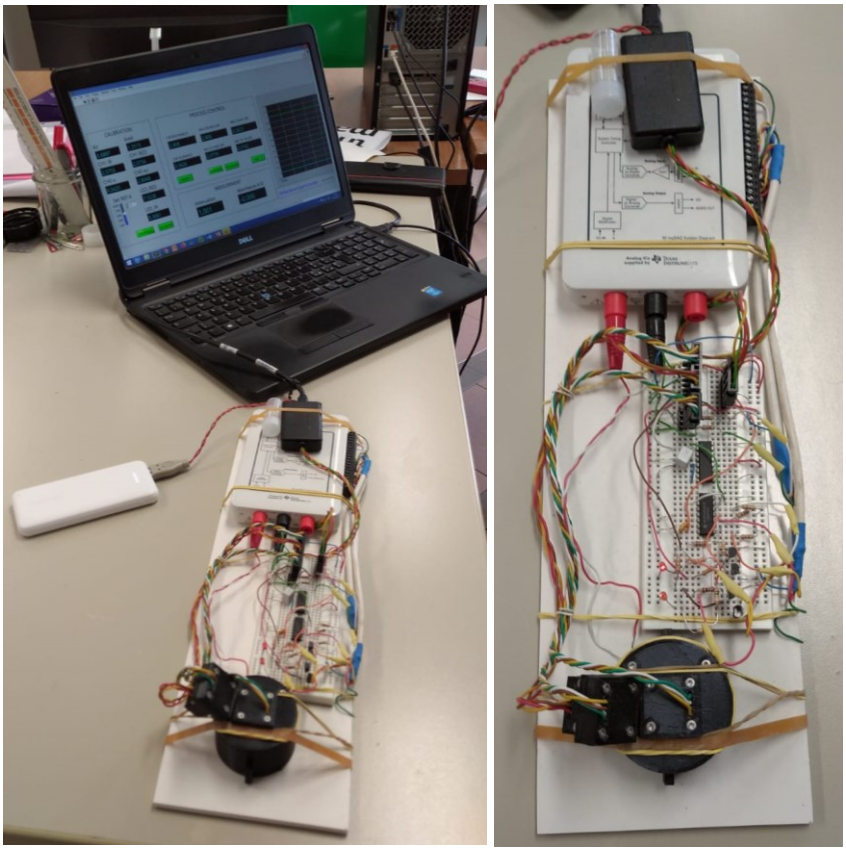

Figure 3.47- Pseudo differential reflection spectrophotometer.

Before evaluating the analytical performances of the two devices, a first test has been carried out by incubating the discs of composition **Me2** (dried in vacuum oven) in 5 vials, each one containing 5 mL of a 2 mM CGA solution prepared in 20 mM carbonate buffer, pH 9.5. Each of the vials has then been treated in a different way:

- vigorous magnetic stirring;
- sonication in a bath;
- bubbling with compressed air to increase the oxygen availability;
- heating at 95°C under stirring;
- addition of hydrogen peroxide as an oxidant, under stirring.

A blank has been prepared reacting a membrane in carbonate buffer, without CGA.

After 35 and 80 minutes of incubation, the discs have been analyzed using the image reader. 11 points have been taken in a cross-like shape for each sample, and for each point the red component has been subtracted to the green one (G-R); then, after subtracting the G-R value for the blank, the average between all the values has been done.

After 35 minutes of reaction all the membranes had already developed a green color and looking at the G – R values, it is possible to see that sonication and simple stirring seem to be the best treatments to obtain green color formation (Figure 3.48).

Repeating the same analysis after 80 minutes of reaction, it is possible to see that all the G-R values increased (apart for the hydrogen peroxide solution for which membranes colored very poorly with a more yellowish

shade), and sonication and stirring confirmed to be the best treatments to obtain more reactivity of the discs (Figure 3.48). Pictures of the discs after 80 minutes of reaction are reported (Figure 3.49). So, for further experiments it has been decided to use simple stirring, since sonication does not significantly improve the performance and introduces a more complicated element in sample treatment.

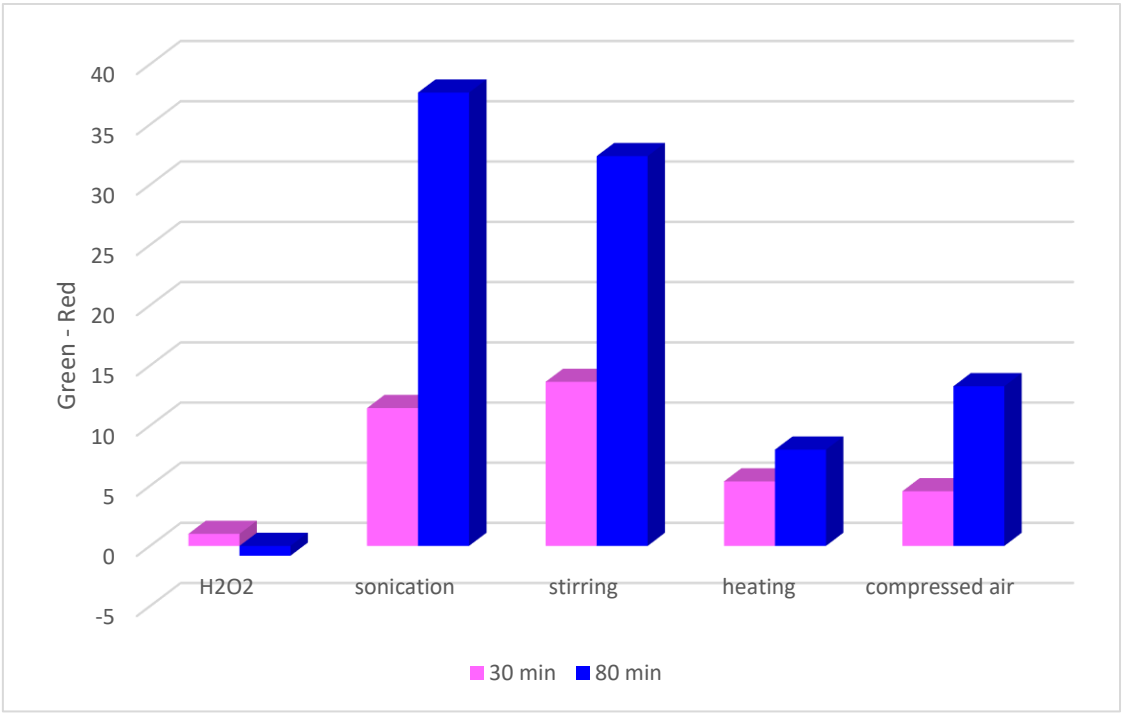

*Figure 3.48- Evaluation of membrane **Me2** reaction conditions by using image reader.*

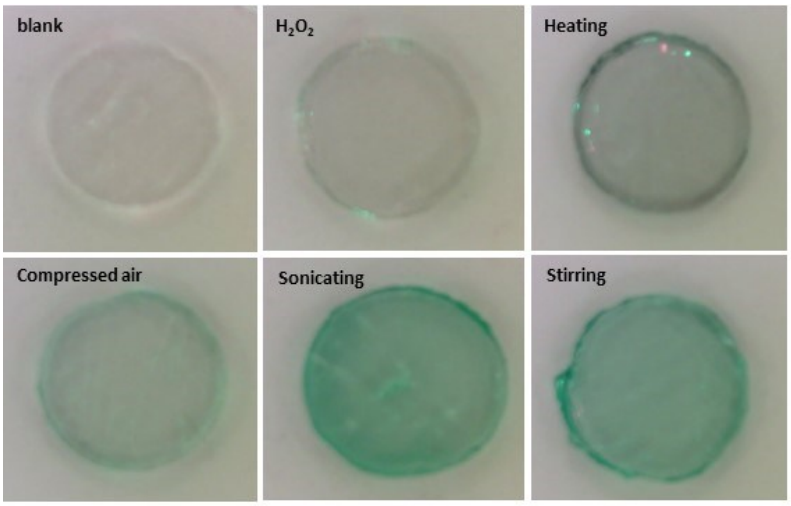

*Figure 3.49- Pictures of **Me2** discs after 80 minutes of incubation in different reaction conditions.*

Once assessing the best conditions for green color development, a test has been carried out incubating **Me2** discs at different concentrations of CGA under magnetic stirring for 1 hour, and then analyzing them with both instruments, to compare their analytical performances. The experiment has been carried out in triplicate, and as a reference three discs have been incubated with only carbonate buffer, without CGA.

Discs have been first analyzed by using pseudo differential reflection spectrophotometer: it has been observed that complete drying of the membranes is necessary, otherwise absorbance values keep changing with the time. By plotting the absorbance values against CGA concentration, a good linear correlation could be found, also with good reproducibility (Figure 3.50 a).

Then, membranes have also been analyzed with the image reader, taking 16 points for each membrane, and then G-R components of each point have been analyzed. Also in this case a good linear correlation could be found, and results from the two instruments appear comparable (Figure 3.50 b).

Based on the linear correlations found for both the pseudo differential reflection spectrophotometer (Eq. 3.13) and the image reader (Eq 3.16), LOD and LOQ values have been calculated according to the ICH guidelines (Eq. 3.14 and 3.15 for the spectrophotometer, 3.17 and 3.18 for the image reader).[13]

- pseudo differential reflection spectrophotometer

$$Abs_{680} = 8.79 \cdot 10^{1}[CGA] + 0.00611 \ (\mathrm{R}^2 = 0.991) \quad \textit{(Eq. 3.13)}$$

$$LOD = \frac{3.3\sigma}{m} = \frac{3.3\times0.001}{87.9} = 3.75 \cdot 10^{-5}\ mol/L \quad \textit{(Eq. 3.14)}^{x}$$

$$LOQ = \frac{10\sigma}{m} = \frac{10\times0.001}{87.9} = 1.14 \cdot 10^{-4}\ mol/L \quad \textit{(Eq. 3.15)}^{x}$$

- Image reader

$$Abs_{680} = 1.57 \cdot 10^{4}\ [CGA] + 1.53 \ (\mathrm{R}^2 = 0.974) \quad \textit{(Eq. 3.16)}$$

$$LOD = \frac{3.3\sigma}{m} = \frac{3.3\times0.5948}{1.57\cdot10^{4}} = 1.25 \cdot 10^{-4}\ mol/L \quad \textit{(Eq. 3.17)}^{x}$$

$$LOQ = \frac{10\sigma}{m} = \frac{10\times0.5948}{1.57\cdot10^{4}} = 3.79 \cdot 10^{-4}\ mol/L \quad \textit{(Eq. 3.18)}^{x}$$

Pictures of the discs after 1 hour of incubation in CGA taken with the image reader are reported in Figure 3.51.

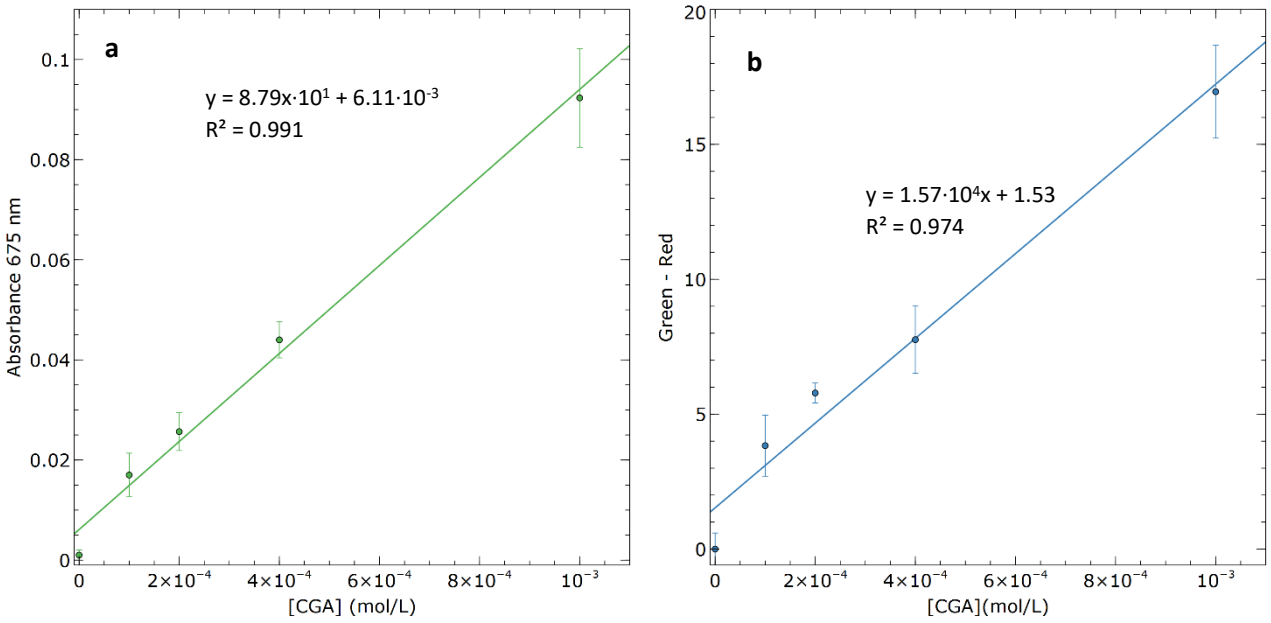

*Figure 3.50- (a) Linear correlation between absorbance at 675 nm of **Me2** discs vs. CGA concentrations measured with the pseudo differential reflection spectrophotometer; (b)linear correlation between green – red components of **Me2** discs vs. CGA concentrations measured with the image reader.*

[x] Where *m* is the slope of the curve and σ is the standard deviation calculated on 3 blank samples.

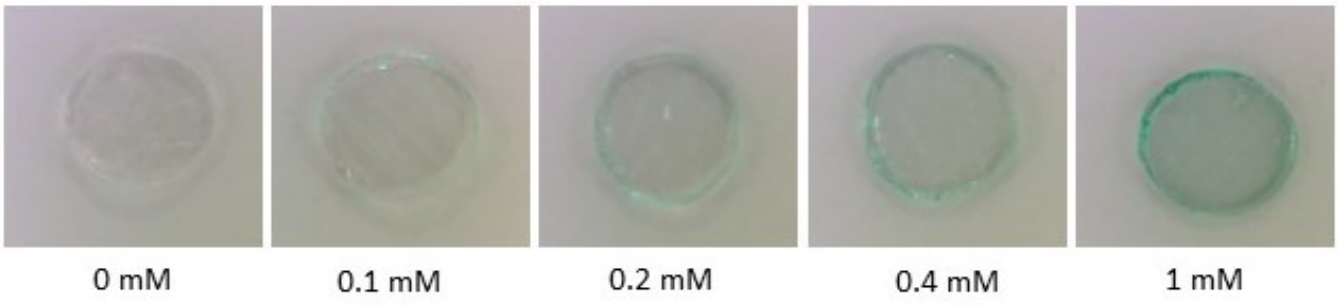

*Figure 3.51- Pictures of **Me2** discs after 60 minutes of incubation with CGA taken with the image reader.*

Preliminary results obtained with the two in-lab built devices are very promising, showing good linear ranges and reproducibility. The performance of the two devices is comparable, with pseudo differential reflection spectrophotometer giving slightly better results in terms of correlation and reproducibility.
Results obtained with the different portable devices are reported in Table 3.6, together with results from *N*α-boc-lysine for comparison purposes. It is possible to see that amongst the portable devices, the best performing one is the pseudo differential reflectance spectrophotometer, having the lowest LOD and LOQ values. With respect to the optical fiber device, both the reflectance spectrophotometer and the image reader perform better. However, both assays with discs perform worse with respect to the in-solution assays, so further improvements on membranes composition will have to be done, but the developed devices are perfectly able to analyze data.

Table 3.6 – comparison between tested assay formats for CGA quantification

Device/Assay	Linear correlation	LOD (mol/L)	LOQ (mol/L)
Optical fiber device	$y = 51.8\,x + 0.0032$ (0.996)	$2.57 \cdot 10^{-4}$	$7.81 \cdot 10^{-4}$
Reflectance spectrophotometer	$y = 87.9x + 0.00611$ (R^2 =0.991)	$3.75 \cdot 10^{-5}$	$1.14 \cdot 10^{-4}$
Image reader	$y = 1.57 \cdot 10^{4}x + 1.53$ (R^2 = 0.974)	$1.25 \cdot 10^{-4}$	$3.79 \cdot 10^{-4}$
***N*α-boc lysine (24h)**	$y = 841x - 0.0133$ (R^2 = 0.994)	$6.0 \cdot 10^{-6}$	$1.8 \cdot 10^{-5}$
***N*α-boc lysine (kinetic mode)**	$y = 0.290x - 4.11 \cdot 10^{-6}$ (R^2 = 1.00)	$5.0 \cdot 10^{-6}$	$1.5 \cdot 10^{-5}$

3.5 FLUORESCENCE OF THE GREEN TBA PIGMENT

Besides the colorimetric properties of the green pigments, it has been decided to investigate if pigment **2** is also fluorescent, which is something never reported in literature. In fact, this might open further possibilities to exploit the reaction for sensing purposes.

Preliminary evaluations about the fluorescent properties of pigment **2** have been done using the purest fraction obtained by SEC (fraction **b**, see paragraph 3.2.1).

Actually, the pigment is fluorescent, and a first scan carried out in the 200 - 600 nm range allowed to define the best excitation and emission wavelengths in carbonate buffer (excitation at 318 nm and emission at 426 nm, Figure 3.52 a).

The fluorescence of solutions containing different pigment **2** concentrations has been measured, and a linear relationship has been found (Figure 3.52 b), according to Equation 3.19:

$$F = 4.37 \cdot 10^5[\mathbf{2}] + 7.84 \ (\mathrm{R}^2 = 0.999) \quad \text{(Eq. 3.19)}$$

LOD (Eq. 3.20) and LOQ (Eq. 3.21) values for the pure pigment have been determined according to the ICH guidelines:[13]

$$LOD = \frac{3.3\sigma}{m} = \frac{3.3\times7.38}{4.37\cdot10^5} = 5.6 \cdot 10^{-5}\ mol/L \qquad (Eq.\ 3.20)^{xi}$$

$$LOQ = \frac{10\sigma}{m} = \frac{10\times7.38}{4.37\cdot10^5} = 1.7 \cdot 10^{-4}\ mol/L \qquad (Eq.\ 3.21)^{xi}$$

Making a comparison with absorbance results working in mixture of *N*α-boc-lysine and CGA, both at the endpoint of the reaction and in kinetic mode (see paragraphs 3.2.3), the LOD and LOQ calculated for the pure pigment **2** in fluorescence mode result to be almost one order of magnitude higher, so it seems that this type of fluorescence analysis is not very sensitive for CGA quantification.

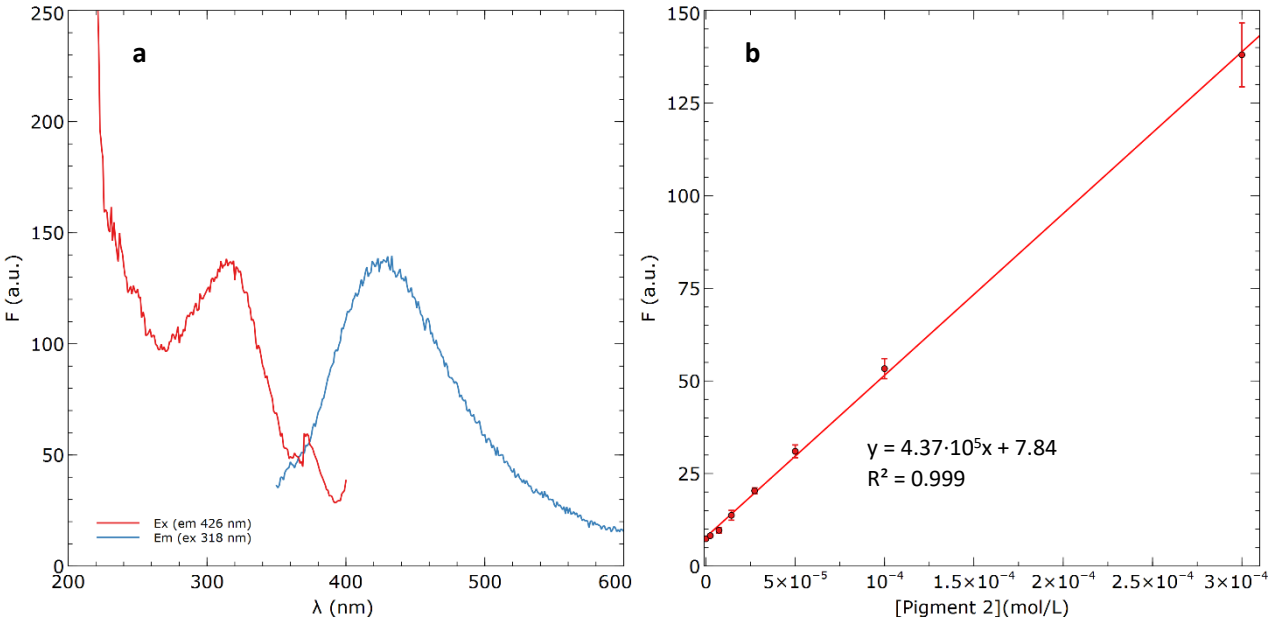

*Figure 3.52 – a) Fluorescence spectra of a 300 µM pigment **2** solution in carbonate buffer 3 mM, pH 9; b) linear correlation between fluorescence emission and pigment **2** concentration.*

[xi] Where *m* is the slope of the curve and σ is the standard deviation calculated on 6 measurements of the blank.

Considering the possibility of performing fluorescence analysis also in mixture -such as in the case of absorbance measurements-, fluorescence of CGA in carbonate buffer at the wavelengths of pigment excitation/emission was investigated. In fact, it is reported in literature that caffeic acid and its esters exhibit fluorescent properties thanks to the presence of the hydroxycinnamic subunit.[26] Unfortunately, a fluorescence emission at 490 nm when exciting at 400 nm could be observed, which might largely interfere with the measurement of the TBA pigment fluorescence. However, a measurement in mixture has been done, to check if fluorescence of the TBA pigment can be distinguished from that of CGA alone. Unfortunately, the obtained spectra show that the CGA fluorescence is predominant with respect to the emission of the TBA pigment at the investigated wavelengths between 450 and 550 nm, so in these conditions it is not possible to exploit the TBA pigment fluorescence for CGA detection. The only way to solve this limit might be that of using the amine immobilized on a support, to allow removal of unreacted CGA. One last attempt has been done trying to distinguish the two fluorescence emissions in kinetic mode, but no resolutive results have been obtained. However, further analyses were carried out and after obtaining preliminary results above described, the fluorescence of the TBA pigment has been investigated in a more precise way, concentrating in particular on possible longer wavelengths fluorescence (above 680 nm).[xii] The presence of a red fluorescence emission would be very interesting because it would be in a region at which no interferences happen, so even in a crude reaction mixture a fluorescence emission in this region would be diagnostic for the formation of the pigment, something which is not true for the fluorescence at 440 nm previously discussed, for which there was a huge interference from CGA itself, and probably also from other species.

To study the fluorescence of the TBA pigment at long wavelengths in a reaction mixture, chlorogenic acid 1.8 mM has been reacted with *N*α-boc-lysine 18 mM in sodium carbonate buffer 180 mM at pH 9.5, for around 40 hours at room temperature to allow formation of a big quantity of pigment **2** in the mixture. Then, the reaction mixture has been diluted in water (final pH around 9) and it has been analyzed with the fluorimeter: at this basic pH no fluorescence emission could be detected in the red region, even by increasing the concentration of the reaction mixture in cuvette. The solution was thus slightly acidified to a neutral pH around 7, to see if changing the pH -and thus the prevalent prototropic form of the pigment- could also change the fluorescence behavior. Surprisingly, after lowering the pH, the pigment exhibited a fluorescence emission at around 710 nm when excited between 630 and 650 nm. By further lowering the pH to the acidic value of 2, the pigment solution appeared to be pink and retained its red fluorescence.

These discoveries are quite interesting, first of all because fluorescence properties of the TBA pigments have never been studied and reported in literature, secondly because red fluorescence would allow target monitoring in a spectral range usually free from interferents.

3.5.1.1 Dependence of the red fluorescence on CGA concentration

After initial preliminary evaluations, a first quantitative experiment has been done to determine if there is a linear correlation between CGA concentration and fluorescence emission of the TBA pigment at 700 nm, working in mixture. For this experiment, *N*α-boc-lysine 18 mM has been reacted with CGA at concentrations ranging between 1.75 mM and 62.5 µM, in carbonate buffer at pH 9.5. A control solution containing CGA at the highest tested concentration without lysine was also prepared to check the fluorescence behavior of the target when no pigment is formed. After 30 minutes of reaction with vials opened, solutions were acidified with hydrochloric acid, obtaining a pH around 3 as measured with pH indicator paper. Fluorescence measurements have been done exciting the acidified solutions at 660 nm (Figure 3.53). By plotting the maximum fluorescence emissions at 695 nm with respect to CGA concentration, it was possible to find a good linear relationship up to 0.5 mM CGA concentration, whereas fluorescence emission for the most concentrated solutions results out of linearity (Figure 3.54): this might be attributed to the presence of an

[xii] Experiments were carried out at the GSOLFA group, at Complutense University, Madrid.

inner-filter effect due to absorption of the red fluorescence emission of the TBA pigments from the pigment itself.

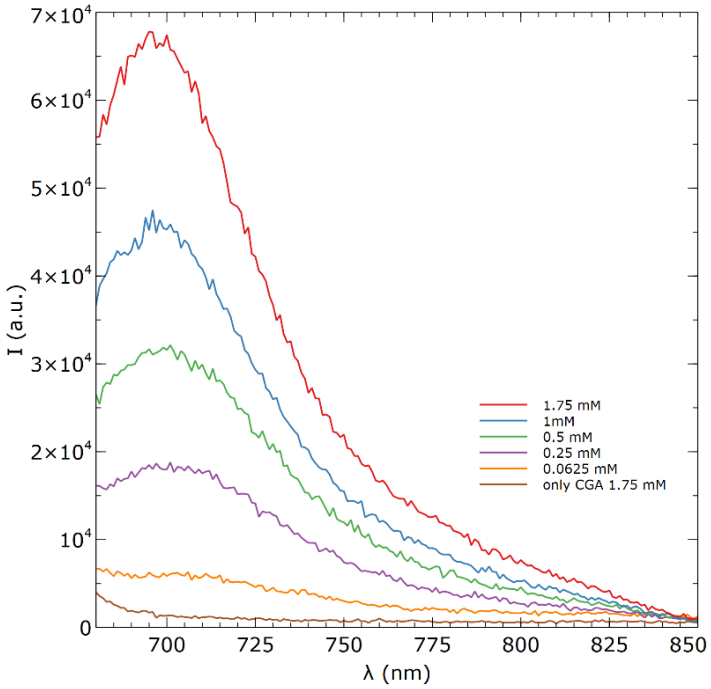

*Figure 3.53- Fluorescence emission of pigment **2** at increasing CGA concentrations (λ_{ex} 660 nm)*

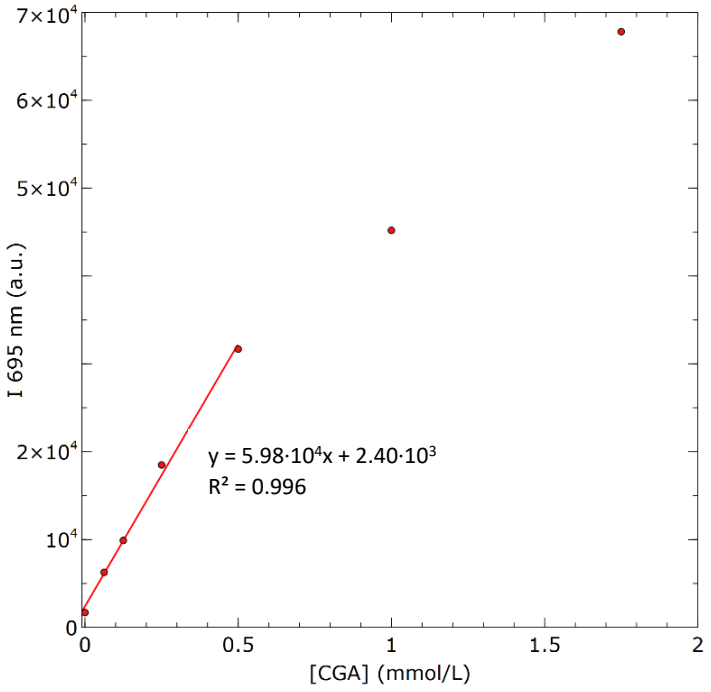

*Figure 3.54- Linear correlation between fluorescence emission of pigment **2** at 695 nm and CGA concentration.*

3.5.1.2 Dependence of the fluorescence emission on pH

After assessing that in the tested conditions there is a linear relationship between fluorescence emission and CGA concentration, which is a good starting point, a study has been done to find the best pH conditions to monitor fluorescence at around 700 nm. As it was difficult to measure in a precise way the pH after acidifying the reaction mixture due to the small reaction volumes, a study has been done preparing a solution of *N*α-

boc-lysine (18.2 mM) and CGA (2.5 mM) in carbonate buffer at pH 9.5, by letting the reaction mixture for almost 4 hours at room temperature to allow extensive formation of the pigment. Then, 300 µL aliquots have been taken from the mother solution and each one has been acidified with different quantities of HCl. Depending on the added HCl volume, different aliquots of water have been added to keep the final volume and the concentration of the TBA pigment constant, while changing only the pH which has been measured with pH indicator paper. Emission spectra have been registered exciting at 620 nm.

Looking at the emission spectra (Figure 3.55) and at the plot correlating maximum emission and HCl volume added (Figure 3.56), it is possible to observe that with the addition of only 10 µL of HCl (pH 9), there is no emission at all, and by adding aliquots between 20 and 50 µL (pH between 8 and 7), emission gradually starts to increase, reaching the maximum for the addition of 60 µL of HCl, which corresponds to a pH around 6. Then, for additions between 65 and 80 µL (pH between 4.5 and 3), fluorescence emission gradually diminishes. Thus, slightly acidic pH is the best pH condition to observe a fluorescence emission of the pigment, which gradually becomes less intense for more acidic pHs. A limit of this analysis has been of course the impossibility to measure pH in a precise way, and the fact that it was not possible to change it in a very controlled way, also due to the presence of the dissociation equilibrium of carbonic acid to carbon dioxide and water, which makes this system quite difficult to reproduce in a precise way. However, this must be considered as a starting point to understand how to use in the best way this quantification system in fluorescence mode.

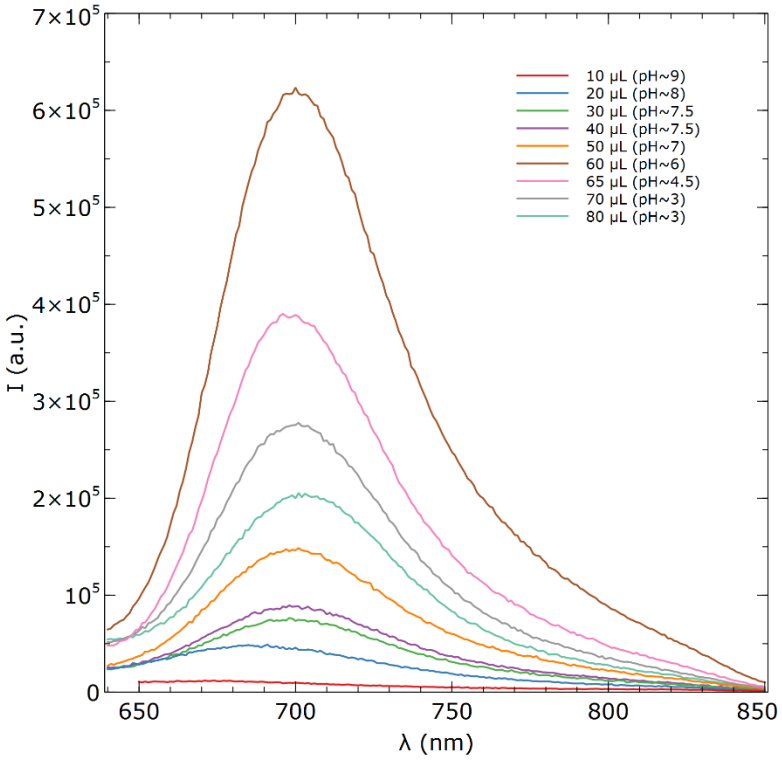

*Figure 3.55- Study of correlation between pigment **2** fluorescence and pH (λ_{ex} 620 nm).*

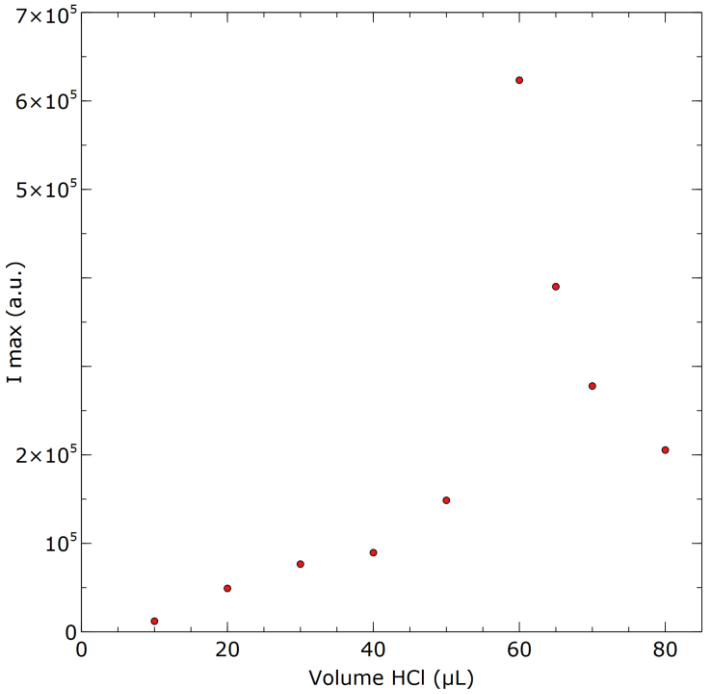

*Figure 3.56- Maximum fluorescence emissions of pigment **2** vs. added volume of HCl 1 M.*

After establishing the best pH conditions to observe TBA pigment fluorescence, a new experiment in carbonate buffer has been done, adopting the lysine concentration of the first concentration-dependent experiment (18 mM) and using CGA concentrations ranging between 1 mM and 20 µM. This time, before acidifying the solutions with HCl, after 15 minutes of reaction, 200 µL of each reaction mixtures were analyzed using a multiwell plate reader to determine the absorbances at 680 nm. This has been done to make a comparison between sensitivity of the fluorescence and the absorbance mode, to understand which is the most promising one. Very good linearity results were obtained in absorbance mode (Figure 3.57 a). Then, all the solutions were acidified obtaining a pH around 6 and were analyzed in fluorescence mode. Contrary to the good absorbance results, the fluorescence ones resulted very unsatisfactory. In fact, no correlation could be found between the fluorescence emission and CGA concentrations, since the 1 mM CGA solution is the only one exhibiting a high fluorescence intensity, whereas all the others emit very poorly (Figure 3.57 b). The difference in behavior with respect to the first concentration-dependent experiment can be partially explained with the different reaction time (15 minutes in the last experiments instead of the 30 of the first one) but it might be ascribed also to the different pH conditions (6 in the last experiment, whereas in the first one it was 3). However, another problem consisted in the difficulty in controlling the acidification of the carbonate solutions due to the dissociation of carbonic acid to carbon dioxide and water, and due to the lack of a precise pH monitoring system, which can make results very unreproducible.

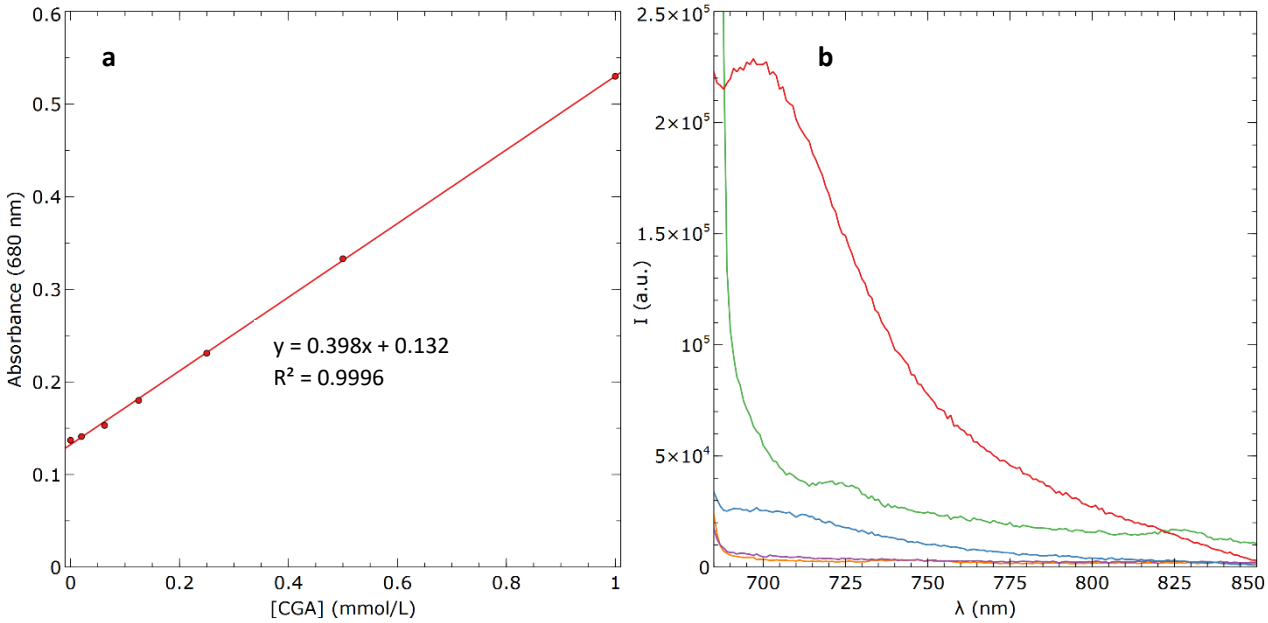

*Figure 3.57- (a)Linear correlation between absorbance at 680 nm of pigment **2** and CGA concentration; fluorescence emission of pigment **2** (acidified) exciting at 660 nm.*

The experiment has been repeated lowering lysine and consequently CGA concentrations, but also in this case no good linearity could be obtained in fluorescence mode.

To try to avoid problems related to carbonate buffer, the conditions of the last carbonate buffer test at higher lysine concentration (18 mM) were reproduced changing to HEPPS (4-(2-Hydroxyethyl)-1-piperazinepropanesulfonic acid) buffer, which has a p*K*a of 8, so quite suitable to be used at the pH around 9 necessary for the reaction to happen (borate buffer and phosphate buffer had already been excluded based on kinetics experiments reported at paragraph 3.2.2.1). However, even at the highest CGA concentration the emission signal resulted quite low, not allowing to finish the titration, thus meaning that even if in this case carbonic acid dissociation problems do not take place, the buffer is not suitable for this type of experiment.

3.5.1.3 Final considerations

On one hand fluorescence mode seemed to be very promising because normally in fluorescence measurements it is possible to obtain higher sensitivities. However, in this case the fluorescence analysis mode resulted to be much more complicated with respect to the absorbance one. Considering the fluorescence at 440 nm, problems were related to the interferences of the CGA intrinsic fluorescence. On the other hand, considering the fluorescence emission at longer wavelengths, which would allow to avoid optical interferences, a first problem arises because sample treatment by lowering the pH with respect to the basic conditions necessary for TBA pigments formation is requested, otherwise no fluorescence is observed. This is additional work that complicates analysis and causes a dilution of the sample. Connected to lowering the pH, it is very complicated to do it in a controlled and reproducible manner, especially without a pH microelectrode. Moreover, although carbonate buffer is a good choice in absorbance mode, it complicates the acidification step due to the existence of dissociation equilibrium of carbonic acid. The poor reproducibility of the fluorescence measurements, with only one experiment showing linear relationship with CGA concentration, might be due to the fact that at slightly acidic pH there is a very complex equilibrium between the different prototropic forms of the pigment, each one having its proper fluorescence behavior (whereas at basic pH the anionic one is prevalent) and for this reason little changes in pH can cause shifts toward one or the other form, thus causing a drift from linearity. This might explain why the only measurement in which a linear relationship could be observed is the first one in which the pH was highly acidic (around 3), and probably the acidic prototropic form was prevalent. So, it seems that working at slightly

acidic pH (around 6) is the most convenient condition in terms of fluorescence emission intensity (see paragraph 3.5.1.2), but the presence of several equilibria between prototropic forms in this environment suggests that measurements should be performed at more acidic pH. In addition, inner filter effect due to absorbance of the pigment might cause loss of linearity at higher concentrations.

Due to the previous considerations, currently, it seems that working in fluorescence mode is more complicated than in absorbance and is also far less sensitive: the only way to apply this approach would be that of trying to obtain a reproducible system.

3.6 THE PIGMENT AS A POTENTIAL FLUORESCENT LABEL FOR PROTEINS

Another application of the green TBA pigment could be its use as a reagent for protein labeling. In this case, reaction of CGA could take place with the ε amino groups of lysine residues inside a protein. This reaction could lead to colored/fluorescent proteins, thus giving a very easy and cheap method for protein labeling, which is something that might be very interesting also from a commercial point of view. In this perspective, the reaction was tested on Bovine Serum Albumin (BSA), which is a 66.5 kDa protein commonly used as a standard in laboratories. The reactivity of BSA with CGA has already been demonstrated by Iacomino and co-worker when they tried to develop a food coloring agent.[10]

Reaction has been done using 75 µM BSA with 1.5 mM CGA in carbonate buffer 0.1 M at pH 9, obtaining a dark green solution that has then been dialyzed to ensure complete CGA removal and finally lyophilized obtaining TBA pigment-modified BSA (**P-BSA**). The UV-visible spectrum of **P-BSA** is reported in Figure 3.58, showing an absorption signal at 640 nm, diagnostic for the TBA pigment in water (pH around neutrality). In this case, it is possible to exclude the presence of CGA thanks to the extensive dialysis. However, purity is unknown due to the fact that some BSA might have not reacted, and it is not known how many ε-amino groups of the 60 lysine residues reacted.[27] Moreover, also the lateral side chains of other amino acid residues might have reacted as previously discussed in the introductive part of this paragraph.[7]

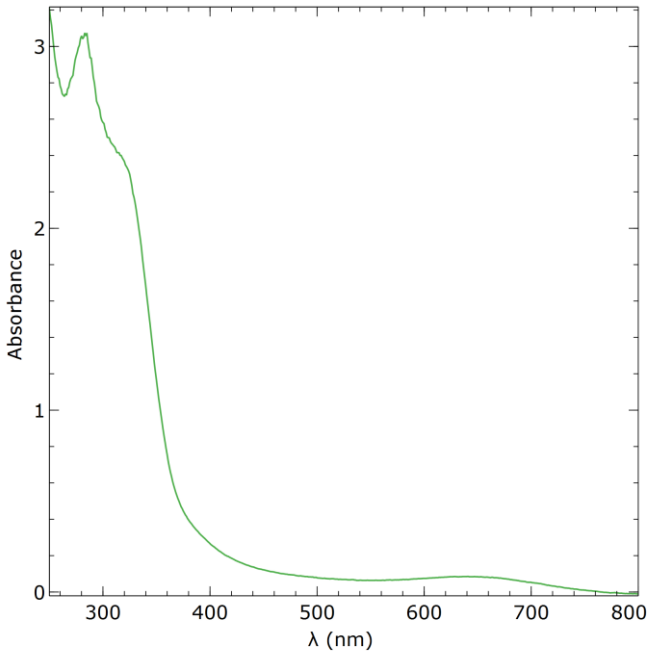

*Figure 3.58- Absorbance spectrum of a **P-BSA** solution.*

Despite all these considerations, fluorescent properties of the purified **P-BSA** have been evaluated by preparing a 32 µM **P-BSA** solution in 10 mM carbonate buffer, pH 9: a maximum of emission has been observed at 470 nm while exciting at 346 nm (Figure 3.59 a). As a control, unmodified BSA has been analyzed, preparing a 62 µM solution in 10 mM carbonate buffer: in this case, exciting at 290 nm, a maximum emission at 341nm could be observed, which is typical for the emission of tryptophan and tyrosine residues, in accordance with the literature (Figure 3.59 b).[28]

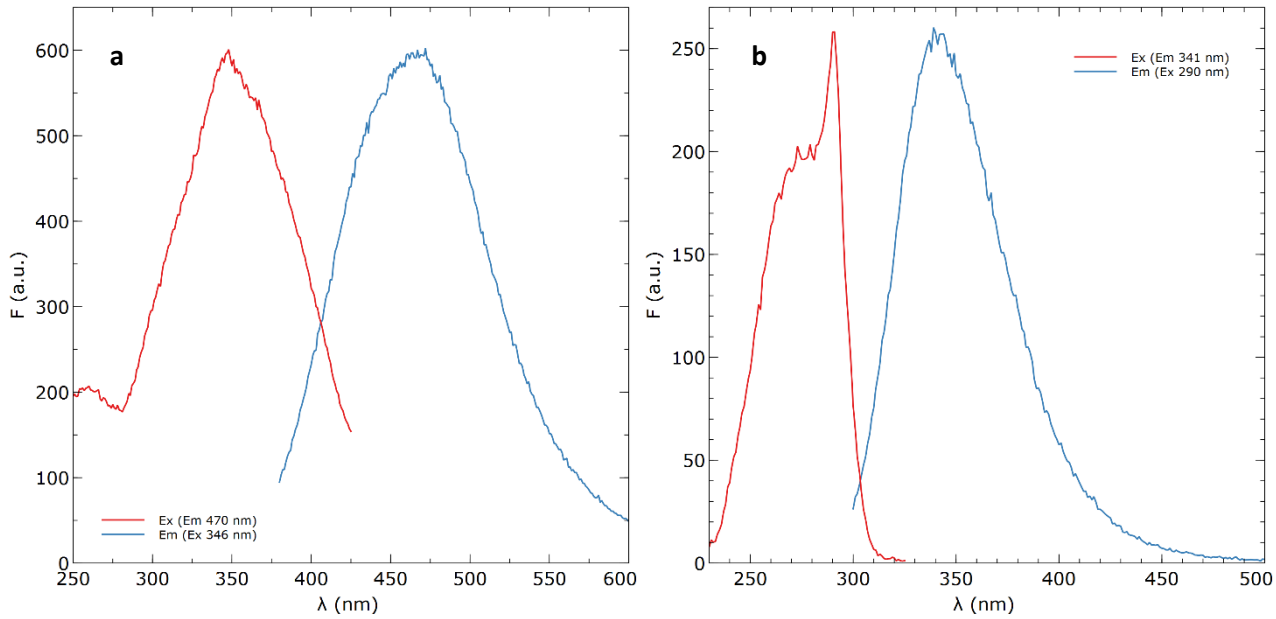

Figure 3.59- (a) -Emission and excitation spectra of 32µM P-BSA in carbonate buffer 10 mM; (b) Emission and excitation spectra of 62 µM BSA in carbonate buffer 10 mM.

It is possible to observe that the emission spectrum of native BSA superimposes well with the excitation one of **P-BSA**, and for this reason the presence of a possible FRET effect has been investigated. For this purpose, a spectrum of **P-BSA** has been registered selecting the excitation wavelength of unmodified BSA (290 nm): in this case it is possible to see a peculiar emission at 450 nm that is not present in native BSA (Figure 3.60). The hypothesis that a FRET effect takes place is supported by the fact that in spatial proximity with Lys222 of BSA (the lysine residue having the lowest pK_a and that is thought to be the first one to react in TBA pigment formation), there is the Trp214 residue (one of the BSA residues responsible for its intrinsic fluorescence).[29] However, this is only an hypothesis and further studies will be carried out to elucidate if a FRET effect takes place.

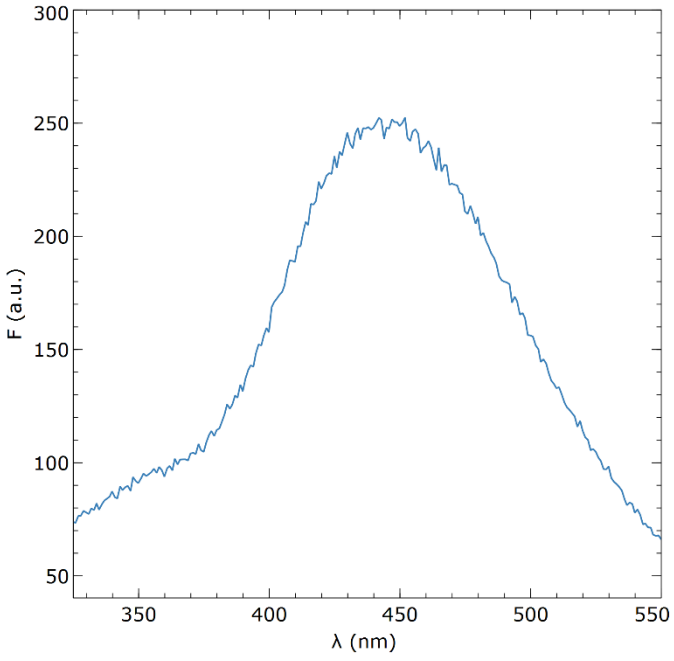

*Figure 3.60- Fluorescence emission of **P-BSA** exciting at the excitation wavelength of BSA (λ_{ex} 290 nm).*

3.6.1.1 Preliminary evaluation on the applicability of P-BSA for protein labeling

As already mentioned, TBA pigment formation might serve as an easy and cheap method for protein labeling. In this perspective, determining the sensitivity limits of **P-BSA** detection in fluorescence mode would be very useful to evaluate the applicability of the reaction for this purpose. In fact, this is a labeling method that could be applied to almost all types of proteins, comprising antibodies, and it would be important to understand if sensitivity of the TBA labeling system allows quantification in the ranges requested for practical applications. The intensity of the emission peak of **P-BSA** has been evaluated in 10 mM carbonate buffer pH 9, at 470 nm when exciting at 346 nm (Figure 3.61), finding the linear correlation in equation 3.22.

$$F = 4.39 \cdot 10^7 [\text{P-BSA}] + 34.6 \ (R^2 = 0.967) \qquad \text{(Eq. 3.22)}$$

According to the ICH guidelines, LOD (Eq. 3.23) and LOQ (Eq. 3.24) have been calculated.[13]

$$LOD = \frac{3.3\sigma}{m} = \frac{3.3 \times 0.479}{4.39 \cdot 10^7} = 3.6 \cdot 10^{-8}\ mol/L \qquad \textit{(Eq. 3.23)}^{\text{xiii}}$$

$$LOQ = \frac{10\sigma}{m} = \frac{10 \times 0.479}{4.39 \cdot 10^7} = 1.09 \cdot 10^{-7}\ mol/L \qquad \textit{(Eq. 3.24)}^{\text{xiii}}$$

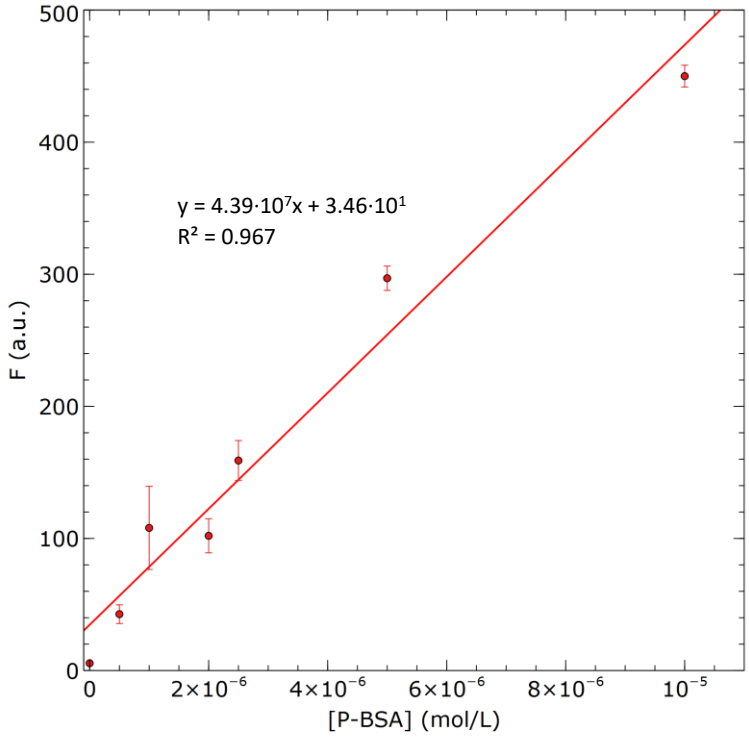

*Figure 3.61- Fluorescence emission of **P-BSA** vs. **P-BSA** concentration in carbonate buffer 10 mM (λ_{ex} 346 nm, λ_{em} 470 nm)*

These preliminary results are very positive, allowing to obtain excellent sensitivity even exploiting fluorescence at lower wavelengths, and further experiments will be done to evaluate use of **P-BSA** for protein labeling also using the fluorescence at higher wavelengths. An idea is also that of making tests by confocal microscopy on TBA-labelled antibodies, to evaluate the applicability of the approach to practical applications.

[xiii] Where *m* is the slope of the curve and σ is the standard deviation calculated on 6 blank samples.

3.7 BIBLIOGRAPHY

(1) Yabuta, G.; Koizumi, Y.; Namiki, K.; Kawai, T.; Hayashi, T.; & Namiki, M. Novel benzacridine derivative in the green pigment from methyl caffeate and butylamine. *Biosci. Biotech. Biochem.*, **1996**, 60(10), 1701-1702.

(2) Matsui, T. Greening Pigments Produced by the Reaction of Ethyl Caffeate with Methylamine., *J. Nutr. Sci. Vitaminol.,* **1981**, 27 (6), 573–582.

(3) Wildermuth, S. R.; Young, E. E.; Were, L. M. Chlorogenic Acid Oxidation and Its Reaction with Sunflower Proteins to Form Green-Colored Complexes. *Compr. Rev. Food Sci. Food Saf.*, **2016**, 15 (5), 829–843.

(4) Yabuta, G.; Koizumi, Y.; Namiki, K.; Hida, M.; & Namiki, M. Structure of Green Pigment Formed by the Reaction of Caffeic Acid Esters (or Chlorogenic Acid) with a Primary Amino Compound. *Biosci. Biotech. Biochem.,* **2001**, 65 (10), 2121–2130.

(5) Namiki, M.; Yabuta, G.; Koizumi, Y.; YANo, M. Development of Free Radical Products during the Greening Reaction of Caffeic Acid Esters (or Chlorogenic Acid) and a Primary Amino Compound. *Biosci. Biotech. Biochem.,* **2001**, 65 (10), 2131–2136.

(6) Schilling, S.; Sigolotto, C.-I.; Carle, R.; Schieber, A. Characterization of Covalent Addition Products of Chlorogenic Acid Quinone with Amino Acid Derivatives in Model Systems and Apple Juice by High-Performance Liquid Chromatography/Electrospray Ionization Tandem Mass Spectrometry. *Rapid Commun. Mass Spectrom.,* **2008**, 22 (4), 441–448.

(7) Prigent, S. V. E.; Voragen, A. G. J.; Li, F.; Visser, A. J. W. G.; van Koningsveld, G. A.; Gruppen, H. Covalent Interactions between Amino Acid Side Chains and Oxidation Products of Caffeoylquinic Acid (Chlorogenic Acid): Covalent Interactions between Amino Acid Side Chains and CQA. *J. Sci. Food Agric.*, **2008**, 88 (10), 1748–1754.

(8) Bongartz, V., Brandt, L., Gehrmann, M. L., Zimmermann, B. F., Schulze-Kaysers, N., Schieber, A. Evidence for the Formation of Benzacridine Derivatives in Alkaline-Treated Sunflower Meal and Model Solutions. *Molecules,* **2016**, 21 (1), 91.

(9) Moccia, F.; Martín, M. Á.; Ramos, S.; Goya, L.; Marzorati, S.; DellaGreca, M.; Panzella, L.; Napolitano, A. A New Cyanine from Oxidative Coupling of Chlorogenic Acid with Tryptophan: Assessment of the Potential as Red Dye for Food Coloring. *Food Chem.,* **2021**, 348, 129152.

(10) Iacomino, M.; Weber, F.; Gleichenhagen, M.; Pistorio, V.; Panzella, L.; Pizzo, E.; Schieber, A.; d'Ischia, M.; Napolitano, A. Stable Benzacridine Pigments by Oxidative Coupling of Chlorogenic Acid with Amino Acids and Proteins: Toward Natural Product-Based Green Food Coloring. *J. Agric. Food Chem.*, **2017**, 65 (31), 6519–6528.

(11) Verona. C. Derivati Covalenti Colorati e Fluorescenti tra Fenoli e Lisina a Scopo Biosensoristico, Master degree thesis, **2020**-**2021**, University of Trieste.

(12) Xie, C.; Yu, K.; Zhong, D.; Yuan, T.; Ye, F.; Jarrell, J. A.; Millar, A.; Chen, X. Investigation of Isomeric Transformations of Chlorogenic Acid in Buffers and Biological Matrixes by Ultraperformance Liquid Chromatography Coupled with Hybrid Quadrupole/Ion Mobility/Orthogonal Acceleration Time-of-Flight Mass Spectrometry. *J. Agric. Food Chem.*, **2011**, 59 (20), 11078–11087.

(13) Guideline, I. H. T. Validation of analytical procedures: text and methodology. Q2 (R1), **2005**, 1(20), 05.

(14) Forzato, C.; Vida, V.; Berti, F. Biosensors and Sensing Systems for Rapid Analysis of Phenolic Compounds from Plants: A Comprehensive Review. *Biosensors,* **2020**, 10 (9), 105.

(15) Crozier, T. W. M.; Stalmach, A.; Lean, M. E. J.; Crozier, A. Espresso Coffees, Caffeine and Chlorogenic Acid Intake: Potential Health Implications. *Food Funct*., **2012**, 3 (1), 30–33.

(16) Balasco, N.; Diaferia, C.; Morelli, G.; Vitagliano, L.; Accardo, A. Amyloid-Like Aggregation in Diseases and Biomaterials: Osmosis of Structural Information. *Front. Bioeng. Biotechnol*., **2021**, 9, 641372.

(17) Cherny, I.; Gazit, E. Amyloids: Not Only Pathological Agents but Also Ordered Nanomaterials. *Angew. Chem. Int. Ed.,* **2008**, 47 (22), 4062–4069.

(18) Lamiable, A.; Thévenet, P.; Rey, J.; Vavrusa, M.; Derreumaux, P.; Tufféry, P. PEP-FOLD3: Faster de Novo Structure Prediction for Linear Peptides in Solution and in Complex. Nucleic Acids Res 2016, 44 (W1), W449–W454.

(19) D.A. Case, H.M. Aktulga, K. Belfon, I.Y. Ben-Shalom, J.T. Berryman, S.R. Brozell, D.S. Cerutti, T.E. Cheatham, III, G.A. Cisneros, V.W.D. Cruzeiro, T.A. Darden, N. Forouzesh, G. Giambaşu, T. Giese, M.K. Gilson, H. Gohlke, A.W. Goetz, J. Harris, S. Izadi, S.A. Izmailov, K. Kasavajhala, M.C. Kaymak, E. King, A. Kovalenko, T. Kurtzman, T.S. Lee, P. Li, C. Lin, J. Liu, T. Luchko, R. Luo, M. Machado, V. Man, M. Manathunga, K.M. Merz, Y. Miao, O. Mikhailovskii, G. Monard, H. Nguyen, K.A. O'Hearn, A. Onufriev, F. Pan, S. Pantano, R. Qi, A. Rahnamoun, D.R. Roe, A. Roitberg, C. Sagui, S. Schott-Verdugo, A. Shajan, J. Shen, C.L. Simmerling, N.R. Skrynnikov, J. Smith, J. Swails, R.C. Walker, J. Wang, J. Wang, H. Wei, X. Wu, Y. Wu, Y. Xiong, Y. Xue, D.M. York, S. Zhao, Q. Zhu, and P.A. Kollman (2023), Amber 2023, University of California, San Francisco.

(20) Schrödinger Release 2023-1: MacroModel, Schrödinger, LLC, New York, NY, 2021.

(21) Calvanese, L.; Caporale, A.; Focà, G.; Iaccarino, E.; Sandomenico, A.; Doti, N.; Apicella, I.; Incisivo, G. M.; De Falco, S.; Falcigno, L.; D'Auria, G.; Ruvo, M. Targeting VEGF Receptors with Non-Neutralizing Cyclopeptides for Imaging Applications. *Amino Acids,* **2018**, 50 (2), 321–329.

(22) Rico-Yuste, A.; González-Vallejo, V.; Benito-Peña, E.; de las Casas Engel, T.; Orellana, G.; Moreno-Bondi, M. C. Furfural Determination with Disposable Polymer Films and Smartphone-Based Colorimetry for Beer Freshness Assessment. *Anal. Chem*., **2016**, 88 (7), 3959–3966.

(23) Alvarez-Rivera, F.; Rey-Rico, A.; Venkatesan, J. K.; Diaz-Gomez, L.; Cucchiarini, M.; Concheiro, A.; Alvarez-Lorenzo, C. Controlled Release of RAAV Vectors from APMA-Functionalized Contact Lenses for Corneal Gene Therapy. *Pharmaceutics,* **2020**, 12 (4), 335.

(24) Krzywinski, M.; Altman, N. Visualizing Samples with Box Plots. *Nat. Methods,* **2014**, 11 (2), 119–120.

(25) https://Www.Effemm2.de/Hardware/Systems_colorimetry.Html.

(26) Navarro-Orcajada, S.; Matencio, A.; Vicente-Herrero, C.; García-Carmona, F.; López-Nicolás, J. M. Study of the Fluorescence and Interaction between Cyclodextrins and Neochlorogenic Acid, in Comparison with Chlorogenic Acid. *Sci. Rep.,* **2021**, 11 (1), 3275.

(27) Richards, D. A.; Thomas, M. R.; Szijj, P. A.; Foote, J.; Chen, Y.; Nogueira, J. C. F.; Chudasama, V.; Stevens, M. M. Employing Defined Bioconjugates to Generate Chemically Functionalised Gold Nanoparticles for in Vitro Diagnostic Applications. *Nanoscale,* **2021**, 13 (27), 11921–11931.

(28) Li, S.; Huang, K.; Zhong, M.; Guo, J.; Wang, W.; Zhu, R. Comparative Studies on the Interaction of Caffeic Acid, Chlorogenic Acid and Ferulic Acid with Bovine Serum Albumin. *Spectrochim. Acta A Mol. Biomol. Spectrosc.,* **2010**, 77 (3), 680–686.

(29) Berti, F.; Bincoletto, S.; Donati, I.; Fontanive, G.; Fregonese, M.; Benedetti, F. Albumin-Directed Stereoselective Reduction of 1,3-Diketones and β-Hydroxyketones to Anti Diols. *Org. Biomol. Chem.,* **2011**, *9* (6), 1987.

4 RESULTS AND DISCUSSION- BORONIC ESTERS

4.1 STATE OF THE ART

From the chemical point of view, boronic acids are trivalent boron compounds, that possess one alkyl or aryl substituent and two hydroxyl groups to fill the remaining valences of the boron atom.[1] Since the boron atom has only six valence electrons, boronic acids are Lewis acids, with a planar sp^2 geometry at boron.[1,2] Thanks to their acidic character, boronic acids can coordinate basic molecules, such as a hydroxide anion, thus forming the tetrahedral boronate ion $[R\text{-}B(OH)_3]^-$, in an analogous way to the borate ion in aqueous solution.[3,4]

A very important type of reactivity of boronic acids is that they are capable of reacting reversibly with bidentate ligands, such as 1,2-diols (including catechols and sugars) forming boronic esters.[5]

The diol can bind to either the trigonal or the tetrahedral form of the boronic acid, thus leading to the corresponding neutral (equilibrium regulated by K_{trig}) and anionic boronic ester (equilibrium regulated by K_{tetra}) respectively: free boronic acids have lower Lewis acid strength compared to that of their neutral boronic esters with 1,2-diols, so $K_a' > K_a$ (Scheme 4.1).[6] This binding process is influenced by several factors such as pH of the medium, nature and concentration of the buffer, proteolitic equilibrium constant (pK_a) of the compound under study, pK_a' of the formed ester, conformation of the diol and temperature.[7]

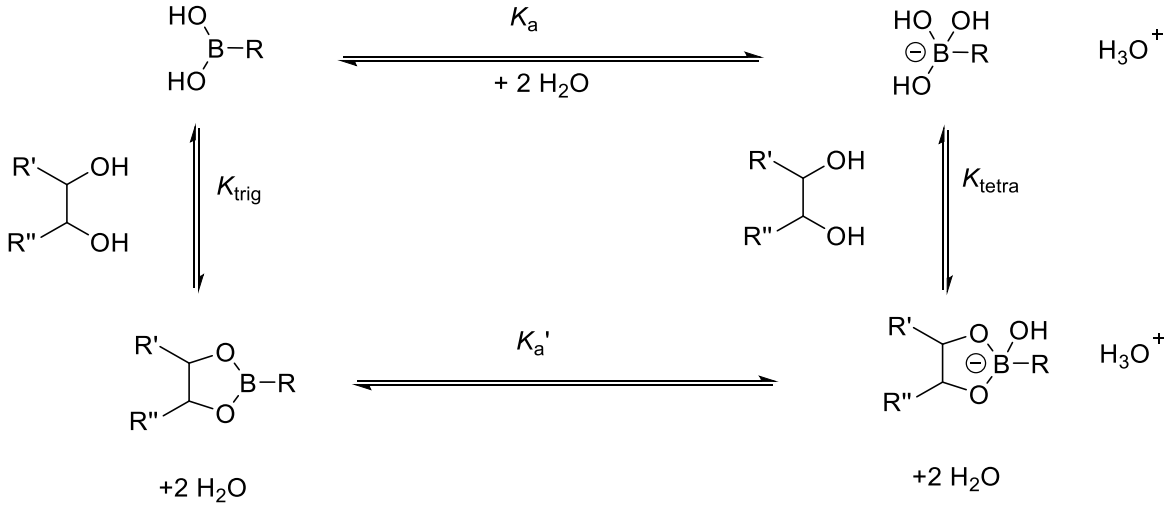

Scheme 4.1- Equilibria of ionization of boronic acids in the presence of a diol (adapted from Marinaro et al.[2] and Bosch et al.[6])

Thanks to their ability to form boronic esters, several examples of their use in developing sensors, for 1,2- or 1,3 diols are present in the literature, exploiting different transduction mechanisms, such as electrochemistry, colorimetry or fluorescence.[8]

Considering electrochemical sensors, a very interesting molecularly imprinted polymer (MIP) used to produce responsive electrodes containing 4-vinylphenylboronic acid as the functional monomer has been developed for potentiometric detection of catechol, based on proton dissociation of the boronic acid group of the MIP upon binding with catechol, which can associate the counterion (X^-) of $TDMA^+$ (tridodecylmethylammonium) in the membrane and diffuse into the aqueous phase, thus promoting movement of anionic species from the membrane phase to the aqueous phase inducing an anionic response. Under acidic conditions, the MIP can be completely regenerated, releasing the diols in solution (Figure 4.1).[9]

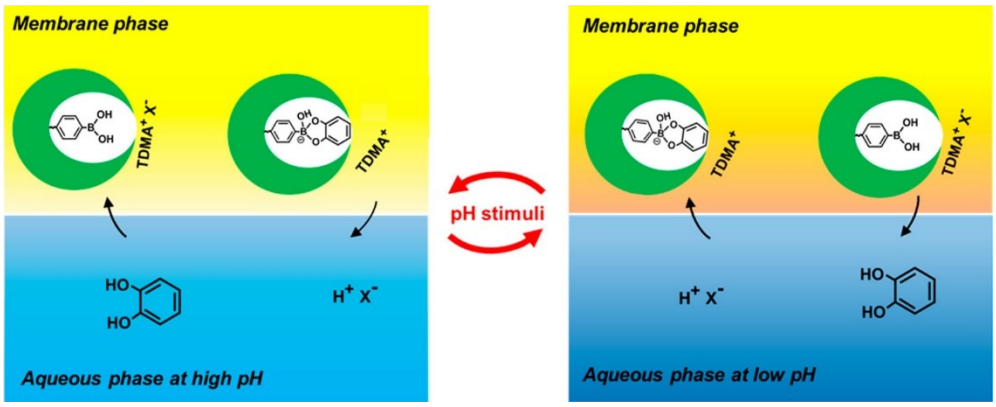

Figure 4.1- Response and regeneration mechanisms of the pH-responsive boronate-affinity MIP-based potentiometric sensor. [9]

Changing detection mechanism, a very interesting colorimetric dye-displacement assay has been developed for saccharides, in which alizarin red and boronic acids have been used to develop a competitive assay (Figure 4.2). In particular, Winson and coworkers synthesized polyacrylamide gel beads containing *meta*-boronophenyl units: such beads have then been exposed to alizarin red, containing a 1,2-diol moiety and thus capable of forming boronic esters with the phenylboronic moiety. After extensive washing, spheres resulted to be orange, which is the typical color for alizarin red esters, whereas in the free form the dye is red. So, by a competitive assay, increasing the concentration of fructose, it was possible to observe increased coloring of the solution, due to release of free alizarin red absorbing at 513 nm.[10]

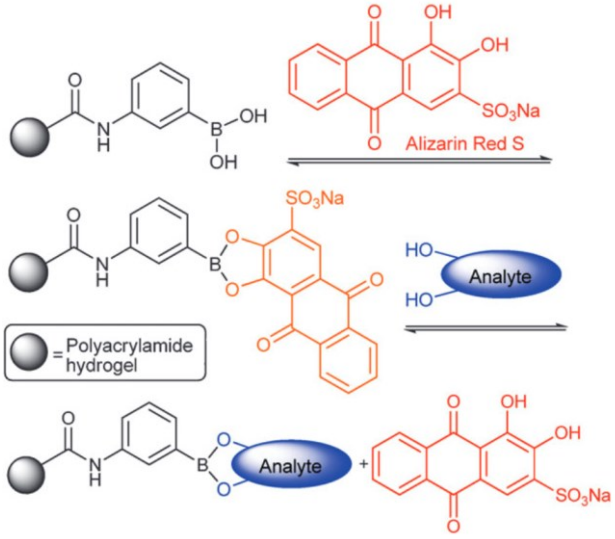

Figure 4.2 General mechanism of dye displacement assay based on Alizarin Red S for saccharides detection.[10]

However, the most common type of boronic acid-based sensor relies on fluorophores containing boronic acid moieties, capable of changing their fluorescence properties upon binding with target molecules.

One of the earliest examples of fluorophores for saccharides sensing is compound **3** reported in Figure 4.3, proposed by James and colleagues in 1994.[11] One year later the same group developed the related compound **4** (Figure 4.3) which, thanks to a cleft like structure, is particularly selective and sensitive for glucose due to the formation of an intramolecular 1:1 complex between the two boronic acids and the 1,2- and 4,6-hydroxyls of glucose.[12] Initially, the mechanism of these sensors was thought to be based on a PET (photoinduced electron transfer) between the *o*-methylphenyl boronic acid and the proximal tertiary amine, causing a change in the N-B bonding strength upon sugar binding.[11] However, this PET fluorescence modulation mechanism resulted to be wrong, and other explanations have been proposed (pK_a switch and aggregation/disaggregation), finally arriving to the conclusion by Sun and colleagues that the role of the

protonated amino group is that of acting primarily as an electron-withdrawing group that lowers the pK_a of the neighboring boronic acid thereby facilitating diol binding at neutral pH, without playing any role in the modulation of the fluorescence of appended fluorophores. Instead, fluorescence turn-on can be consistently tied to vibrational-coupled excited-state relaxation (a loose-bolt effect). According to this explanation, O-H vibrations of the boronic acid in water quench the fluorescence of the fluorophore by accepting the electronic excitation energy. Upon boronic ester formation, quenching from $B(OH)_3^-$ vibrations does not take place, since O-H bonds are replaced by groups having lower vibration frequencies, and this causes a turn-on of fluorescence emission.[13]

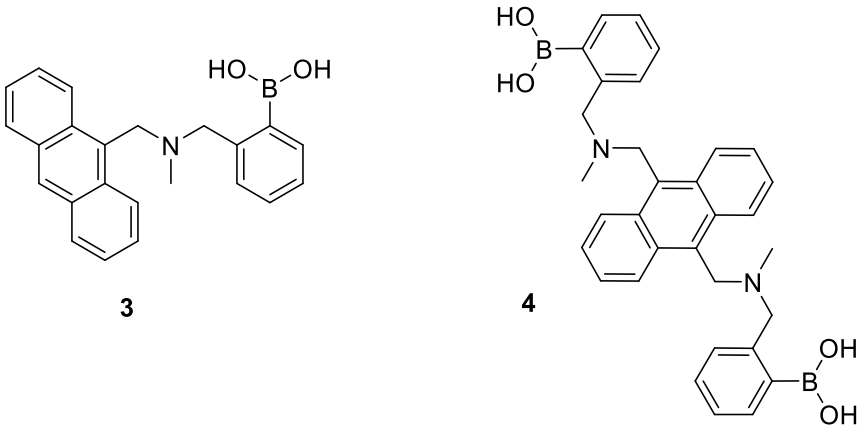

*Figure 4.3- Structures of fluorophores **3** and **4**.*

A very interesting fluorophore that is capable of tuning its fluorescence upon binding with target molecules -both *ortho*-diphenols and saccharides- is 2-(4-boronophenyl)quinoline-4-carboxylic acid **5** (Scheme 4.2).[14] The characteristic of this fluorophore is the fact that the fluorescent moiety is not directly bound to the boronic acid, and the presence of the carboxylic group allows its insertion in more complex structures.[14] The native fluorophore **5** has been reported to show fluorescence increase upon binding with several monosaccharides, showing the highest fluorescence increase in the presence of fructose.[14] Considering the equilibrium of boronic esters formation with monosaccharides (Scheme 4.2), the *pK*a of the neutral boronic acid is of 7.9, which lowers to 5.2 when the boronic acid forms a boronic acid with a sugar. However, it must be considered that the boronate form for the anionic sugar-boronic acid complex is far more fluorescent than the corresponding boronate form of the free acid (Scheme 4.2): so, the intensity increase of the fluorophore at physiological pH in the presence of the sugar is not entirely due to the ionization state change of the boron, but also due to diol-binding's perturbation.[14]

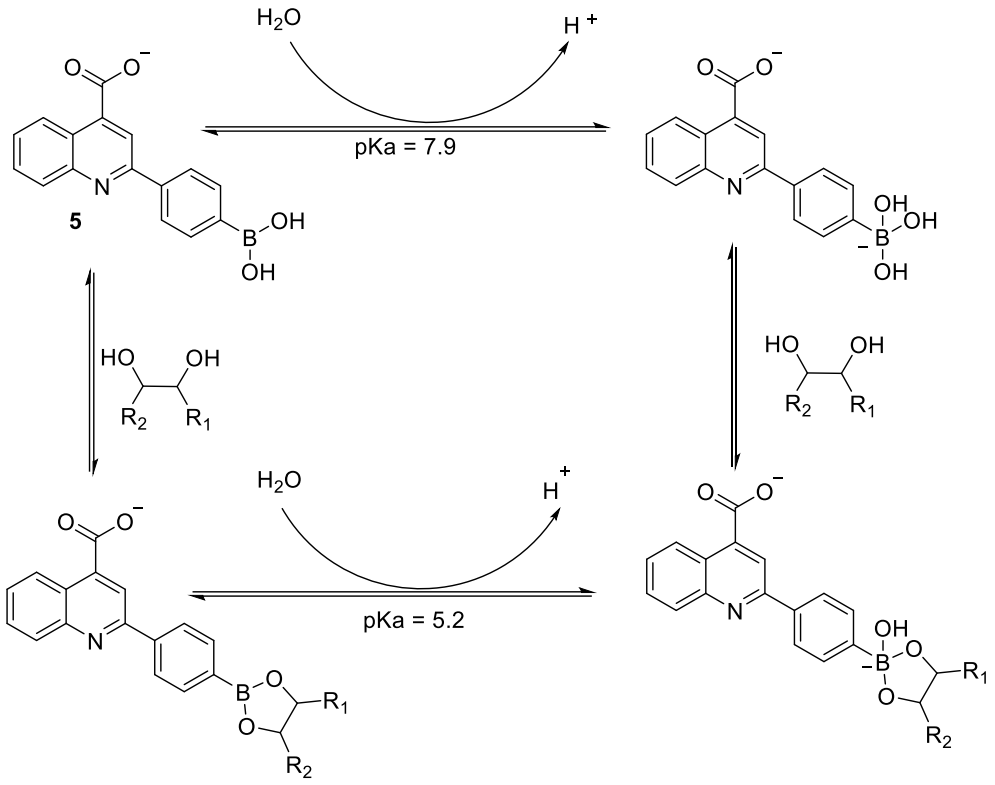

*Scheme 4.2- Equilibria in solution for fluorophore **5.** [14]*

Fluorophore **5** has been used also for the development of more complex sensing systems. A very interesting case is that of Yao and colleagues that in 2019 proposed a diboronic acid fluorescent sensor capable of selectively quenching its fluorescence in the presence of D-ribose, while increasing or not changing its fluorescence in the presence of other carbohydrates.[15] The same group in 2020 further modified the sensor, preparing more conjugated derivatives in order to enhance the Stokes shift (excitation at 350 nm, emission at 500 nm), based on aggregation induced emission.[16] In 2019, another very interesting sensor based on **5** inserted in a diboronic acid sensor was developed, capable of selectively increase of its fluorescence in the presence of sorbitol, while showing only poor interferences with other sugars.[17]

Nucleus **5**, however, has been used not only for the construction of carbohydrate sensors, but also for recognition of *ortho*-diphenolic compounds. Wang and colleagues tested the performance of **5** alone in the presence of catechol, demonstrating that its fluorescence is quenched in the presence of the simplest *ortho*-diphenol. They confirmed the importance of the formation of boronic ester for fluorescence quenching by demonstrating that in the absence of the boronic acid moiety, quenching does not occur increasing catechol concentration, and they also demonstrated that *meta* and *para* diphenols do not quench the fluorescence of the sensor. They hypothesized that fluorescence quenching might be due to a PET effect occurring from catechol into the excited state of the quinoline moiety (Figure 4.4).[18]

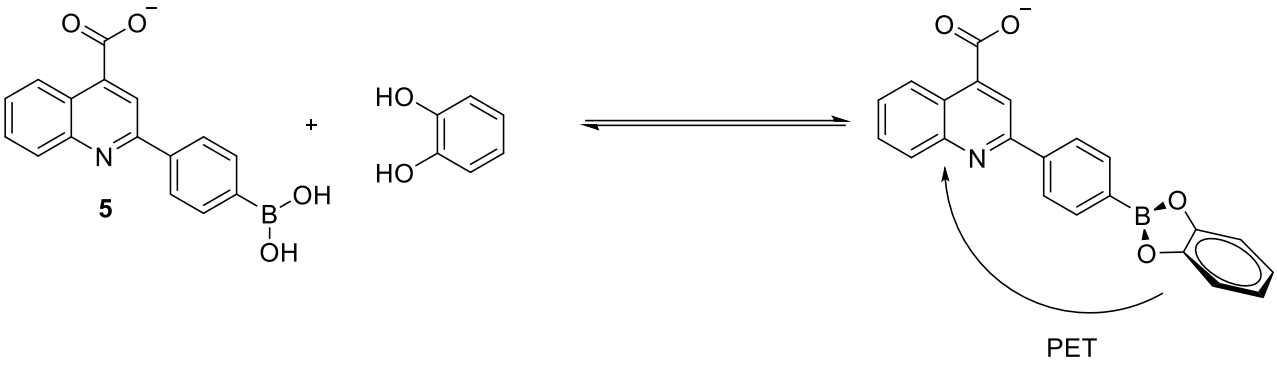

*Figure 4.4- Hypothesized PET mechanism of fluorescence quenching of **5** with catechol (adapted form [18]).*

A very interesting double site recognition sensor is that realized by Bian and coworkers containing the fluorescent nucleus **5** combined with a positively charged guanidinium group at a suitable distance for recognition of caffeic acid: the boronic acid can form a boronic ester with the *ortho*-diphenolic moiety, whereas the guanidinium group can establish ionic interactions with the carboxylic group. This sensor is based on inner filter effect, showing fluorescence quenching upon adding increasing quantities of the target molecule (Figure 4.5).[19]

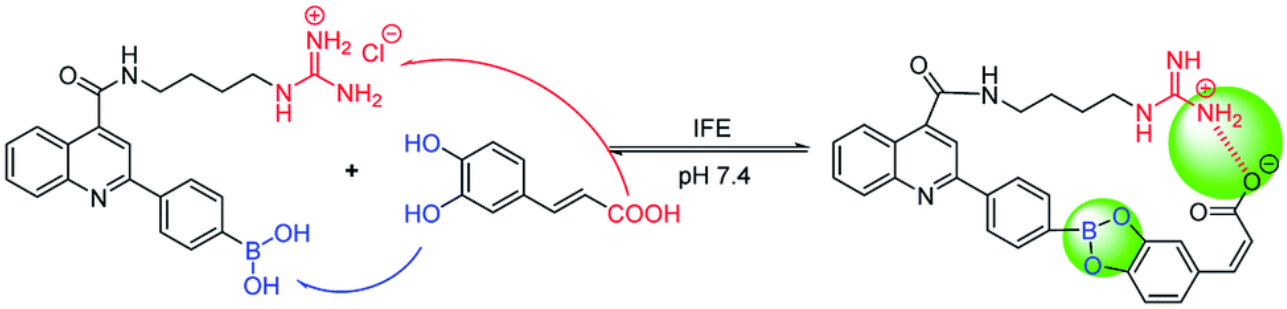

*Figure 4.5- Mechanism for the double site recognition sensor based on **5** for caffeic acid sensing.[19]*

The fluorophore has also been used to synthesize fluorescent MIPs for glycoprotein recognition prepared by introducing **5** as fluorescent monomer on the bead surface, then obtaining a molecularly imprinted surface by polymerizing the surface with aniline after template glycoprotein immobilization thanks to boronic esters formation with immobilized fluorescent reporter. The developed fluorescent MIP particles could exhibit fluorescence emission upon binding with target molecule, being able of specific recognition of model glycoprotein, while showing only poor fluorescence in the absence of the target (Figure 4.6).[20]

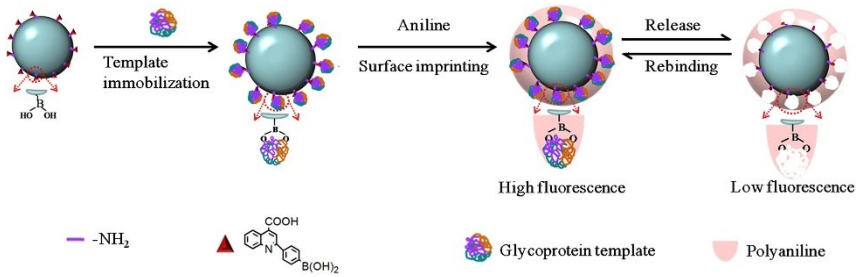

*Figure 4.6- Fluorescent MIP based on monomer **5** for glycoprotein recognition.[20]*

Fluorophore **5** has also been used for the development of recognition elements for analysis of metals such as Fe(III)[21] and Pd(II)[22].

Another very interesting fluorescent core that has been extensively reported in literature for sensing purposes, including the development of boronic acid containing molecules, is the 1,8-naphtalimide nucleus

(Figure 4.7).[23] In 2002, Lakowicz's group proposed two *N*-phenyl-1,8-naphthalimide derivatives, **6** and **7**, having the boronic acid moiety in *ortho* and *para* position respectively with respect to the *N*-phenyl group (Figure 4.7). Both molecules have an excitation wavelength of 345 nm, with emissions at around 400 nm in phosphate buffer at pH 7.5, and exhibited a pronounced fluorescence quenching passing from the neutral to the anionic form of the boronic acid moiety, as well as upon boronic esters formation with sugars.[24] Mohr's group designed another very interesting fluorescent probe, **8**, based on the 4-amino-1,8-naphtalimide nucleus (Figure 4.7). Such fluorophore has a large Stokes shift, with emission at 530 nm when exciting at 410 nm, and shows increase in its fluorescence upon sugar binding, showing particular selectivity for D-fructose.[25]

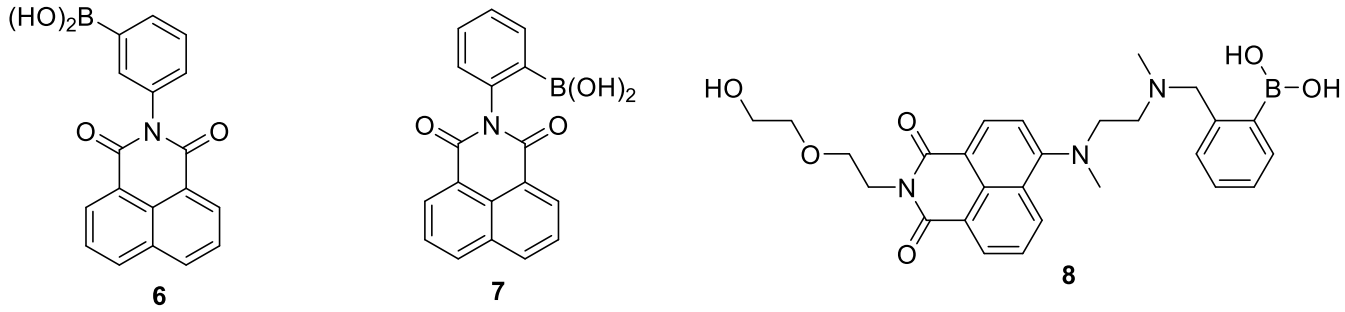

*Figure 4.7- Structure of 1,8-naphtalimide derivatives **6**, **7** and **8**.*

Other very interesting compounds were developed by Wang and colleagues (compounds **9a**-**9c** in Figure 4.8), which differ for the substitution at the 4-amino group of the naphthalimide ring. While compound **9a** having the amino group substituted with a benzyl group was decreasing its fluorescence upon binding with sugars, **9b** and **9c**, having a methyl and hydrogen atom respectively as the third substituent on the amino group, were increasing their fluorescence. **9c** was identified as the best candidate for further studies, being the one emitting at longer wavelength (570 nm) and being completely soluble in PBS (phosphate buffered saline) at the investigated concentrations without the need for adding other solvents.[26] Starting from **9c** structure, the same group investigated also the influence of inserting substituents on the aromatic ring in *para* position with respect to the boronic acid moiety. All four compounds **10a**-**10d** (Figure 4.8) exhibited very similar affinities and spectroscopic properties, thus meaning that the *para*-substituent does not make much difference. All of them had good water solubility, and the excitation and emission wavelengths were respectively 493 and 567 nm.[27]

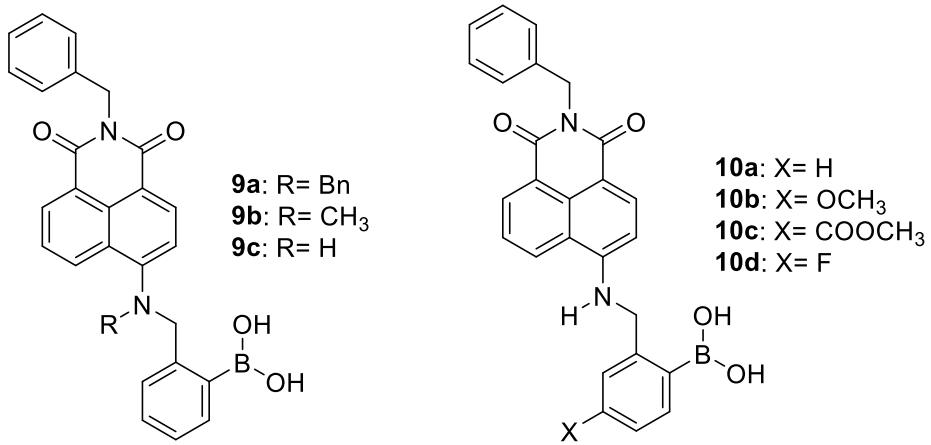

*Figure 4.8- Structures of naphthalimide derivatives **9a**-**9c** and **10a**-**10d**.*

4.2 FLUORESCENCE STUDY ON THE QUINOLINIC FLUOROPHORE

Amongst the different fluorophores for 1,2-diols sensing, comprising *ortho*-diphenols, the first building block tested was 2-(4-boronophenyl)quinoline-4-carboxylic acid **5**, which has been described in paragraph 4.1. In this work, due to the interest in targeting several molecules sharing the catechol moiety, such as caffeic acid, chlorogenic acid and hydroxytyrosol (Figure 4.9), the first step has been that of investigating the fluorescence behavior of fluorophore **5** in the presence of target molecules, by fluorescence titration experiments. Several of the experiments of chapter 4 of the present thesis have been done in collaboration with the master student Giulia Ciani, during her Master thesis internship.[28]

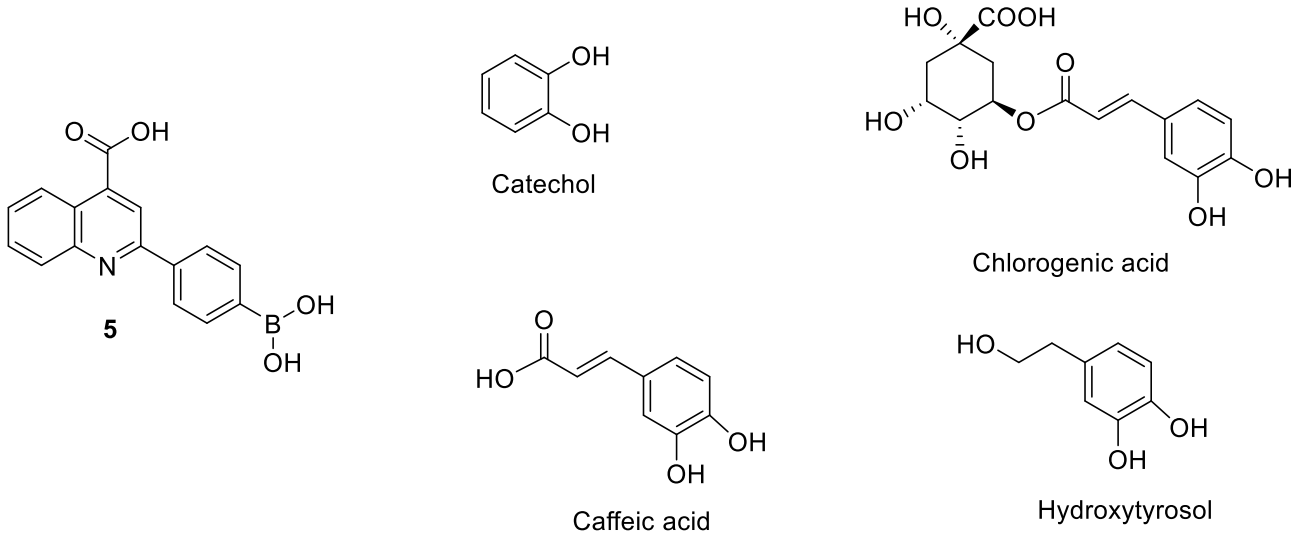

*Figure 4.9- Structure of fluorophore **5** and of target ortho-diphenols.*

4.2.1 Catechol

The first investigated compound was catechol (CC), the simplest molecule containing the *ortho*-diphenolic nucleus which is at the basis of molecular recognition of the other targets of interest, and whose interactions with **5** have already been reported in literature.[18] As a starting point, an emission spectrum has been registered on a 32 µM solution of **5** in phosphate buffer (100 mM, pH 7.4), observing a fluorescence emission at 390 nm when exciting at 335 nm, which is in accordance with data reported in literature (Figure 4.10 a). By adding increasing concentrations of CC in the range 354 nM-380 µM, a progressive fluorescence quenching was observed. According to Wu and colleagues, this effect can be attributed to the PET effect from the excited state of catechol to the quinolinic fluorescent nucleus, resulting in fluorescence quenching upon boronic ester formation.[18] By making a plot of the relative fluorescence emissions of the fluorophore with respect to CC concentration expressed on a logarithmic scale, a sigmoidal trend can be observed, even if further target concentrations should be considered to obtain the complete curve (Figure 4.10 b).

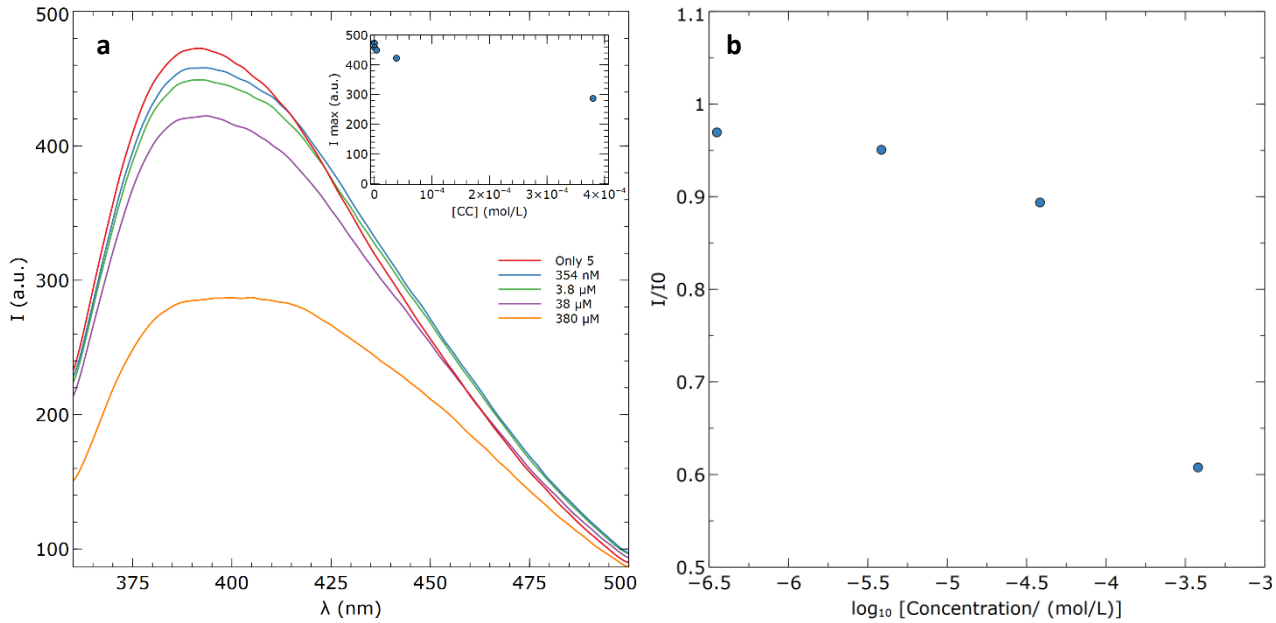

*Figure 4.10- (a) Fluorescence titration of 32 µM **5** with catechol (phosphate buffer 100 mM, pH 7.4, λ_{ex}= 335 nm); (b) Plot of relative fluorescence emission of **5** vs. CC concentration expressed on a logarithmic scale.*

4.2.2 Chlorogenic acid

After preliminary tests with catechol, a fluorescence titration has been conducted with CGA, one of the targets of interest. Also in this case, a 32 µM concentration of **5** in phosphate buffer has been used, adding increasing CGA concentrations in the range 393 nM-4 mM. A little fluorescence quenching could be observed between 393 nM and 43 µM concentrations. However, between 43 µM and 408 µM CGA concentrations, fluorescence was almost completely extinguished, and a huge red shift of 60 nm is observed (Figure 4.11 a). For this reason, the range of concentrations between 40 and 400 µM has been investigated in more details, repeating the titration in the range 37.8-897.5 µM (Figure 4.11 b). Even for the first investigated concentration, 37.8 µM, a 50% quenching can be observed, with the appearance of a tail in the emission at longer wavelengths. Fluorescence emission keeps diminishing at increasing CGA concentration, arriving at a complete red shift and emission quenching for the 897.5 µM concentration.

In this case, the hypothesis is that there might be an inner filter contribution to the fluorescence quenching, because CGA absorbs at around 330 nm, which means in the region of fluorophore **5** excitation, and might thus attenuate the quantity of radiation arriving to the fluorophore. To confirm this hypothesis, an inner filter correction has been applied (Equation 4.1) [29]

$$I_{corr} = I_{obs} \cdot 10^{\frac{A_{ex}+A_{em}}{2}} \quad \text{(Eq 4.1)}$$

Where I_{corr} is the fluorescence emission corrected for the inner filter effect, I_{obs} is the fluorescence emission experimentally measured, A_{ex} and A_{em} are the absorbances of the quencher -in this case CGA- calculated with the molar extinction coefficients at the excitation and emission wavelengths, whose values have been experimentally determined to be 8380 $L \cdot mol^{-1} \cdot cm^{-1}$ at the excitation wavelength (335 nm) and 1250 $L \cdot mol^{-1} \cdot cm^{-1}$ at the emission wavelength (390 nm). However, after inner filter correction, this effect has been proved to be negligible, and in any case, it would not account for the shift in emission wavelengths.

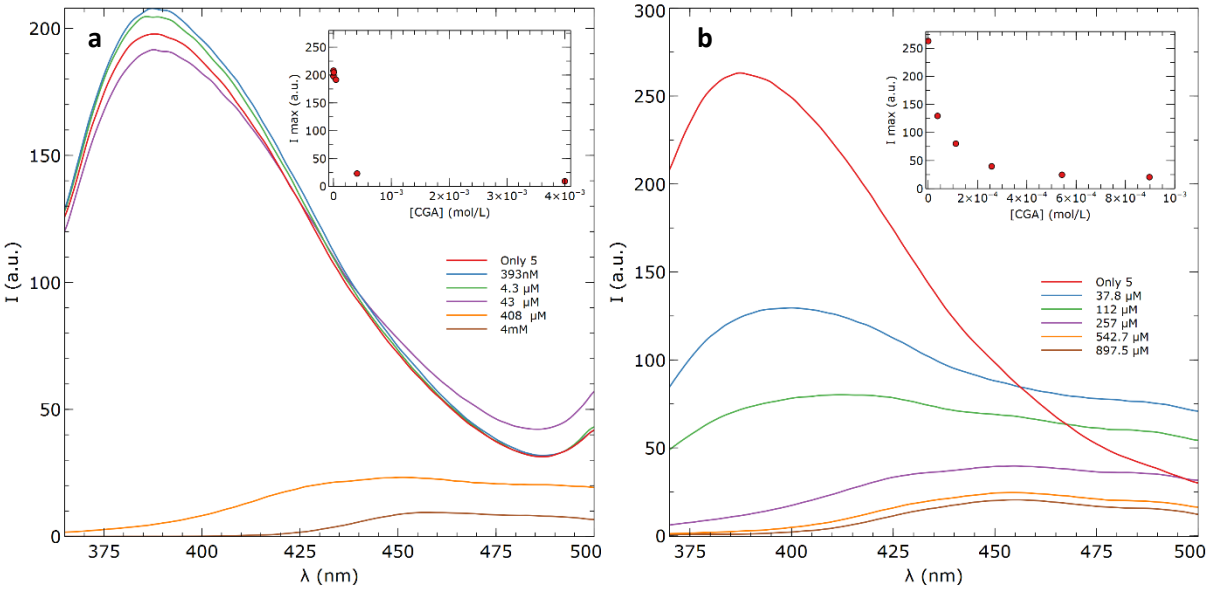

*Figure 4.11- (a) Fluorescence titration of 32 µM **5** at increasing CGA concentrations (393 nM-4 mM) (phosphate buffer 100 mM, pH 7.4, λ_{ex}= 335 nm); (b) Fluorescence titration of 32 µM **5** at increasing CGA concentrations (37.8-897.5 µM) (phosphate buffer 100 mM, pH 7.4, λ_{ex}= 335 nm).*

4.2.3 Hydroxytyrosol and caffeic acid

Since sensitivity of **5** was not very high during previous titrations with catechol and chlorogenic acid, its concentration has been increased to 66 µM in the following measurements with caffeic acid (CA) (Figure 4.12a) and hydroxytyrosol (HT) (Figure 4.12 b), whose concentrations have been investigated in the range 393 nM-4.5 mM.

In the case of caffeic acid, the fluorescence trend during titration is the same observed for CGA, with a fluorescence quenching accompanied by a marked red shift, reaching a 92% fluorescence quenching after the last addition. On the other hand, with HT, fluorescence quenching was not accompanied by any red shift, and quenching reached only the 59% for the highest HT concentration tested.

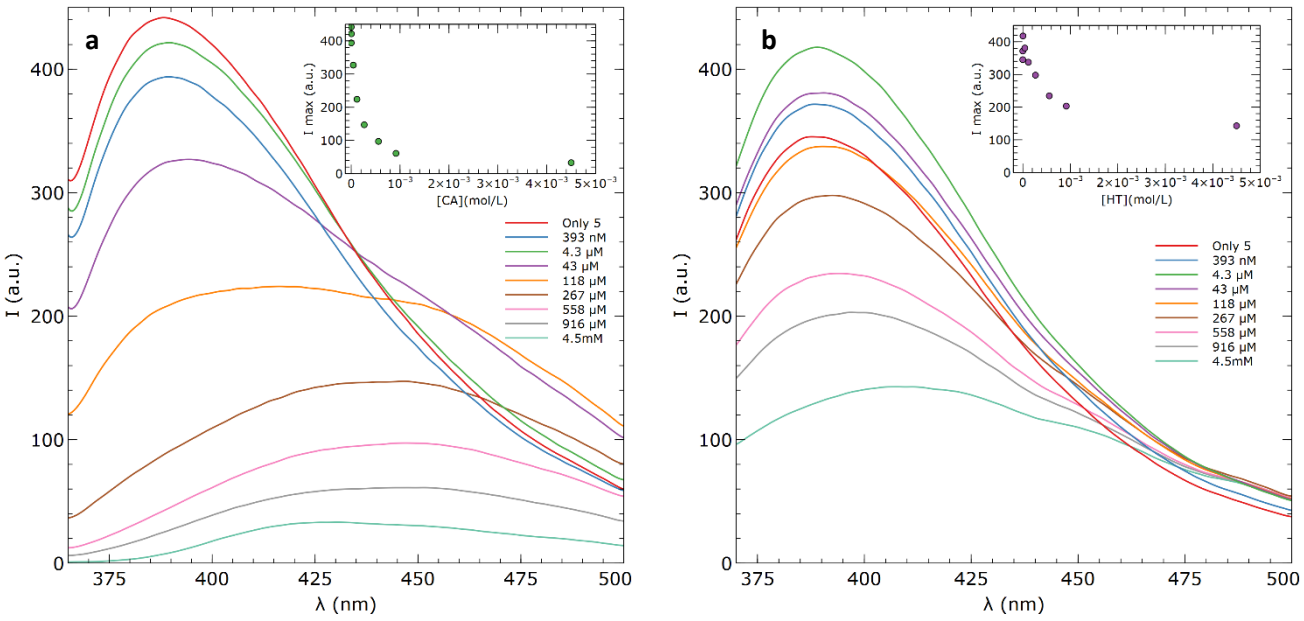

*Figure 4.12- (a) Fluorescence titration of 66 µM **5** at increasing CA concentrations (393 nM-4.5 mM) (phosphate buffer 100 mM, pH 7.4, λ_{ex}= 335 nm); (b) Fluorescence titration of 66 µM **5** at increasing HT concentrations (393 nM-4.5 mM) (phosphate buffer 100 mM, pH 7.4, λ_{ex}= 335 nm).*

4.2.4 Stern-Volmer analyses

A Stern-Volmer analysis based on Equation 4.2[29] has been performed, to elucidate the type of quenching occurring.

$$\frac{I_0}{I} = 1 + K_{SV}[Q] = 1 + k_q\tau_0[Q] \quad \text{(Eq 4.2)}$$

Where I_0 is the fluorescence emission of the fluorophore alone, I is the fluorescence intensity in the presence of a certain concentration of target (which acts as the quencher), K_{SV} is the Stern-Volmer constant and [Q] is the concentration of the target/quencher. From the Stern-Volmer constant, obtained from linear plots in Figure 4.13, it is possible to calculate the quenching constant k_q, since K_{SV} is the product of k_q and τ_0, which is the lifetime of the excited state of the fluorophore in the absence of the quencher. Depending on the obtained k_q values, it is possible to distinguish between a static and dynamic process. In fact, according to literature,[29] a value of k_q inferior to $1{\cdot}10^{10}$ $L{\cdot}mol^{-1}{\cdot}s^{-1}$, is diagnostic for a dynamic quenching, which means that the fluorescence quenching is due to collisions of the fluorophore with the quencher.

In this case, it is important to remark that the k_q values reported in Table 4.1 are approximated, since they have been calculated using a τ_0 value of 1.2 ns taken from the literature for a modified **5** structure and in a different solvent (methanol/water in a ratio 10:90).[16]

Table 4.1- Stern-Volmer analysis on CGA, CA, CC and HT

Analyte	K^{app}_{SV} ($L{\cdot}mol^{-1}$)	k_q ($L{\cdot}mol^{-1}{\cdot}s^{-1}$)
CGA	$2.15{\cdot}10^4$	$1.79{\cdot}10^{13}$
CA	$7.37{\cdot}10^3$	$6.15{\cdot}10^{12}$
HT	$1.00{\cdot}10^3$	$8.36{\cdot}10^{11}$
CC	$1.62{\cdot}10^3$	$1.35{\cdot}10^{12}$

Looking at the calculated k_q values, all of them are higher than the limit value, even if the parameters have been calculated using a τ_0 from literature for a different compound and in different solvent conditions. This seems to be indicative of a static quenching process for the interaction between the *ortho*-diphenolic analytes and the boronic acid derivative **5** (bearing in mind that the k_q values should be revised after determining the actual emission lifetime value for compound **5**).

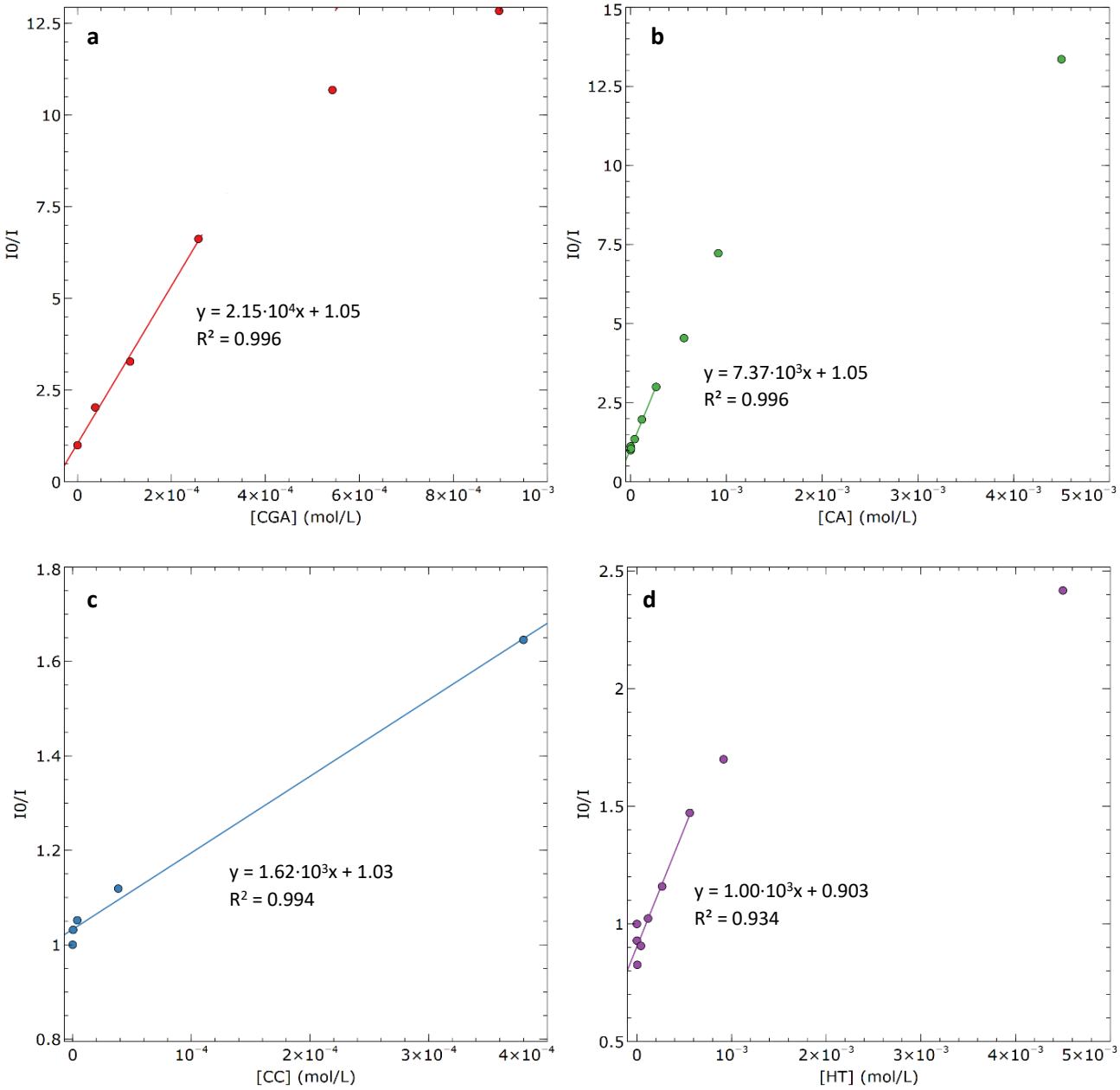

Figure 4.13 – Stern-Volmer plots of CGA (a), CA (b), CC(c) and HT (d) (phosphate buffer 100 mM, pH 7.4, λ_{ex} = 335 nm).

4.2.5 *p*-coumaric acid

After observing the red shift in fluorescence emission for CGA and CA, an attempt has been done to understand which portion is responsible for this behavior, not observed for the other two targets HT and CC. For this reason, fluorescence titrations have been carried out with *p*-coumaric acid (*p*-CA) (Figure 4.14), possessing the conjugated cinnamic acid portion present also in CGA and CA, with the difference of having only one hydroxyl group instead of the *ortho*-diphenolic moiety. As it can be seen in Figure 4.15, also in this case a quenching associated with a red shift can be observed, meaning that the shift at longer wavelengths is due to the cinnamic acid portion. Despite the impossibility to form a cyclic boronic ester as in the cases of *ortho*-diphenols, *p*-CA quenches the 62% of the initial **5** fluorescence. It is difficult to rationalize such behavior. One hypothesis is that the shift at longer wavelengths is caused by the formation of boronic esters with cinnamoyl derivatives (cyclic esters in the case of CGA and CA, non-cyclic in the case of *p*-CA). However, another possibility is that the shift is caused by non-covalent interactions with the hydroxycinnamic portion, such as π-π stacking interactions.

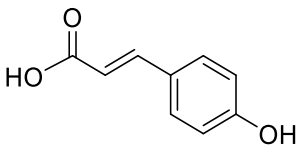

p-coumaric acid

Figure 4.14- Structure of p-coumaric acid.

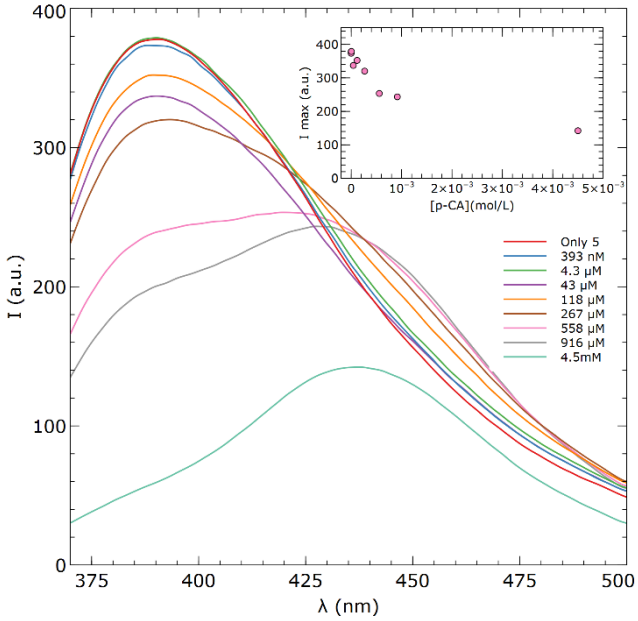

*Figure 4.15- Fluorescence titration of **5** 66 µM at increasing p-CA concentrations (393nM-4.5mM) (phosphate buffer 100 mM, pH 7.4, λ_{ex} = 335 nm).*

4.2.6 Quinic acid

Finally, considering that chlorogenic acid can in principle form boronic esters both through the *ortho*-diphenolic moiety and through the quinic acid portion -that can be assimilated to a monosaccharide-, titrations have been carried out also with quinic acid (QA), to understand if formation of boronic esters occurs also at this site of CGA molecule (Figure 4.16).

Also in this case a 66 µM **5** solution in phosphate buffer has been titrated using increasingly high quantities of target quinic acid, in a range between 393 nM and 558 µM (Figure 4.17). Differently from all the other tested molecules, but coherently with what reported in the literature for monosaccharides, a fluorescence increase has been observed. Therefore, since for CGA titrations a fluorescence quenching is observed, this experiment confirms that for chlorogenic acid the *ortho*-diphenolic moiety is the one responsible for binding.

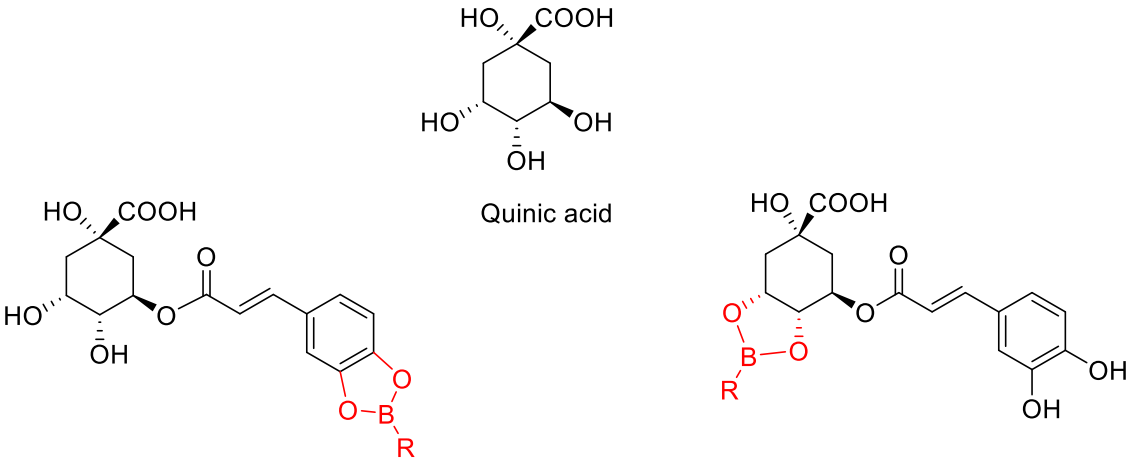

Figure 4.16- Structure of quinic acid and possibilities of boronic esters formation of CGA.

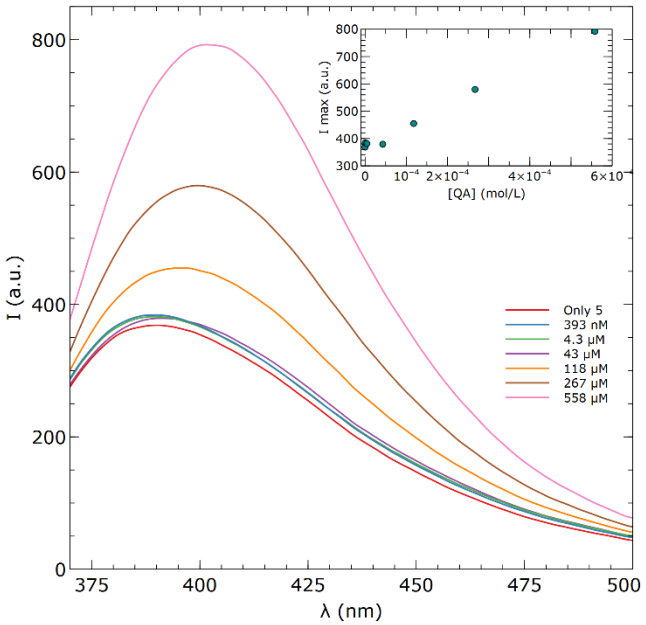

*Figure 4.17- Fluorescence titration of **5** 66 µM at increasing QA concentrations (393nM-558 µM) (phosphate buffer 100 mM, pH 7.4, λ_{ex} = 335 nm).*

.

4.2.7 Final considerations

Fluorophore **5**, as already mentioned in paragraph 4.1, has already found application for the detection of *ortho*-diphenols, showing a fluorescence quenching upon target molecule addition. It has been employed in the detection of catechol alone,[18] but derivatives of this compound have also been applied to detection of more complex molecules. For example, **5** has been conjugated to multi-walled carbon nanotubes for dopamine detection,[30] and diboronic acid derivatives have been used to quantify the same target with a detection limit of $7.7 \cdot 10^{-6}$ mol $\cdot$ L^{-1}.[31] The **5** derivative containing the guanidinium moiety already mentioned at paragraph 4.1 has been already employed for analysis of one of the target of interest, caffeic acid, showing a quenching of fluorescence, with a calculated LOD of $1.81 \cdot 10^{-6}$ mol $\cdot$ L^{-1}.[19] Despite the fact that Bian and colleagues already stated that **5** alone performs worse than when it is inserted into the double-site receptor, before using this fluorophore for the construction of peptide recognition elements, our idea was that of testing in more details the performances of **5** both with caffeic acid and with other target molecules never tested before. In particular, the hope was that of observing for CGA the fluorescence enhancement that very often **5** exhibits with saccharide molecules, thanks to the presence on CGA of the saccharide-like quinic acid

moiety, that might in principle be involved in boronic esters formation instead of the *ortho*-diphenolic one. However, after preliminary results obtained, despite the application of **5** is well documented in literature - very recently in 2022 it was applied to the synthesis of a double-site receptor for gallic acid-[32], it was decided to change the type of fluorophore. This choice has been taken in the perspective of observing a fluorescence emission at longer wavelengths, thus having a fluorescence quenching independent from the inner filter effect at lower wavelengths, in which plenty of optical interferents might cause problems when analyzing real samples.

4.3 NAPHTHALIMIDE FLUOROPHORE

The second reporter selected for *ortho*-diphenols is fluorophore **20**: it is composed by a 4-amino-1,8-naphthalimide portion, responsible for its fluorescent properties, functionalized with a phenylboronic acid moiety, necessary to covalently bind *ortho*-diphenols or 1,2-/1,3-diols through the formation of boronic esters. This structure is inspired to naphthalimide derivative **9c** proposed by Wang and coworkers for the recognition of sugars previously discussed at paragraph 4.1,[26] but instead of having the benzyl moiety linked to the naphthalimide nitrogen, a primary amino group to allow further conjugation of the fluorophore has been introduced (Figure 4.18). Due to changes made on the fluorophore structure, some steps of the synthetic pathway had to be modified with respect to the one proposed by Wang and colleagues.

It is important to highlight that application of analogues of the fluorophore **20** has never been reported in literature for *ortho*-diphenols detection, nor their application to the development of peptide recognition elements.

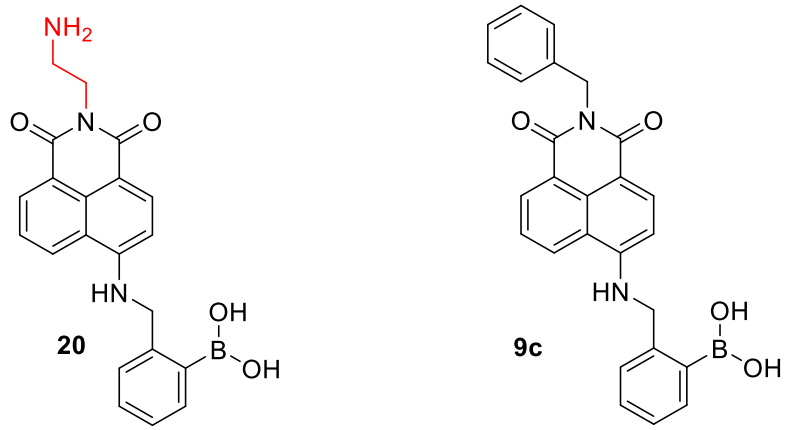

*Figure 4.18- Comparison between structure of fluorophore **20** and fluorophore **9c**.*

4.3.1 Synthesis of the fluorophore 20

The naphthalimide fluorophore **20** has been synthesized according to the procedure reported in Scheme 4.3.

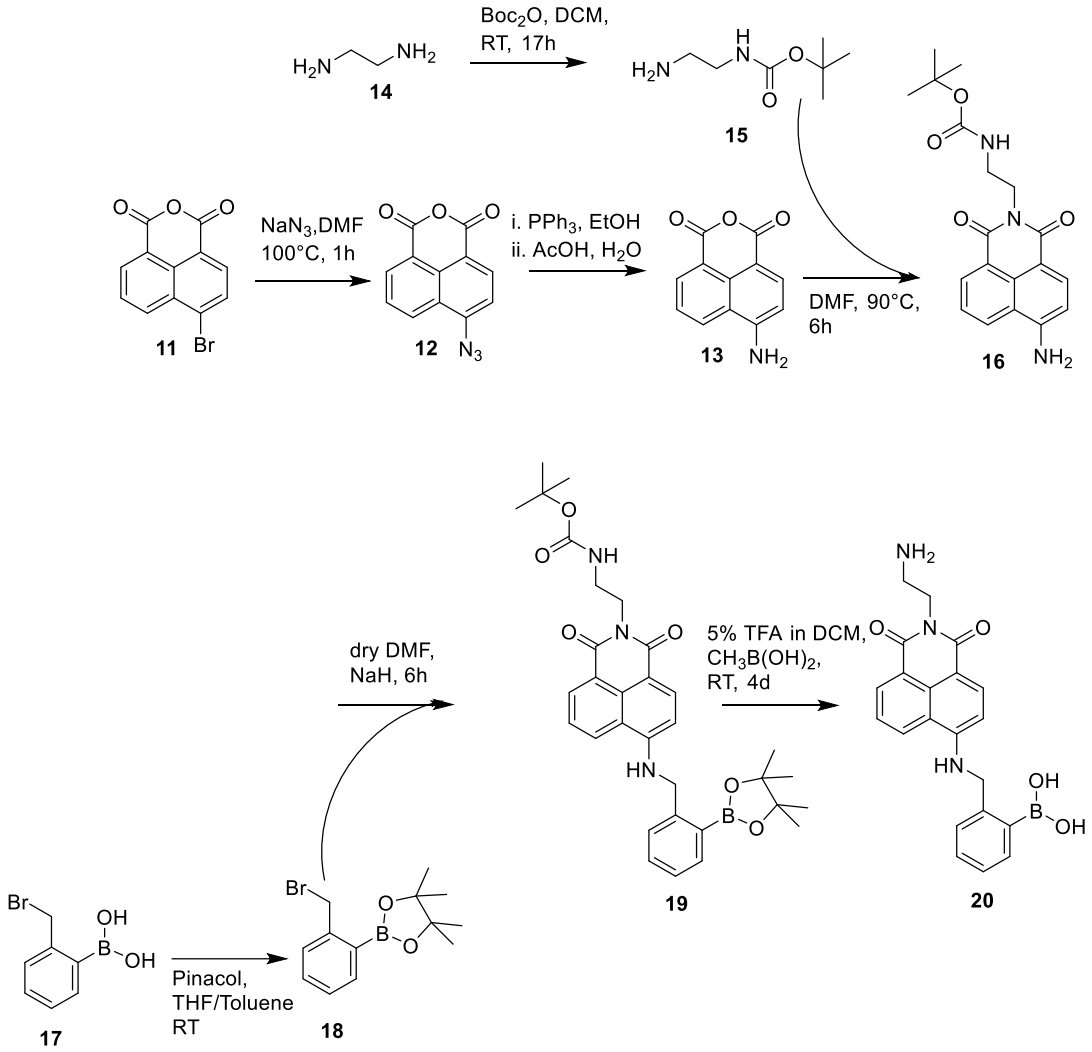

*Scheme 4.3- Synthetic pathway to obtain fluorophore **20**.*

The first step is the synthesis of 4-amino-1,8-naphthalic anhydride **13** starting from 4-bromo-1,8-naphthalic anhydride **11**, according to a procedure reported in the literature[33] proceeding through the nucleophilic aromatic substitution on **11** with sodium azide, carried out heating the reaction mixture in DMF for 1 hour at 100°C. A Staudinger reaction is then performed on compound **12** with triphenylphosphine, obtaining **13** with a yield of 82%. In parallel *N*-boc-ethylenediamine **15** has been synthesized by reacting ethylenediamine **14** in excess with di-*tert*-butyl-dicarbonate, with a yield of 82%.[34] Then, **15** has been reacted with **13**, obtaining naphthalimide **16** with a 89% yield.[35]

In order to obtain compound **19**, the initial idea based on the procedure of Wang and colleagues for a similar compound,[26] was that of reacting **16** with 2-bromobenzyl bromide **21**, and then performing a Miyaura reaction on the intermediate **22** to obtain the boronic ester **19** (Scheme 4.4). However, after obtaining the intermediate bromide **22**, the Miyaura reaction, successfully applied in other cases, did not work.

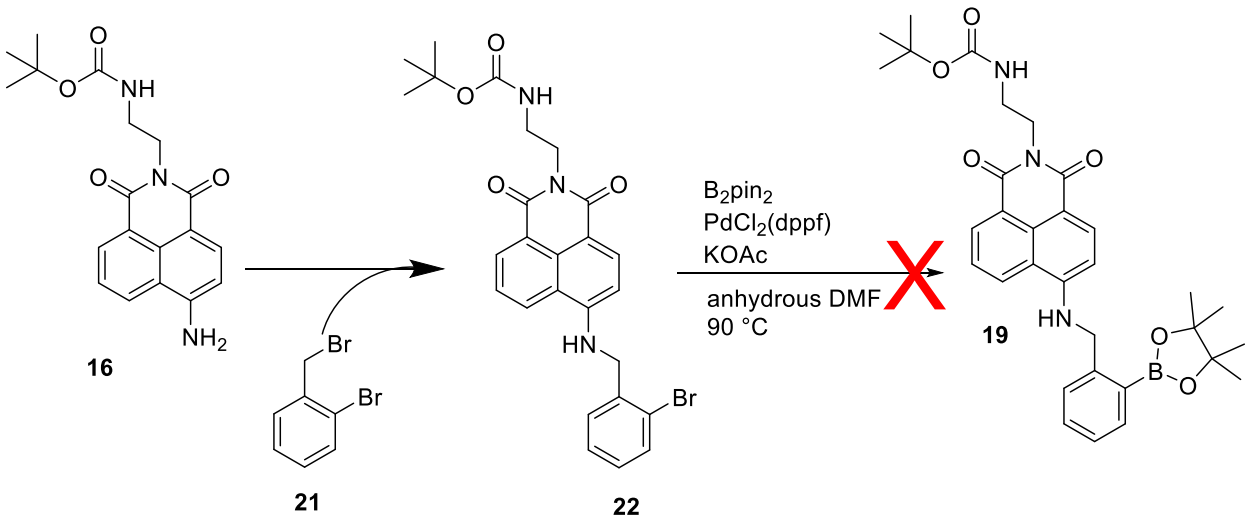

*Scheme 4.4- Unsuccessful reaction pathway to obtain **19**.*

Therefore, it has been decided to use directly the phenylboronic acid moiety **18**, protected in the form of the boronic ester to avoid collateral reactions. Protection of the boronic acid has been achieved by reacting 2-bromomethyl phenylboronic acid **17** with the diol pinacol,[36] obtaining **18** with a 99% yield (Scheme 4.5).

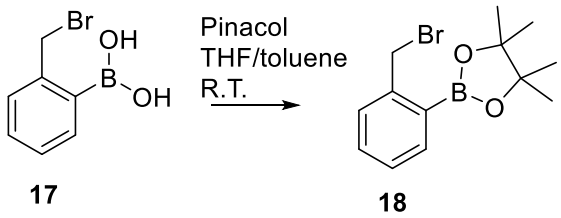

*Scheme 4.5- Synthesis of **18** from **17**.*

At this point, **16** and **18** have been reacted in a nucleophilic substitution reaction, working under inert atmosphere, using sodium hydride as a strong base to allow deprotonation of the aromatic amine of **16**. After analysis by ^{1}H-NMR (Figure 4.19), ^{13}C-NMR and bidimensional NMR spectra, it has been possible to conclude that by this way product **19** has been obtained pure enough, with a yield of 77%.

Looking at the ^{1}H-NMR spectrum in DMSO-d_6 (Figure 4.19), it is possible to observe two singlets at 1.24 ppm and 1.30 ppm, integrating for 9 and 12 protons respectively, that can be assigned to the three methyl groups of Boc and to the four methyl groups of pinacol boronic ester. The quartet at 3.48 ppm and the triplet at 4.07 ppm, each integrating for 2 protons can be attributed to the methylene protons respectively in α and β position with respect to the carbamate nitrogen. The doublet at 4.85 ppm can be assigned to the benzyl methylene. The spectral area between 6.64 and 8.72 ppm comprises all the aromatic, carbamic and amino protons of the molecule.

Moreover, in the mass spectrum it is possible to observe two peaks of interest at 594.4 m/z, corresponding to the $[M+Na]^+$ adduct and at 572.5 m/z, corresponding to the $[M+H]^+$ adduct.

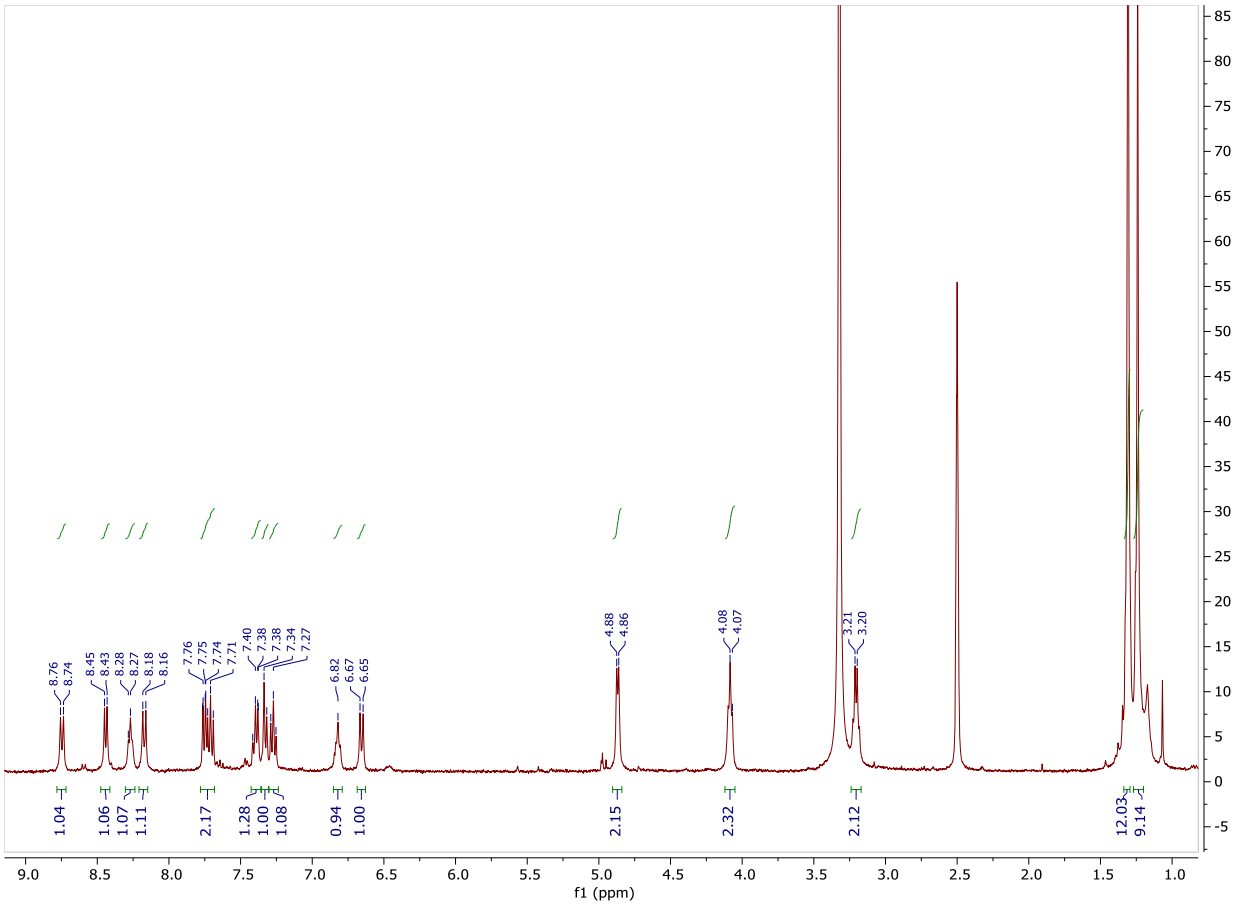

*Figure 4.19- ^{1}H-NMR of **19** (DMSO-d_6).*

Finally, the last step has been the deprotection of the *tert*-butoxycarbonyl protecting group from the aliphatic amine and of the boronic ester moiety to obtain the free boronic acid. Deprotecting the boronic ester has proved to be a quite problematic issue since it required 7 days of reaction with 90% TFA with 10% of water. To decrease such a long reaction time in concentrated acid, based on the work by Hinkes and Klein,[37] a new protocol has been tested consisting of the transesterification reaction of the boronic ester **19** with methylboronic acid in DCM with 5% of TFA: this allowed formation of the methylboronic acid ester with pinacol and deprotection of **19**. Since methylboronic ester with pinacol is volatile, it is possible to evaporate the mixture to obtain **20** in the completely deprotected form (Scheme 4.6).

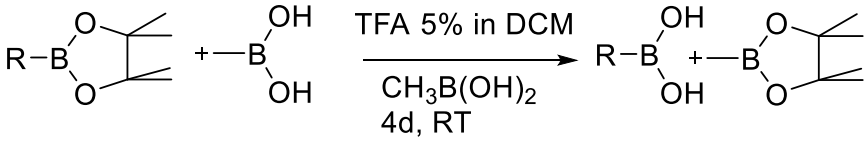

Scheme 4.6- Deprotection of boronic acids using methylboronic acid.

Characterization of **20** has been performed by ^{1}H-NMR (Figure 4.20), ^{13}C- and bidimensional NMR spectra. Looking at the ^{1}H-NMR spectrum in DMSO-d_6 (Figure 4.20), it is possible to observe the disappearance of the Boc and pinacol ester signals present in the spectrum of the precursor **19**, whereas at 8.31 ppm there is the appearance of a singlet integrating for 2 protons diagnostic for the two hydroxyl protons of the deprotected boronic acid moiety. Signals at 3.10, 4.25 and 4.82 ppm are attributable to the three methylene groups in the molecule, whereas between 6.6 and 8.8 ppm all the 14 aromatic, amino and boronic acid protons of fluorophore **20** can be detected.

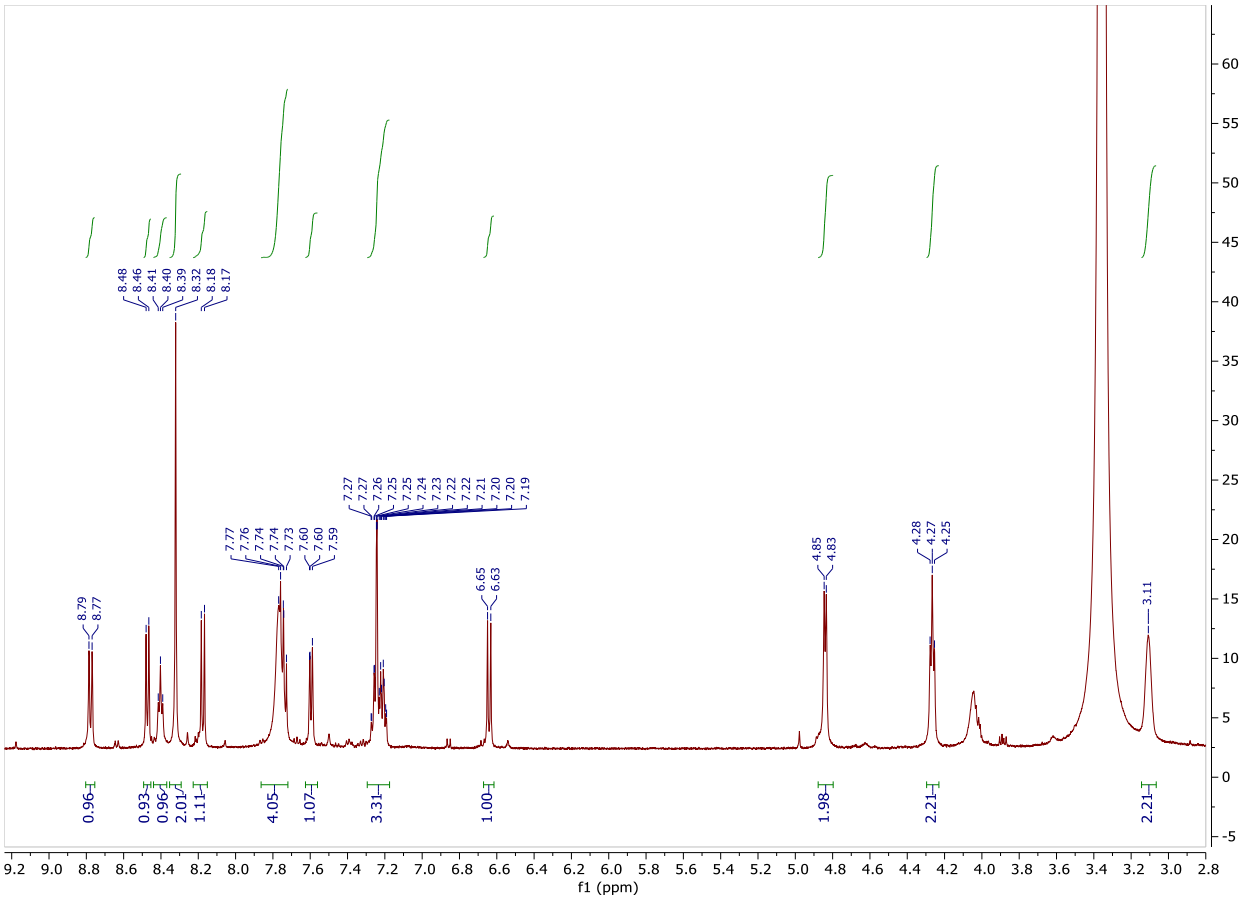

*Figure 4.20- ^{1}H-NMR of **20** (DMSO-d_6).*

4.3.2 Fluorescence experiments with fluorophore 20

Fluorescence behavior of fluorophore **20** has been studied in the presence of increasing concentrations of target molecules. In fact, structures very similar to fluorophore **20** have been reported to change their fluorescent properties upon binding with different monosaccharides, showing an increase in their fluorescence.[26,27] However, such compounds have never been studied in the presence of *ortho*-diphenols.

4.3.2.1 Catechol, caffeic acid, chlorogenic acid and hydroxytyrosol

As in the case of fluorophore **5**, catechol, which is not a target of interest for us but is the simplest *ortho*-diphenol available, has been the first investigated molecule, allowing to study the influence of the catecholic portion, present in all the targets of interest, without having other structures influencing the interaction.

The emission spectrum of the fluorophore alone at a 52 µM concentration has been registered in sodium phosphate buffer 0.1 M, pH 7.4, as previously done for **5**: by exciting at 490 nm, a maximum emission at 550 nm could be observed. To the same solution, aliquots containing increasing quantities of catechol have been added, in a range between 393 nM and 10.4 mM, registering an emission spectrum after each addition, waiting some minutes to let the system to equilibrate. For all the tested concentrations, a fluorescence quenching could be observed, reaching almost complete quenching with the 10.4 mM concentration (Figure 4.21 a).

After assessing that there is a quenching of fluorescence in the presence of catechol, the same analysis has been performed also for the other target CGA, CA and HT, using target concentrations in the range 393 nM-4.5 mM (10.4 mM for HT) (Figure 4.21 c-d): in all cases fluorescence quenching has been observed.

Considering CGA, as already mentioned (paragraph 4.2.6) since it has two possibilities of boronic esters formation (through caffeic acid moiety and quinic acid portion), fluorescence titrations with quinic acid alone have been carried out in the same conditions: in this case, emission changed in an irregular way, and this result seems to confirm that chlorogenic acid reacts with **20** through the caffeic acid portion.

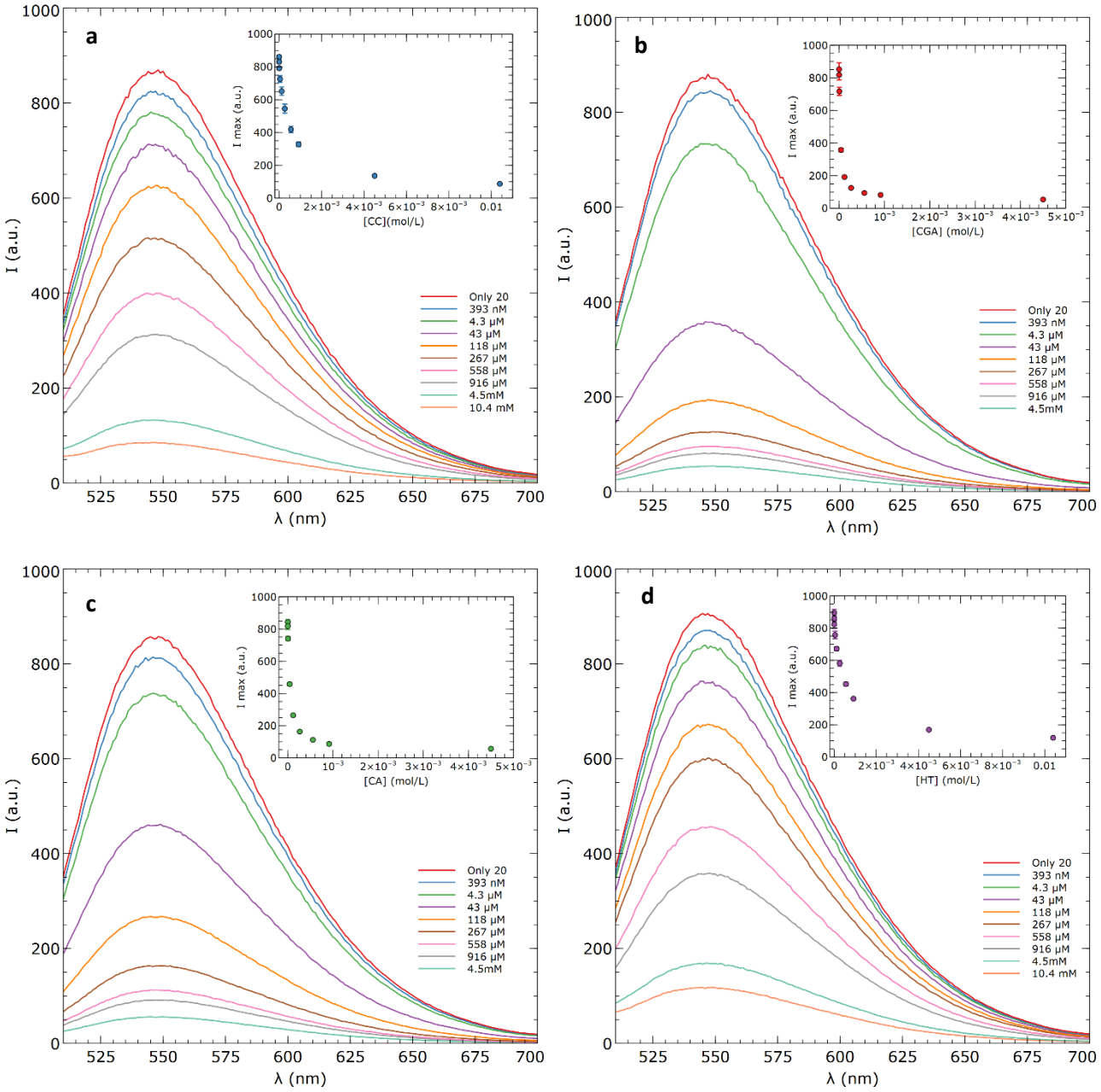

*Figure 4.21- Fluorescence titration of **20** 52 µM at increasing concentrations of catechol (a), chlorogenic acid (b), caffeic acid (c) and hydroxytyrosol (d)(phosphate buffer 100 mM, pH 7.4, λ_{ex} = 490 nm).*

Then, for all the four targets the Stern-Volmer analysis has been performed, to elucidate if the quenching is of a static or dynamic nature, according to the Stern-Volmer Equation (see paragraph 4.2.4) (Eq 4.2)

$$\frac{I_0}{I} = 1 + K_{SV}[Q] = 1 + k_q\tau_0[Q] \qquad \text{(Eq. 4.2)}$$

After obtaining the K_{SV} from the slopes of the Stern-Volmer plots (Figure 4.22), the quenching constant k_q has been obtained by dividing the K_{SV} for the τ_0 value of 0.07 ns in ethanol, found in the literature for a similar

fluorophore structure containing a 4-amino-1,8-naphthalimide core.[38] The K_{SV} and k_q values obtained for all the four compounds have been reported in Table 4.2. In all the cases τ_0 values higher than the limit value of $1 \cdot 10^{10}$ have been found, thus indicating the presence of a static quenching mechanism, which would be in agreement with covalent boronic esters formation as the fluorescence quenching mechanism.

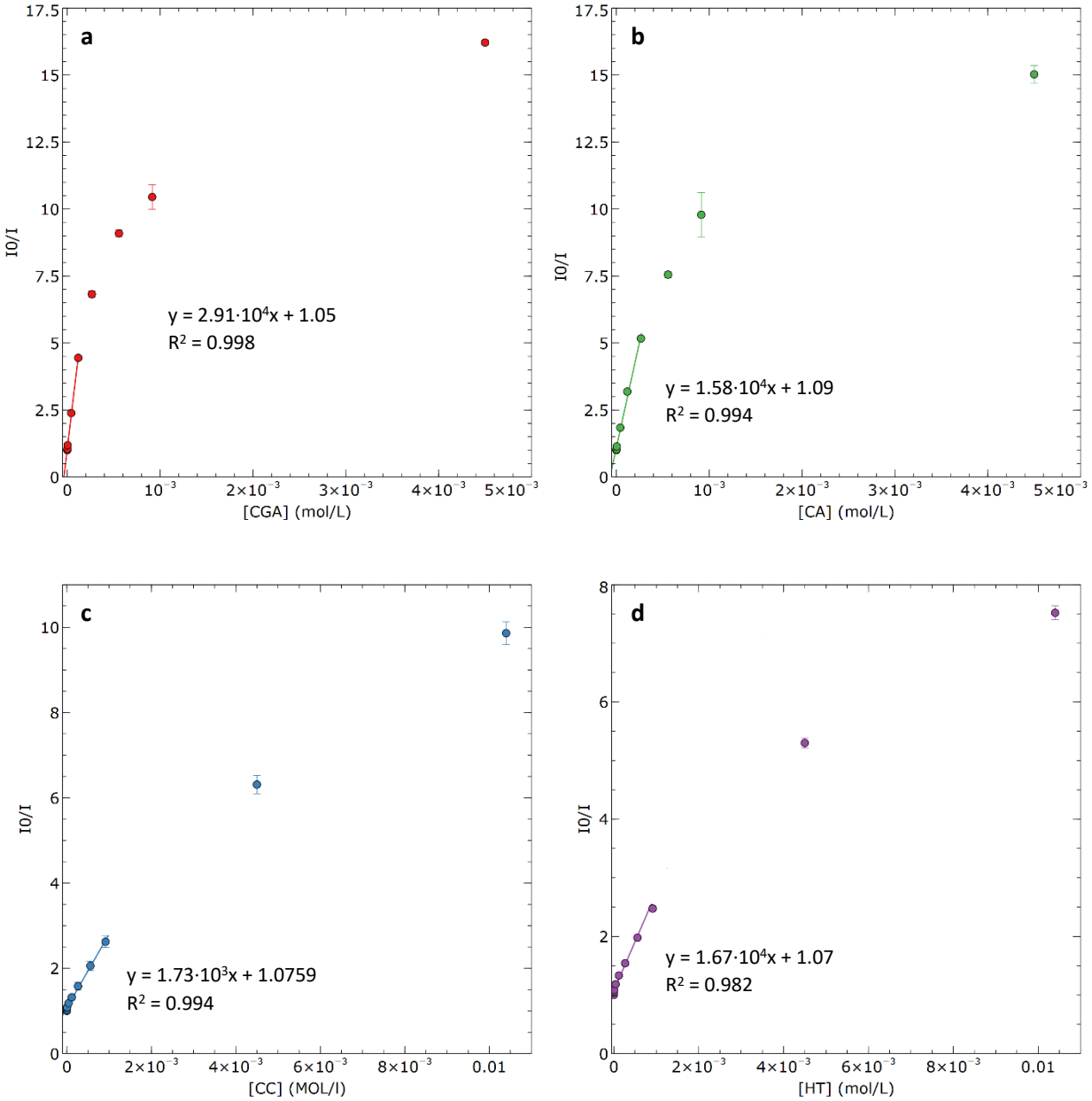

*Figure 4.22- Stern-Volmer plots for fluorescence titrations of **20** with chlorogenic acid (a), caffeic acid (b), catechol (c) and hydroxytyrosol (HT) (phosphate buffer 100 mM, pH 7.4, λ_{ex} = 490 nm).*

*Table 4.2- Parameters obtained from Stern-Volmer analysis of **20** with CGA, CA, HT and CC.*

Analite	K^{app}_{SV} ($L \cdot mol^{-1}$)	k_q ($L \cdot mol^{-1} \cdot s^{-1}$)
CGA	$2.91 \cdot 10^4 \pm 6.7 \cdot 10^2$	$4.15 \cdot 10^{14}$
CA	$1.58 \cdot 10^4 \pm 2.2 \cdot 10^2$	$2.26 \cdot 10^{14}$
HT	$1.67 \cdot 10^3 \pm 9.6$	$2.39 \cdot 10^{13}$
CC	$1.73 \cdot 10^3 \pm 1.4 \cdot 10^2$	$2.47 \cdot 10^{13}$

After the Stern-Volmer analysis, the selectivity of the fluorophore **20** towards the different targets has been evaluated, by plotting the ratio I/I_0 with respect to the logarithm of the target concentration.

For all the considered molecules, it is possible to observe a sigmoidal trend (Figure 4.23). Since boronic ester formation is a reversible reaction, this type of shape might reflect an equilibrium situation between the bound and unbound fluorophore, hypothesizing that fluorescence emission at each concentration is proportional to the fraction of free fluorophore. This is suggested also by the shape of the curves, with an 85% quenching occurring within two orders of magnitude, as suggested by the Langmuir isotherm, describing this type of phenomena by a simple model of reversible interactions with a 1:1 stoichiometry. Moreover, the slope of the curves in the linear region can be approximated to be the same, which suggests that the four binding phenomena obey to the same stoichiometry.

In these conditions, using the approximation of the Langmuir model (Eq. 4.3), the inflection point can be considered as correlated to the value of the apparent dissociation constant (K_d^{app}) of the reaction:

$$\frac{[RL]}{[R_0]} = \frac{[L_0]}{[L_0] + K_D} \quad \text{(Eq. 4.3)}$$

where $[R_0]$ is the initial concentration of the receptor (in this case fluorophore **20**), $[L_0]$ is the initial ligand concentration (in this case one of the *ortho*-diphenolic molecules), [RL] is the concentration of the complex receptor-ligand and K_d is the dissociation constant. This is only an apparent value (K_d^{app}), which is valid only for the fluorophore concentration used for the measurements, but it allows to compare the ligands.

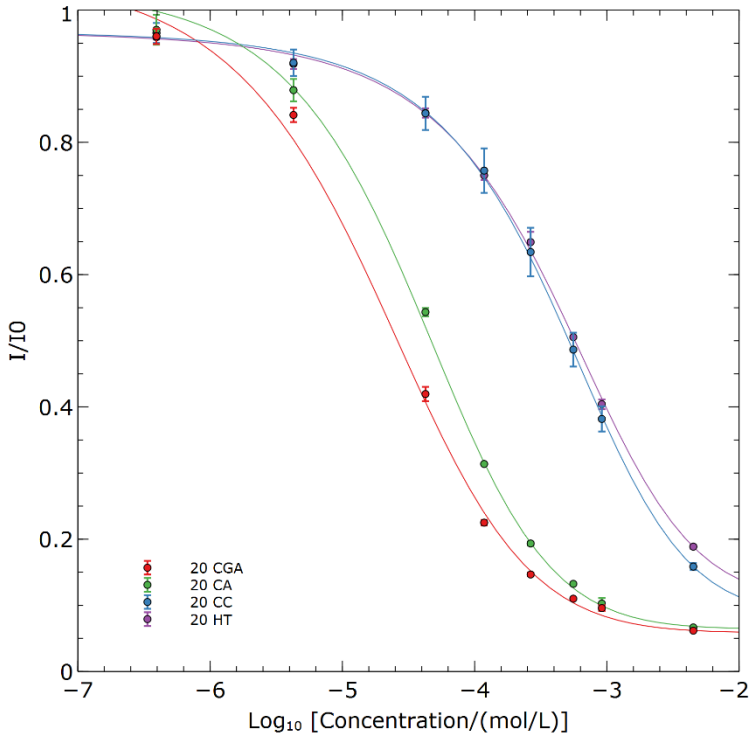

*Figure 4.23- Binding isotherms on a logarithmic scale for **20**.*

*Table 4.3- Apparent K_d values of **20** with CGA, CA, HT and CC.*

Analite	K_d^{app} **20 (mol/L)**
CGA	$2.55 \cdot 10^{-5} \pm 1.4 \cdot 10^{-6}$
CA	$4.37 \cdot 10^{-5} \pm 1.4 \cdot 10^{-6}$
HT	$4.70 \cdot 10^{-4} \pm 7.5 \cdot 10^{-6}$
CC	$4.58 \cdot 10^{-4} \pm 4.7 \cdot 10^{-5}$

Looking at the apparent K_d, (Table 4.3), it is possible to observe that chlorogenic acid and caffeic acid values are one order of magnitude lower with respect to catechol and hydroxytyrosol, and this might be due to the different structure of the molecules. In fact, CA and CGA have an extended conjugated system that in the boronic esters also involves the boron atom, thus providing further stabilization to the structure. On the other side, catechol and hydroxytyrosol cannot exploit such conjugation, and their K_d^{app} values are very similar and less favorable.

4.3.2.2 p-coumaric acid and tyrosol

After testing the performance of the fluorophore **20** in the presence of molecules containing an *ortho*-diphenolic moiety, the behavior of **20** has been further studied with molecules structurally related to the analyzed targets, but lacking the *ortho*-diphenolic portion, to confirm that the mechanism behind fluorescence changes is the formation of covalent cyclic boronic esters.

For this purpose, *p*-coumaric acid and tyrosol have been selected, being the analogues of caffeic acid and hydroxytyrosol respectively, with only one phenolic group, performing fluorescence titrations in the same conditions as previously done. In the case of tyrosol (Figure 4.24 a), fluorescence remains almost constant with all the additions. On the other hand, considering *p*-coumaric acid (Figure 4.24 b), starting from the 267 µM concentration there is a quenching of fluorescence, even if to a less extent with respect to the one observed for the *ortho*-diphenolic targets. In fact, fluorescence quenching reaches a maximum of 20% adding the highest *p*-coumaric acid concentration, whereas at the same concentration CA reached a 92% of quenching. Such results can be attributed to non-covalent interactions in fluorescence quenching. Probably, since the quenching is observed for *p*-coumaric acid and not for tyrosol, the ionic interactions involving the deprotonated carboxylic group of the target and the protonated amino group of the fluorophore might be responsible for the non-covalent interactions, even if also the extended conjugated system of cinnamic acid derivatives might play a role. Another possibility is that also esters with only one hydroxyl group might form, even if they are much less stable. However, the most important contribution seems to be the boronic ester formation with *ortho*-diphenolic moieties.

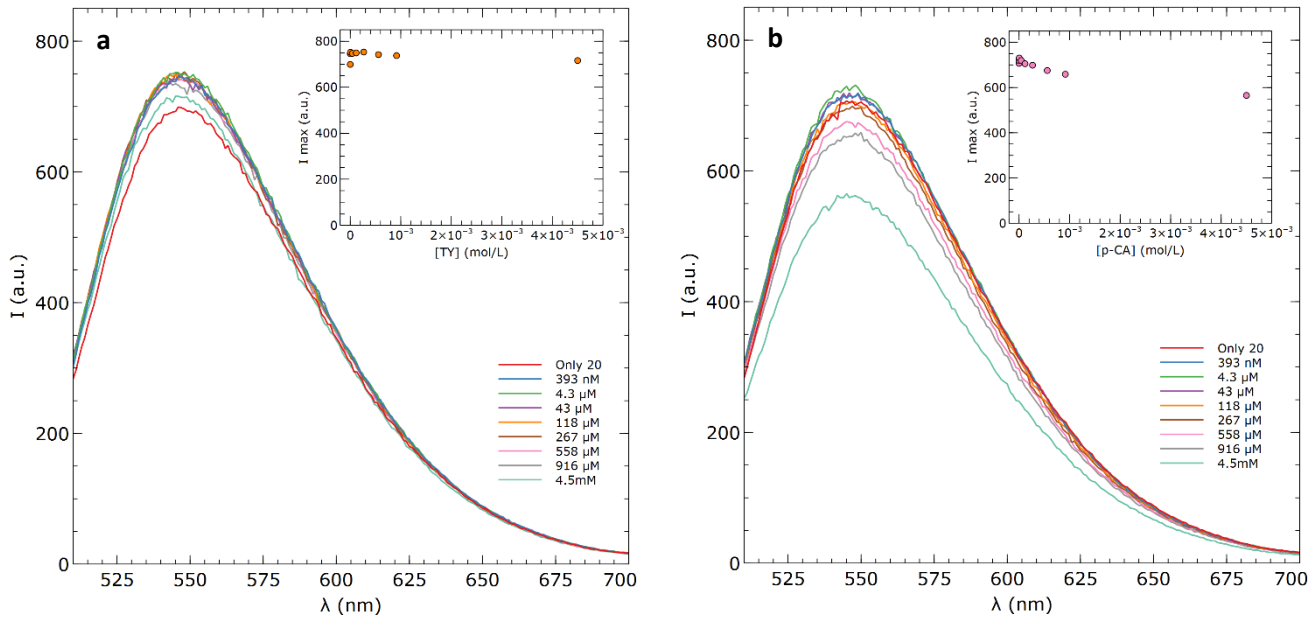

*Figure 4.24- Fluorescence titration of **20** 52 µM at increasing concentrations of tyrosol (a) and p-coumaric acid (b) (phosphate buffer 100 mM, pH 7.4, λ_{ex} = 490 nm).*

4.4 FLUORESCENT PEPTIDES

After testing the performances of **5** and **20**, the naphthalimide fluorophore **20** was selected as the most promising one due to its fluorescent properties. In fact, it is the one showing the highest fluorescence emission and it emits at longer wavelengths (550 nm with respect to the 390 nm of the **5** fluorophore), and for this reason, the inner filter effect should not be relevant (also considering possible optical interferences in real samples), with the only covalent boronic esters formation reaction responsible for the change in the fluorescence emission of the reporter.

20 was so used for the development of fluorescent peptides, inserting the fluorophore into a peptide sequence capable of promoting the interaction with the target molecule and providing some selectivity, due to increasing affinities for the target molecules.

Three peptide sequences have been selected:

-**P3**: **20**-succinyl-dPro-Pro-Trp-NH_2

-**P4**: Acetyl-Arg-Gly-Glu(**20**)-Gly-NH_2

-**P5**: Acetyl-Arg-Gly-Glu(**20**)-dPro-Pro-Ala-His-Glu-NH_2.

4.4.1 Peptide P3

4.4.1.1 Synthesis and characterization

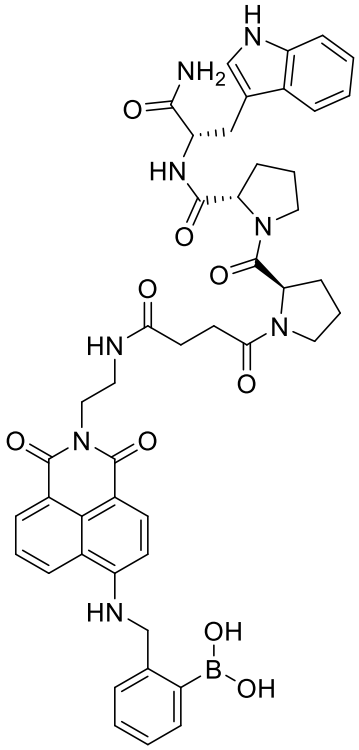

*Figure 4.25- Structure of peptide **P3.***

P3 (Figure 4.25), having the sequence **20**-succinyl-dPro-Pro-Trp-NH_2, was selected as a short explorative tripeptide to investigate the influence on target binding of a proline diad conferring a secondary loop structure, and that of tryptophan capable of establishing π-π stacking interactions with the aromatic benzene ring of *ortho*-diphenolic targets. The synthesis of the peptide scaffold has been carried out in solid state as

previously described[i] (see paragraph 3.3.2, peptides **P1** and **P2**): the only difference with respect to synthesis of peptides **P1** and **P2**, is the fact that in this case the first and the second coupling with the amino acids have been done with two different strategies:

-using ethyl cyano(hydroxyimino)acetate (OXYMA) / *N*,*N*'-diisopropylcarbodiimide (DIC) for the first one;

-using 2-(1H-Benzotriazole-1-yl)-1,1,3,3-tetramethylaminium tetrafluoroborate (TBTU), 1-Hydroxybenzotriazole hydrate (HOBT) and diisopropylethylamine (DIPEA) for the second one.

After synthesizing the peptide scaffold, coupling with the fluorophore **20** has been performed by introducing on the amino-terminal D-Proline a succinyl linker to be reacted with the free amino group of **20**. Coupling with the fluorophore has then been done using HATU (1-[Bis(dimethylamino)methylene]-1H-1,2,3-triazolo[4,5-b]pyridinium 3-oxide hexafluorophosphate) as coupling agent, HOBT as nucleophilic catalyst and collidine as the base, performing the coupling for 24 hours at room temperature twice.

Subsequently, cleavage from the resin and deprotection of the protecting group on the lateral side chain (in this case, boc of the tryptophan residue) have been performed in TFA at 95% with triisopropylsilane (TIS) and water as scavengers. Then, the crude peptide has been precipitated with diethyl ether and analyzed by mass-spectrometry.

Peptide **P3** has been purified by preparative HPLC, using a gradient of water and acetonitrile, and identification was performed by mass spectrometry. In fact, the fraction of interest showed a peak at m/z 869.4, corresponding to the $[M+H]^+$ adduct, a peak at m/z 891.4, corresponding to the $[M+Na]^+$ adduct, and a peak at m/z 907.4 corresponding to the $[M+K]^+$ adduct (Figure 4.26).

Peptide **P3** has been also characterized by NMR spectroscopy, dissolving the peptide in DMSO-d_6 (presaturating the water signal due to presence of residual water) and registering ^{1}H-NMR (Figure 4.27, Table 4.4), ^{1}H-^{1}H-COSY NMR and ^{1}H-^{1}H-TOCSY NMR spectra.

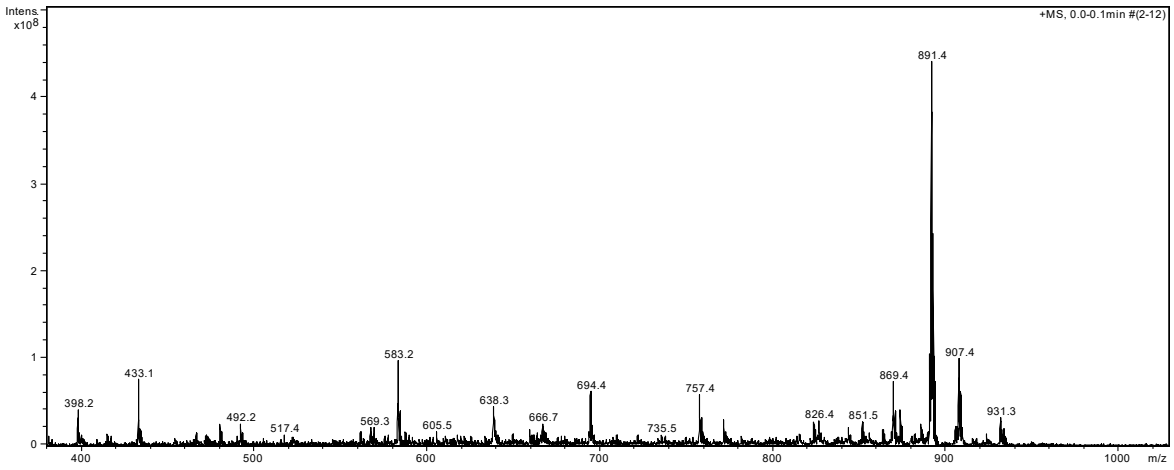

*Figure 4.26- Mass spectrum of **P3** in positive mode.*

[i] Synthesis of the peptides has been carried out at the Department of Life Sciences of the University of Trieste, under the supervision of Dott. Andrea Caporale.

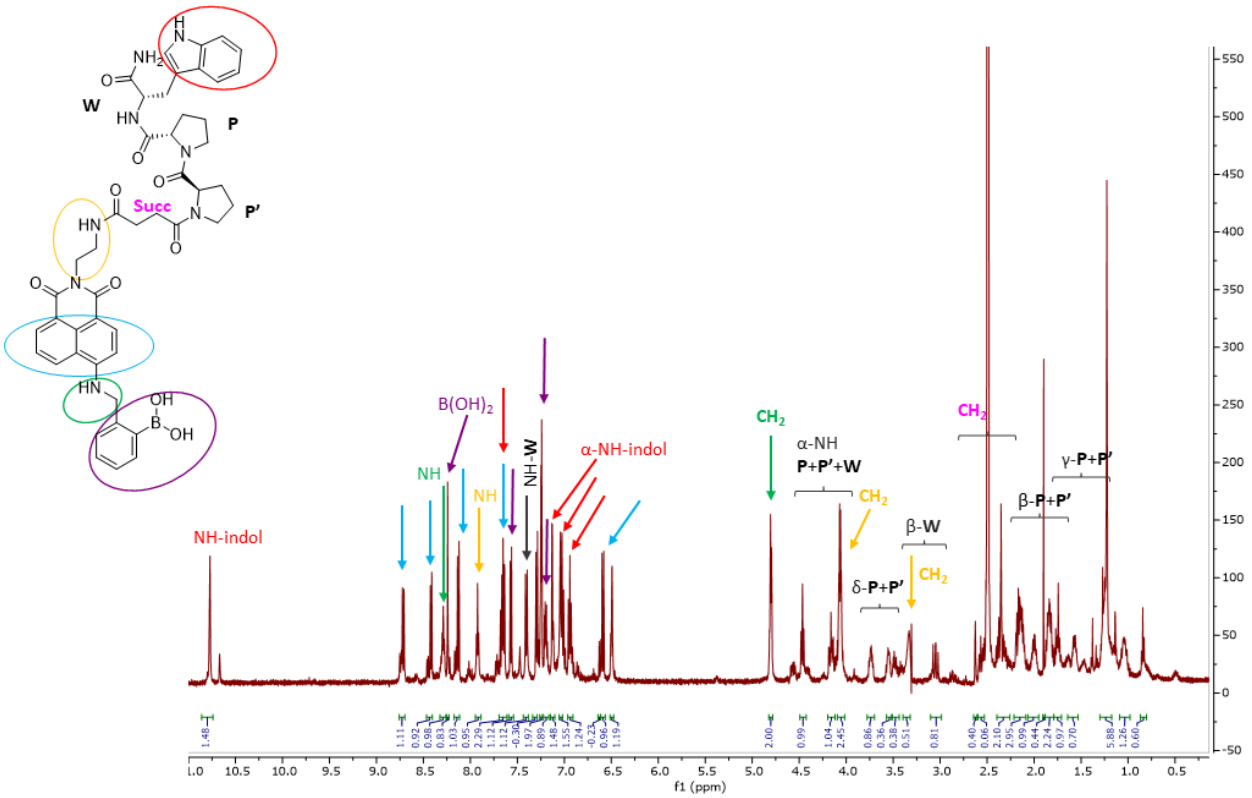

*Figure 4.27- ^{1}H-NMR spectrum of **P3** (DMSO-d_6).*

In the region between 8.73 and 6.50 ppm it is possible to distinguish the amide and the aromatic protons of the fluorophore and of tryptophan lateral side chain.

Starting from signals of **20**, at 8.73, 8.43 and 7.66 ppm it is possible to find the first set of signals of the naphthalimide portion of the fluorophore (in light blue), whereas at 8.14 and 6.60 there are the other two signals (light blue). At 7.58, 7.26 and 7.21 ppm it is possible to distinguish the protons of the boronic acid aromatic ring (purple), whereas the boronic acid hydroxyl protons can be found at 8.25 ppm. The amino group at 8.30 ppm couples with the benzylic methylene signal at 4.80 ppm (green), whereas the triplet of the amide proton deriving from the aliphatic amine at 7.93 ppm couples with the two methylene signals at 4.06 and 3.34 ppm (yellow).

Considering the three amino acids present, tryptophan is the only one having the amide proton at 7.41 ppm, forming the same spin system with the α signal at 4.17 ppm and the two diasterotopic β signals at 3.33 and 3.06 ppm respectively. The lateral side chain generates one indolic amino proton at 10.78 ppm, coupling with its α proton at 7.14 ppm, and four aromatic protons at 7.66 ppm, 7.30, 7.04 and 6.95 ppm. L-proline and D-proline do not have amide protons, and it is possible to distinguish the α, β, γ and δ signals belonging to one spin system respectively at 4.47, 2.16, 1.76, 3.56 ppm, whereas the signals of the other proline are at 4.08, 1.85, 1.28, 3.75 ppm. In this case, it has been possible to distinguish the spin systems of the two prolins but it is not possible to distinguish between the L and D one.

*Table 4.4. ^{1}H-NMR signals of amino acidic backbone of **P3.***

Amino acid	N-H amide (δ)	α-NH (δ)	β-NH (δ)	γ-NH (δ)	δ-NH (δ)
Pro		4.47	2.16	1.76	3.56
Pro		4.08	1.85	1.28	3.75
Trp	7.41	4.17	3.33, 3.06		

4.4.1.2 Fluorescence measurements

Fluorescence of the peptide **P3** has been tested in the same conditions of the fluorophore **20** alone. Measurements have been carried out at a 66 µM peptide concentration, in 0.1 M phosphate buffer at pH 7.4, adding increasing concentrations of the target molecules CGA, CA, HT and CC, ranging between 393 nM to 4.5 mM (in the case of HT and CC an additional concentration of 8 mM has been considered). Also for the peptide **P3**, as for the fluorophore alone, fluorescence quenching has been observed for all the target molecules investigated (Figure 4.28).

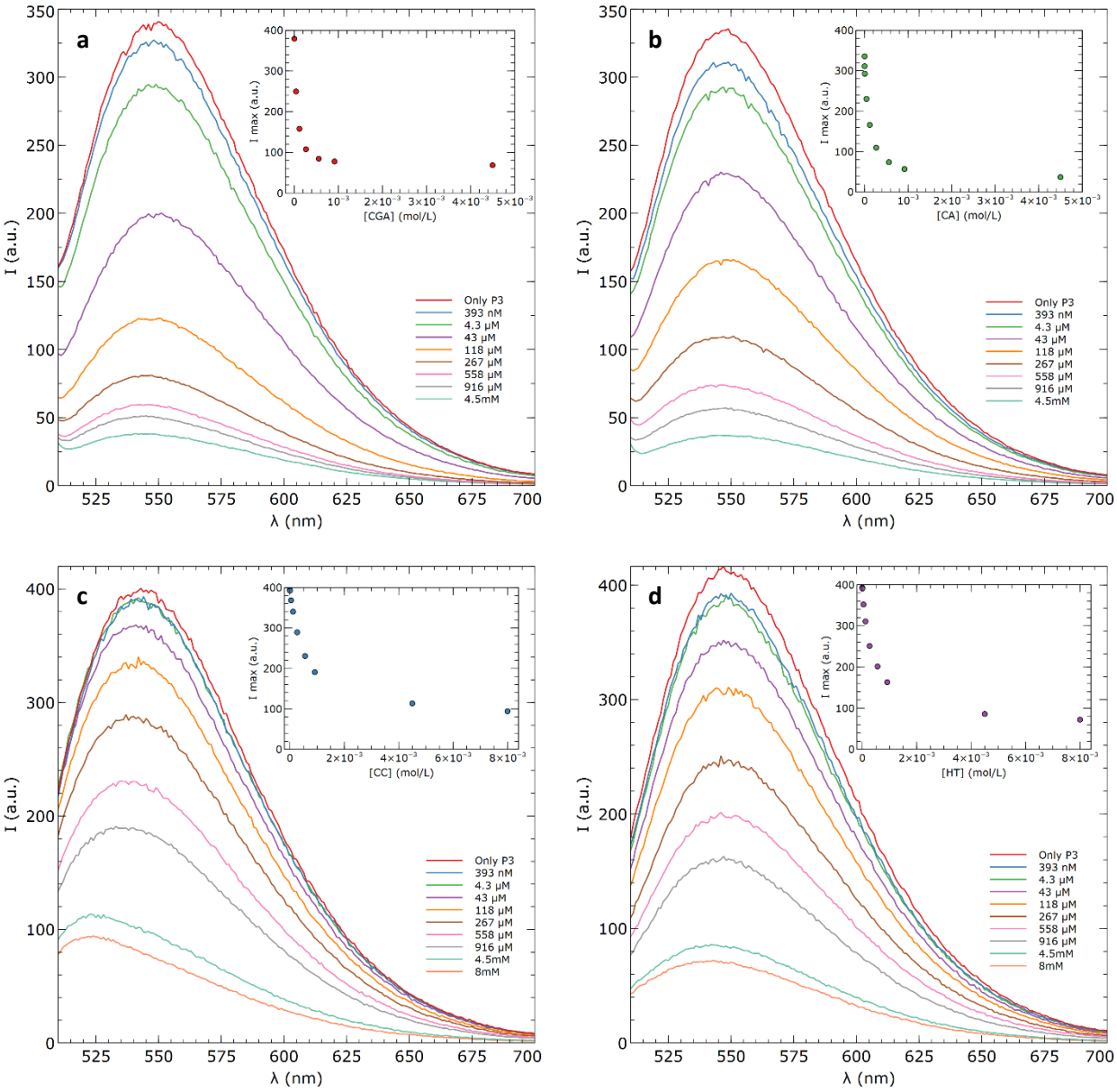

*Figure 4.28- Fluorescence titration of **P3** 66 µM at increasing concentrations of chlorogenic acid (a), caffeic acid (b) catechol (c), and hydroxytyrosol (d) (phosphate buffer 100 mM, pH 7.4, λex = 490 nm).*

Then, as previously done for the fluorophore **20** alone, Stern-Volmer analysis has been performed, and the k_q values have been calculated using the same τ_0 value adopted for **20** (Table 4.5). By comparing the values of the constants of **P3** with those obtained for **20**, it is possible to observe that for CGA, CA and CC the values are higher for the fluorophore alone, whereas in the case of HT there is a little increase of the values for **P3**.

*Table 4.5-Comparison between parameters obtained from Stern-Volmer analysis of peptide **P3** and fluorophore **20**.*

Analite	K_{SV}^{app} 20 [L·mol^{-1}]	k_q 20 [L·mol^{-1}·s^{-1}]	K_{SV}^{app} P3 [L·mol^{-1}]	k_q P3 [L·mol^{-1}·s^{-1}]
CGA	$2.91\cdot10^{4}\pm6.7\cdot10^{2}$	$4.15\cdot10^{14}$	$1.22\cdot10^{4}\pm1.8\cdot10^{2}$	$1.75\cdot10^{14}$
CA	$1.58\cdot10^{4}\pm2.2\cdot10^{2}$	$2.26\cdot10^{14}$	$7.50\cdot10^{3}$	$1.07\cdot10^{14}$
HT	$1.67\cdot10^{3}\pm9.6$	$2.39\cdot10^{13}$	$2.33\cdot10^{3}$	$3.32\cdot10^{13}$
CC	$1.73\cdot10^{3}\pm1.4\cdot10^{2}$	$2.47\cdot10^{13}$	$1.30\cdot10^{3}$	$1.86\cdot10^{13}$

By comparing the binding isotherms (see paragraph 4.3.2.1, Eq. 3.4) for fluorophore **20** with those obtained for peptide **P3** (Figure 4.29), it is possible to see that in general **20** alone shows a slightly higher affinity for charged molecules (Table 4.6). This might be due to the fact that the fluorophore has a free amino group - that in the peptide is employed in an amide bond with the succinyl linker- that might make an ionic interaction with the negatively charged carboxylate groups of CGA and CA. However, the slope of the curves in the linear range is almost the same for all the targets and receptor, thus indicating that the stoichiometry of the interaction should be the same in all cases, even if with different affinities.

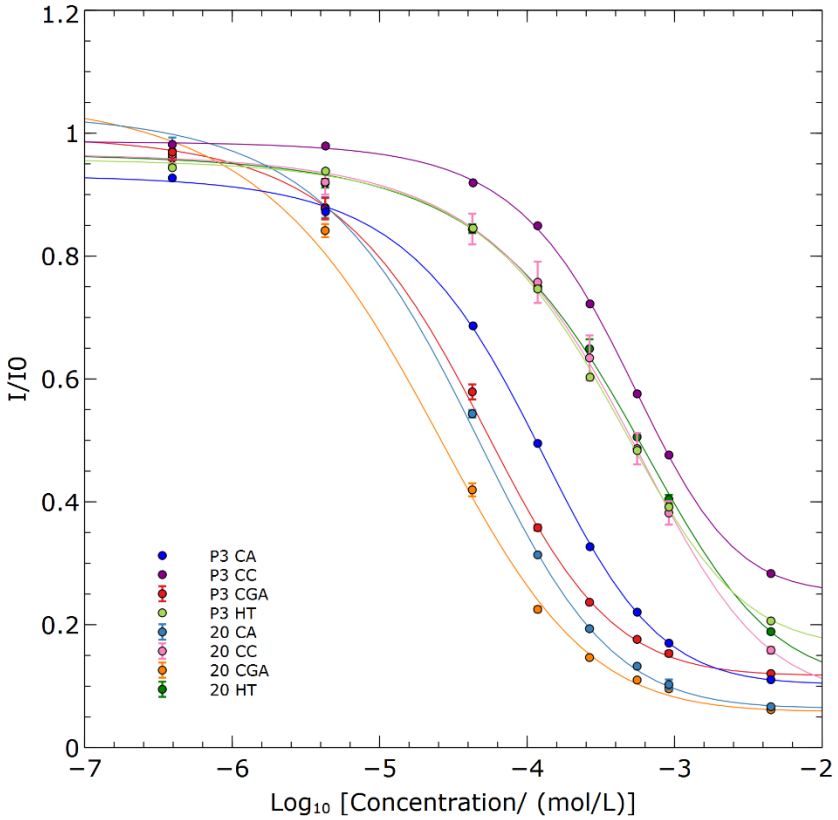

*Figure 4.29- Binding isotherms on a logarithmic scale for **20** and **P3**.*

*Table 4.6- Apparent dissociation constants for **20** and **P3**.*

Analite	K_d^{app} 20 (mol/L)	K_d^{app} P3 (mol/L)
CGA	$2.55\cdot10^{-5}\pm1.4\cdot10^{-6}$	$4.70\cdot10^{-5}\pm4.4\cdot10^{-6}$
CA	$4.37\cdot10^{-5}\pm1.4\cdot10^{-6}$	$1.05\cdot10^{-4}$
HT	$4.70\cdot10^{-4}\pm7.5\cdot10^{-6}$	$3.58\cdot10^{-4}$
CC	$4.58\cdot10^{-4}\pm4.7\cdot10^{-5}$	$4.56\cdot10^{-4}$

Cross reactivity has been calculated to evaluate the capability of the two receptors **20** and **P3** to discriminate between the targets. Such value is normally used for antibodies, to evaluate their ability to discriminate between antigens.[39] In this case, since for both **20** and **P3** chlorogenic acid shows the highest affinity, the ratio has been done between the K_d^{app} of CGA (which is the lowest) with respect to the K_d^{app} of the other targets CA, HT and CC: the lower the ratio is, the higher is the capability to discriminate between the two structures (Table 4.7).

*Table 4.7- Cross reactivity of **20** and **P3***

	20	***P*3**
CGA/HT	5%	13%
CGA/CC	6%	10%
CGA/CA	58%	45%

Since **20** and **P3** perform similarly, the peptide is not capable of providing selectivity with respect to the fluorophore alone. For both **20** and **P3**, cross reactivity with CA is high (58% and 44% respectively), so neither the fluorophore nor the peptide can discriminate efficiently between these two targets, and this can be explained considering the structural similarities of the two molecules, that share the cinnamoyl portion responsible for binding to the receptors. In the case of HT and CC the ability to discriminate them from CGA is higher, with slightly better results for **20** with respect to the peptide.

4.4.2 Peptides P4 and P5

4.4.2.1 Design of the peptides

After demonstrating with the simple peptide **P3** that the fluorophore can be exploited successfully also inside a peptide, two slightly more complex peptides were considered. Thus, the sequence Acetyl-Arg-Gly-Glu(**20**)-dPro-Pro-Ala-His-Glu-NH_2 (Figure 4.30) has been designed as a possible biosensing element for chlorogenic acid and caffeic acid. The *N*-terminal arginine residue has been inserted due to the presence of the positively charged guanidinium group in the lateral side chain, which should confer the capability of interacting with negatively charged molecules, such as chlorogenic acid and caffeic acid which are present in the anionic form at neutral pH. Differently from peptide **P3**, the fluorophore in this case has been placed in the middle of the peptide sequence, binding it to the lateral side chain of an internal glutamic acid residue, trying to increase the influence of the peptide structure on the recognition of target molecule. The proline diad (in this case D- and L-), already applied for the synthesis of peptide **P1** (paragraph 3.3), introduces a conformational block due to the formation of a secondary loop structure, which should lead to a central cavity in the peptide sequence suitable for hosting target molecule: in this central position, covalent binding with the target should benefit from other non-covalent interactions such as π-stacking interactions involving also the lateral side chain of the histidine residue. The conformation of the proposed structure has been analyzed by using the modeling suite Schrödinger,[40] to understand if it might work as recognition element for target molecules.

Initially, the idea was that the γ-carboxylic group of the *C*-terminal glutamic acid might form a salt-bridge with the positively charged guanidinium group of arginine: however, looking at the simulation, it can be seen that actually this electrostatic interaction is replaced by a non-electrostatic interaction between guanidinium group and carbonyl group of glutamic acid, which in any case favors folding of the structure. By looking at the simulated structures in the absence and in presence of target molecule caffeic acid (Figure 4.31), the proposed structure might be suitable for target molecule binding.

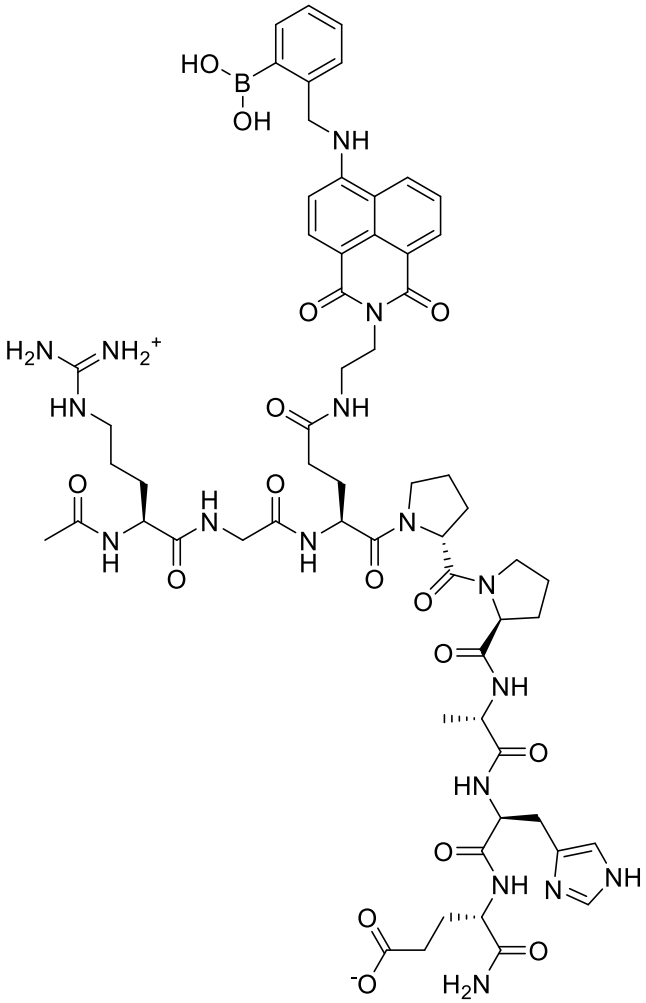

*Figure 4.30- Structure of peptide Acetyl-Arg-Gly-Glu(**20**)-dPro-Pro-Ala-His-Glu-NH_2.*

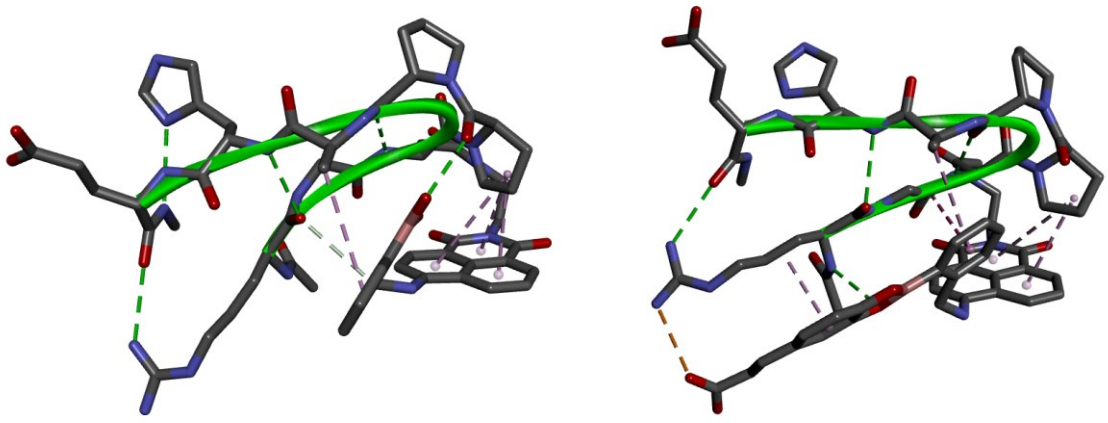

*Figure 4.31- Simulated structure of free peptide Acetyl-Arg-Gly-Glu(**20**)-dPro-Pro-Ala-His-Glu-NH_2 (on the left) and bound to caffeic acid (right).*

However, to establish the influence of the loop structure on target molecule recognition (according to the simulations it seems to be not very relevant) the shorter tetrapeptide Acetyl-Arg-Gly-Glu(**20**)-Gly-NH_2 (Figure 4.32) was also synthesized. The first three amino acids are in common with the longer peptide structure

proposed, but instead of the proline diad and the rest of the sequence, a simple glycine has been introduced. Thanks to the presence of the arginine amino acid, also the tetrapeptide should be capable of interacting electrostatically with target CGA and CA, but without further stabilizations from the loop and other interactions.

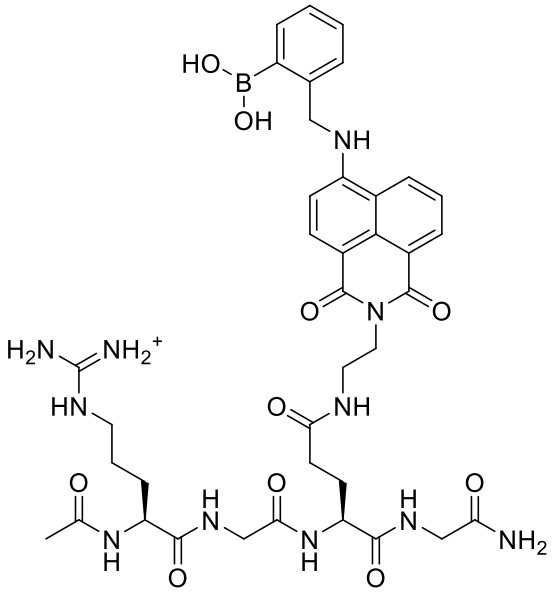

*Figure 4.32- Structure of peptide Acetyl-Arg-Gly-Glu(**20**)-Gly-NH_2.*

4.4.2.2 Synthesis of the peptides

With respect to peptide **P3**, the new peptides have been synthesized introducing an important change in the strategy adopted for coupling to the fluorophore. In fact, since peptide **P3** has been obtained at low yields, probably due to collateral reactions connected with the presence of the free boronic acid moiety during coupling to the peptide backbone, this time the peptides have been synthesized using the fluorophore **20** having the boronic acid protected, performing deprotection at the end of the synthesis.

Therefore, the first preliminary step has been that of obtaining from the precursor **19** (paragraph 4.3.1) the fluorophore with only the amino group deprotected (**23**). This has been achieved by treating **19** with 50% TFA in DCM for 3 hours (Scheme 4.7), then eliminating solvents and deprotection volatile byproducts (carbon dioxide and isobutene) by co-evaporation with DCM. ^{1}H-NMR spectrum of the reaction product registered in DMSO-d_6 confirmed the disappearance of the Boc signal at 1.24 ppm (originally present in **19**), while retaining the boronic ester moiety at 1.31 ppm (Figure 4.33).

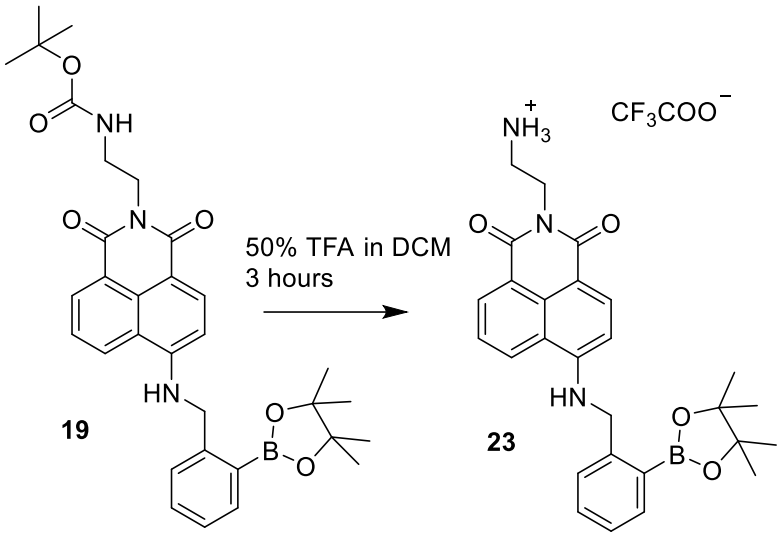

*Scheme 4.7 – Synthesis of **23** from **19**.*

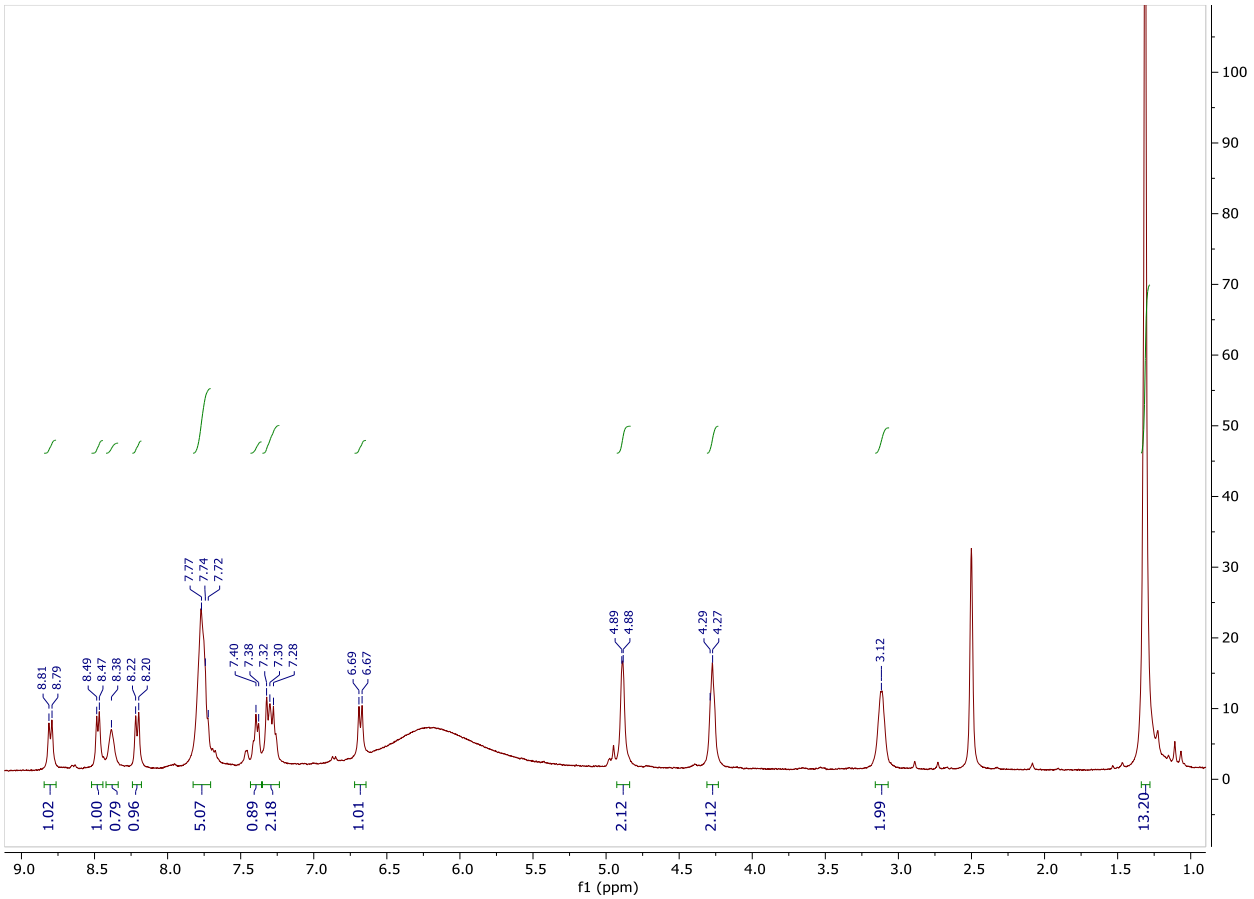

*Figure 4.33- ^{1}H-NMR of **23** (DMSO-d_6).*

Finally, to synthesize the Acetyl-Arg-Gly-Glu(**20**)-Gly-NH_2 (**P4**) and Acetyl-Arg-Gly-Glu(**20**)-dPro-Pro-Ala-His-Glu-NH_2 (**P5**) peptides, it has been necessary to insert in the sequence a glutamic acid protected on the lateral side chain with a protecting group that can be selectively removed with respect to the others, also avoiding cleavage of the peptide from the resin. This is to allow coupling of **23** on an internal glutamic acid residue before peptide cleavage from the resin. For this purpose, the Dmab (4-{N-[1-(4,4-dimethyl-2,6-dioxocyclohexylidene)-3-methylbutyl]-amino} benzyl) ester has been selected. The Dmab group contains a 1-(4,4-dimethyl-2,6dioxocyclohexylidene)-3-methylbutyl (ivDde) group which can be conveniently removed by

treatment with 2% hydrazine. Following ivDde removal, the residual aminobenzyl moiety is reported to spontaneously eliminate to afford the corresponding free carboxylate (see Scheme 4.8).[41] The main advantages of Dmab with respect to other orthogonal protecting groups, is the ease of deprotection in the presence of hydrazine, without the need for expensive catalysts; moreover, the ivDde group, that generates during deprotection, absorbs in the UV at around 290 nm, thus allowing a method to monitor the reaction progress spectrophotometrically.

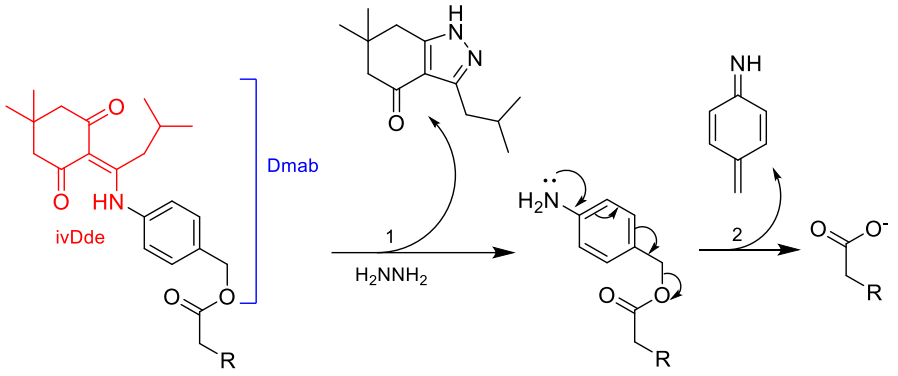

Scheme 4.8- Deprotection of Dmab protecting group.

As for the synthesis of the peptides, FMOC approach in solid phase has been adopted, using the same conditions previously reported for **P3** (double coupling with DIC/OXYMA and HOBT/TBTU/DIPEA, paragraph 4.4.1.1). Both **P4** precursor Acetyl-Arg-Gly-Glu(Dmab)-Gly-NH_2 and **P5** precursor Acetyl-Arg-Gly-Glu(Dmab)-dPro-Pro-Ala-His-Glu-NH_2 have been synthesized having the internal glutamic acid residue protected with Dmab, while having the other amino acids lateral side chains protected with acid labile groups removable during peptide cleavage.

After peptide scaffolds synthesis, the Dmab group has been removed by first treating the functionalized resin with aliquots of 2% hydrazine in DMF, analyzing the collected fractions by reading absorbance at 290 nm to check the complete removal of the ivDde moiety. Subsequently, resin has been treated with NaOH 5mM in water/methanol in a ratio 1:1, which favors removal of the aminobenzyl moiety, thus obtaining the free carboxylic group of glutamic acid residue, available for functionalization with the fluorophore.[41]

Coupling with **23** has been achieved performing a double coupling with HATU ([Bis(dimethylamino)methylene]-1H-1,2,3-triazolo[4,5-b]pyridinium 3-oxid hexafluorophosphate), HOBT and collidine, for 24 hours each.

Then, to remove the pinacol moiety thus obtaining the free boronic acid on the fluorophore, the resin has been treated for around 60 hours with 5% TFA in DCM, in the presence of 10 equivalents of methylboronic acid, to favor faster deprotection of the boronic acid as previously explained (paragraph 4.3.1). After the 60 hours, the acidic liquid phase used for deprotection has been filtered away from the resin. Since long exposure to acidic conditions (even if mild) might have caused partial undesired release of the peptide from the resin, the solution has been treated by first removing solvent and subsequently adding cold diethyl ether, achieving precipitation of an orange solid for both peptides **P4** and **P5** (the obtained solid from this first precipitation process will be called fraction I).

On the other hand, cleavage has been performed on the resin still bound to peptides now having the deprotected boronic acid, in the usual conditions, i.e. 95% TFA with TIS and water as scavengers. For both peptides, the solution containing the cleaved peptide has been treated as explained for fraction I and it has been precipitated with diethyl ether, obtaining an orange precipitate (fraction II).

Both crude fractions I and II of peptides **P4** and **P5** revealed the presence of signals diagnostic for desired peptides functionalized with fluorophore **20** when analyzed by MS, and have thus been purified by preparative HPLC, using different gradients of water and acetonitrile. In both cases fraction II, the one obtained after cleavage with 95% TFA, resulted to be much cleaner with respect to fraction I. The purified peptides have been lyophilized and analyzed by mass spectrometry and NMR spectroscopy.

Characterization of peptide P4

Looking at the mass spectrum of peptide **P4** purified by preparative HPLC, it is clearly possible to distinguish the signal at m/z 830.5, corresponding to the $[M+H]^+$ adduct (Figure 4.34).

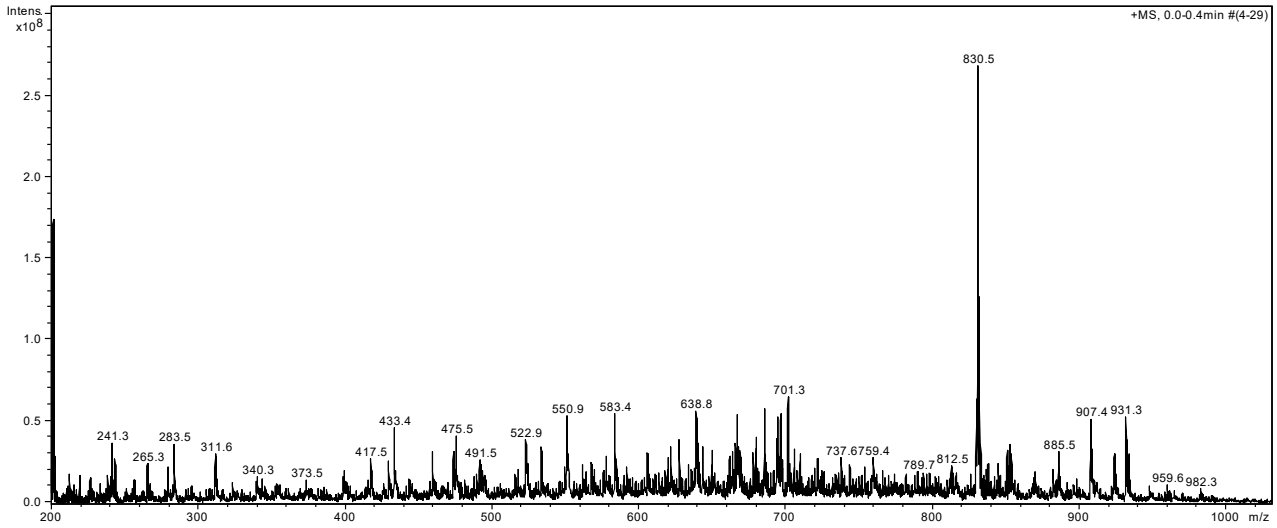

*Figure 4.34- Mass spectrum of **P4.***

The peptide has also been analyzed by NMR spectroscopy, registering the ^1H, ^1H-^1H-COSY and the ^1H-^1H-TOCSY NMR in water plus 10% of D_2O, suppressing the water peak.[42]

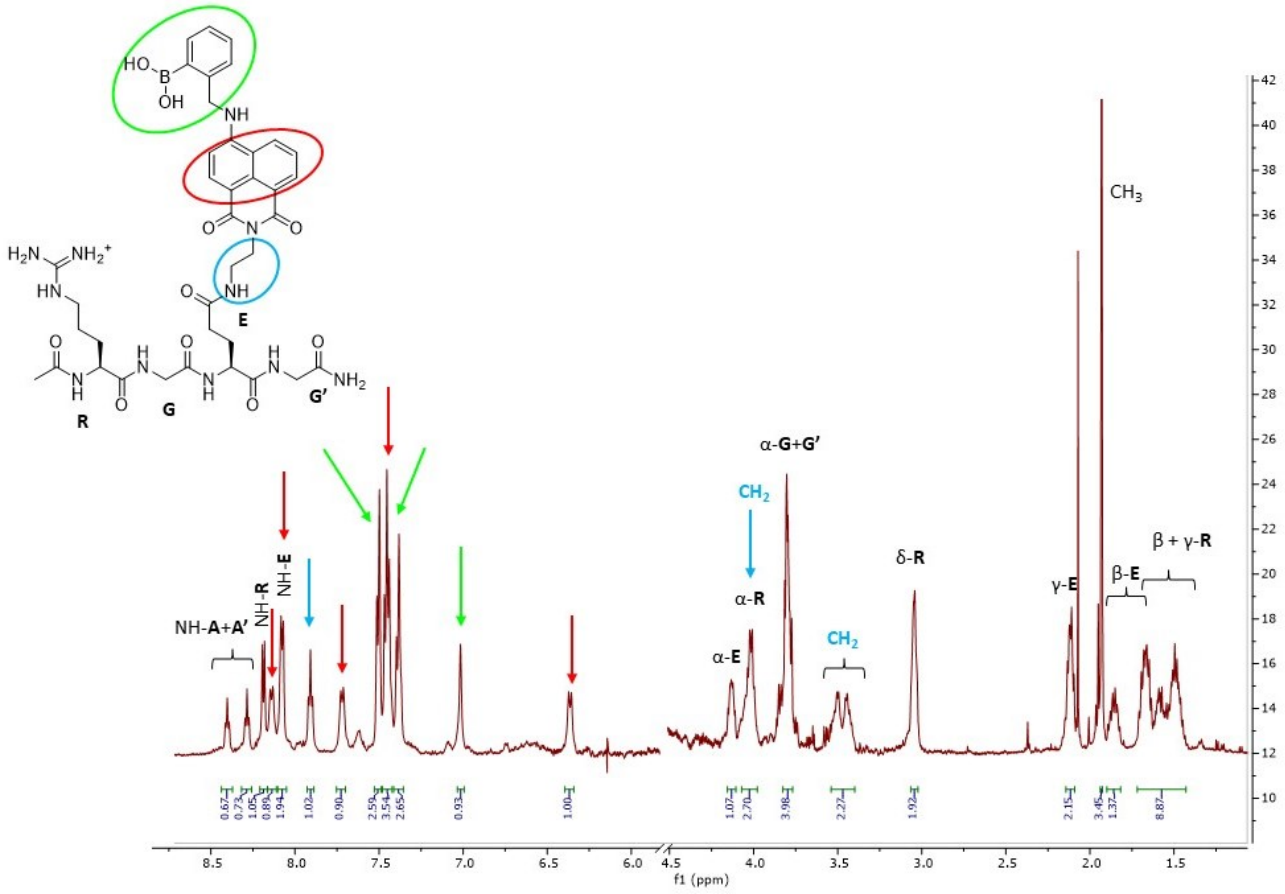

*Figure 4.35- ^{1}H-NMR of peptide **P4** (water + 10% D_2O).*

Looking at the ^{1}H NMR spectrum (Figure 4.35, Table 4.8), in the region between 8.40 and 6.36 ppm, there are the amide protons, the guanidinium protons and the aromatic signals of the fluorophore.

In particular, the amide protons of the two glycine residues can be distinguished by the two triplets at 8.40 and 8.29 ppm, each one coupling with the corresponding α protons at 3.80 ppm (two for each glycine).

The arginine system is composed by the *N*α-amide proton at 8.18 ppm, correlating with the α proton at 4.03 ppm, the two diastereotopic β signals at 1.67 and 1.58 ppm, the γ signals at 1.50 ppm, and the δ hydrogens at 3.02 ppm.

Another spin system is composed by the amide proton of the glutamic acid residue at 8.07 ppm, correlating with the α proton at 4.13 ppm, the two β diastereotopic protons at 1.85 and 1.67 ppm and the γ protons at 2.12 ppm.

The ethylene linker between naphthalimide fluorophore and glutamic acid residue has one methylene signal at 4.02, and the protons of the other one at 3.49 and 3.44 ppm, these last correlating in the COSY spectrum with amide proton at 7.91 ppm.

Looking at the signals of fluorophore **20**, at 8.13 and 8.07 ppm there are the two protons of the naphthalimide nucleus, coupling with the central hydrogen located under the group of signals at 7.45 ppm, whereas the other two doublets, correlating one with each other, can be found at 7.72 and 6.37 ppm. The aromatic protons of the phenylboronic portion are under the group of signals between 7.51 and 7.38 ppm, plus the signal at 7.01 ppm.

*Table 4.8- ^{1}H-NMR signals of peptide **P4.***

Amino acid	N-H amide (δ)	α-NH (δ)	β-NH (δ)	γ-NH (δ)	δ-NH (δ)
Arg	8.18	4.03	1.67, 1.58	1.50	3.02
Gly	8.40	3.80			
Glu	8.07	4.13	1.85,1.67	2.12	
Gly	8.29	3.80			

Characterization of peptide P5

The purified peptide **P5** has been analyzed by mass spectrometry (Figure 4.36).

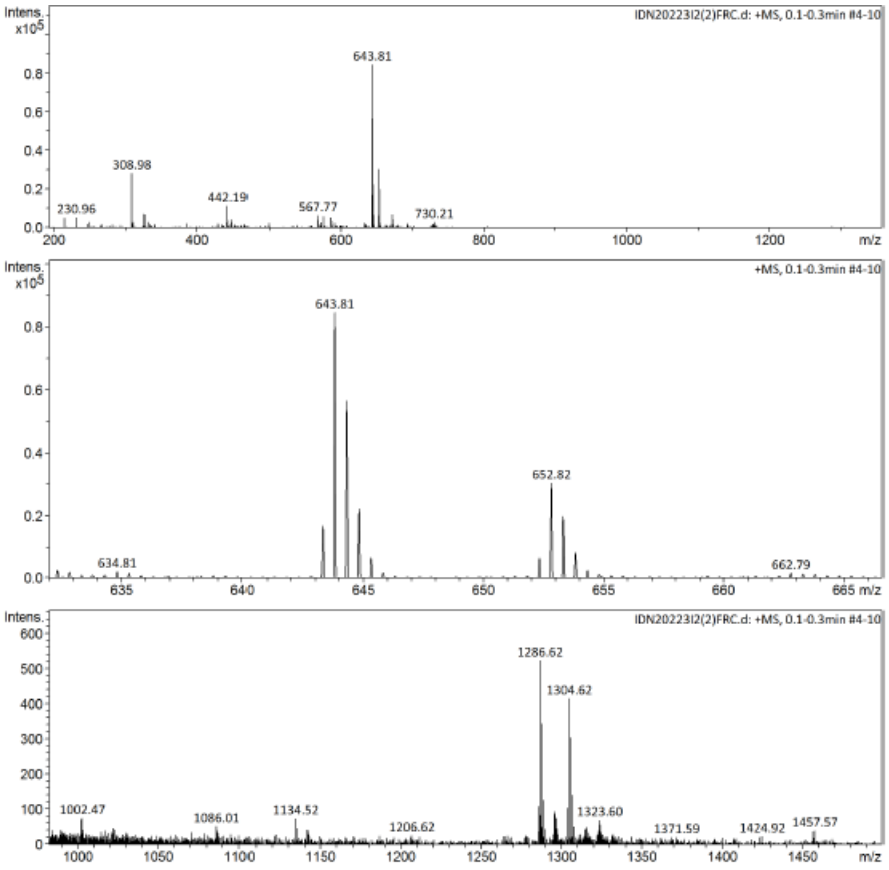

*Figure 4.36- mass spectrum of **P5.***

As it can be seen in Figure 4.36, it is possible to recognize the signals corresponding to the positively charged peptide [**P5**+H]$^{+}$ and also to the double charged [**P5**+2H]$^{2+}$ adduct at 1304.62 m/z (very low intensity, visible only in the zoomed section) and 652.82 m/z respectively. However, two other signals can be distinguished at 1286.62 and 643.81m/z, which can be possibly be attributed to the single charged and double positively-charged peptide **P5** adduct reported in Figure 4.37, resulting from cyclization reaction between the γ carboxylic group of glutamic acid and its amidated α carboxylic group: in any case, the reaction should not interfere much with the ability of the peptide to bind the target CGA and CA.

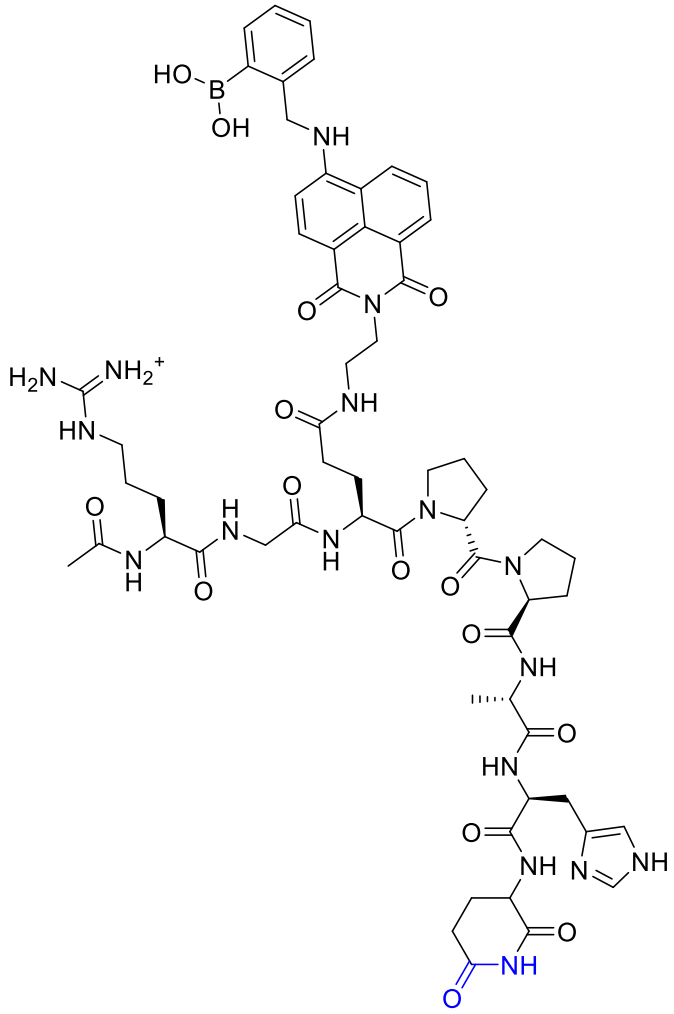

*Figure 4.37- Cyclic byproduct of **P5.***

4.4.2.3 Fluorescence characterization of peptides P4 and P5

The performance of peptides **P4** and **P5** has been evaluated with target molecules CGA, CA, HT and CC in the conditions previously explained for fluorophore **20** and peptide **P3**, titrating a 52 µM solution of each peptide with target molecules, in a range of concentrations between 393 nM and 10.3 mM, working in phosphate buffer 100 mM at pH 7.4.

Fluorescence titrations with all the four targets are reported in Figure 4.38 and Figure 4.39 for peptide **P4** and peptide **P5** respectively.

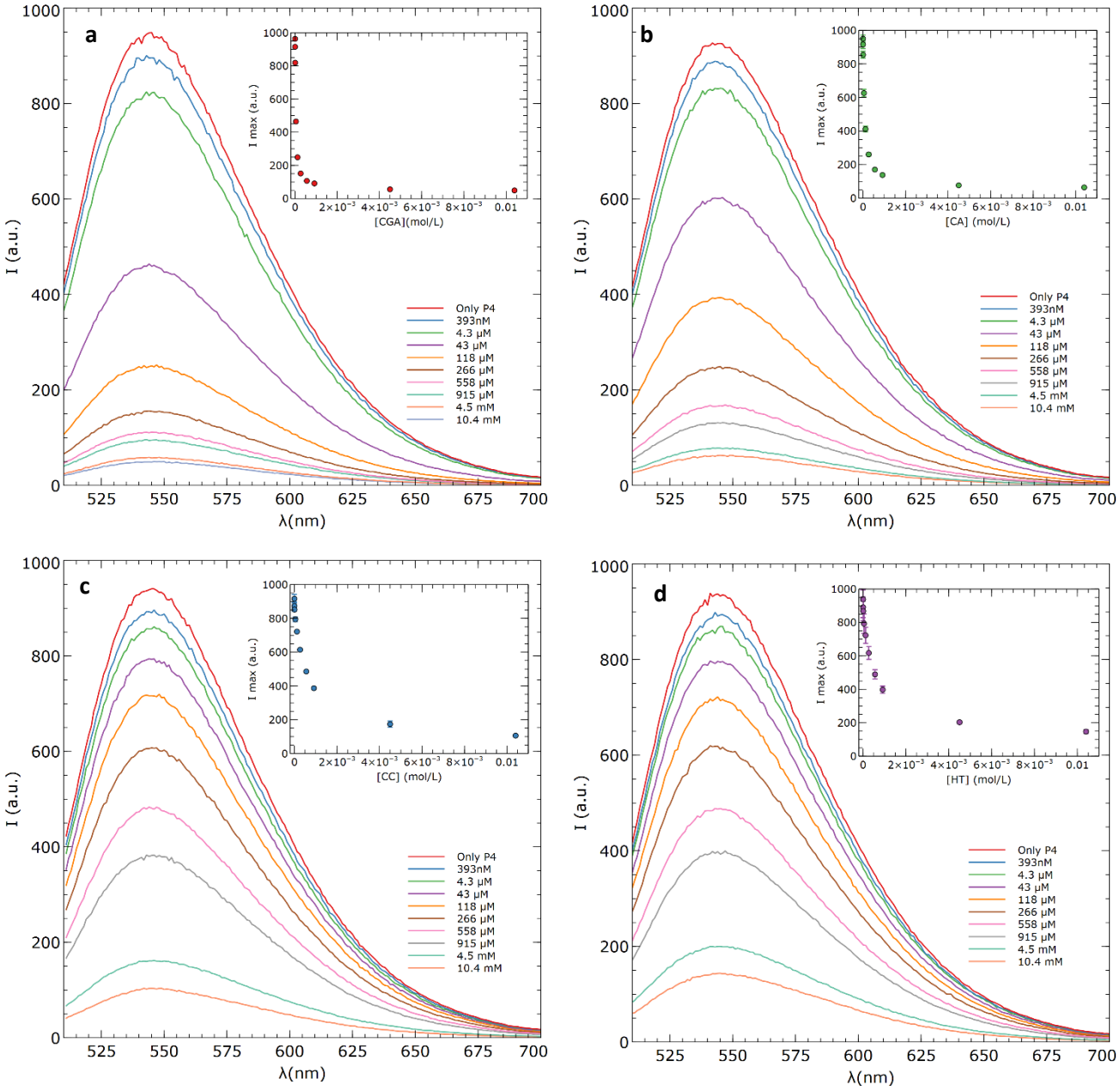

*Figure 4.38- Fluorescence titration of **P4** 52 µM at increasing concentrations of chlorogenic acid (a), caffeic acid (b) catechol (c) and hydroxytyrosol (d) (phosphate buffer 100 mM, pH 7.4, λ_{ex} = 490 nm).*

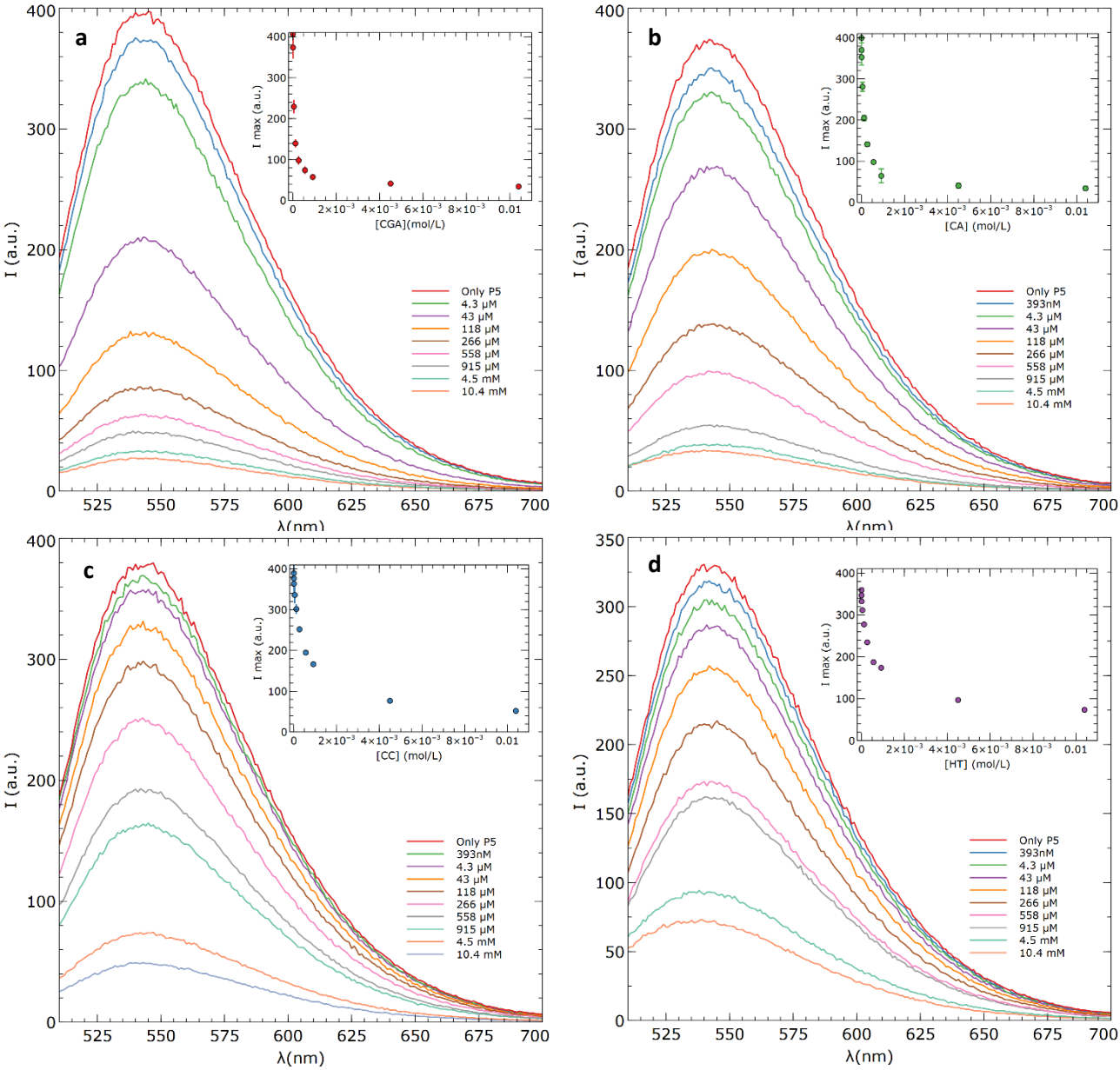

*Figure 4.39- Fluorescence titration of **P5** 52 µM at increasing concentrations of chlorogenic acid (a), caffeic acid (b) catechol (c) and hydroxytyrosol (d) (phosphate buffer 100 mM, pH 7.4, λ_{ex} = 490 nm).*

As obtained also for **20** and **P3**, for both **P4** and **P5** the highest K_{SV} value is observed for CGA followed by CA (Table 4.9). For the other two molecules CC and HT K_{SV} are lower and very similar in value.

*Table 4.9- Stern Volmer constants and quenching constants for peptides **P4** and **P5** with CGA, CA, HT and CC.*

	K_{SV}^{app} P4 [L·mol^{-1}]	k_q P4 [L·mol^{-1}·s^{-1}]	K_{SV}^{app} P5 [L·mol^{-1}]	k_q P5 [L·mol^{-1}·s^{-1}]
CGA	$2.05 \cdot 10^4 \pm 2.0 \cdot 10^3$	$2.92 \cdot 10^{14}$	$1.28 \cdot 10^4 \pm 9.3 \cdot 10^2$	$1.83 \cdot 10^{14}$
CA	$9.93 \cdot 10^3 \pm 2.5 \cdot 10^2$	$1.42 \cdot 10^{14}$	$6.73 \cdot 10^3 \pm 9.3 \cdot 10^2$	$9.61 \cdot 10^{13}$
HT	$1.45 \cdot 10^3 \pm 1.7 \cdot 10^1$	$2.07 \cdot 10^{13}$	$1.88 \cdot 10^3 \pm 7.5 \cdot 10^1$	$2.69 \cdot 10^{13}$
CC	$1.45 \cdot 10^3 \pm 7.2 \cdot 10^1$	$2.07 \cdot 10^{13}$	$1.74 \cdot 10^3 \pm 1.5 \cdot 10^2$	$2.48 \cdot 10^{13}$

The binding isotherms for the four ligands are reported in Figure 4.40 for **P4** and Figure 4.41 for **P5** and the K_d^{app} values for **P4** and **P5** are provided in Table 4.11.

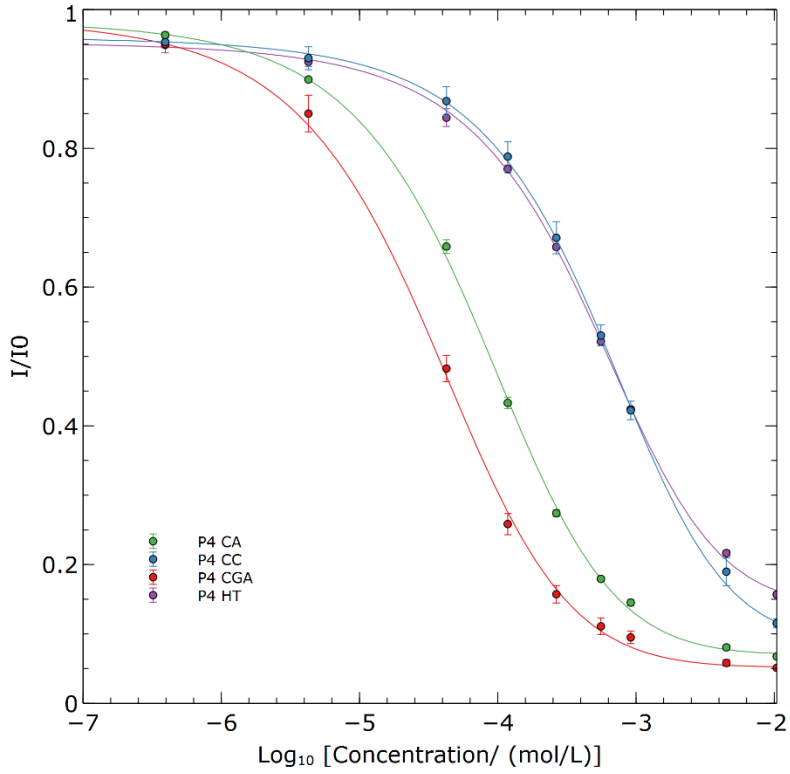

*Figure 4.40- Binding isotherms on a logarithmic scale for **P4** with CGA, CA, HT and CC.*

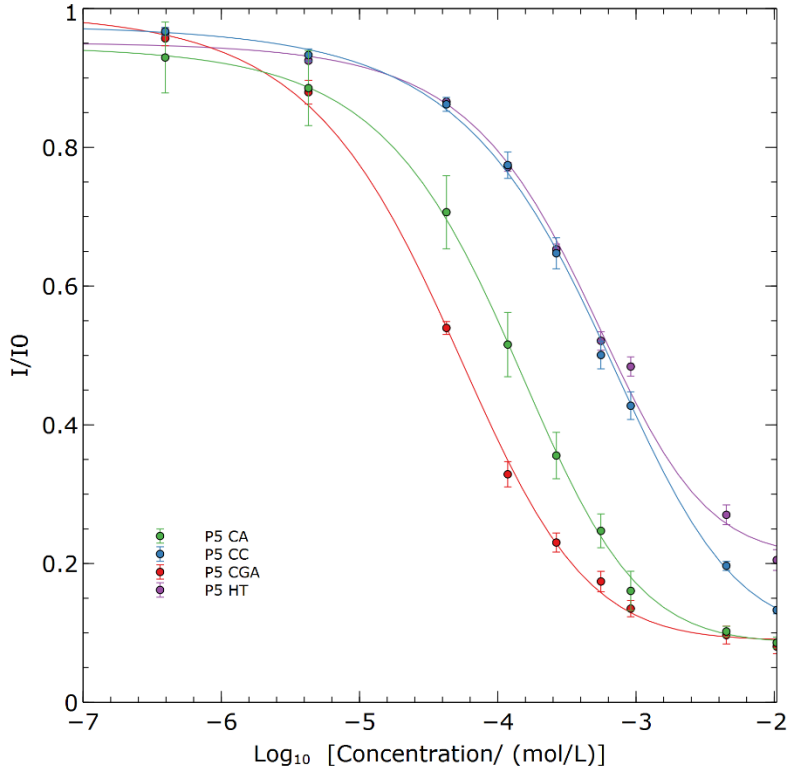

*Figure 4.41- Binding isotherms on a logarithmic scale for **P5** with CGA, CA, HT and CC.*

4.4.3 Conclusions

To sum-up obtained results, considering the Stern-Volmer analysis, **20** has the highest k_q for CGA and CA, followed by **P4**, **P5**/**P3**. In the case of catechol and hydroxytyrosol, all the k_q values are quite similar and in general lower with respect to CA and CGA, with **P5** and **20** having higher values for CC and **P3** for HT (Table 4.10).

*Table 4.10- Quenching constants for **20** and peptides **P3, P4** and **P5** with CGA, CA, HT and CC.*

	k_q **20** [L·mol^{-1}·s^{-1}]	k_q **P3** [L·mol^{-1}·s^{-1}]	k_q **P4** [L·mol^{-1}·s^{-1}]	k_q **P5** [L·mol^{-1}·s^{-1}]
CGA	$4.15\cdot10^{14}$	$1.75\cdot10^{14}$	$2.92\cdot10^{14}$	$1.83\cdot10^{14}$
CA	$2.26\cdot10^{14}$	$1.07\cdot10^{14}$	$1.42\cdot10^{14}$	$9.61\cdot10^{13}$
HT	$2.39\cdot10^{13}$	$3.32\cdot10^{13}$	$2.07\cdot10^{13}$	$2.69\cdot10^{13}$
CC	$2.47\cdot10^{13}$	$1.86\cdot10^{13}$	$2.07\cdot10^{13}$	$2.48\cdot10^{13}$

The trend is confirmed also considering the K_d^{app} values of peptides **P4** and **P5**, together with those for **20** and **P3** (Table 4.11), and all the peptides and the fluorophore **20** show very similar K_d values for catechol and hydroxytyrosol. Therefore, the results obtained drive to the conclusion that **20** is the best one in recognizing CGA and CA, followed by **P4**, which also has good affinities. Despite the presence of the motif Arg-Gly-Glu in common with **P4**, **P5** always performs worse.

*Table 4.11- Comparison between the dissociation constants of **20, P3, P4** and **P5** with CGA, CA, HT and CC.*

Analite	K_d^{app} **20 (mol/L)**	K_d^{app} ***P3*** **(mol/L)**	K_d^{app} ***P4*****(mol/L)**	K_d^{app} ***P5*** **(mol/L)**
CGA	$2.55\cdot10^{-5}\pm1.4\cdot10^{-6}$	$4.70\cdot10^{-5}\pm4.4\cdot10^{-6}$	$3.52\cdot10^{-5}\pm3.1\cdot10^{-6}$	$4.14\cdot10^{-5}\pm7.4\cdot10^{-7}$
CA	$4.37\cdot10^{-5}\pm1.4\cdot10^{-6}$	$1.05\cdot10^{-4}$	$7.86\cdot10^{-5}\pm3.4\cdot10^{-6}$	$1.22\cdot10^{-4}\pm1.8\cdot10^{-5}$
HT	$4.70\cdot10^{-4}\pm7.5\cdot10^{-6}$	$3.58\cdot10^{-4}$	$4.61\cdot10^{-4}\pm5.6\cdot10^{-5}$	$4.51\cdot10^{-4}\pm3.7\cdot10^{-5}$
CC	$4.58\cdot10^{-4}\pm4.7\cdot10^{-5}$	$4.56\cdot10^{-4}$	$5.61\cdot10^{-4}\pm3.1\cdot10^{-5}$	$4.81\cdot10^{-4}\pm5.1\cdot10^{-5}$

Finally, cross reactivity has been calculated to evaluate the capability of the receptors to discriminate between the targets. Also in this case, as previously done for **20** and **P3**, calculations have been done considering the ratio between K_d^{app} for the reference chlorogenic acid (since also **P4** and **P5** show the highest affinity for this target) and the K_d^{app} value for another target (Table 4.12).

*Table 4.12- Cross reactivity comparison between **20, P3, P4** and **P5**.*

	20	**P3**	**P4**	**P5**
CGA/HT	5%	13%	8%	9%
CGA/CC	6%	10%	6%	9%
CGA/CA	58%	45%	45%	34%

All the recognition elements can discriminate well between chlorogenic acid and HT and CC, with cross-reactivity values ranging between 5 and 13%. As to the cross reactivity between CGA and CA, which are both carboxylic acids and share the same cinnamoyl structure, **P5** is more selective than **20** and the other peptides.

4.5 BIBLIOGRAPHY

(1) Hall, D.G. Structure, properties, and preparation of boronic acid derivatives. Overview of their reactions and applications. In Boronic acids: preparation and applications in organic synthesis and medicine, D.G. Hall Ed., **2005**, 1-99.

(2) Marinaro, W. A.; Prankerd, R.; Kinnari, K.; Stella, V. J. Interaction of Model Aryl- and Alkyl-Boronic Acids and 1,2-Diols in Aqueous Solution. *J. Pharm. Sci.,* **2015**, 104 (4), 1399–1408.

(3) Lorand, J. P.; Edwards, J. O. Polyol Complexes and Structure of the Benzeneboronate Ion. *J. Org. Chem.,* **1959**, 24 (6), 769–774.

(4) Edwards, J. O.; Morrison, G. C.; Ross, V. F.; Schultz, J. W. The Structure of the Aqueous Borate Ion. *J. Am. Chem. Soc.,* **1955**, 77 (2), 266–268.

(5) Suzuki, Y.; Kusuyama, D.; Sugaya, T.; Iwatsuki, S.; Inamo, M.; Takagi, H. D.; Ishihara, K. Reactivity of Boronic Acids toward Catechols in Aqueous Solution. *J. Org. Chem*., **2020**, 85 (8), 5255–5264.

(6) Bosch, L. I.; Fyles, T. M.; James, T. D. Binary and Ternary Phenylboronic Acid Complexes with Saccharides and Lewis Bases. *Tetrahedron,* **2004**, 60 (49), 11175–11190.

(7) Geethanjali, H.S.; Melavanki, R. M.; Nagaraja D.; Bhavja P.; Kusanur, R. A. Binding of Boronic Acids with Sugars in Aqueous Solution at Physiological PH - Estimation of Association and Dissociation Constants Using Spectroscopic Method. *J. Mol. Liq.,* **2017**, 227, 37–43.

(8) Egawa, Y.; Seki, T.; Takahashi, S.; Anzai, J. Electrochemical and Optical Sugar Sensors Based on Phenylboronic Acid and Its Derivatives. *Mater. Sci. Eng. C,* **2011**, 31 (7), 1257–1264.

(9) Qi, L.; Liang, R.; Qin, W. Stimulus-Responsive Imprinted Polymer-Based Potentiometric Sensor for Reversible Detection of Neutral Phenols. *Anal. Chem*., **2020**, 92 (6), 4284–4291.

(10) Ma, W. M. J.; Pereira Morais, M. P.; D'Hooge, F.; van den Elsen, J. M. H.; Cox, J. P. L.; James, T. D.; Fossey, J. S. Dye Displacement Assay for Saccharide Detection with Boronate Hydrogels. *Chem. Commun.,* **2009**, 5, 532–534.

(11) James, T. D.; Sandanayake, K. R. A. S.; Shinkai, S. Novel Photoinduced Electron-Transfer Sensor for Saccharides Based on the Interaction of Boronic Acid and Amine. *J. Chem. Soc., Chem. Commun*., **1994**, 4, 477.

(12) James, T. D.; Sandanayake, K. R. A. S.; Iguchi, R.; Shinkai, S. Novel Saccharide-Photoinduced Electron Transfer Sensors Based on the Interaction of Boronic Acid and Amine. *J. Am. Chem. Soc.,* **1995**, 117 (35), 8982–8987.

(13) Sun, X.; Chapin, B. M.; Metola, P.; Collins, B.; Wang, B.; James, T. D.; Anslyn, E. V. The Mechanisms of Boronate Ester Formation and Fluorescent Turn-on in Ortho-Aminomethylphenylboronic Acids. *Nat. Chem*., **2019**, 11 (9), 768–778.

(14) Yang, W.; Lin, L.; Wang, B. A New Type Of Water-Soluble Fluorescent Boronic Acid Suitable For Construction Of Polyboronic Acids For Carbohydrate Recognition. *Heterocycl. Commun.,* **2004**, 10 (6), 383-388.

(15) Wang, H.; Fang, G.; Wang, H.; Dou, J.; Bian, Z.; Li, Y.; Chai, H.; Wu, Z.; Yao, Q. A Diboronic Acid Fluorescent Sensor for Selective Recognition of D -Ribose via Fluorescence Quenching. *New J. Chem*., **2019**, 43 (11), 4385–4390.

(16) Fang, G.; Wang, H.; Bian, Z.; Zhang, G.; Guo, M.; Wu, Z.; Yao, Q. 2-(4-Boronophenyl)Quinoline-4-Carboxylic Acid Derivatives: Design and Synthesis, Aggregation-Induced Emission Characteristics, and Binding Activity Studies for D-Ribose with Long-Wavelength Emission. *J. Chem. Res.,* **2020**, 44 (3–4), 152–160.

(17) Fang, G.; Bian, Z.; Liu, D.; Wu, G.; Wang, H.; Wu, Z.; Yao, Q. Water-Soluble Diboronic Acid-Based Fluorescent Sensors Recognizing D -Sorbitol. *New J. Chem*., **2019**, 43 (35), 13802–13809.

(18) Wu, Z.; Li, M.; Fang, H.; Wang, B. A New Boronic Acid Based Fluorescent Reporter for Catechol. *Bioorganic Med. Chem. Lett.,* **2012**, 22 (23), 7179–7182.

(19) Bian, Z.; Fang, G.; Wang, R.; Zhan, D.; Yao, Q.; Wu, Z. A Water-Soluble Boronic Acid Sensor for Caffeic Acid Based on Double Sites Recognition. *RSC Adv.,* **2020**, 10 (47), 28148–28156.

(20) Wei, J.; Ni, Y.; Zhang, W.; Zhang, Z.; Zhang, J. Detection of Glycoprotein through Fluorescent Boronic Acid-Based Molecularly Imprinted Polymer. *Anal. Chim. Acta,* **2017**, 960, 110–116.

(21) Fang, G.; Wang, H.; Bian, Z.; Guo, M.; Wu, Z.; Yao, Q. A Novel Boronic Acid-Based Fluorescent Sensor for Selectively Recognizing Fe $^{3+}$ Ion in Real Time. *RSC Adv*., **2019**, 9 (35), 20306–20313.

(22) Fang, G.; Zhan, D.; Wang, R.; Bian, Z.; Zhang, G.; Wu, Z.; Yao, Q. A Highly Selective and Sensitive Boronic Acid-Based Sensor for Detecting Pd^{2+} Ion under Mild Conditions. *Bioorganic Med. Chem. Lett.,* **2020**, 30 (17), 127397.

(23) Huang, S.; Jia, M.; Xie, Y.; Wang, J.; Xu, W.; Fang, H. The Progress of Selective Fluorescent Chemosensors by Boronic Acid. *Curr. Med. Chem.,* **2012**, 19 (16), 2621–2637.

(24) DiCesare, N., Adhikari, D. P., Heynekamp, J. J., Heagy, M. D.,; Lakowicz, J. R. Spectroscopic and photophysical characterization of fluorescent chemosensors for monosaccharides based on *N*-phenylboronic acid derivatives of 1, 8-naphthalimide. *J. Fluoresc.*, **2002**, 12(2), 147-154.

(25) Trupp, S.; Schweitzer, A.; Mohr, G. J. A Fluorescent Water-Soluble Naphthalimide-Based Receptor for Saccharides with Highest Sensitivity in the Physiological PH Range. *Org. Biomol. Chem*., **2006**, 4 (15), 2965.

(26) Wang, J.; Jin, S.; Akay, S.; Wang, B. Design and Synthesis of Long-Wavelength Fluorescent Boronic Acid Reporter Compounds. *Eur. J. Org. Chem*., **2007**, 2007 (13), 2091–2099.

(27) Jin, S.; Wang, J.; Li, M.; Wang, B. Synthesis, Evaluation, and Computational Studies of Naphthalimide-Based Long-Wavelength Fluorescent Boronic Acid Reporters. *Chem. Eur. J.,* **2008**, 14 (9), 2795–2804.

(28) Ciani, G. Biosensori peptidici contenenti acidi boronici per il riconoscimento covalente di *orto*-difenoli, Master degree thesis, **2021**-**2022**, University of Trieste.

(29) Lakowicz, J. R. Principles of Fluorescence Spectroscopy, 3rd ed.; Springer: New York, **2006**.

(30) Wu, W.; Zhu, H.; Fan, L.; Liu, D.; Renneberg, R.; Yang, S. Sensitive Dopamine Recognition by Boronic Acid Functionalized Multi-Walled Carbon Nanotubes. *Chem. Commun*., **2007**, 23, 2345-2347.

(31) Wang, H.; Fang, G.; Wang, K.; Wu, Z.; Yao, Q. Determination of Dopamine Using 2-(4-Boronophenyl)Quinoline-4-Carboxylic Acids as Fluorescent Probes. *Anal. Lett.,* **2019**, 52 (4), 713–727.

(32) Zhan, D.; Bian, Z.; Li, H.; Wang, R.; Fang, G.; Yao, Q.; Wu, Z. Novel Detection Method for Gallic Acid: A Water Soluble Boronic Acid-Based Fluorescent Sensor with Double Recognition Sites. *Bioorg. Med. Chem. Lett.,* **2022**, 57, 128483.

(33) Yang, C., Chen, K., Chen, M., Hu, X., Huan, S. Y., Chen, L., Song, g.; Zhang, X. B. (2019). Nanoscale metal–organic framework based two-photon sensing platform for bioimaging in live tissue. *Anal. Chem.*, **2019**, 91(4), 2727-2733.

(34) Jensen, K. B.; Braxmeier, T. M.; Demarcus, M.; Frey, J. G.; Kilburn, J. D. Synthesis of Guanidinium-Derived Receptor Libraries and Screening for Selective Peptide Receptors in Water. *Chem. Eur. J.,* **2002**, 8 (6), 1300–1309.

(35) Chen, H.; Wang, H.; Qin, X.-J.; Chen, C.; Feng, L.; Chen, L.-Z.; Du, L.-P.; Li, M.-Y. A Bestatin-Based Fluorescent Probe for Aminopeptidase N Cell Imaging. *Chin. Chem. Lett.,* **2015**, 26 (5), 513–516.

(36) Hebel, M.; Riegger, A.; Zegota, M.M.; Kizilsavas, G.; Gačanin, J.; Pieszka, M.; Lückerath, T.; Coelho, J.A.S.; Wagner, M.; Gois, P. M. P; Ng, D. Y. W.; Weil, T. Sequence programming with dynamic boronic acid/catechol binary codes. *J. Am. Chem. Soc*., **2019**, 141(36), 14026-14031.

(37) Hinkes, S. P.; Klein, C. D. Virtues of volatility: A facile transesterification approach to boronic acids. *Org. Lett.*, **2019**, 21(9), 3048-3052.

(38) Wagner, R.; Wan, W.; Biyikal, M.; Benito-Peña, E.; Moreno-Bondi, M. C.; Lazraq, I.; Rurack, K.; Sellergren, B. Synthesis, Spectroscopic, and Analyte-Responsive Behavior of a Polymerizable Naphthalimide-Based Carboxylate Probe and Molecularly Imprinted Polymers Prepared Thereof. *J. Org. Chem.,* **2013**, 78 (4), 1377–1389.

(39) Frank, S. A. Immunology and Evolution of Infectious Disease; Princeton University Press: Princeton, **2002**.

(40) Schrödinger Release 2023-1: MacroModel, Schrödinger, LLC, New York, NY, 2021.

(41) Conroy, T.; Jolliffe, K. A.; Payne, R. J. Efficient Use of the Dmab Protecting Group: Applications for the Solid-Phase Synthesis of N-Linked Glycopeptides. *Org. Biomol. Chem*., **2009**, 7 (11), 2255- 2258.

(42) Calvanese, L.; Caporale, A.; Focà, G.; Iaccarino, E.; Sandomenico, A.; Doti, N.; Apicella, I.; Incisivo, G. M.; De Falco, S.; Falcigno, L.; D'Auria, G.; Ruvo, M. Targeting VEGF Receptors with Non-Neutralizing Cyclopeptides for Imaging Applications. *Amino Acids,* **2018**, 50 (2), 321–329.

5 RESULTS AND DISCUSSION- DIAZO-COUPLING REACTION

Our group has recently obtained several interesting results on the fluorescence changes of fluorescein inserted into molecularly imprinted polymers upon binding with target molecules tyrosol, hydroxytyrosol and oleuropein; rebinding of the phenols led to a fluorescence enhancement, rather than to a quenching.[1] As the enhancement of a signal is much better than its decrease from the analytical point of view, we have tried to do the same also on peptides, synthesizing a short model peptide Acetyl-*p*NH_2Phe-(D)Pro-(L)Pro-Lys(FITC)-NH_2 (**P6**) functionalized with fluorescein isothiocyanate (FITC)(Figure 5.1). The peptide contains fluorescein as the fluorescent reporter and an aromatic amino acid to favor π-π stacking interactions with the target phenols, linked together by a proline diad to introduce a conformational block and promote a double interaction of the target with both the fluorophore and the aromatic amino acid. The idea has been that of using the non-natural amino acid *p*-amino-phenylalanine (*p*NH_2Phe), in the perspective of having peptides capable also of forming covalent diazo-coupling products thanks to the presence of the aromatic amino group, thus providing a possible double application for the same peptide for both non-covalent and covalent target molecule recognition. Since diazo coupling products are usually colored, in this case the influence of the diazo-coupling product on the fluorescence of fluorescein might be used as transduction mechanism. Based on the idea of studying the non-covalent interactions of a peptide containing a fluorescent moiety with a different structure and being excited/emitting at lower wavelengths (thus more favorable to observe a FRET effect with diazo-coupling product obtained from *p*NH_2Phe and tyrosol), a second peptide has been synthesized, possessing 5-((2-aminoethyl)amino)naphthalene-1-sulfonic acid (EDANS) as the fluorophore, with an aromatic core capable of interacting by π-π stacking interactions with the target molecule. Moreover, the amino acidic sequence has been changed to EDANS-succinyl-(D)Pro-(L)Pro-*p*(NH_2)Phe-Ala-His-Glu-NH_2 (**P7**) (Figure 5.1), maintaining the proline diad to favor structural constraint and the *p*-NH_2-phenylalanine amino acid. By the insertion of another residue capable of π-π stacking interactions -histidine- and a glutamic acid residue, an enhancement of water solubility of the peptide and further possibilities of interaction by hydrogen bonds formation should be obtained. Experiments of chapter 5 of the present thesis related to the synthesis and study of fluorescent peptides have been done in collaboration with the master student Elena Maria Tamburello, during her Master thesis internship.[2]

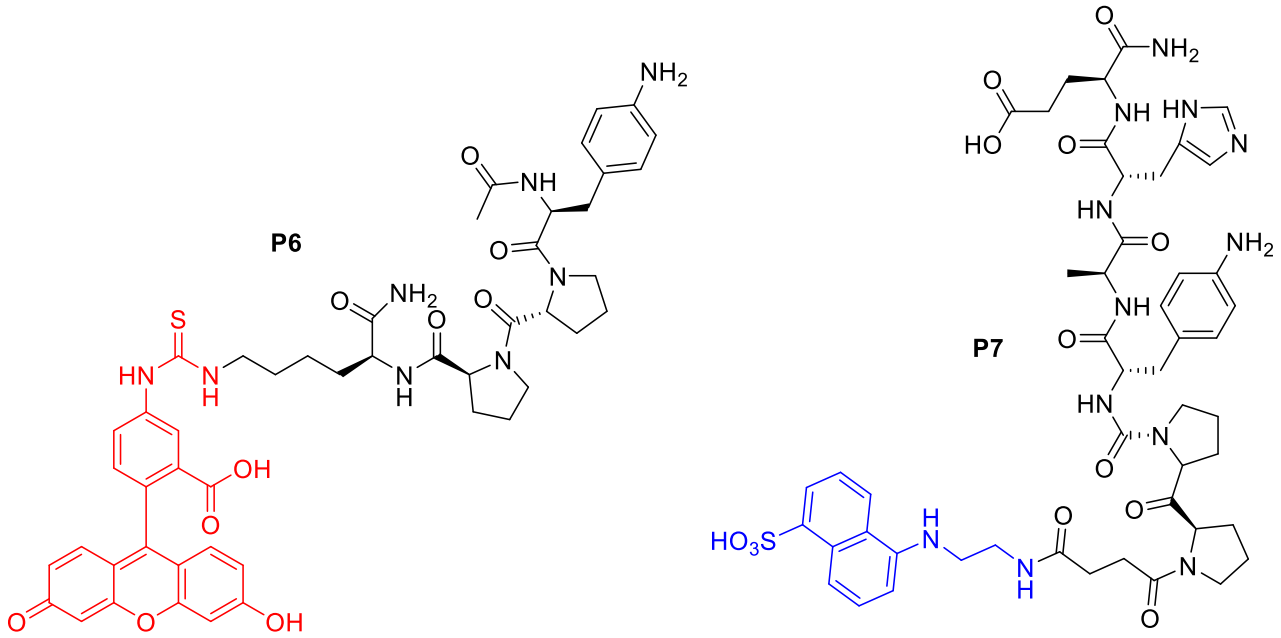

*Figure 5.1- Structure of the two peptides Acetyl-pNH_2Phe-(D)Pro-(L)Pro-Lys(FITC)-NH_2 (**P6**) and EDANS-succinyl-(D)Pro-(L)Pro-p(NH_2)Phe-Ala-His-Glu-NH_2 (**P7**).*

5.1 SYNTHESIS AND CHARACTERIZATION OF THE PEPTIDES

The synthesis of the two peptides **P6** and **P7** has been done by solid phase synthesis with an automatic microwave synthesizer,[i] using Rink amide MBHA resin and traditional FMOC approach. For coupling of amino acids, a double conjugation approach has been adopted as previously described (see paragraph 3.3.2 and 4.4.1.1), using for the first coupling OXYMA-DIC and for the second TBTU-HOBT and DIPEA.

In the case of **P6**, coupling of the fluorescent label FITC has been obtained exploiting the ε-amino group of lysine, protected with the 4-methyltrityl (MTT) group that can be selectively removed in slightly acidic conditions avoiding cleavage of the peptide from the resin and deprotection of the other lateral side chain protecting groups. Then, after selective deprotection of lysine ε-amino group, it has been reacted with the isothiocyanate group of fluorescein, leading to the formation of a disubstituted *N*,*N*'-thiourea.

To conjugate EDANS to **P7**, a succinyl linker has been added to the amino terminal residue of the peptide (D-Pro), using TBTU, HOBT and DIEA to activate the carboxylic functionality for coupling with the amino group of the fluorophore.

Both peptides have been cleaved from the resin using concentrated TFA and scavengers, and purified by preparative HPLC, using a gradient of water and acetonitrile with 0.05% of TFA.

As already explained in previous chapters, mass spectrometry and NMR analyses confirmed the obtainment of the two peptides. In the case of **P6** it has been possible to see the double charged peak of the adduct $[M+2H]^{2+}$ at 467.1821 m/z, together with less intense peaks at 933.3592 and 955.3419, corresponding to the $[M+H]^+$ and $[M+Na]^+$ adducts. In the case of **P7**, it has been possible to distinguish the signals at m/z of 1059.8, 1081.6 and 1097.6, corresponding respectively to the adducts $[M+H]^+$, $[M+Na]^+$ and $[M+K]^+$.

For peptide **P7**, obtained in larger quantities, also ^1H, ^1H-^1H-COSY and ^1H-^1H-TOCSY NMR characterization has been performed. The sample has been prepared in water plus 10% D_2O, operating suppression of the water peak, even if only partial assignment of the signals could be done.[3]

[i] Peptides have been synthesized at the Department of Life sciences of the University of Trieste, under the supervision of Dott. Andrea Caporale.

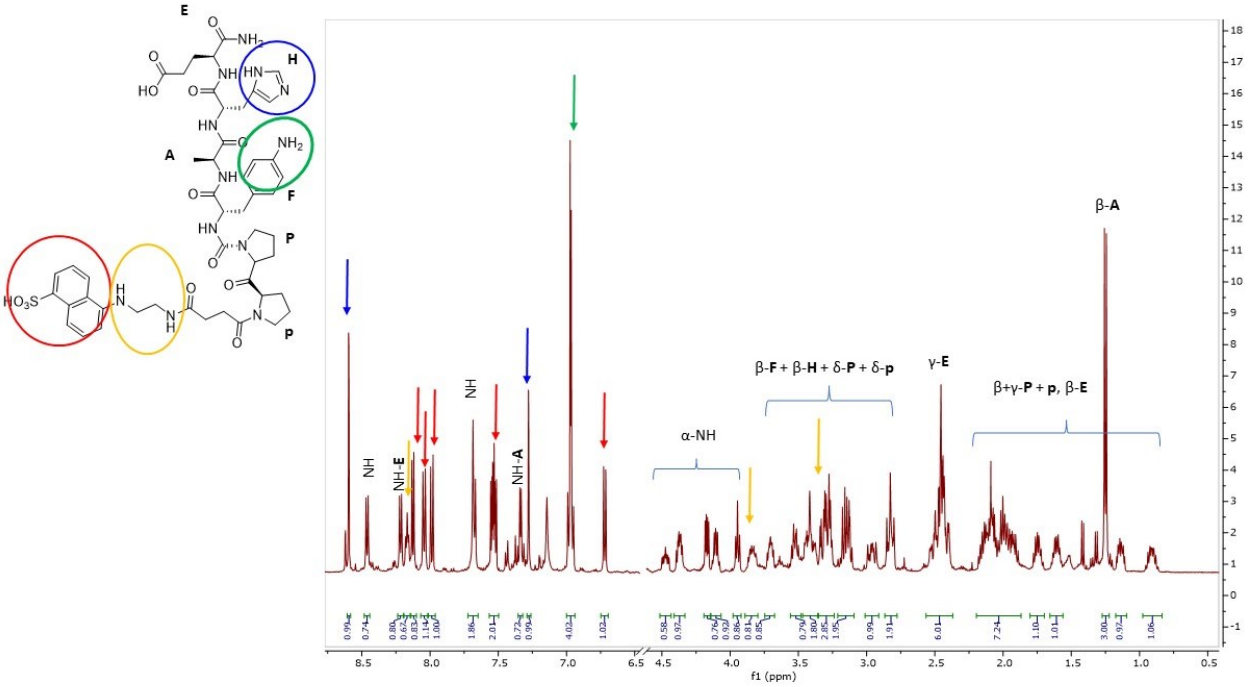

*Figure 5.2- ^{1}H-NMR spectrum of **P7** (water + 10% D_2O).*

In this case, only partial assignation could be done.

Looking at the ^{1}H-NMR spectrum (Figure 5.2), in the region between 8.60 and 6.71 ppm there are the amide protons, together with aromatic amino groups and aromatic protons of EDANS, *para*-amino phenylalanine and histidine. The α protons can be found between 4.71 and 3.95 ppm, and at lower ppm all the other protons of the lateral side chains.

The alanine system is easily recognizable because the characteristic doublet of the β protons at 1.25 ppm correlates with the α proton at 4.11 ppm and with the amide proton at 7.34 ppm.

The glutamic acid signals can also be distinguished because this amino acid has the longest spin system of the peptide, comprising the NH and α protons at 8.21 and 4.38 ppm respectively, the two diastereotopic β protons at 1.98 and 2.14 ppm and the two γ protons at 2.44 ppm.

The backbone of phenylalanine and histidine has the same type of pattern composed by NH, α and β diastereotopic protons, since the aromatic portion does not correlate with the protons in the principal peptide skeleton, and it has not been possible to distinguish amongst these two amino acids. In the case of histidine, the two imidazole protons can be found at 8.59 ppm and 7.28 ppm.

As for the two proline systems, they can be distinguished from the other amino acids because they do not have correlations with amide protons. However, a more complicated pattern then it was expected has been observed, possibly due to rigidity of the proline diad system creating many splitted signals even for non-diastereotopic protons, also causing important variations in the chemical shifts.

EDANS aromatic signals can be distinguished between 8.13 and 6.72 ppm.

5.2 STUDY OF THE NON-COVALENT INTERACTIONS OF THE PEPTIDES WITH TYROSOL

Using a multiwell plate reader, measurements of **P6** at a 19 µM concentration alone and with increasing concentrations of tyrosol (TY) ranging between 626 nM and 50 µM, have been taken, working in a basic environment to favor the dianionic form of fluorescein. In Figure 5.3 spectra registered exciting fluorescein at 483 nm are reported. It is possible to see that by increasing tyrosol concentration, there is an increase in the fluorescence emission at 525 nm. As already mentioned, previous work from our group regarding molecularly imprinted polymers containing fluorescein, demonstrated that the polymers were capable of increasing their fluorescence upon binding with target molecules tyrosol, hydroxytyrosol and oleuropein, and this was attributed to the capability of the binding event to shift the equilibrium between fluorescein protonation forms toward the formation of the dianionic form, the most fluorescent one, predominant at basic pH above 7.5.[1] However, since in the case of the peptides interaction takes place at basic pH, where the dianionic form is already predominant, it is possible to assume that the increase in fluorescence might be attributed to the nature of the peptide. In fact, the peptide has a very hydrophobic nature and, also thanks to the presence of the turn-promoting motif provided by the two prolines, it might bend on itself, so that fluorescein has a less polar environment around it. The binding event with tyrosol might thus cause a change in the conformation of the peptide, leading to an increase in the fluorescence of fluorescein due to increased polarity of the environment. On the other hand, examples of aggregates made of fluorophores such as fluorescein containing a xanthine core have already been reported in literature, forming H or J type dimers. H aggregates form by parallel card-pack disposition of the molecules, and cause a blue shift and fluorescence quenching, whereas J aggregates form by a head to tail scheme, and cause a red shift and fluorescence enhancement.[4,5] So, another hypothesis is that tyrosol favors the formation of J-type aggregates, thus causing fluorescent enhancement.

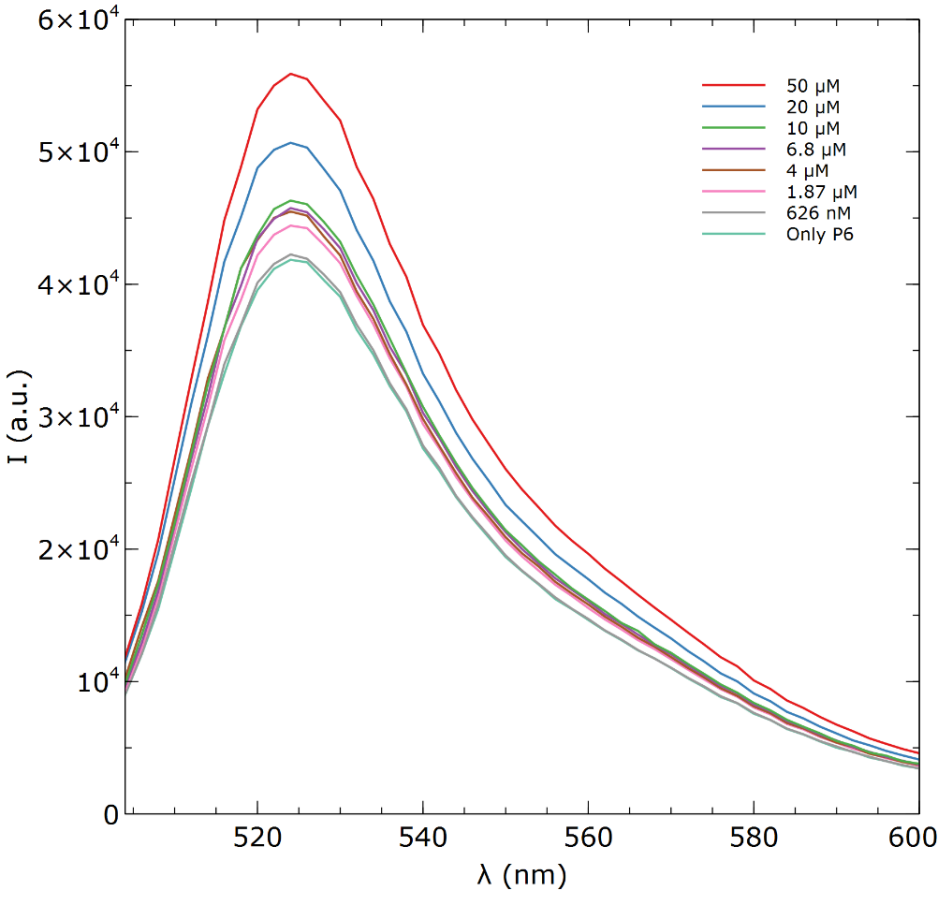

*Figure 5.3 Fluorescence titration of **P6** with tyrosol (spectra registered in a mixture of sodium carbonate with DMF, λ_{ex}= 483 nm).*

Considering **P7** containing EDANS, the same approach has been adopted, measuring fluorescence of 19 µM peptide solutions with increasing quantities of tyrosol, also this time working in a basic environment, but exciting the fluorophore at 336 nm (Figure 5.4). An increase in the fluorescence of the peptide has been observed also in this case and, as already mentioned for **P6**, one possible explanation might be the change in conformation of the peptide upon interaction with the target molecule, which might cause a change in the polarity around the fluorophore.

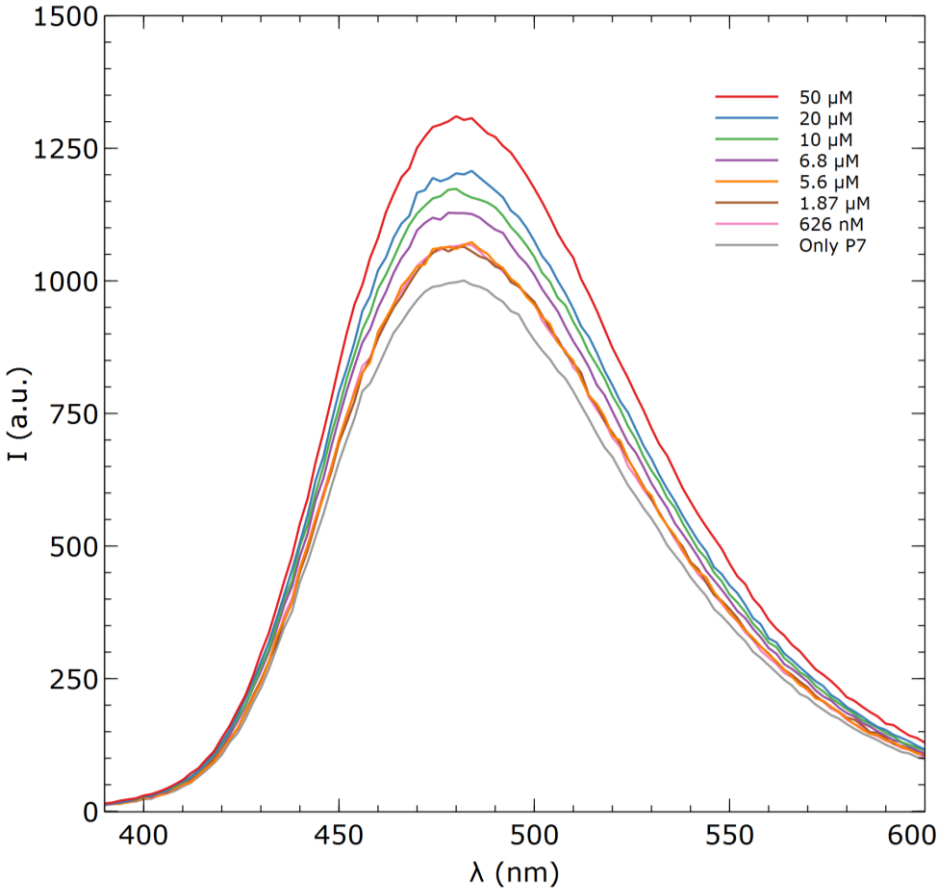

*Figure 5.4- Fluorescence titration of **P7** with tyrosol (spectra registered in a mixture of sodium carbonate with DMF, λ_{ex}= 336 nm).*

The increase in the fluorescence of the two peptides (Figure 5.5) follows a similar trend showing an overall increase emission of about 30%, which is quite promising in a sensing perspective. However, a lack of linearity is observed in both cases, together with high standard deviations. In this sense, further studies will have to be done, for example changing solvent composition and pH, also investigating the performance of the two peptides with other target molecules.

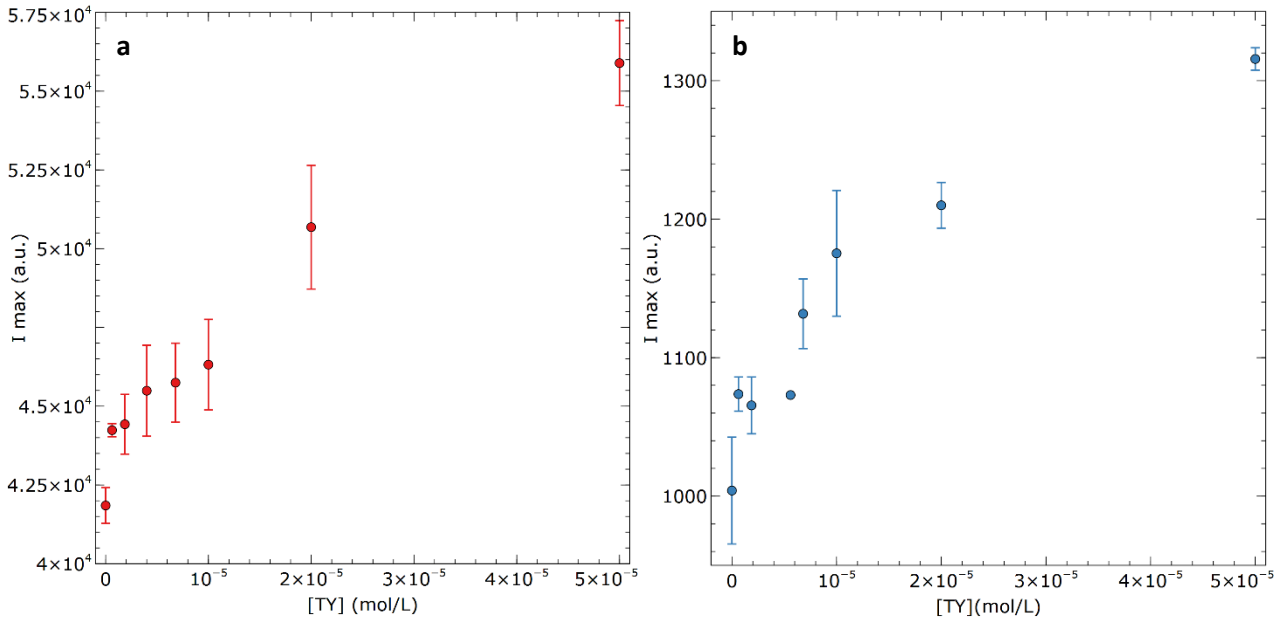

*Figure 5.5- Fluorescence intensities variation of **P6** (a) and **P7** (b) at increasing tyrosol concentrations.*

5.3 STUDY OF THE COVALENT INTERACTIONS OF THE PEPTIDES WITH TYROSOL

After testing the changes in the fluorescence behavior of the peptides induced by non-covalent interactions with tyrosol, the idea was that of testing their reactivity in the diazo-coupling reaction thanks to the presence of the *p*-NH_2-phenylalanine moiety, to investigate the influence of a diazo-coupling product formation on the fluorescence behavior of the two fluorophores present in the peptides.

5.3.1 Study of a model system

As a starting point, a simple model system has been studied, reacting the amino acid *p*-NH_2-Phe and tyrosol, with the aim of testing mild reaction conditions and to isolate and characterize the diazo-coupling product. The reaction was performed on the protected amino acid Acetyl-*p*NH_2Phe-OMe **24** with the α amino group acetylated and the carboxylic group protected in the form of the methyl ester to avoid unwanted influence on reactivity of groups different from the aromatic amine. The protocol has been adapted from the literature[6] and is a two steps reaction. The formation of the diazonium salt **25** was performed in 0.1 M HCl, with the addition of a solution of sodium nitrite in water. Subsequently a solution of tyrosol TY dissolved in sodium carbonate 0.1 M has been added drop by drop and the formation of a dark orange precipitate has been immediately observed (Scheme 5.1). NMR analyses confirmed the obtainment of the diazo coupling product **26** in a pure form, with a yield of 82%.

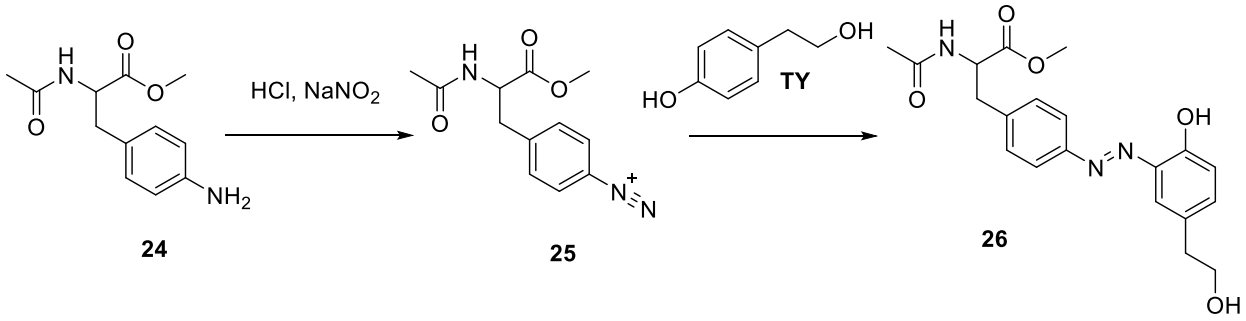

*Scheme 5.1- Diazo-coupling reaction of **24** with tyrosol to obtain **26.***

From the ^{1}H-NMR spectrum in DMSO-d_6 (Figure 5.6), it is possible to observe the characteristic three aromatic protons of tyrosol at 7.59 ppm (doublet with a J_{meta} of 2.26 Hz), at 7.27 ppm (a doublet of doublets, J_{ortho} of 8.5 Hz and J_{meta} of 2.2 Hz) and at 6.97 ppm (doublet with a J_{ortho} of 8.4 Hz), which is consistent with the formation of a diazo-coupling product.

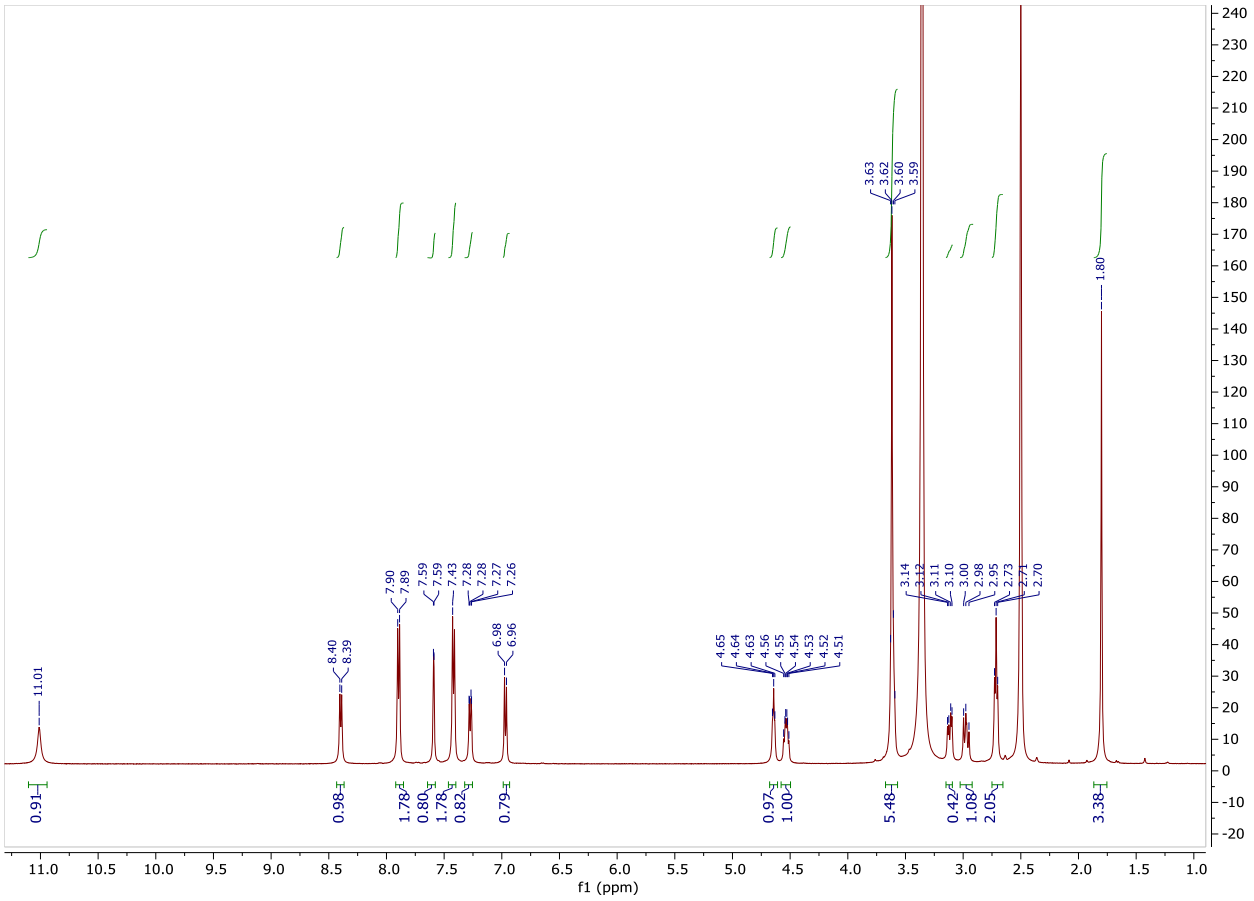

*Figure 5.6 – ^{1}H-NMR of **26** (DMSO-d_6).*

Looking at the mass spectrum in positive mode (Figure 5.7), it is possible to distinguish three diagnostic peaks at m/z 386.2, 408.2 and 424.1, corresponding respectively to the $[M+H]^+$, $[M+Na]^+$ and $[M+K]^+$ adducts.

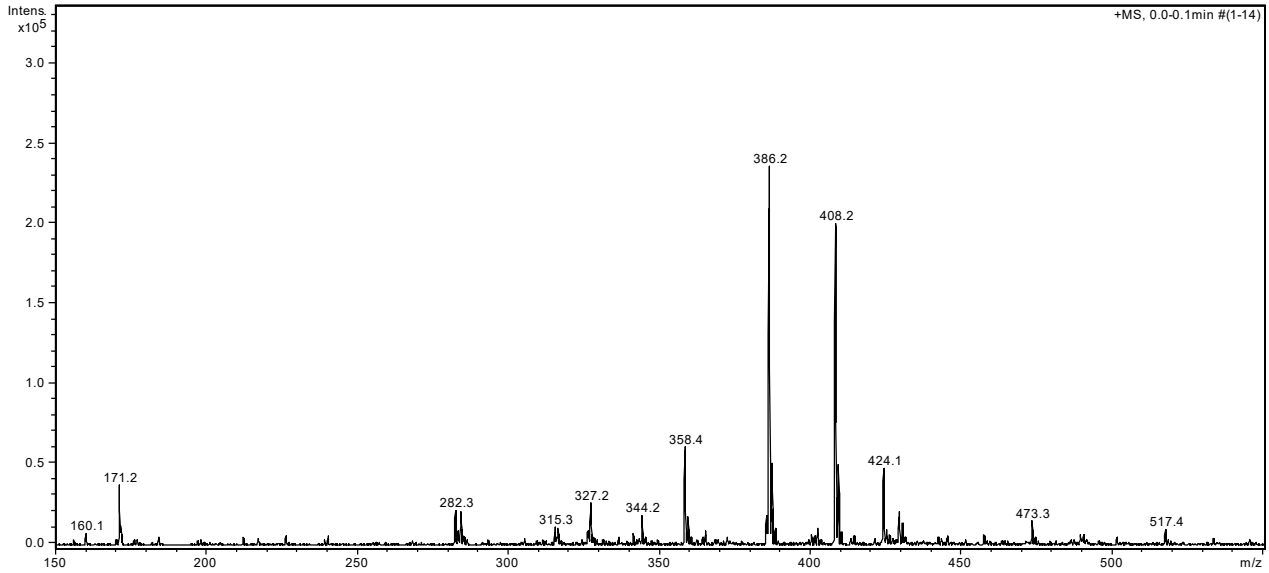

*Figure 5.7- Mass spectrum of **26.***

Since **26** is highly colored, UV-visible spectra have been registered in two different solvents: water and DMF, both at a 50 µM concentration (Figure 5.8). Although the two spectra are very similar, the spectrum in DMF shows higher absorbance: both present a higher peak at 330 nm and a less intense peak at 390 nm, while a

tail is present in the visible region up to 500 nm, which is responsible for the red-orange color of the compound.

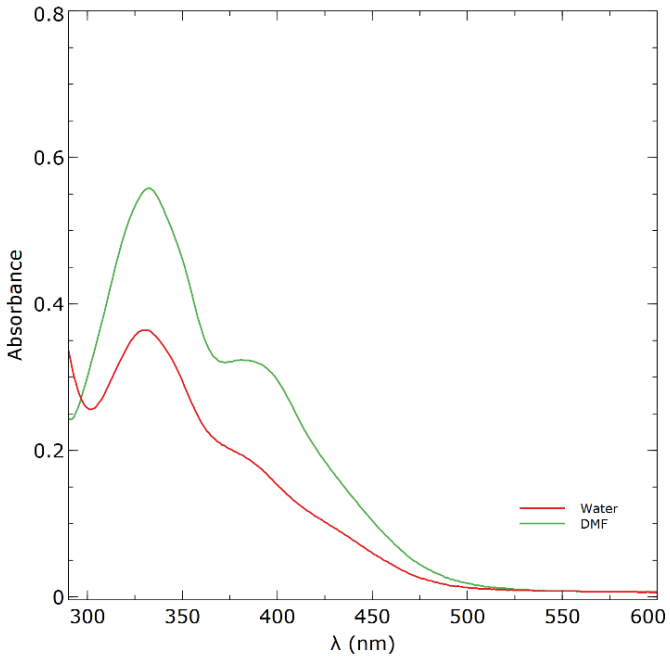

*Figure 5.8 absorption spectra of **26** in water and DMF.*

After obtaining and characterizing compound **26**, the reaction was tried on peptides **P6** and **P7** containing the *p*-amino-Phenylalanine amino acid, monitoring changes in the fluorescence emission of FITC and EDANS after formation of colored diazo-coupling compounds on the peptides. However, despite several attempts, this strategy resulted unsuccessful, due to the irreproducibility of the diazo-coupling reaction, caused by the instability of the intermediate diazonium salt that is rapidly hydrolyzed at room temperature. Moreover, in the case of **P7**, complete fluorescence quenching was observed after diazonium salt formation, before diazo-coupling reaction, due to its absorbance at 330 nm, the region in which EDANS is excited.

5.4 A NEW DIAZADIENE REACTION

5.4.1 Discovery of the reaction

In the attempt to apply the diazo-coupling reaction to target molecules different from tyrosol, aniline was reacted with different phenolic molecules, cinnamic acids, a very important class of compounds that can be found both in coffee and olive oil. The reactions performed did not lead to the expected diazo compounds but led surprisingly to new diazadiene compounds which were fully characterized and tested as antimicrobial and antitumoral compounds. The results obtained in this part of the thesis have been already published and will be briefly summarized here,[7] although this outcome is far from the main aim of the work.

Since hydroxycinnamic acids are widely present in the plant kingdom and have a backbone of a phenylpropanoid C6-C3 structure with hydroxyl groups on the phenyl ring, several substituted cynnamic acids have been considered, extending the trial also to substituents different from the hydroxyl.

As a first attempt *p*-coumaric acid (**28a**) was used in the reaction with the diazonium salt obtained from aniline **27**, formed as already described in the reaction with tyrosol (paragraph 5.3.1). The stoichiometry of the reaction was 1:2 aniline and *p*-coumaric acid respectively. The red precipitate formed was analyzed by ^{1}H-NMR, revealing the unexpected formation of the 1,2-diaza-1,3-diene **29a** (DD), obtained in 92% yield instead of the diazo-coupling product **30** (Scheme 5.2). The structure assignment was confirmed by mass spectrometry and ^{13}C-NMR spectroscopy (Figure 5.9 and Figure 5.10), with the help of bidimensional spectra ^{1}H-^{13}C HSQC and ^{1}H-^{13}C HMBC.

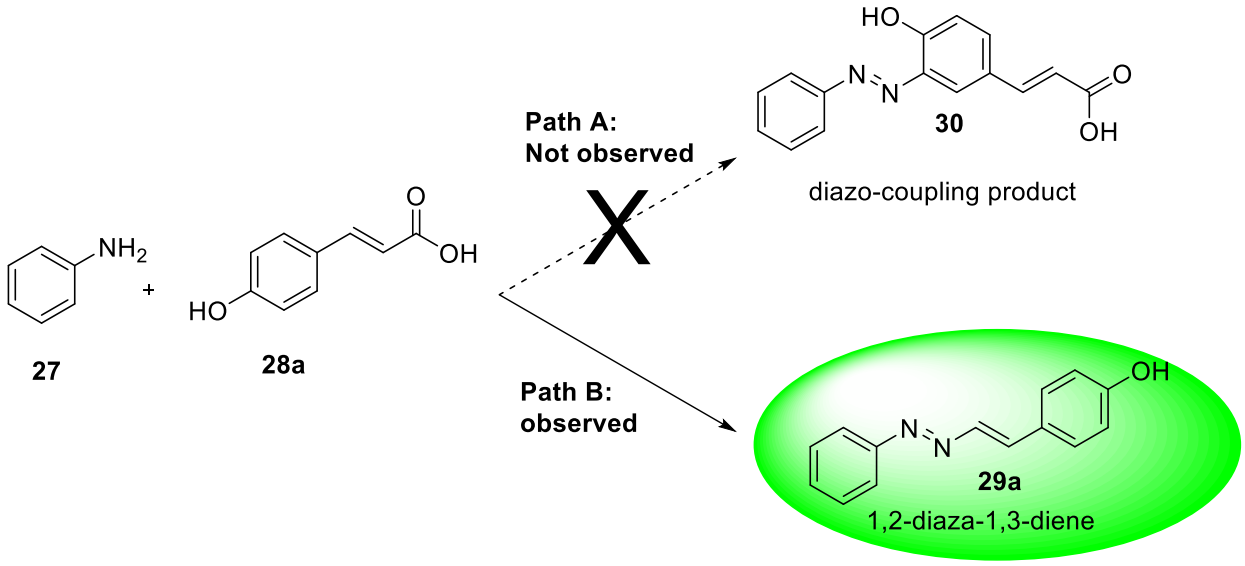

*Scheme 5.2 – Possible reaction pathways of aniline **27** with p-coumaric acid **28a** leading to formation of diazo-coupling product **30** (path A) or to 1,2-diaza-1,3-diene **29a**.*

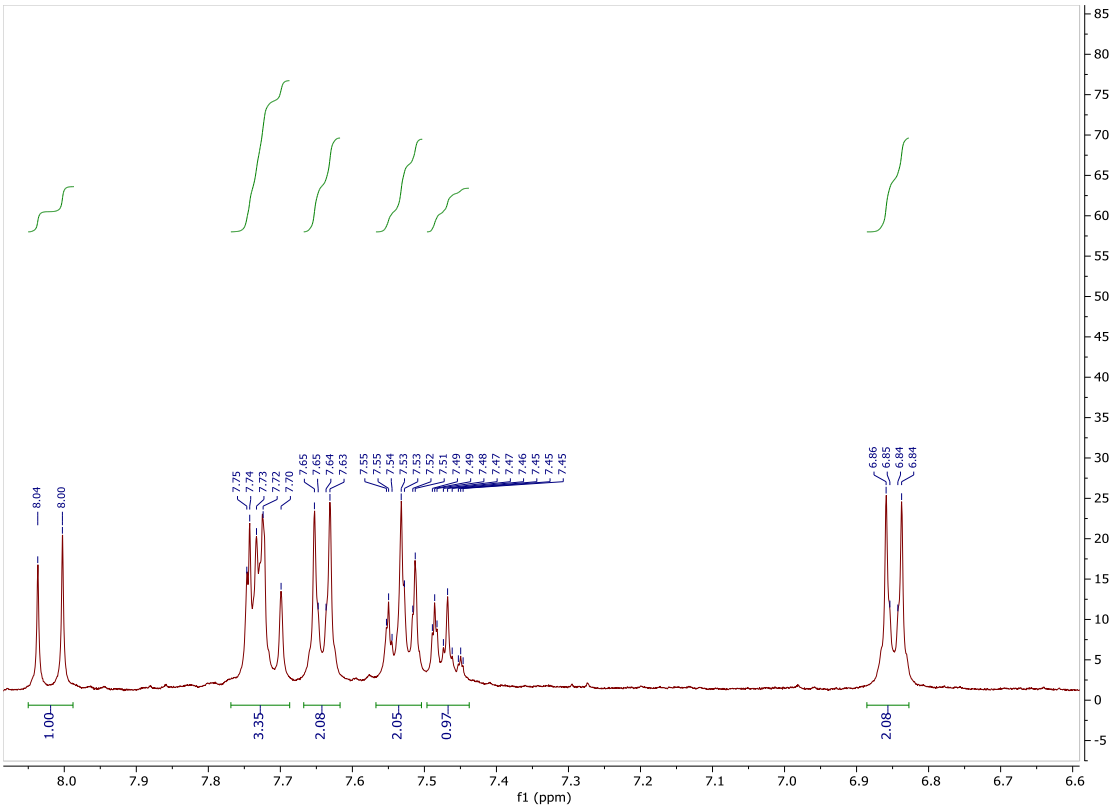

*Figure 5.9- ^{1}H-NMR spectrum of **29a** (DMSO-d_6).*

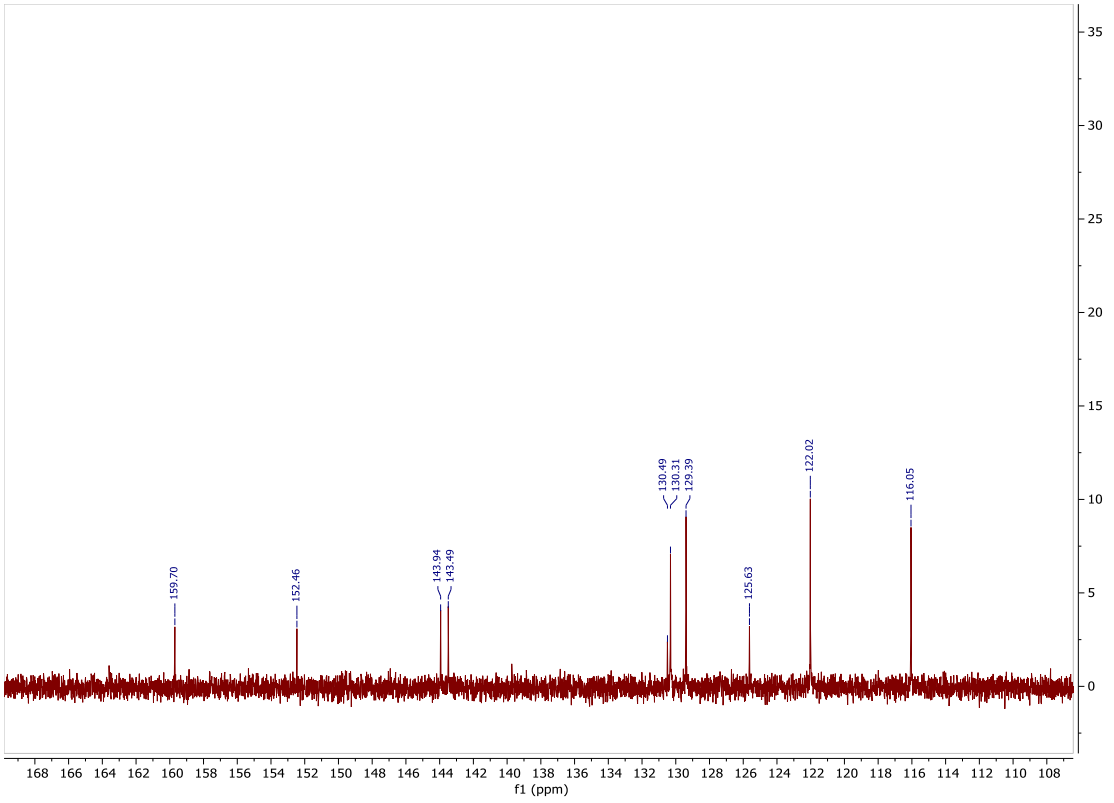

*Figure 5.10- ^{13}C-NMR spectrum of **29a** (DMSO-d_6).*

Since this kind of reactions was never observed till now, further experiments have been done to understand in which conditions this innovative reactivity takes place.

The reactions between aniline **27** and the following cinnamic acids were so studied: ferulic acid (**28b**), 4-(dimethylamino)cinnamic acid (**28c**) and *o*-coumaric acid (**28d**) (Scheme 5.3). Different stoichiometric ratios were used, and results are summarized in Table 5.1. By ^{1}H-NMR, ^{13}C-NMR and mass spectrometry analyses it was possible to determine that ferulic acid and 4-(dimethylamino)cinnamic acid gave a diazadiene as the product while *o*-coumaric acid reacted through a traditional diazo-coupling reaction.

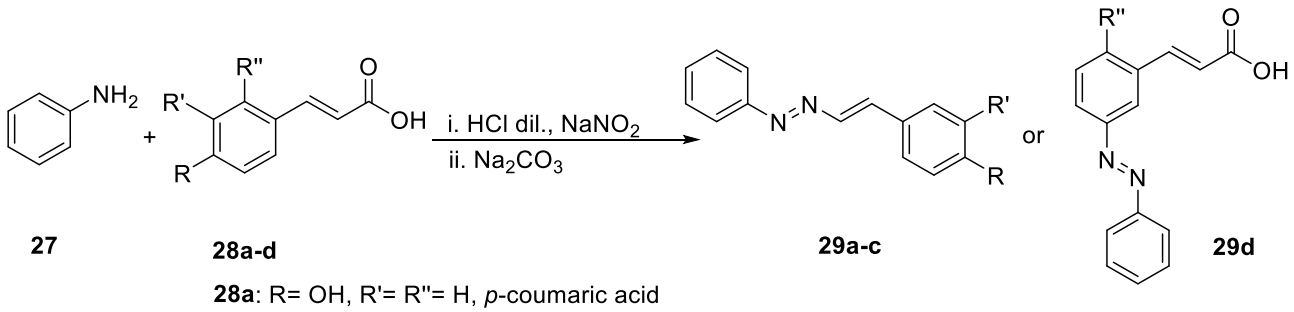

27 **28a-d** **29a-c** **29d**

28a: R= OH, R'= R''= H, *p*-coumaric acid
28b: R= OH, R'= OCH_3, R''= H, ferulic acid
28c: R= $N(CH_3)_2$, R$^{'}$= R''= H, 4-(dimethylamino)cinnamic acid
28d: R$^{''}$= OH, R=R$^{'}$= H, *o*-coumaric acid

Scheme 5.3 - General reaction scheme for the reaction of aniline with cinnamic acids.

After testing different cinnamic acids, also a different aromatic amine was used, Ac-*p*NH_2Phe-OMe **24**, as already mentioned in paragraph 5.3.1. This choice was based with the idea to use this reaction to develope a peptide sensing element as in the case of diazo-coupling reaction with tyrosol. **24** was so reacted with *p*-coumaric acid **28a**, ferulic acid **28b** and 4-(dimethylamino)cinnamic acid **28c**, and in all three cases the corresponding DDs **31a-c** have been obtained with yields ranging between 71 and 96% (Scheme 5.4, Table 5.1).

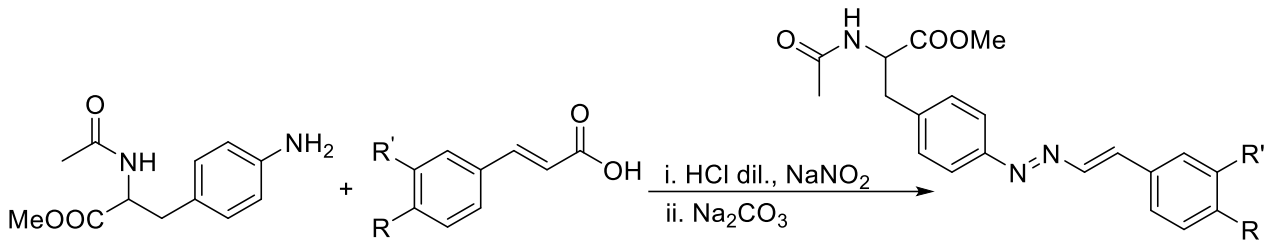

24 **28a-c** **31a-c**

28a: R= OH, R' = H, *p*-coumaric acid
28b: R=OH, R$^{'}$ = OCH_3, ferulic acid
28c: R= $N(CH_3)_2$, R' = H, 4-(dimethylamino)cinnamic acid

*Scheme 5.4 Reaction scheme of **24** with cinnamic acids.*

*Table 5.1- Stoichiometric ratios and yield for DDs **29a-c** and **31a-c.***

Compound	Stoichiometric ratio amine: cinnamic acid	Yield
29a	1:2	92%
29b	1:2	98%
29c	1:1	81%
31a	1:3	96%
31b	1:1	77%
31c	1:1	71%

5.4.2 Reaction mechanism

Based on the reactivity of the tested cinnamic acid, a bielectronic mechanism of reaction has been hypothesized, involving the nucleophilic attack of the carbon in α position with respect to the carboxylic group towards the electrophilic diazonium salt, promoted by the electron donating group in *para* position with respect to the conjugated double bond. Then, decarboxylation of the intermediate reestablishes the aromaticity, resulting in the completely conjugated DD (Scheme 5.5). The proposed mechanism is very different from that of other reactions involving diazonium salts and unsaturated compounds, such as the Meerwein arylation reaction, resulting in the formation of the corresponding stilbene when applied to aryl-diazonium salts and cinnamic acid.[8,9] The only somehow-correlated reaction happening with a mechanism similar to the one we hypothesized for DDs formation, has been reported in literature for the synthesis of 4,4-dialkylthio-1,2-diaza-1,3-butadienes based on the azo-coupling decarboxylation of α-carboxy ketene dithioacetals with aryldiazonium salts.[10]

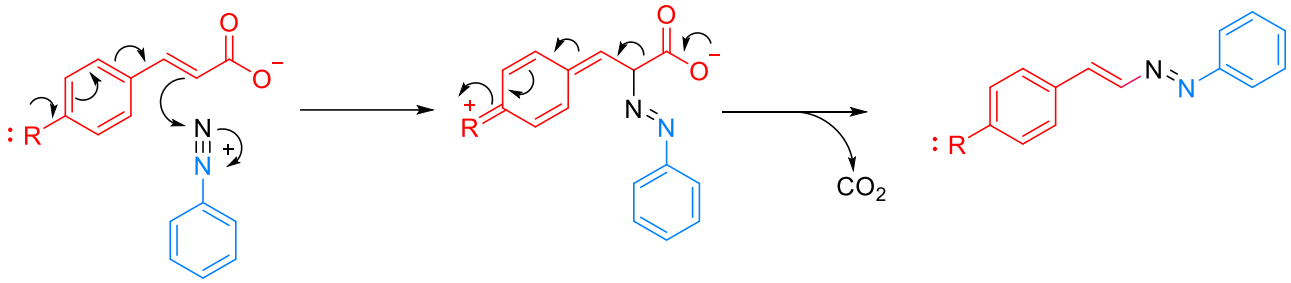

Scheme 5.5- Hypothesized reaction mechanism for DDs formation.

5.4.3 Biological tests

Since the newly discovered diazadienes seemed to be very interesting from the biological point of view, preliminary studies have been carried out to test their antimicrobial and antitumor activity.[ii]

In particular, the antitumor activity of the six DDs has been evaluated by comparing the response of normal hTERT-immortalized human uterine smooth muscle cells and the tumorous counterpart, leiomyosarcoma (LMS) SK-UT-1 cells. Compound **29c** resulted to be the most promising one, inducing a selective response against cancer cells with respect to normal ones, and the mechanism involved in its differential action might be the object of further studies in the future.

Considering the antibacterial activity, the minimum concentrations inhibiting the growth (MIC) of DDs has been tested on a standard strain of *E. coli* (ATCC 25922) and *S. aureus* (ATCC 25923), as representative of a Gram-negative and -positive pathogen, respectively. None of the tested compounds resulted to be effective on *E. coli*, but some of them, in particular **29a** and **29b**, exerted some antibacterial activity.

[ii] Antitumor activity of DDs has been tested in collaboration with the group of Professor Brancolini, of the Department of Medical Sciences of the University of Udine, whereas the antimicrobial activity has been tested in collaboration with Professor Scocchi of the Department of Life Sciences of the University of Trieste.

5.5 BIBLIOGRAPHY

(1) Stavro Santarosa, A.; Berti, F.; Tommasini, M.; Calabretti, A.; Forzato, C. Signal-On Fluorescent Imprinted Nanoparticles for Sensing of Phenols in Aqueous Olive Leaves Extracts. *Nanomaterials,* **2020**, 10 (6), 1011.

(2) Tamburello, E. M. Piccoli peptidi per riconoscimento covalente di composti fenolici presenti nell'olio EVO con applicazioni sensoristiche, Master degree thesis, **2021**-**2022**, University of Trieste.

(3) Calvanese, L.; Caporale, A.; Focà, G.; Iaccarino, E.; Sandomenico, A.; Doti, N.; Apicella, I.; Incisivo, G. M.; De Falco, S.; Falcigno, L.; D'Auria, G.; Ruvo, M. Targeting VEGF Receptors with Non-Neutralizing Cyclopeptides for Imaging Applications. *Amino Acids,* **2018**, 50 (2), 321–329.

(4) Das, S.; Chattopadhyay, A. P.; De, S. Controlling J Aggregation in Fluorescein by Bile Salt Hydrogels. *J. Photochem. Photobiol. A,* **2008**, 197 (2–3), 402–414.

(5) Khan, F.; Liu, P.; Yang, S.; Ma, Y.; Qiu, Y. Concentration-Dependent Dye Aggregation in the LbL-Assembly of Fluorescein Isothicyanate Labeled Poly(Allylamine Hydrochloride) and Poly(Acrylic Acid) on Cotton Fabrics. *Dyes Pigm.,* **2017**, 142, 358–364.

(6) Liu, Y.; Zhou, P.; Da, H.; Jia, H.; Bai, F.; Hu, G.; Zhang, B.; Fang, J. An Azo Coupling Strategy for Protein 3-Nitrotyrosine Derivatization. *Chem. Eur. J.,* **2019**, 25(48), 11228-11232.

(7) Vida, V.; Minisini, M.; Mardirossian, M.; Brancolini, C.; Scocchi, M.; Forzato, C.; Berti, F. Novel Synthesis of 1,2-Diaza-1,3-Dienes with Potential Biological Activity from Cinnamic Acids and Diazonium Salts of Anilines. *RSC Adv*., **2023**, 13 (1), 456–463.

(8) Schroll, P.; Hari, D. P.; König, B. Photocatalytic Arylation of Alkenes, Alkynes and Enones with Diazonium Salts. *ChemistryOpen,* **2012**, 1 (3), 130–133.

(9) Rondestvedt, C.S. Arylation of Unsaturated Compounds by Diazonium Salts (The Meerwein Arylation Reaction) *Org. Reactions*, **2004**, 24, 225-259.

(10) Xu, X.-X.; Wang, M.; Liu, Q.; Pan, L.; Zhao, Y.-L. Azo-Coupling Decarboxylation Reaction Of α-Carboxy Ketene Dithioacetals in Water–a New Route to 1,2-Diaza-1,3-Butadienes. *Chin. J. Chem*., **2006**, 24 (10), 1431–1434.

6 CONCLUSIONS

In conclusion, during this PhD project, several approaches have been developed for the detection and quantification of bioactive phenols present in olive oil - tyrosol and hydroxytyrosol- and coffee -chlorogenic acid and caffeic acid-. The first focus of the research has been that of screening amongst different reactions for covalent target molecule recognition, capable of providing changes in spectroscopic signals upon reaction with target molecules (TMs). The identified reactions are:

1. TBA (trihydroxybenzacridine) pigments formation from reaction of CGA with primary amino groups;
2. Boronic esters formation between *ortho*-diphenols and boronic acids labeled with fluorophores;
3. Diazo coupling reaction between the non-natural amino acid *p*-amino-phenylalanine and phenols.

After testing the reactions on the single building blocks responsible for covalent binding, the reactions have been applied to peptide systems, with the aim of combining the covalent recognition with the non-covalent interactions provided by the peptide scaffold, that might be beneficial to improve the affinity and selectivity of the sensing elements for target molecules.

6.1 TBA PIGMENT REACTION

TBA pigment formation is a particular reaction involving primary amino groups and esters of caffeic acid in an aqueous oxidizing environment, leading to the formation of green pigments showing a characteristic absorbance around 680 nm at basic pH. Such reaction has been extensively reported in literature, but it has never been applied to CGA sensing. The first step has been that of isolating the pigment obtained from reaction between CGA and the amino acid *N*α-boc-lysine, purifying it by SEC and characterizing it by HPLC-MS to confirm its formation in the reaction conditions adopted. Then, the kinetics of TBA pigment formation in excess of lysine has been studied spectrophotometrically by measuring the increase in the diagnostic absorbance at 680 nm, observing the presence of a linear range during the first 15 minutes of reaction, while the reaction reaches completion in around 24 hours. The effect of different buffering conditions at pH 9 - namely carbonate, phosphate and borate buffer- has been evaluated, thus selecting carbonate buffer for further studies.

Application of the reaction to CGA quantification has thus been investigated from the analytical point of view, working in excess of amino receptor lysine at different CGA concentrations, either at the end point of the reaction or in kinetic mode monitoring the first 15 minutes of reaction.

In the end point mode, after 24 hours of reaction, a good linear range could be found, obtaining a 6 µM calculated LOD. In the kinetic mode, a LOD of 5 µM was obtained, thus comparable with result from the end-point method, but with the advantage of monitoring the reaction for only 15 minutes. The experiment in kinetic mode has been replicated also using an in-lab built photometer obtaining very interesting preliminary results that suggest a higher sensitivity of such instrument with respect to the laboratory spectrophotometer.

After these preliminary studies, the reactive lysine residue has been inserted into two different peptides, Ac-Phe-Phe-Ala-Pro-Pro-Lys-Ala-Ser-Glu-NH_2 (**P1**) and Ac-Phe-Phe-Ala-Glu-Ser-Lys-Ala-Ser-Glu-NH_2 (**P2**), obtained by solid phase synthesis. By comparing the performance of **P1** and **P2** with results obtained with lysine alone, it emerged that **P1** improves the reaction rate, while **P2** makes it slower, and the positive performance of **P1** has been confirmed also by a preliminary study at different CGA concentrations.

Due to positive outcomes from the TBA pigment formation reaction working in solution, with the idea of passing to an approach even more suitable for sensing applications, during the six months period spent at Universidad Complutense de Madrid, the reaction has been applied to the synthesis of polymeric films capable of turning green upon CGA reaction thanks to the presence of reactive primary amino monomers.

The composition of the polymers has been optimized, testing two types of amino-monomers -*N*-(3-aminopropyl)methacrylamide APMA and 2-aminoethyl methacrylamide AEM- and varying the ratio between amino-monomer and the other components, analyzing the performance of the obtained polymeric discs by using a multiwell plate reader to measure increased absorbance of the discs at 680 nm upon CGA reaction. After selecting **Me2** as the most promising composition, its performance at different CGA concentrations has been studied both using the multiwell plate reader and portable devices, i.e. an optical fiber photometer and two in-lab built devices- an image reader and a pseudo-differential reflection spectrophotometer-. By testing CGA in a range of concentrations between 0.1 and 1 mM, the best performing device resulted to be the reflectance spectrophotometer, obtaining a LOD of 37.5 µM: this value is one order of magnitude higher with respect to those obtained in solution for lysine alone. However, the possibility of working on polymeric discs with easy in-lab built devices, is very advantageous in the perspective of realizing the final biosensor, and further improvements on this approach might be made to obtain better results.

To explore the possibility of using also other sensing strategies apart from the colorimetric approach, fluorescence of the TBA pigment has been studied. A first fluorescence emission in basic environment could be found when exciting the purified TBA pigment at 318 nm and measuring emission at 426 nm, with a LOD of 56 µM. Such value is one order of magnitude higher than the one observed for the lysine system in absorbance mode. Moreover, the interference from CGA own emission in this region makes it impossible to use the reaction working in mixture as previously done for the absorbance approach. For this reason, a second screening has been done searching for possible other emissions, finding a very interesting emission at 700 nm when the pigment is excited between 620 and 660 nm, provided the pH is equal or below 7. This fluorescence is very interesting because it is in a region far from possible interferences from other compounds in solution - including CGA- thus allowing to work in a mixture. The emission in the red region has been studied to quantify CGA: however, despite some positive preliminary results, the system resulted to be very complicated, and not suitable for CGA quantification in the present configuration. One possible reason for this probably resides in the fact that an acidification step is required with respect to the basic environment in which TBA pigment formation takes place, and using carbonate buffer complicates this step because of the dissociation equilibrium of carbonic acid to carbon dioxide and water. Another critical point is the existence of different prototropic forms of TBA pigment, exhibiting different spectroscopic properties, and at a slightly acidic pH (around 6) these forms might coexist at the same time.

Finally, the TBA pigment reaction has been studied as a possible method for protein labeling, using BSA as a model protein. Fluorescence emission of the TBA pigment at 460 nm has been used as the detection method and the sensitivity of the system has been evaluated to determine if the proposed method might be applied to protein labeling. Very good results could be obtained, with a linear range between 2.5-300 µM and a 28 nM calculated LOD. Further tests will be carried out to study protein labeling in fluorescence mode also at longer wavelengths.

As a future perspective, it will be interesting to test the performance of the developed colorimetric systems -both in solution and based on polymeric discs- on real samples analysis, for example analyzing green coffee beans extracts. In the case of polymeric discs, an option might be that of testing the performance also on coffee brews, thanks to the possibility of washing the discs to remove dark colored non-reacted products prior to analysis with the in-lab built devices, thus avoiding the presence of interferent colored compounds.

6.2 BORONIC ACIDS

The first step has been the evaluation of two different fluorescent molecules containing a boronic acid moiety suitable for boronic ester formation with *ortho*-diphenolic targets, but also possessing a functionality suitable for conjugation to peptides.

The first tested fluorescent monomer has been 2-(4-boronophenyl)quinoline-4-carboxylic acid **5**, whose application has been extensively reported in literature for sensing of saccharides but also on *ortho*-diphenols. The performance of **5** has been analyzed by fluorescence titrations with target molecules CC, CGA, CA and HT, observing in all cases a fluorescence quenching, in accordance with the literature. In the case of CGA and CA, fluorescence quenching was accompanied by a shift of the emission at longer wavelengths from 390 nm to 450 nm when exciting at 335 nm. To try to go deeper into the phenomenon, the experiment has been repeated also on *p*-coumaric acid, observing the same effect, even if with a less pronounced fluorescence quenching.

A second type of fluorophore has then been evaluated, **20**, containing a 1,8 naphthalimide core, taking inspiration from an analogous structure reported in literature, but slightly changing it to provide a site for future conjugation to peptides. The fluorophore has been synthesized according to a procedure partially adapted from literature. After synthesizing **20**, which emits at 550 nm when excited at 490 nm, fluorescence titrations have been carried out with TMs CC, CGA, CA and HT, observing for all of them a fluorescence quenching adding concentrations in the range 393 nM-4.5 mM, without shifts in the emission wavelengths. Calculating the bimolecular quenching constant k_q from the Stern-Volmer plot, all the molecules resulted to have a static fluorescence quenching mechanism, which might hint to a covalent quenching mechanism. Considering the apparent K_d values calculated according to the Langmuir Isotherm model, CGA exhibited the highest affinity, followed by CA and, with a K_d around one order of magnitude higher, by CC and HT. **20** was also tested with possibly interfering molecules tyrosol, *p*-coumaric acid and quinic acid, showing partial fluorescence quenching only at the highest concentrations of *p*-coumaric acid, thus suggesting that the quenching mechanism in this case is mainly ascribed to formation of cyclic boronic esters with *ortho*-diphenolic molecules. **20** has been selected for further conjugation with peptides, due to the most favorable fluorescent properties with respect to **5**. In fact, **20** is excited and emits at longer wavelengths with respect to **5**, where less interferences should verify, also exhibiting best quenching performance and less interferences from other related compounds. Three different peptides have been synthesized, **P3** (**20**-succinyl-dPro-Pro-Trp-NH_2), **P4** (Acetyl-Arg-Gly-Glu(**20**)-Gly-NH_2) and **P5** (Acetyl-Arg-Gly-Glu(**20**)-dPro-Pro-Ala-His-Glu-NH_2). While **P3** is uncharged, in the case of **P4** and **P5** a positively charged residue of arginine has been inserted into the peptide, capable of interacting electrostatically with the carboxylate of targets which are negatively charged at the 7.4 pH at which analyses are performed. After synthesizing the peptides, fluorescence titrations have been carried out with target *ortho*-diphenols as already performed for fluorophore **20** alone. By making a comparison of the peptides with **20** alone, all the sensing elements exhibited the highest affinity for CGA, followed by CA and then HT and CC behaving very similarly in all cases. **20** showed the highest affinity for CGA, followed by peptides **P4**, **P5** and finally **P3**, and the same order is maintained also for caffeic acid, with only a shift between **P5** and **P3**. The generally best performance of the positively charged fluorophore **20** and of peptides **P4** and **P5** with the acidic targets, can be at least partially ascribed to the additional electrostatic interactions formed with the negatively charged carboxylate of CGA and CA. As to the cross reactivity, all the recognition elements are capable of discriminating well between CGA and HT and CC, with cross-reactivity values ranging between 5% and 13%, whereas in all cases capability of discriminating between CGA and CA is much worse (58% for **20**, 45% for **P3** and **P4**), with only **P5** performing a bit better, with a cross reactivity value of 34%: this can be ascribed to the high structural similarity of the two compounds, sharing the caffeoyl moiety.

An interesting perspective for the future would be that of projecting other peptides supported by a more sophisticated computational approach, to target specifically one of the desired targets.

6.3 DIAZO-COUPLING REACTION

Based on previous experience of our group about fluorescein as a reporter for the recognition of phenols in imprinted polymers, fluorescein-labeled peptides have been prepared to test the same process on such scaffold. However, to study these peptides also in covalent mode, the non-natural amino acid *p*-amino-phenylalnine (*p*NH_2Phe) has been inserted into the peptide structure, which might react in a diazo-coupling reaction with phenolic compounds. In this perspective, peptide **P6** (Acetyl-*p*NH_2Phe-(D)Pro-(L)Pro-Lys(FITC)-NH_2) has been synthesized. Based on the same principle, also a second peptide has been synthesized, having the sequence EDANS-succinyl-(D)Pro(L)Pro-*p*(NH_2)Phe-Ala-His-Glu-NH_2 (**P7**) retaining the *p*NH_2Phe and the proline diad motif, but changing to a different fluorophore- EDANS-, inserting few more amino acids capable of hydrophobic interactions and also to enhance water solubility. Both peptides have been synthesized in solid phase, and their performance in tyrosol recognition has been tested by the non-covalent approach. In both cases, a fluorescence enhancement has been observed, even if, unfortunately, without a clear linear trend.

Before evaluating the covalent interactions of peptides **P6** and **P7** with TM tyrosol, the reactivity of the amino acid Acetyl-*p*NH_2Phe-OMe with tyrosol has been studied to assess mild reaction conditions suitable for performing diazo-coupling reaction on peptides, obtaining the corresponding red-colored diazo-coupling product **26**. Several unsuccessful attempts have been carried out to apply the diazo-coupling reaction also to peptides **P6** and **P7**.

As a side project of the diazo coupling reaction approach, while studying the reactivity of phenolic compounds different from tyrosol -substituted cinnamic acids- in diazo coupling reaction, a new reactivity involving *p*-substituted cinnamic acids and aromatic amines has been discovered, leading to formation of novel 1,2-diaza-1,3-dienes, which have been fully characterized and have been also tested in biological tests as potential antitumor and anti-microbial agents.

7 EXPERIMENTAL PART

7.1 INSTRUMENTATION

Size Exclusion Chromatography (SEC) has been performed on a column having a radius of 1.25 cm, a section of 4.9 cm^2, a length of 52 cm and a volume of 255 mL, using a peristaltic pump to flow solvent through it. As the stationary phase, a Bio-Gel P-4 resin (Bio-Rad) has been used (hydrated bead size = 90-180 µm, hydrated bed volume/mass dry gel = 4 mL/g, typical flow rate = 15-20 cm/h, molecular weight fractionation range = 800-4000 Da).

Spectrophotometric measurements have been performed on a UV-Visible Shimadzu UV-2450 spectrophotometer, coupled with a Shimadzu TCC-Controller thermostat. Kinetic measurements have been registered at 25°C, all the others at room temperature. Quartz cuvettes from Hellma having a 1 cm optical path have been used.

Fluorescence measurements have been carried out on a Perkin Elmer LS50B fluorometer (non thermostated) or, if not differently stated, on a Varian Cary Eclipse spectrophotometer coupled to a Varian Cary thermostat, performing measurements at 25°C. If not differently stated, all the measurements have been done using quartz cuvettes having a 0.5 cm optical path, using an adaptator.

Fluorescence measurements of pigment 2 in the red region (around 700 nm) have been carried out using a HORIBA Fluoromax-4TCSPC steady-state spectrofluorometer, having a red-sensitive Hamamatsu R928P photomultiplier tube (PMT) sensitive from 200 to 850 nm. 2x10 mm cuvettes from Hellma have been used.

Fluorescence and absorbance measurements using a multiwall plate reader have been done using a Tecan Infinite M1000 Pro instrument, taking all the measurements at 25°C. Thermo Fisher Scientific-Nunclon 96 Flat Bottom Black Polystyrene multiwell plates have been used for fluorescence measurements, transparent polystyrene Greiner 96-well plates have been used for absorbance measurements.

Absorbance measurements on polymeric discs using a multiwell plate reader have been done using a CLARIOstar reader from BMG Labtech (Ortenberg, Germany), working at 25°C, using transparent polystyrene Greiner 96-well plates and using MARS software.

Optical fiber absorbance measurements were carried out with a portable optical fiber spectrometer (Ocean Insights FLAME-S-VIS-NIR-ES-200 model, response in the 350-1000 nm range) connected to a 3.2 mm dia. 50/50 randomly bifurcated bundle made of individual borosilicate optical glass fibers (Vydas, UK). The light source is composed by a high-intensity white light LED (SL1-LED, StellarNet, Fla., USA). The mini-spectrometer acquisition and signal display are provided by a laptop computer connected via its USB port using the Ocean Optics Spectrasuite software v2.0.

HPLC-MS measurements have been carried out using an HPLC instrument consisting of a degasser, a quaternary pump, a thermostated column compartment, a Diode Array Detector (DAD) Agilent Technologies 1260 Infinity and an Agilent technologies 6120 Quadrupole LC/MS mass spectrometer. The column was a Phenomenex Gemini (150x2mm, 3 µm, C18 110 angstrom, 0.2 mL/min flow).

Preparative HPLC to purify peptides has been done using a Thermo Scientific Dionex HPLC UltiMate Vanquish 3000 instrument, consisting of a degasser, a quaternary pump, autosampler, thermostated column compartment, UV-Vis detector and fraction collector. The column was a Phenomenex Gemini (250x10 mm, C18, 5 µm, 5 mL/min flow).

Peptide synthesis has been carried out in solid phase with a microwave Biotage Initiator + Alstra automatic synthesizer, using polystirenic Rink Amide MBHA resin as the solid support for peptide synthesis by FMOC approach.

NMR spectra have been recorded on a Varian 400 or a Varian 500 spectrometer using deuterated solvents as specified in the text, taking the solvent peak as the reference: for ^{1}H NMR, references were selected at 4.79 ppm for D_2O, at 7.26 ppm for $CDCl_3$, at 2.50 ppm for DMSO-d_6, at 4.87 ppm for MeOD; ^{13}C NMR spectra have been registered only in DMSO-d_6, taking as the reference the DMSO-d_6 solvent peak at 39.52 ppm. The chemical shift values are expressed as ppm (δ), whereas coupling constants (J) values are expressed in Hz. Resonance multiplicity is described as s (singlet), d (doublet), t (triplet), q (quartet), m (multiplet), dd (doublet of doublets), or br (broad signal).

Mass spectra were registered on a microTOF-Q-Bruker having an electrospray ionization (ESI) source and a time of flight (TOF) analyzer, and on an Esquire 4000-Bruker, having an ESI source and an ion trap analyzer.

Infrared spectra (IR) were registered on an ATR-IR IRAffinity-1S Fourier transform infrared spectrophotometer (Shimadzu).

pH measurements have been carried out using a pH-meter HANNA instruments, edge$^{®pH}$ model (HI12002) provided with a kit HI13310 including a digital electrode with temperature sensor and standard calibration solutions.

Lyophilizations have been carried out using a SCANVAC CoolSafe 55/110 lyophilizer.

Dialysis has been carried out using Dialysis membranes with MWCO of 3500 Da purchased from Spectrumlabs.

In-lab built devices

The **photometer** for measurements in cuvette is composed by a LED source (λ_{em} = 675 nm, Δλ = 24 nm), Silicon blue enhancement detectors and a dedicated section for analogic signal treatment. The whole is controlled by a software for digital processing.
The **image reader** for measurements on polymeric discs is composed by a high-resolution commercial USB camera, mounted on a white chamber containing a sample compartment. On top of the chamber, around the camera, red (λ = 675 nm) and green (λ = 520 nm) LEDs are mounted to illuminate the chamber with wavelengths of interest. The image is then processed using a freeware (Just Color Picker) for data elaboration, capable of distinguishing red, green and blue color coordinates. Multiple points are taken for each disc (diameter around 5 mm) and after making the difference between the green and red coordinates for each point and subtracting the average blank value to each of them, results are mediated to obtain the final value.
Pseudo differential reflection spectrophotometer for measurements on polymeric discs is composed by two LED sources operating at the wavelengths of interest at λ =675 nm and λ=860 nm (also serving as the reference), and an optical fiber mixer collimating the two sources on a white diffusive surface of reference. The two optical sensors are positioned so that the light emitted by the light sources (sensor 1) and light retro diffused by the sample (sensor 2) can be measured. The sample slot is white, whereas all the rest of the surfaces are black. A first calibration test with the blank sample is requested, then it is possible to pass to sample measurement.

7.2 MATERIALS

2-hydroxyethyl methacrylate (HEMA) (≥99%, containing ≤50 ppm monomethyl ether hydroquinone as inhibitor) was purchased from Sigma Aldrich and used after passing it through Inhibitor remover replacement

packing, for removing hydroquinone and monomethyl ether hydroquinone (Sigma-Aldrich). Ethylene glycol dimethacrylate (EGDMA) was used after distillation. Hydroxytyrosol has been purchased from Carbosynth. The fluorophore 2-(4-boronophenyl)quinoline-4-carboxylic acid) has been purchased from Ambeed. The amino acid acetyl-*p*-amino-phenylalanine-O-methyl ester has been purchased from Bachem. EDANS has been purchased from MP Biomedicals. Collidine has been purchased from Fluka. All the amino acids, 2-(1H-Benzotriazole-1-yl)-1,1,3,3-tetramethylaminium tetrafluoroborate (TBTU), 1-hydroxybenzotriazole (HOBT), 1-[Bis(dimethylamino)methylene]-1H-1,2,3-triazolo[4,5-b]pyridinium 3-oxid hexafluorophosphate (HATU), *N*,*N*'-Diisopropylcarbodiimide (DIC), Ethyl cyano(hydroxyimino)acetate (Oxyma) and the MBHA Rink amide resin have been purchased from Iris Biotech GmbH. DMF for peptide synthesis has been purchased from Romil. Protecting groups on lateral side chains of amino acids are: *tert*-butoxycarbonyl (boc), O-*tert*-butyl (O-tbu), 2,2,4,6,7-pentamethyldihydrobenzofuran-5-sulfonyl (Pbf), 4-{*N*-[1-(4,4-dimethyl-2,6-dioxocyclohexylidene)-3-methylbutyl]-amino} benzyl ester (ODmab), trityl (Trt), 4-methyltrityl (Mtt).

All the other solvents and reagents have been purchased from Sigma Aldrich and have been used without further purification.

7.3 SYNTHETIC PROCEDURES

7.3.1 TBA pigment

7.3.1.1 Synthesis and purification of pigment 2

28 mM CGA and *N*α-boc-lysine **1** solutions have been prepared by dissolving 100 mg and 69 mg of CGA and **1** respectively in 10 mL of 0.1 M carbonate buffer, pH 9. The two solutions have been put to react together under stirring and pH has been adjusted to 9 with few drops of a 0.1 M NaOH solution, repeating this operation after 10 and 30 minutes from the beginning of the reaction. Already after the first minutes of reaction a green color started to develop, increasing with time. The mixture has been left to react for 24 hours at room temperature keeping the recipient open.

The reaction mixture has been purified by size exclusion chromatography (SEC) using a Bio-Gel P4 resin with a molecular fractionation range of 800-4000 Da, using distilled water as eluent at a rate of 96 mL/h. After discarding the first mL of colorless liquid, the eluate has been collected into falcon tubes, checking the pH of each one and regulating it to 9 with NaOH 0.1 M, if necessary. To select the purest fractions containing the TBA pigment, the UV-visible spectra of each fraction has been registered, diluting with water if necessary. Fraction **a** and fraction **b** have been taken separately and lyophilized, having a ratio A_{680}/A_{330} lower than 0.3.[1] After lyophilization, 90 mg of dark green solid have been obtained from fraction **a**, 79 mg of blue solid have been obtained from fraction **b**. These fractions have been characterized by HPLC-DAD-MS (peaks reported in Table 7.1). The elution conditions used for purification are reported in Table 7.2.

To determine retention times of CGA byproducts, also a control solution, composed by only 3 mM CGA in carbonate buffer 0.1 M (pH 9) left to react for 36 hours in an open vial, has been analyzed in the same conditions of elution.

*Table 7.1- Retention times and mass signals obtained from HPLC-MS analysis of pigment **2**.*

Sample	Compound	R_t(min)	$[M+H]^+$ (m/z)	$[M-H]^-$ (m/z)
Fraction a	**2**	29.484	928.6	
		30.817	928.6	926.6
		31.461	928.6	926.6
		31.951	928.6	926.8
		32.261	928.8	927.6
Fraction b	**2**	29.506	929.2	927.0
		30.376	929.0	926.8
		30.634	928.8	
		31.890	929.8	
		32.245	929.2	926.8
		32.341	929.0	929.8
		33.453	929.0	927.0
		34.484	928.8	926.6

*Table 7.2-Elution conditions for HPLC-MS analysis of pigment **2***

Time (min)	Flow (mL/min)	% H_2O + 0.1 % formic acid	% CH_3CN + 0.1 % formic acid
0	0.2	97	3
35	0.2	40	60
45	0.2	40	60
50	0.2	97	3

7.3.1.2 P-BSA synthesis

A 75 µM BSA solution has been prepared by dissolving 49.8 mg of BSA in 5 mL of 0.1 M carbonate buffer. A 1.5 mM CGA solution has been prepared by dissolving 10.7 mg of CGA in 10 mL of 0.1 M carbonate buffer. The BSA and CGA solutions have been mixed and, after 30 minutes of reaction, pH has been adjusted to 9 by adding 0.1 M NaOH: the reaction mixture has been left under stirring for 24 hours at room temperature keeping the vessel open. A green solution has been obtained and it has been dialyzed against distilled water using a Spectra Pore membrane with molecular weight cutoff of 12-14 kDa. Water has been changed three times during the first 24 hours. After 36 hours, a pale green solution has been obtained inside the dialysis membrane, with some visible precipitate. The dialyzed material has been lyophilized obtaining 31.9 mg of a pale green solid. An UV-visible spectrum has been registered dissolving 6.0 mg of modified BSA (**P-BSA**) in 1.4 mL of distilled water, filtering the solution with a 0.45 µm PTFE filter to remove undissolved particles.

7.3.2 Boronic acids

7.3.2.1 Synthesis of fluorophore 20

Synthesis of 13

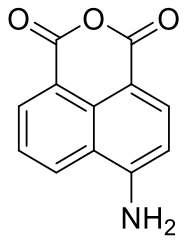

Synthetic procedure has been slightly adapted from a work present in literature.[2]

In a round bottomed flask, 0.5070 g (1.83 mmol) of 4-bromo-1,8-naphthalic anhydride **11** and 0.2202 g (3.39 mmol) of sodium azide have been dissolved in 10 mL of DMF. The flask has been covered with aluminium foil to avoid the presence of light, and the reaction mixture has been heated at 100°C for 1 hour. The solution becomes black with green shades. The reaction mixture has been left to cool at room temperature, then 25 mL of water have been added thus observing precipitation of an ochre solid, which has been isolated by filtration on a Gooch crucible obtaining the azide derivative **12**.

4-azido-1,8-naphthalic anhydride **12** has then been transferred into a new round bottomed flask, and it has been dissolved in 10 mL of ethanol. 0.6993 g (2.67 mmol) of triphenylphosphine have been added, and the mixture has been reacted for 30 minutes at room temperature. Then, 2.9 mL of acetic acid and 3.8 mL of water have been added to the flask, leaving the mixture to react under stirring for 15 more hours. After this time, 35 mL of water have been added, and precipitation of an ochre solid has been observed. The solid has been isolated by filtration on a Gooch crucible, and it has been washed with several mL of water. It has been possible to observe the presence of white triphenylphosphine oxide crystals, which have been removed using a tweezer. After this, the solid has been further washed with 50 mL of a mixture of petroleum ether with 5% of DCM. The solid has been vacuum dried over the pump and in the desiccator. 0.3178 g of 4-amino-1,8-naphthalic anhydride **13** have been obtained, with a yield of 82%.

NMR spectrum has been registered in DMSO-d_6 and it is in accordance with the literature.[3]

^{1}H-NMR (DMSO-d_6): δ (ppm) = 8.69 (d, ^{3}J = 8.4 Hz, 1H), 8.43 (d, ^{3}J = 7.3 Hz, 1H), 8.19 (d, ^{3}J = 8.5 Hz, 1H), 7.78 (s, 2H), 7.69 (t, ^{3}J = 7.9 Hz, 1H), 6.88 (d, ^{3}J = 8.5 Hz, 1H).

Synthesis of 15

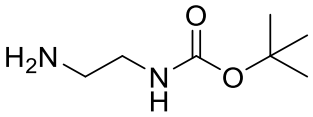

Synthetic procedure has been slightly adapted from literature.[4]

In a round bottomed flask, 4 mL of ethylenediamine **14** (59.73 mmol) have been dissolved in 147 mL of DCM. 2.14 g (9.81 mmol) of di-*tert*-butyl-dicarbonate Boc_2O have been dissolved in 50 mL of DCM, and they have been loaded on a dropping funnel. The system has been cooled in an ice bath at 0°C, and Boc_2O has been added to the ethylenediamine solution dropwise in around 8 hours, keeping the system at 0°C. The formation of a white precipitate could be observed. After finishing addition of Boc_2O, the system has been left under stirring for 17 hours at room temperature. The day after, the mixture has been filtered on paper to remove the white solid, and DCM has been removed from the solution by rotary evaporator. The oily residue has

been dissolved in 126 mL of a 5% sodium carbonate solution, and then the aqueous phase has been extracted with 4 aliquots of DCM. The whole organic phase has been anhydrified over anhydrous sodium sulphate. Then, after filtering the Na_2SO_4, the solvent has been removed by rotary evaporator, obtaining 1.28 g (7.99 mmol) of **15** as an oil, with a yield of 82%.

NMR spectrum has been registered and is in accordance with the literature.[5]

^{1}H-NMR ($CDCl_3$): δ (ppm) = 5.11 (s, 1H), 3.10 (q, ^{3}J = 5.9 Hz, 2H), 2.72 (t, ^{3}J = 5.9 Hz, 2H), 1.37 (s, 9H), 1.33 (s, 2H).

Synthesis of 16

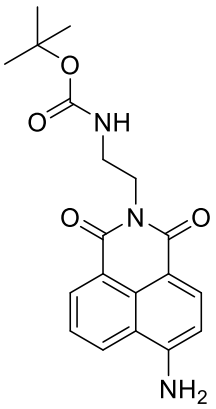

The synthetic procedure has been taken from literature.[6]

In a round bottomed flask, 0.336 g (1.58 mmol) of **13** and 0.473 g (2.95 mmol) of **15** have been dissolved in 10 mL of DMF. A dark green solution has been obtained, and it has been reacted at 90°C under stirring for 6 hours. Then, the flask has been left to cool and, after reaching room temperature, it has been put in an ice bath. After 15 minutes, 50 mL of water have been added, thus observing the precipitation of an orange solid, which has been isolated by filtration over a Gooch crucible and has then been left to dry. 0.498 g (1.41 mmol) of compound **16** have been obtained as an orange solid, with a yield of 89%.

Compound has been analyzed by NMR, and data obtained are in accordance with the literature.[6]

^{1}H-NMR (DMSO-d_6): δ (ppm) = 8.59 (d, ^{3}J = 8.5 Hz, 1H), 8.41 (d, ^{3}J = 7.2 Hz, 1H), 8.18 (d, ^{3}J = 8.3 Hz, 1H), 7.64 (t, ^{3}J = 7.8 Hz, 1H), 7.38 (s, 2H), 6.83 (d, ^{3}J = 8.3 Hz, 2H), 4.08 (t, ^{3}J = 6.2 Hz, 2H), 3.21 (q, ^{3}J = 6.2 Hz, 2H), 1.26 (s, 9H).

Synthesis of 18

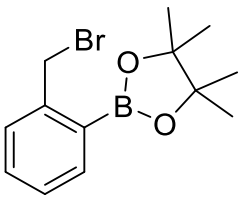

The synthesis has been adapted from that for a different compound.[7]

0.411 g of 2-bromomethyl phenylboronic acid **17** and 0.221 g (1.87 mmol) of pinacol have been placed inside a round bottom flask, and they have been dissolved in 20 mL of a 50:50 mixture of anhydrous THF and toluene (THF has been previously distilled over sodium/benzophenone ketyle). The reaction mixture has been left to react for 20 minutes under stirring at room temperature, then the solvent has been removed by rotary evaporator. The residue has been redissolved in 20 mL of the THF/toluene mixture, and after 15 minutes of

reaction, solvent has been removed one more time with rotary evaporator, repeating the same operation of adding solvent and then evaporating it 2 more times. After completing the last evaporation, 0.552 g (1.86 mmol) of **18** have been obtained, with a yield of 99%.

NMR spectrum has been registered and it is in accordance with the literature.[8]

^{1}H-NMR ($CDCl_3$): δ (ppm) = 7.82 (d, ^{3}J = 7.7 Hz, 1H), 7.43 – 7.36 (m, 2H), 7.31 – 7.27 (m, 1H), 4.92 (s, 2H), 1.37 (s, 12H).

Synthesis of 19

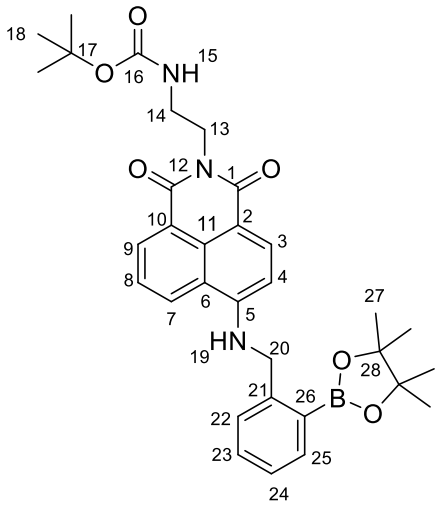

The synthesis has been adapted from literature.[9]

0.3121 g (0.88 mmol) of **16** have been dissolved with 10 mL of anhydrous DMF in a 3-necks round bottomed flask, creating an inert system under a flux of argon that has been maintained for all the reaction. 0.0793 g of NaH in a mineral oil dispersion (1.98 mmol considering it is a 60% dispersion) have been washed with hexane, and then they have been inserted into the reaction vessel. The mixture passes from a green color to a dark red one, due to formation of the anion on the aromatic amine of **16**. After 20 minutes of reaction, 0.348 g (1.17 mmol) of **18** dissolved in 10 mL of DMF have started to be added, drop by drop, over 4 hours of reaction, always under a flux of argon. At a certain point reaction mixture returns green. After finishing addition, reaction has been continued for 1 more hour, then the reaction has been quenched by adding 5% citric acid (100 mL): precipitation of an orange solid has been observed. The solid has been filtered over a Gooch crucible, it has been extensively washed with water and it has been dried under vacuum in a desiccator. 0.3909 g of pure **19** compound have been obtained, with a yield of 77%.

Characterization of compound **19** has been done by ^{1}H and ^{13}C- NMR spectroscopy and mass spectrometry. Assignments of ^{1}H and ^{13}C signals has been done by ^{1}H-^{1}H COSY, ^{1}H-^{13}C HSQC and ^{1}H-^{13}C HMBC spectra.

^{1}H NMR (DMSO-d_6): δ (ppm) = 8.74 (d, ^{3}J = 8.4 Hz, 1H, H-7), 8.44 (d, ^{3}J = 7.3 Hz, 1H, H-9), 8.27 (t, ^{3}J = 5.9 Hz, 1H, H-19), 8.17 (d, ^{3}J = 8.5 Hz, 1H, H-3), 7.75 (dd, ^{3}J = 7.4 Hz, ^{4}J= 1.5 Hz, 1H, H-25), 7.70 (dd, ^{3}J = 8.4, 7.3 Hz, 1H, H-8), 7.45 – 7.36 (m, 1H, H-23), 7.33 (d, ^{3}J = 7.6 Hz, 1H, H-22), 7.27 (td, ^{3}J = 7.3 Hz, ^{4}J=1.3 Hz, 1H, H-24), 6.82 (t, ^{3}J = 6.1 Hz, 1H, H-15), 6.65 (d, ^{3}J = 8.5 Hz, 1H, H-4), 4.87 (d, ^{3}J = 5.5 Hz, 2H, H-20), 4.08 (t, ^{3}J = 6.0 Hz, 2H, H-13), 3.21 (q, ^{3}J = 6.1 Hz, 2H, H-14), 1.30 (s, 12H, H-28), 1.24 (s, 9H, H-18).

^{13}C NMR (DMSO-d_6): δ (ppm) = 163.97 (C-12), 163.11 (C-1), 155.66 (C-16), 150.45 (C-5), 144.32 (C-21), 135.95 (C-25), 133.88 (C-3), 131.28 (C-23), 130.56 (C-9), 129.54 (C-11), 128.31 (C-7), 126.46 (C-22 or C-24), 126.36 (C-22 or C-24), 124.37 (C-8), 122.23 (C-10), 120.19 (C-6), 108.40 (C-2), 104.29 (C-4), 83.68 (C-27), 77.39 (C-17), 45.86 (C-20), 38.00 (C-14), 28.11 (C-18), 24.66 (C-28).

ESI mass (m/z) = 572.5 $[M+H]^+$ (calculated 572.3), 594.4 $[M+Na]^+$ (calculated 594.3)

Synthesis of 23

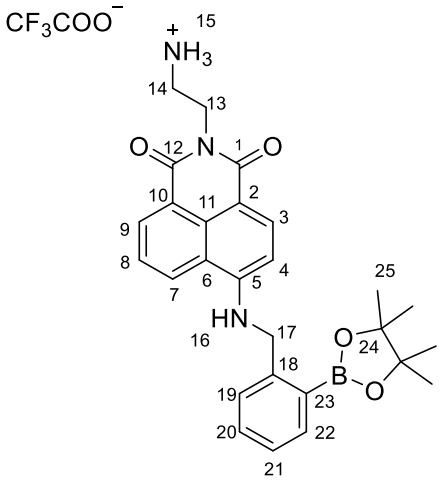

0.1312 g of compound **19** have been dissolved in 10 mL of a 50:50 mixture of TFA and DCM, and it has been left under stirring for 3 hours at room temperature. Then, solvent has been removed by rotary evaporator, and multiple aliquots of DCM have been added to the round bottom flask and then evaporated by rotary evaporator to allow complete removal of TFA and evaporation of boc-deprotection byproducts. 0.1135 g of amino-deprotected **23** have been obtained as a brilliant orange solid, with a yield of 98%.

^{1}H NMR (DMSO-d_6): δ (ppm) = 8.80 (d, ^{3}J = 8.4 Hz, 1H, H-7), 8.48 (d, ^{3}J = 7.3 Hz, 1H, H-9), 8.38 (t, J = 5.9 Hz, 1H, H-16), 8.21 (d, ^{3}J = 8.6 Hz, 1H, H-3), 7.75 (m, 5H, H-8, H-15, H-22), 7.50 – 7.20 (m, 3H, H-19+H-20+H-21), 6.68 (d, ^{3}J = 8.6 Hz, 1H, H-4), 4.89 (d, ^{3}J = 5.6 Hz, 2H, H-17), 4.27 (t, ^{3}J = 6.0 Hz, 2H, H-13), 3.11 (m, 2H, H-14), 1.32 (d, J = 8.2 Hz, 12H, H-25).

Synthesis of 20

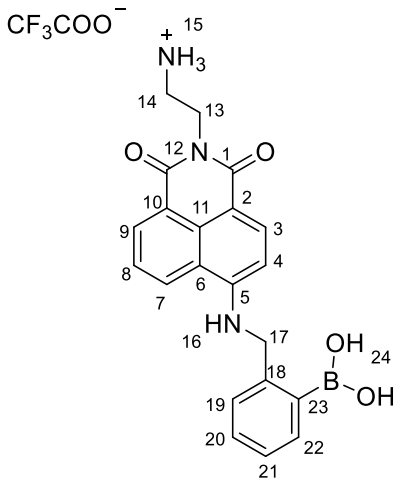

0.1272 g (0.22 mmol) of **19** and 0.1335 g (2.23 mmol) of methylboronic acid have been transferred into a round bottom flask and they have been dissolved in 20 mL of 5% TFA in DCM. The flask has been left under stirring 4 days at room temperature. The solvent has then been evaporated under reduced pressure, thus obtaining 0.083 g of **20** completely deprotected as an orange solid with a yield of 97%.

The compound has been characterized by ^{1}H and ^{13}C-NMR, and assignment of the signals has been done by bidimensional ^{1}H-^{1}H COSY, ^{1}H-^{13}C HSQC and ^{1}H-^{13}C HMBC NMR spectra.

^{1}H NMR (DMSO-d_6): δ ppm = 8.78 (d, ^{3}J= 8.4 Hz, 1H, H-7), 8.48 (d, ^{3}J = 7.3 Hz, 1H, H-9), 8.41 (t, ^{3}J = 6.0 Hz, 1H, H-16), 8.32 (s, 2H, H-24), 8.18 (d, ^{3}J = 8.5 Hz, 1H, H-3), 7.83 – 7.69 (m, 4H, H-8 + H-15), 7.60 (d, ^{3}J = 7.1 Hz, 1H, H-22), 7.28 – 7.16 (m, 3H, H-19 + H-20 + H-21), 6.64 (d, ^{3}J = 8.5 Hz, 1H, H-4), 4.84 (d, ^{3}J = 5.8 Hz, 2H, H-17), 4.27 (t, ^{3}J = 5.9 Hz, 2H, H-13), 3.11 (s, 3H,m, H-14).

^{13}C NMR (DMSO-d_6): δ (ppm) = 164.50 (C-12), 163.48 (C-1), 150.81 (C-5), 141.95 (C-18), 134.15 (C-3 or C-22), 134.03 (C-3 or C-22), 130.81 (C-9), 129.71 (C-11), 129.15 (C-20), 128.73 (C-7), 126.01 (C-21), 125.51 (C-19), 124.54 (C-8), 122.14 (C-10), 120.31 (C-6), 108.04 (C-2), 104.60 (C-4), 46.32 (C-17), 37.92 (C-14), 37.18 (C-13).

ESI (m/z) = 390.0 $[M+H]^{+}$ (calculated 390.2)

7.3.3 Diazo-coupling reaction

7.3.3.1 Diazo-coupling compound 26

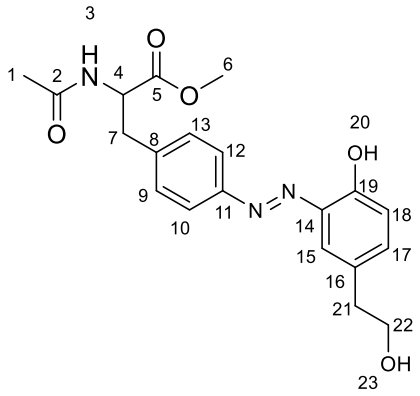

Reaction conditions have been adapted from literature.[10]
15 mg of acetyl-*p*-amino-phenylalanine-methyl ester **24** (0.063 mmol) have been dissolved in 2 mL of 0.1 M HCl. The solution has been cooled to 0°C in an ice bath. 5.2 mg (0.075 mmol) of sodium nitrite have been dissolved in 0.4 mL of distilled water and the solution has been added dropwise to **24**, then leaving the solution to react for 15 minutes at 0°C to allow formation of the diazonium salt. In the meantime, a tyrosol TY solution has been prepared dissolving 26.3 mg (0.190 mmol) of TY in 2 mL of sodium carbonate 0.1M, pH 9 (so the ratio between **24** and TY is 1:3). The tyrosol solution has been added to the diazonium salt solution dropwise: a red precipitate forms immediately. The reaction mixture has been left to react for 30 minutes at 0°C, and for one more hour at room temperature. The solid has been recovered by filtration on a Gooch crucible, washing the filtrate with water and then letting it dry in a desiccator for one night.
23.2 mg of compound **26** have been obtained as a red solid, with a yield of 97%.
The compound has been characterized by ^{1}H and ^{13}C-NMR, and assignment of the signals has been done by bidimensional ^{1}H-^{1}H COSY, ^{1}H-^{13}C HSQC and ^{1}H-^{13}C HMBC NMR spectra.

^{1}H NMR (DMSO-d_6): δ (ppm) = 11.01 (s, 1H, H-20), 8.40 (d, ^{3}J = 7.9 Hz, 1H, H-3), 7.89 (d, ^{3}J = 8.0 Hz, 2H, H-10 + H-12), 7.59 (d, ^{4}J = 2.3 Hz, 1H, H-15), 7.42 (d, ^{3}J = 8.0 Hz, 2H, H-9 + H-13), 7.27 (dd, ^{3}J = 8.5 Hz, ^{4}J = 2.3 Hz, 1H, H-17), 6.97 (d, ^{3}J = 8.5 Hz, 1H, H-18), 4.64 (t, ^{3}J = 5.2 Hz, 1H, H-23), 4.53 (m, 1H, H-4), 3.62 (s, br, 5H, H-6 + H-22), 3.12 (dd, ^{2}J = 13.8 Hz, ^{3}J= 5.6 Hz, 1H, H-7), 2.97 (dd, ^{2}J = 13.8 Hz, ^{3}J =9.4 Hz, 1H, H-7'), 2.71 (t, ^{3}J = 6.8 Hz, 2H, H-21), 1.80 (s, 3H, H-1).

^{13}C NMR (DMSO-d_6): δ (ppm) = 172.05 (C-5), 169.42 (C-2), 152.63 (C-19), 150.20 (C-11), 140.91 (C-8), 137.88 (C-14), 134.31 (C-17), 131.06 (C-16), 130.14 (C-9 + C-13), 123.36 (C-15), 122.47 (C-10 + C-12), 117.85 (C-18), 62.10 (C-22), 53.35 (C-4), 51.93 (C-6), 37.90 (C-21), 36.58 (C-7), 22.26 (C-1).

ESI mass (m/z)= 386.2 $[M+H]^+$ (calculated 386.2), 408.2 $[M+Na]^+$ (calculated 408.2), 424.1 $[M+K]^+$(calculated 424.2)

UV-visible spectra of 50µM solutions of **26** have been registered in water and DMF.

7.3.3.2 Diaza-dienes

Synthetic procedures for 1,2-diaza-2,3-dienes **29a-c** and **31a-c** and for diazo-compound **29d** can be found in the published article.[11]

7.4 PEPTIDES SYNTHESIS

7.4.1 General procedure

Peptides have been synthesized in solid phase with an automatic microwave synthesizer. The usual FMOC (Fluorenylmethyloxycarbonyl) approach has been adopted, having the amino acids protected at the amino terminal with FMOC (FMOC-AA-OH) and reactive lateral side chains protected with acid-labile groups, using Rink MBHA resin, with a loading of 0.56 mmol/g.

Swelling of the resin has been performed in DMF at 70°C for 20 minutes. Then, following steps have been deprotection of the amino groups on the resin, initially FMOC-protected, washing to remove side products, double coupling with amino acid and washing steps, according to procedure reported Table 7.3. The same procedure has been adopted for all amino acids until the amino terminal.

Table 7.3 – General conditions for peptides synthesis

Operation	Conditions	Time	Temperature (°C)
FMOC deprotection	Piperidine 20% in NMP	1) 3 min 2) 5 min	50
Washing (x6)	DMF	3 min	R.t.
Double coupling (3 eq)	FMOC-AA-OH 0.2 M; i. DIC-OXYMA; ii: TBTU 0.2M; HOBT 0.2 M; DIEA 0.2 M (in NMP)	1) 7.5 min 2) 7.5 min	70
Washing (x4)	DMF	3 min	R.t.

When necessary, coupling with fluorescent moieties has been performed according to conditions specified in the corresponding paragraph.

Before performing deprotection of lateral side chains and cleavage of the peptide, the resin has been dried to completely remove DMF, performing multiple washing steps in DCM. Finally, the resin has been treated with a mixture of 95% TFA with 2.5% TIS and 2.5% water for three hours. Then, the liquid phase containing the cleaved peptide has been filtered away from the resin, which has been further washed with TFA. TFA has been removed under a flux of nitrogen, and after obtaining a semi-solid residual, peptides have been precipitated by adding *t*-butyl methyl ether or diethyl ether, keeping them overnight at -20°C. Precipitated peptides have then been centrifuged (10 min, 5000 rpm), and after removing the surnatant, they have been dried overnight in the desiccator.

Purification has been performed by preparative HPLC using a gradient of water and acetonitrile containing 0.05% of TFA as reported in dedicated paragraphs.

7.4.2 TBA pigment

7.4.2.1 Peptides P1 and P2

Amino acids used for **P1** and **P2** synthesis are:

- FMOC-Phe-OH
- FMOC-Ala-OH
- FMOC-Pro-OH
- FMOC-Lys(boc)-OH
- FMOC-Ser(Otbu)-OH
- FMOC-Glu(Otbu)-OH

In this case, instead of using OXYMA-DIC for the first coupling as indicated in Table 7.3 at paragraph 7.4.1, TBTU/HOBT/DIPEA have been used twice.

After deprotection of the amino terminal residue, acetylation of the *N*-terminal amino group has been performed with 10 equivalents of acetic anhydride in the presence of DIEA as a base.
To remove volatile impurities possibly present and obtain more soluble products for HPLC purification, the crude peptides have been dissolved in a mixture of water: acetonitrile in a 10:1 ratio and they have been lyophilized. Purification has been performed by preparative HPLC using a gradient of water and acetonitrile containing 0.05% of TFA as reported in Table 7.4. After collecting fractions corresponding to the major peak for each peptide, acetonitrile and TFA have been removed by rotary evaporation and water has been removed by lyophilization, obtaining 18.9 mg of purified peptide **P1** and 23.8 mg of purified peptide **P2**.

*Table 7.4 – Elution conditions for purification of peptides **P1** and **P2** by preparative HPLC*

Time (min)	Flow (mL/min)	% H_2O + 0.05% TFA	% CH_3CN+ 0.05% TFA
0	5.0	85	15
2	"	85	15
12	"	65	45
13.5	"	10	90
16.5	"	10	90
18	"	85	15

Both peptides have been characterized by mass spectrometry.
ESI mass **P1** (m/z) = 1034.7 $[M+H]^+$(calculated 1034.5), 1072.6 $[M+K]^+$(calculated 1072.5)
ESI mass **P2** (m/z) = 1054.6 $[M-H]^-$ (calculated 1054.5), 1056.6 $[M+H]^+$ (calculated 1056.5)
Both peptides have also been characterized by ^{1}H-NMR, ^{1}H-^{1}H-COSY and ^{1}H-^{1}H-TOCSY NMR spectroscopy, registering spectra in water + 10% D_2O, suppressing the water peak (assignments can be found in tables 3.1 and 3.2, paragraph 3.3.2).

7.4.3 Boronic acids

7.4.3.1 Peptide P3

Amino acids used are:

- Fmoc-(D)Pro-OH
- Fmoc-Pro-OH
- Fmoc-Trp(Boc)-OH

Swelling and synthesis have been performed as indicated at paragraph 7.4.1
After deprotection of the amino terminal residue, coupling with succinic anhydride and fluorophore **20** has been performed operating manually on the resin (Table 7.5).

*Table 7.5 – Coupling conditions of peptide **P3** to fluorophore **20***

Operation	Conditions	Time
FMOC deprotection	Piperidine 20% in NMP	1) 3 min 2) 10 min
Washing (x3)	DMF	
Coupling with succinic anhydride	Succinic anhydride 5 eq; DIPEA 5 eq.	30 min
Double coupling with **20**	**20** 1.5 eq; HATU 1.5 eq; HOBT 1.5 eq; collidine 3 eq.	1) 24 h 2) 24 h
washing (x3)	DMF; DCM; diethyl ether	

Then, cleavage from the resin has been performed as explained in the general procedure at paragraph 7.4.1 Purification has been carried out by preparative HPLC, dissolving the peptide in a mixture water: acetonitrile in a ratio 70:30, using a gradient of water and acetonitrile containing 0.05% of TFA as reported in Table 7.6 .

*Table 7.6 - Elution conditions for purification of peptide **P3** by preparative HPLC*

Time (min)	Flow (mL/min)	% H_2O + 0.05 % TFA	% CH_3CN + 0.05 % TFA
0	5.0	95	5
2	5.0	95	5
16	5.0	10	90
20	5.0	10	90
25	5.0	95	5

After collecting fractions acetonitrile has been removed by rotary evaporation and water has been removed by lyophilization.

Peptide **P3** has been characterized by mass spectrometry.

ESI mass **P3** (m/z) = 869.4 $[M+H]^+$ (calculated 369.4), 891.4 $[M+Na]^+$ (calculated 891.4), 907.4 $[M+K]^+$ (calculated 907.3).

P3 has also been characterized by ^1H-, ^1H-^1H-COSY and TOCSY NMR spectroscopy, registering spectra in DMSO-d_6 (assignments can be found in section 4.4.1.1 of the discussion part).

7.4.3.2 Peptides P4 and P5

Amino acids used are:

- Fmoc-Arg-OH
- Fmoc-Gly-OH
- Fmoc-Glu(ODmab)-OH
- Fmoc-(D)-Pro-OH
- Fmoc-Pro-OH
- Fmoc-Ala-OH
- Fmoc-His(Trt)-OH
- Fmoc-Glu(tBu)-OH

Procedure for peptide synthesis is the same reported in the general procedure at paragraph 7.4.1.
The procedure has been repeated until the amino terminal residue (Arg), whose amino terminal group has been acetylated with 10 equivalents of acetic anhydride and a catalytic quantity of DIEA. Then, the internal glutamic acid residue has been deprotected from Dmab by adding to 60 mg of functionalized resin 3 mL of a

2% v/v solution of hydrazine in DMF (prepared from a hydrazine hydrate solution approximatively 80%), shaking manually for 3 minutes and then filtering the liquid which has been collected in a vial. The operation has been repeated 5 more times. Then, the 6 collected solutions have been analyzed by UV-Visible spectroscopy, by registering spectra between 200 and 500 nm, to monitor the absorbance at 290 nm of the Dmab iVde deprotection byproduct. A progressive decrease of the absorption at 290 nm has been observed, meaning that Dmab deprotection takes place already after the first additions of hydrazine. Then, to complete Dmab deprotection removing the *p*-amino benzyl ester, 3 mL of a 5 mM NaOH solution in H_2O/MeOH 1:1 v/v have been added. After 3 hours of reaction, the liquid phase has been removed and the resin has been washed with 3 mL of MeOH (5x), 3 mL of DMF (5x), 3 mL of DCM (5x), 3 mL of DMF (5x).[12]
Functionalization with fluorophore **23** has been performed with 1.5 eq of **23**, 1.5 eq of HATU, 1.5 eq of HOBT, 3 eq of collidine in 1.5 mL of NMP, reacting them 24 hours at room temperature, repeating the procedure one more time. After the second coupling, the liquid has been removed and resin has been washed with 3 mL of DMF (5x), 3 mL of DCM (5 x), 3 mL of diethyl ether (5x). The resin has been vacuum-dried.
Then, deprotection of the boronic acid moiety has been performed by adding 10 eq of methylboronic acid in 1.5 mL of 5% TFA in DCM, reacting the system for 4 days at room temperature. Since part of the peptide might have been cleaved from the resin in the acidic conditions used for deprotecting the boronic acid, the liquid phase (fraction I) has been collected from the resin, it has been dried under a flux of argon, and cold diethyl ether has been added, thus obtaining an orange precipitate. After few hours in the freezer, the sample has been centrifuged (10 minutes, 5000 rpm) and after removing the surnatant, the residual has been dried under vacuum.
In the meantime, the resin has been deprotected by adding 1 mL of 95% TFA with 2.5% TIS and 2.5% water. After 3 hours under stirring, the liquid has been removed from the resin and, after further washing of the resin with TFA, the filtered liquid (fraction II) has been evaporated under a flux of argon, and it has been precipitated and treated as explained for fraction I.
The two peptides **P4** and **P5** have been analyzed by HPLC-MS, dissolving the samples in 30% acetonitrile (+0.1% formic acid) and 70% water (+ 0.1% formic acid), filtering the solutions through 0.2 µm filters before injection. The elution gradient is reported in Table 7.7.

*Table 7.7 – Elution conditions for HPLC-MS analysis of peptides **P4** and **P5***

Time (min)	Flow (mL/min)	% H_2O + 0.1% formic acid	% CH_3CN + 0.1% formic acid
0	0.2	85	15
4	0.2	85	15
15	0.2	10	90
20	0.2	10	90
30	0.2	85	15

Then, peptides have been purified by preparative HPLC, using the gradient of water and acetonitrile (+ 0.05% TFA) reported in Table 7.8 for **P4**, in Table 7.9 for **P5**. Samples have been dissolved in 30% acetonitrile (+0.05% TFA) and 70% water (+ 0.05% TFA), filtering the solutions through 0.2 µm filters before injection.

*Table 7.8 Elution conditions for purification of peptide **P4** by preparative HPLC.*

Time (min)	Flow (mL/min)	% H_2O + 0.05% TFA	% CH_3CN + 0.05% TFA
0	5	80	20
2	5	80	20
16	5	40	60
20	5	10	90
25	5	10	90
30	5	80	20

*Table 7.9 Elution conditions for purification of peptide **P5** by preparative HPLC.*

Time (min)	Flow (mL/min)	% H_2O + 0.05% TFA	% CH_3CN + 0.05% TFA
0	5	95	5
2	5	95	5
16	5	10	90
20	5	10	90
25	5	95	5

After collecting the fractions of interest, showing the characteristic absorbance at 490 nm of the fluorophore, they have been lyophilized.
Both peptides have been characterized by mass spectrometry.
ESI mass **P4** (m/z) = 830.5 $[M+H]^+$ (calculated 830.4).
ESI mass **P5** (m/z) = 1304.62 $[M+H]^+$ (calculated 1304.60), 652.79 $[M+2H]^{2+}$ (calculated 652.80). Cyclization derivative of **P5** (m/z) = 1286.62 $[M+H]^+$ (calculated 1286.59), 643.81 $[M+2H]^{2+}$(calculated 643.80).
Peptide **P4** has been characterized also by ^1H-, ^1H-^1H- COSY and ^1H-^1H- TOCSY NMR spectra in water + 10% D_2O, suppressing the water peak (assignments can be found in section 4.4.2.2 and table 4.8 of the discussion part).

7.4.4 Diazo coupling reaction

7.4.4.1 Peptide P6

Amino acids used are:

- Fmoc-Phe(NHBoc)-OH
- Fmoc-(D)-Pro-OH
- Fmoc-(L)-Pro-OH
- Fmoc-Lys(Mtt)-OH

Swelling of the resin and coupling has been performed as described at paragraph 7.4.1. At the end of the coupling procedure, the peptide has been acetylated using 10 equivalents of acetic anhydride and DIEA. Then, the resin has been extensively washed with DCM and diethyl ether to remove DMF and dry it. Functionalization with FITC has been achieved by first deprotecting the MTT group from lysine using 1 mL of a mixture of 1% TFA, 3% of TIS and 96% of DCM for 2 days. To be sure of effective removal of the MTT protecting group, the Kaiser test has been performed on a little aliquot of resin, to check if there are some free amines. After confirming the deprotection of MTT thanks to the purple coloration of the Kaiser test, coupling with FITC has been performed by reacting peptide on the resin with 2 equivalents of FITC and 3 equivalents of DIEA.
Finally, cleavage from the resin has been performed as described at paragraph 7.4.1.
Purification has been performed by preparative HPLC, dissolving the peptide in a mixture water: acetonitrile in a ratio 90:10, using a gradient of water and acetonitrile containing 0.05% of TFA as reported in Table 7.10.

*Table 7.10- Elution conditions for purification of **P6** by preparative HPLC*

Time (min)	Flow (mL/min)	% H_2O + 0.05% TFA	% CH_3CN+ 0.05% TFA
0	5.0	90	10
2	"	90	10
12	"	50	50
14	"	10	90
18	"	10	90
20	"	90	10

After collecting fractions acetonitrile has been removed by rotary evaporation and water has been removed by lyophilization. **P6** has been characterized by mass spectrometry.
ESI mass **P6** (m/z) = 467.18 $[M+2H]^{2+}$ (calculated 467.18 m/z), 933.36 $[M+H]^+$ (calculated 933.36), 955.34 $[M+Na]^+$ (calculated 955.34).

7.4.4.2 Peptide P7

- Amino acids used are:
- Fmoc-Phe(NHBoc)-OH
- Fmoc-(D)-Pro-OH
- Fmoc-(L)-Pro-OH
- Fmoc-Ala-OH
- Fmoc-Glu(tbu)-OH
- Fmoc-His(Trt)-OH.

Synthesis of the peptide has been done as described at paragraph 7.4.1 After coupling the *N*-terminal amino acid D-proline, coupling with succinic anhydride has been performed to obtain a free carboxylic group for coupling with the amino group of EDANS. Then, coupling with EDANS has been performed using a procedure taken from the literature[13] by dissolving EDANS (4 eq) in the minimum possible volume of DMSO with DIEA (4 eq) and then adding it to the resin. An equal volume of NMP has then been added together with HBTU (2 eq) and HOBT (2 eq) and the mixture has been reacted for 24 hours. The coupling with EDANS has been performed twice. After extensive washing of the resin, cleavage of the peptide has been performed as explained at paragraph 7.4.1.
Purification has been performed by preparative HPLC, dissolving the peptide in a mixture water: acetonitrile in a ratio 90:10, using a gradient of water and acetonitrile containing 0.05% of TFA as reported in Table 7.11.

*Table 7.11 Elution conditions for purification of **P7** by preparative HPLC*

Time (min)	Flow (mL/min)	% H_2O + 0.05% TFA	% CH_3CN+ 0.05% TFA
0	5.0	95	5
2	"	95	5
16	"	10	90
20	"	10	90
25	"	95	5

After collecting fractions acetonitrile has been removed by rotary evaporation and water has been removed by lyophilization. **P7** has been characterized by mass spectrometry.
ESI mass **P7** (m/z) = 1059.8 $[M+H]^+$ (calculated 1059.4 m/z), 1081.6 $[M+Na]^+$ (calculated 1081.4 m/z) , 1097.6 $[M+K]^+$ (calculated 1097.4 m/z).
Peptide **P7** has been characterized also by ^1H, ^1H-^1H COSY and ^1H-^1H TOCSY NMR spectra in water + 10% D_2O, suppressing water peak (partial assignments are reported at paragraph 5.1).

7.5 FABRICATION OF POLYMERIC DISCS

All the membranes have been prepared using a mold formed by two glass slides 10 × 10 cm (previously treated with dichlorodimethyl silane), held together with metal clips and separated by a 0.5-mm-thick silicon spacer (around 1-cm-wide). If not otherwise stated, polymeric discs used have been cut with a 5 mm diameter puncher.

7.5.1 Silanization procedure of glass slides

The surface of the glass slides used to prepare polymers has been painted with dichlorodimethyl silane in order to make them hydrophobic and make it easier to detach membranes after synthesis. At first, one face of the glass slide has been painted with the silane. After drying for 15-20 minutes under the hood at room temperature, the other side of the glass slide has been painted with the silane, and it has been left to dry for other 15-20 minutes. Then, silanized glass sides have been extensively washed with acetone, water, a detergent solution and water again, with the help of a sponge to eliminate the excess of silane. Then, the glass slides have been put to dry in the oven at around 70°C.

7.5.2 Synthesis of the polymers (general procedure)

The procedure has been adapted from the work of Alvarez-Rivera and colleagues.[14]

The amino monomer (APMA or AEM) has been first dissolved in anhydrous DMSO. In another vial, AIBN has been dissolved in EGDMA and a portion of the HEMA monomer, and it has then been added to the amino-monomer mixture; the remaining volume of HEMA has been also added. After vortexing the mixture, it has been flushed with nitrogen for 5 minutes, it has then been inserted with a syringe into the mold formed by two silanized glass slides 10 × 10 cm, held together with metal clips and separated by a 0.5-mm-thick silicone spacer (around 1-cm-wide), and it has been put to polymerize in the oven at 70°C for 24 hours.
After finishing polymerization, the polymer has been removed from the glass slides and it has been submerged for 15 minutes in hot water for washing away all residual monomers. Then, the polymeric film has been cut into discs with a metal puncher.

In the case of the composition taken from Alvarez-Rivera,[14] no anhydrous DMSO has been used.

When dried membranes have been used, dry discs have been obtained from the wet ones (preserved in distilled water) by placing them in a vacuum oven at room temperature until complete removal of water.
Compositions of the synthesized APMA polymers are reported in Table 7.12, those of AEM polymers in Table 7.13 (molar concentrations are calculated only with respect to APMA, not considering DMSO and EGDMA volumes).

*Table 7.12 Composition of APMA polymers **Mp1**, **Mp2**, **Mp3**, **Mp4**, **Mp5**, **Mp6** and **Mp7**.*

Polymer	HEMA (mL)	DMSO (mL)	APMA* (mg/mM)	EGDMA* (µL/mM)	AIBN* (mg/mM)
Alvarez-Rivera[14]	3	/	42.8/80	45.2	5.24/11
Mp1	1.5	0.250	63.39/236	23/81.3	4.27/17
Mp2	1.5	0.500	216.6/808	23/81.3	4.3/17
Mp3	0.750	0.375	53.7/401	11.3/79.9	2.39/19.4
Mp4	1.0	0.167	42.8/240	150.7/799	4.85/29.5
Mp5	1.0	0.333	143.4/803	150.7/799	5/30.5
Mp6	0.750	0.375	53.87/402	56.5/399	2.3/18.7
Mp7	0.750	0.375	107.28/801	33.9/240	2.55/20.7

***** All the concentration values are calculated with respect to HEMA volume only.

*Table 7.13- Composition of membranes **Me1**, **Me2**, **Me3**.*

Membrane	HEMA (mL)	DMSO (mL)	AEM (mg/mM)*	EGDMA (µL/mM)*	AIBN (mg/mM)*
Me1	1.5	0.250	59.37/237	23/80.1	4.41/17.6
Me2	1.5	0.750	98.85/394	23/78.7	3.5/14.0
Me3	1.5	0.750	98.84/394	67.8/236	3.39/13.6

***** All the concentration values are calculated with respect to HEMA volume only.

7.6 SPECTROPHOTOMETRIC MEASUREMENTS

7.6.1 TBA pigment

7.6.1.1 Pigment 2

Spectrophotometric study of pigment 2 formation in kinetic mode

The kinetics of reaction between CGA and *N*α-boc-lysine **1** over the first 24 hours of reaction has been studied by dissolving 6.2 mg of of CGA (0.0175 mmol) and 41.0 mg of **1** (0.166mmol) in 10 mL of carbonate buffer 175 mM, thus obtaining CGA and **1** concentrations of 1.75 mM and 17 mM respectively. Kinetics of reaction has been measured inserting 2 mL of the solution in the cuvette an taking a point every 20 minutes for the first 24 hours of reaction.

Then, kinetics of reaction during the first 3 hours of reaction at the same concentrations has been measured by preparing a 10.4 mM CGA mother solution (3.7 mg of CGA in 1 mL) and a 74.7 mM **1** mother solution (9.2 mg in 0.5 mL). Then, after registering the blank with a 175 mM carbonate buffer solution (pH 9), reagents have been mixed according to Table 7.14 directly in the cuvette. The concentrated buffer has been added last, and the kinetics has been registered taking a point every 60 seconds for 3 hours.

*Table 7.14- Spectrophotometric study of **2** formation in kinetic mode*

Reagent	[mother solution]	Volume from mother solution	Final concentration
CGA	10.4 mM	335 µL	1.75 mM
1	74.7 mM	468 µL	17.5 mM
Buffer	1 M	350 µL	175 mM
Water		846 µL	

Kinetic study of pigment 2 formation in excess of CGA

A 56 mM CGA mother solution has been prepared by dissolving 29.6 mg of CGA in 3.0 mL of distilled water. A 15 mM **1** solution has been prepared dissolving 3.7 mg of compound into 1 mL of distilled water. Three kinetic studies have been conducted, adding directly in the cuvette aliquots from the two mother solutions, 1 M carbonate buffer and water (Table 7.15). CGA and buffer concentrations have been kept constant, while changing that of **1** by adding different amounts from its mother solution, adding variable amounts of water to reach a 2 mL volume. Buffer has been the last component to be added because it starts the reaction. Absorbances at 680 nm have been measured for 960 s, taking a point every 60 seconds.

*Table 7.15- Solutions for the spectrophotometric study of **2** formation in excess of CGA*

Solution	Mother CGA vol. (µL)	Mother 1 vol. (µL)	Water vol. (µL)	Buffer vol. (µL)	[CGA] (mol/L)	[1] (mol/L)
1	1260	130	260	350	$1.8 \cdot 10^{-2}$	$1.0 \cdot 10^{-3}$
2	"	70	330	"	"	$5.0 \cdot 10^{-4}$
3	"	30	360	"	"	$2.5 \cdot 10^{-4}$

Buffer effect - carbonate

A 4.06 mM CGA mother solution has been prepared by dissolving 14.4 mg of CGA in 10 mL of distilled water. A 138 mM **1** mother solution has been prepared by dissolving 34.1 mg of **1** in 1 mL of distilled water. Three reactions have been conducted: for each one, aliquots of mother solutions, 1 M carbonate buffer (pH 9) and water have been added directly in the cuvette, so that **1** and CGA concentrations remain constant, while changing carbonate buffer concentration, adding variable amounts from the 1 M solution, keeping constant

the volume of reaction at 1 mL by adding different aliquots of water (Table 7.16). The buffer has been the last component to be added to the reaction mixture because it starts **2** formation reaction. Immediately after buffer addition, the kinetics of each reaction has been measured by monitoring absorbance at 680 nm for 1200 s, taking a point every 60 seconds.

*Table 7.16- Solutions for spectrophotometric study of **2** formation at different carbonate buffer concentrations.*

Solution	Mother CGA Vol. (µL)	Mother 1 Vol.(µL)	Water vol. (µL)	Buffer vol. (µL)	[CGA] (mol/L)	[1] (mol/L)	[carbonate buffer] (mol/L)
1	425	125	191	259	$1.73 \cdot 10^{-3}$	$1.73 \cdot 10^{-2}$	0.259
2	"	"	275	175	"	"	0.175
3	"	"	364	86	"	"	0.086

Buffer effect - phosphate

A 4.06 mM CGA mother solution has been prepared by dissolving 14.4 mg of CGA in 10 mL of distilled water. A 138 mM **1** mother solution has been prepared by dissolving 34.1 mg of **1** in 1 mL of distilled water. Three reactions have been conducted: for each one, aliquots of CGA and **1** mother solutions, 0.286 M phosphate buffer (pH 9) and water have been added directly in the cuvette, so that **1** and CGA concentrations remain constant, while changing phosphate buffer concentration, adding variable amounts from the 0.286 M solution, keeping constant the volume of reaction at 1 mL by adding different aliquots of water (Table 7.17). The buffer has been the last component to be added to the reaction mixture because it starts **2** formation reaction. Immediately after buffer addition, the kinetics of each reaction has been measured by monitoring absorbance at 680 nm for 1200 s, taking a point every 60 seconds.

*Table 7.17 Solutions for spectrophotometric study of **2** formation at different phosphate buffer concentrations*

Solution	Mother CGA Vol. (µL)	Mother 1 Vol.(µL)	Water vol. (µL)	Buffer vol. (µL)	[CGA] (mol/L)	[1] (mol/L)	[phosphate buffer] (mol/L)
1	73	22	0	905	$1.73 \cdot 10^{-3}$	$1.73 \cdot 10^{-2}$	0.259
2	"	"	293	612	"	"	0.175
3	"	"	605	300	"	"	0.086

Colorimetric quantification of CGA over 24 hours

A 11 mM CGA mother solution has been prepared by dissolving 7.8 mg of CGA in 2 mL of carbonate buffer 56 mM. A 11.5 mM mother solution of **1** has been prepared dissolving 14.2 mg of compound in 5 mL of carbonate buffer 56 mM. Starting from the mother solutions and carbonate buffer 56 mM, seven different solutions have been prepared, containing **1** in excess and CGA at different concentrations (Table 7.18). A solution containing only **1** at a 5.75 mM concentration has been prepared. All the solutions have been left under stirring at room temperature for 24 hours with vials opened, then they have been analyzed by registering UV-Vis spectra in the range between 200 and 800 nm, using carbonate buffer 56 mM for registering the baseline. Three measurements have been done on each solution, mediating results to calculate average absorbance value at 680 nm. The procedure has been carried in triplicate.

*Table 7.18- Solutions for spectrophotometric study for **2** quantification over 24 hours.*

Solution	Mother CGA volume (µL)	Mother 1 volume (µL)	Buffer volume (µL)	[CGA] (mol/L)	[1] (mol/L)	Average A_{680} (n=3)	Std. Dev.	Error%
blank	0	500	500	0	$5.75\cdot10^{-3}$	$2.6\cdot10^{-3}$	$1.5\cdot10^{-3}$	60
1	100	"	400	$1.1\cdot10^{-3}$	"	$9.3\cdot10^{-1}$	$7.6\cdot10^{-3}$	8.1
2	80	"	420	$8.8\cdot10^{-4}$	"	$7.7\cdot10^{-1}$	$1.5\cdot10^{-1}$	18
3	60	"	440	$6.6\cdot10^{-4}$	"	$4.9\cdot10^{-1}$	$5.7\cdot10^{-2}$	11
4	40	"	460	$4.4\cdot10^{-4}$	"	$3.3\cdot10^{-1}$	$1.9\cdot10^{-2}$	5.7
5	20	"	480	$2.2\cdot10^{-4}$	"	$1.4\cdot10^{-1}$	$6.3\cdot10^{-2}$	46
6	5	"	495	$5.5\cdot10^{-5}$	"	$3.4\cdot10^{-2}$	$4.3\cdot10^{-3}$	13
7	2	"	498	$2.2\cdot10^{-5}$	"	$1.4\cdot10^{-2}$	$4.3\cdot10^{-3}$	30

Colorimetric assay for CGA quantification in kinetic mode ([1] 17.3 mM)

A 2.5 mM CGA mother solution has been prepared by dissolving 3.6 mg of CGA in 4 mL of distilled water. A 138 mM **1** mother solution has been prepared by dissolving 68.2 mg in 2 mL of distilled water. Six reactions have been conducted: for each one, aliquots of mother solutions, 1 M carbonate buffer and water have been added directly in the cuvette, so that **1** and carbonate buffer concentrations remain constant, while changing CGA concentration adding variable amounts from the mother solution, keeping constant the volume of reaction at 2 mL by adding different aliquots of water (Table 7.19). The buffer has been the last component to be added to the reaction mixture because it starts the reaction. Immediately after buffer addition, the kinetics of each reaction has been measured by monitoring absorbance at 680 nm for 960 s taking a point every 60 seconds. For the blank a 17.3 mM **1** solution in 180 mM carbonate buffer has been used. The entire procedure has been repeated three times (starting from newly prepared mother solutions)

*Table 7.19 -Solutions for spectrophotometric study for **2** quantification in kinetic mode ([**1**] 17.3mM)*

Sol.	Mother CGA Vol. (µL)	Mother 1 Vol.(µL)	Water vol. (µL)	Buffer vol. (µL)	[CGA] (mol/L)	[1] (mol/L)	Average $\Delta A_{680}/\Delta t$ (s^{-1})	Std. Dev. (s^{-1})	Error %
Blank	0	250	1400	350	0	$1.73\cdot10^{-2}$	$-2.3\cdot10^{-7}$	$4.4\text{x}10^{-7}$	191
1	1380	"	20	"	$1.8\cdot10^{-3}$	"	$5.0\cdot10^{-4}$	$7.2\cdot10^{-5}$	14
2	790	"	610	"	$1.0\cdot10^{-3}$	"	$4.0\cdot10^{-5}$	$2.0\cdot10^{-5}$	14
3	390	"	1000	"	$5.0\cdot10^{-4}$	"	$1.4\cdot10^{-4}$	$2.2\cdot10^{-5}$	15
4	200	"	1200	"	$2.5\cdot10^{-4}$	"	$6.9\cdot10^{-5}$	$9.6\cdot10^{-6}$	14
5	100	"	1300	"	$1.3\cdot10^{-4}$	"	$3.1\cdot10^{-5}$	$4.4\cdot10^{-6}$	14
6	50	"	1350	"	$6.0\cdot10^{-5}$	"	$1.2\cdot10^{-5}$	$1.5\cdot10^{-6}$	13

Colorimetric assay for CGA quantification in kinetic mode ([1] 1.9mM)

A 2.2 mM solution of **1** has been prepared by dissolving 5.5 mg of **1** in 10 mL of distilled water. A 14 mM mother solution of CGA has been prepared by dissolving 9.8 mg of CGA in 1.98 mL of distilled water (M_1). By progressive dilutions from M_1, mother solutions M_2, M_3 and M_4 have been prepared, having the CGA concentrations of 7 mM, 3.5 mM and 1.75 mM respectively. Four reactions have been conducted: for each one, aliquots of mother solutions, 1 M carbonate buffer and water have been added directly in the cuvette, so that **1** and carbonate buffer concentrations remain constant, while changing CGA concentration adding each time the same aliquot from a different mother solution (M_1-M_4)(Table 7.20). The buffer has been the last component to be added to the reaction mixture because it starts the **2** formation reaction. Immediately

after buffer addition, the kinetics of each reaction has been measured by monitoring absorbance at 680 nm for 1740 s taking a point every 60 seconds. For registering the baseline, a 19 mM carbonate buffer solution has been used.

*Table 7.20 -Solutions for spectrophotometric study for **2** quantification in kinetic mode ([**1**] 1.9mM)*

Solution	Mother CGA Vol. (µL)	Mother 1 Vol.(µL)	Water vol. (µL)	Buffer vol. (µL)	[CGA] (mol/L)	[1] (mol/L)
1	7 (from M_1)	432	51.5	9.5	$1.96\cdot10^{-4}$	$1.9\cdot10^{-3}$
2	7 (from M_2)	"	"	"	$9.8\cdot10^{-5}$	"
3	7 (from M_3)	"	"	"	$4.9\cdot10^{-5}$	"
4	7 (from M_4)	"	"	"	$2.5\cdot10^{-5}$	"

Studies with in-lab built photometer

Preliminary studies with the in-lab built photometer have been done exactly in the same way described for experiment with the spectrophotometer. The first measurement at a 100 µM CGA concentration has been done starting from a 3.3 mM CGA mother solution in water (M_1), whereas for the other experiments at lower CGA concentrations a 10-fold diluted mother solution 0.33 mM in water (M_2) has been prepared. For all the experiments a 270 mM mother solution of **1** in water and carbonate buffer 1 M (pH 9) have been used. **1** and buffer concentrations have been kept constant for all the kinetic experiments, while changing the CGA concentration by adding different volumes from the 2 mother solutions, keeping constant the 3 mL volume in the cuvette by adding water. Quantities are reported in Table 7.21. To determine scattering noise, a sample of distilled water has been used.

*Table 7.21 Solutions for spectrophotometric study of **2** formation using the in-lab built photometer*

Solution	Mother CGA vol. (µL)	Mother 1 Vol. (µL)	Water volume (µL)	Buffer vol. (µL)	[CGA] (mol/L)	[1] (mol/L)	$\Delta A_{680}/\Delta t$ (s^{-1})
1	90 (From M_1)	195	2190	525	$1.0\cdot10^{-4}$	$1.75\cdot10^{-2}$	$2.2\cdot10^{-5}$
2	90 (From M_2)	"	2190	"	$1.0\cdot10^{-5}$	"	$9.2\cdot10^{-7}$
3	45 (From M_2)	"	2235	"	$5.0\cdot10^{-6}$	"	$2.1\cdot10^{-7}$
4	9 (From M_2)	"	2270	"	$1.0\cdot10^{-6}$	"	$-1.0\cdot10^{-7}$

7.6.1.2 Peptides P1 and P2

Spectrophotometric study of peptide P1 reactivity with CGA in kinetic mode

A 1.9 mM peptide **P1** solution has been prepared by dissolving 1.0 mg of peptide in 500 µL of distilled water. A 12 mM CGA mother solution has been prepared by dissolving 2.2 mg of CGA in distilled water. Before starting the kinetic measurement with the spectrophotometer, the baseline has been acquired using a 19 mM carbonate buffer solution. 500 µL of the peptide solution have been inserted directly in the cuvette (1cm optical path, volume 500-1000 µL) together with 8 µL of the CGA mother solution and 10 µL of carbonate buffer 1 M (pH 9), thus obtaining final concentrations in solution of 1.9 mM for peptide **P1**, 0.19 mM for CGA and 19 mM for buffer. Immediately after making the last addition of buffer, kinetic measurement has been started, measuring the absorbance at 680 nm for 2.5 hours, taking a point every 60 seconds. At the end of the kinetic study, a complete absorbance spectrum has been registered between 200 and 800 nm.

Spectrophotometric study of peptide P2 reactivity with CGA in kinetic mode

A 3 mM solution of peptide **P2** has been prepared by dissolving 1.57 mg of peptide in 500 µL of distilled water. A 15 mM CGA mother solution has been prepared by dissolving 2.6 mg of CGA in distilled water. The baseline has been acquired using a 19 mM carbonate buffer solution. 300 µL of **P2** solution have been inserted directly in the cuvette (1 cm optical pathway, volume 500-1000 µL) together with 6 µL of the CGA mother solution, 180 µL of distilled water and 10 µL of carbonate buffer 1 M (pH 9), thus obtaining final concentrations in solution of 1.9 mM **P2**, 0.19 mM CGA and 19 mM buffer. Immediately after making the last addition of buffer, kinetic measurement has been started, measuring the absorbance at 680 nm for 2 hours, taking a point every 60 seconds. At the end of the kinetic study and after 24 hours, a complete absorbance spectrum has been registered between 200 and 800 nm.

Colorimetric assay for CGA quantification in kinetic mode (P1)

A 6 mM CGA mother solution has been prepared by dissolving 1.3 mg of CGA in 0.6 mL of distilled water. A 1.9 mM **P1** mother solution has been prepared by dissolving 3.8 mg in 2 mL of distilled water. Four reactions have been conducted: for each one, aliquots of mother solutions, 1 M carbonate buffer and water have been added directly in the cuvette, so that **P1** and carbonate buffer concentrations remain constant, while changing CGA concentration adding variable amounts from the mother solution, keeping constant the volume of reaction at 515 µL by adding different aliquots of water (Table 7.22). The buffer has been the last component to be added to the reaction mixture because it starts the **2** formation reaction. Immediately after buffer addition, the kinetics of each reaction has been measured by monitoring absorbance at 680 nm for 960 s taking a point every 60 seconds. For the blank a 19 mM carbonate buffer solution has been used.

*Table 7.22 -Solutions for spectrophotometric study for **2** quantification in kinetic mode*

Solution	Mother CGA Vol. (µL)	Mother 1 Vol.(µL)	Water vol. (µL)	Buffer vol. (µL)	[CGA] (mol/L)	[1] (mol/L)
1	15	490	0	10	$1.8 \cdot 10^{-4}$	$1.8 \cdot 10^{-3}$
2	8	"	7	"	$9.7 \cdot 10^{-5}$	"
3	4	"	11	"	$4.9 \cdot 10^{-5}$	"
4	2	"	13	"	$2.4 \cdot 10^{-5}$	"

Reactivity of P1 and 1 with CGA and ethyl caffeate

A 2.2 mM mother solution of **1** has been prepared by dissolving 5.5 mg (0.0223 mmol) of **1** in 10 mL of distilled water.

A 2 mM **P1** solution has been prepared by dissolving 2.15 mg of **P1** (0.00208 mmol) in 1.040 mL of distilled water.

A 14 mM mother solution of CGA has been prepared by dissolving 4.3 mg (0.0121 mmol) of CGA in 864 µL of distilled water.

A 14 mM ethyl caffeate (EtCA) mother solution has been prepared by dissolving 5.6 mg (0.0269 mmol) in 1.920 mL of a solvent mixture composed by 10% of DMSO and 90% of distilled water (due to solubility problems DMSO must be added before water and to avoid precipitation the solution must be prepared right before performing analysis).

For the kinetic experiments, the different components have been added directly in cuvette, adding last 1 M carbonate buffer (pH 9). Immediately after buffer addition, the kinetics of each reaction has been measured by monitoring absorbance at 680 nm for 2 hours, taking a point every 60 seconds. Quantities and concentrations are reported in Table 7.23 (experiments with **1**) and Table 7.24 (experiments with **P1**).

*Table 7.23 Solutions for spectrophotometric study of **1** reaction with CGA and EtCA*

Solution	Mother CGA/CA vol. (µL)	Mother 1 vol. (µL)	Buffer volume (µL)	Water (µL)	[CGA] (mol/L)	[1] (mol/L)	[buffer] (mol/L)
1-CGA	432 (CGA)	7	9.5	51.5	$1.9 \cdot 10^{-4}$	$1.9 \cdot 10^{-3}$	$1.9 \cdot 10^{-2}$
1-EtCA	432 (EtCA)	"	"	"	"	"	"

*Table 7.24 Solutions for spectrophotometric study of **P1** reaction with CGA and EtCA*

Solution	Mother CGA/CA vol. (µL)	Mother P1 vol. (µL)	Buffer vol. (µL)	Water vol. (µL)	[CGA] (mol/L)	[P1] (mol/L)	[buffer] (mol/L)
P1-CGA	475 (CGA)	7	9.5	8.5	$1.9 \cdot 10^{-4}$	$1.9 \cdot 10^{-3}$	$1.9 \cdot 10^{-2}$
P1-EtCA	475 (EtCA)	"	"	"	"	"	"

7.6.1.3 Polymeric films

Kinetic and time-point measurements of the discs using a multiwell plate reader: general procedure

One disc has been placed in each well of a transparent flat-bottomed multiwell plate, adding to each well 200 µL of CGA solution at the desired concentration, prepared in carbonate buffer 20 mM, pH 9.5. A multiwell plate reader has been used to measure at regular timepoints the absorbance at 680 nm of the green TBA pigments that form upon reaction of the amino groups on the polymeric discs with CGA: the map reading mode has been used, by making a map of each well 15x15. A measurement was taken at time 0 (t_0), which means immediately after adding chlorogenic acid to the membranes.

During all the kinetic measurements, membranes have been left in the wells submerged in the CGA solutions, measuring absorbances at 680 nm at regular timepoints.

In the case of measurements at different CGA concentrations at specific time points, the discs have been incubated at different CGA concentrations, and measurements taken at the beginning (t_0) and at one (or more) specific time point(s).

In all cases, measurements have been performed in triplicate. Data elaboration has been performed as explained at paragraph 3.4.1.

Experiments with optical fiber device: general procedure

Me2 discs cut with a 10 mm puncher have been put to incubate in solutions of CGA at concentrations 1 mM, 0.5 mM, 0.4 mM, 0.3 mM, 0.2 mM, 0.1 mM in carbonate buffer 20 mM, pH 9.5. Three discs were incubated for 1 hour in 10 mL of each CGA solution. Three discs have also been incubated in 10 mL of carbonate buffer without CGA to be used as reference. After incubation, discs have been left to dry for around 10 minutes and then they have been analyzed with the optical fiber. In all the cases, a white sheet of paper has been used as the background on which putting the membranes for measurements with optical fiber. Membranes incubated in only buffer were used as the blank. Spectra were corrected at 590 nm, to report all the spectra at the same baseline level. Then, corrected absorbance values at 691 nm have been taken and correlation with CGA concentration has been extrapolated.

CGA detection using in-lab built devices: evaluation of reaction conditions

A 2 mM CGA solution has been prepared by dissolving 18.1 mg of CGA in 25 mL con carbonate buffer 20 mM, pH 9.5. 5 mL of the CGA solution have been placed in 5 vials, each one containing two **Me2** discs, and the 5 vessels have been treated in different ways: the first has been put under simple magnetic stirring, the second has been sonicated, the third has been bubbled with compressed air, the fourth has been heated at 95°C under stirring and the last one has been treated with the addition of hydrogen peroxide as an oxidant, under stirring (5.5 µL, which correspond to 10 equivalents of H_2O_2 with respect to CGA, taken from a 30% commercial solution in water). A blank has been prepared reacting a membrane in carbonate buffer, without CGA. All the membranes have been incubated keeping vessels opened. After 35 minutes, all the discs have been analyzed using the image reader, taking for each disc 11 points in a cross-like shape. Then, discs have been placed again in the respective incubation vessels (more H_2O_2 has been added to the corresponding vial), and they have been put to react again, reaching in total 80 minutes. Then, they have been analyzed again.

Data processing has been done subtracting the red component (R) to the green one (G) for each of the 11 points taken for each membrane; then, the average blank value has been subtracted to all the G-R values, and the average between all the blank-corrected values has been done.

CGA quantification using in-lab built devices: evaluation of the two devices performances

A 2 mM CGA mother solution has been prepared by dissolving 18.5 mg of CGA in 25 mL of carbonate buffer 20 mM, pH 9.5. By diluting the 2 mM mother solution, diluted CGA solutions (10 mL volume) have been prepared at the concentrations 1 mM, 0.4 mM, 0.2 mM and 0.1 mM. The 10 mL CGA solutions in the range of concentration 1 mM – 0.1 mM have been poured in 4 vials, each one containing three **Me2** discs (diameter around 5 mm). A blank sample has also been prepared by incubating three discs in only carbonate buffer 20 mM. The vials have been kept under vigorous magnetic stirring for 60 minutes, keeping them opened. After drying the membranes for around 30 minutes (otherwise measured values are not stabile) they have been first analyzed with the pseudo differential reflection spectrophotometer and then with the image reader, taking 16 points for each membrane (data analysis as explained in the previous paragraph). Then average, standard deviation and relative error have been calculated for both devices measurements.

7.7 FLUORESCENCE

7.7.1 TBA Pigment

7.7.1.1 Pigment 2 fluorescence

LOD of pigment 2 in fluorescence mode (lower wavelength)

A 1.8 mM **2** mother solution (fraction **b** obtained from purification of **2** by SEC, paragraph 7.3.1.1) has been prepared by dissolving 3.3 mg of **2** in 2 mL of carbonate buffer 3 mM. Fluorescence cuvettes 5x5 mm have been used, setting excitation and emission slits at 10-20 nm respectively; excitation (200-400 nm) and emission spectra (350-600 nm) have been registered, finding excitation and emission maxima at 318 nm and 426 nm respectively. By successive dilutions from the 1.8 mM mother solution, seven solutions at decreasing concentrations ranging between 300 µM and 2.5 µM have been prepared. The emission spectrum of each solution (λ_{ex}=318 nm) has been registered three time, making an average of the maxima emission intensity at 426 nm. The procedure has been repeated other two times (three replicates) (Table 7.25).

*Table 7.25- Solutions to calculate LOD of **2** in fluorescence mode*

Solution	[2] (mol/L)	Average F (a.u.)	Std. deviation	Error %
0 (Blank)	0	7.4	0.27	3.6
1	$3.0 \cdot 10^{-4}$	$1.4 \cdot 10^{2}$	8.6	6.2
2	$1.0 \cdot 10^{-4}$	53	2.7	5.1
3	$5.0 \cdot 10^{-5}$	31	1.7	5.5
4	$2.7 \cdot 10^{-5}$	20	0.78	3.9
5	$1.4 \cdot 10^{-5}$	14	1.3	9.7
6	$7.3 \cdot 10^{-6}$	9.7	0.77	7.9
7	$2.5 \cdot 10^{-6}$	8.2	0.39	4.7

CGA fluorescence

A 2.8 mM CGA solution has been prepared by dissolving 4.0 mg of CGA in 4 mL of distilled water. 125 µL of the CGA solution have been added in the cuvette, together with 540 µL of distilled water and 35 µL of carbonate buffer 1 M (pH 9). The concentrations in cuvette resulted to be [CGA] = 0.5 mM, [buffer] = 50 mM. Immediately after preparation, the fluorescence of the solution has been measured in excitation (200-450 nm) and emission mode (450-600 nm). The following peaks have been found: λ_{ex} = 252 nm, 335 nm, 418 nm; λ_{em} = 490 nm (slits 10-20 nm).

Quantification of CGA in fluorescence mode at 700 nm

A 138 mM mother solution of **1** has been prepared dissolving 69.10 mg in 2.033 mL of carbonate buffer 180 mM, pH 9.45. A 2.5 mM mother solution of CGA has been prepared dissolving 4.53 mg of CGA in 5.114 mL of the same carbonate buffer. Starting from the mother solutions and from carbonate buffer 180 mM, six different solutions have been prepared, containing **1** in excess (17.9 mM) and CGA at different concentrations ranging between 1.75 mM and 62.5 µM, keeping the volume constant at 2 mL by adding aliquots of carbonate buffer (Table 7.26). One solution containing only CGA at the highest tested concentration has also been prepared as a reference, to analyze its fluorescence behavior in the absence of lysine (control). After 30 minutes of reaction with vials opened, 1 mL of each solution has been taken and acidified with 225 µL of HCl 1 M: after acidifying, a pH around 3 was measured with pH indicator paper. For each analysis the cuvette was filled with 400 µL of each acidified solution, exciting at 660 nm, with slits of excitation and emission set at 10-10 nm.

*Table 7.26- Solutions to study **2** formation at different CGA concentrations in fluorescence mode*

Solution	Mother CGA vol. (µL)	Mother 1 vol. (µL)	Buffer vol. (µL)	[CGA] (mol/L)	[1] (mol/L)
0 (control)	1400	0	600	$1.75 \cdot 10^{-3}$	0
1	1400	260	340	$1.75 \cdot 10^{-3}$	$1.79 \cdot 10^{-2}$
2	800	"	940	$1.00 \cdot 10^{-3}$	"
3	400	"	1340	$5.00 \cdot 10^{-4}$	"
4	200	"	1540	$2.50 \cdot 10^{-4}$	"
5	100	"	1640	$1.25 \cdot 10^{-4}$	"
6	50	"	1690	$6.25 \cdot 10^{-5}$	"

Dependence of the fluorescence emission at 700 nm from the pH

Due to the impossibility to measure in a precise way the pH after acidifying the reaction mixture with the pHmeter, pH values have been measured using pH indicator papers.

A 5 mM CGA mother solution has been prepared dissolving 5.11 mg of CGA in 2.88 mL of carbonate buffer 180 mM, pH 9.45. 13.42 mg of **1** have been weighted directly in the reaction vessel. 1.5 mL of the CGA mother solution have been added to the vial containing **1**, and 1.5 mL of carbonate buffer have been added bringing the final volume to 3 mL. Final concentrations in solution thus resulted to be 18.2 mM of **1**, 2.5 mM of CGA, 180 mM of carbonate buffer. The reaction mixture has been stirred for around 4 hours at room temperature keeping the vial opened. After 4 hours, nine aliquots of 300 µL each have been taken from the reaction mixture, and each one has been acidified with different quantities of HCl 1 M ranging between 10 and 80 µL, adding different quantities of water to keep a constant volume of 500 µL for all the acidified aliquots, in order to change the pH while maintaining equal concentrations of the different components in solution (Table 7.27). Excitation has been set at 620 nm, with slits of excitation and emission of 10-10 nm.

*Table 7.27 – Solutions to study the dependence of **2** fluorescence depending on the pH*

Solution	Reaction mixture volume (µL)	Volume of added HCl 1M (µL)	Volume of added water (µL)	pH (measured with pH indicator paper)
1	300	10	190	9
2	300	20	180	8
3	300	30	170	7/8
4	300	40	160	7/8
5	300	50	150	7
6	300	60	140	6
7	300	65	135	4/5
8	300	70	130	3
9	300	80	120	3

Quantification of CGA in absorbance mode at 680 nm and in fluorescence mode at 700nm

A 138 mM mother solution of **1** has been prepared dissolving 51.51 mg in 1.515 mL of carbonate buffer 180 mM, pH 9.5. A 2.5 mM mother solution of CGA has been prepared dissolving 4.50 mg of CGA in 5.080 mL of the same carbonate buffer. Starting from the mother solutions and from carbonate buffer 180 mM, six different solutions have been prepared, containing **1** in excess (17.9 mM) and CGA at different concentrations ranging between 1 mM and 20 µM, keeping the volume constant at 1.5 mL by adding aliquots of carbonate buffer. A blank solution containing **1** without CGA has also been prepared (Table 7.28). After 15 minutes of reaction with vessels opened, 200 µL of each solution have been taken and their absorbance at 680 nm has been analyzed using a multiwell plate reader. Then, 500 µL of each solution have been acidified with 106 µL of HCl 1 M: after acidifying, a pH around 6 was measured with pH indicator paper. For each analysis, the cuvette was filled with 400 µL of each acidified solution, exciting at 660 nm, with slits of excitation and emission of 15-15 nm.

*Table 7.28- Solutions to study **2** formation at different CGA concentrations in fluorescence mode ([**1**] 18mM)*

Solution	Mother CGA s vol. (µL)	Mother 1 Vol. (µL)	Buffer vol. (µL)	[CGA] (mol/L)	[1] (mol/L)
0 (blank)	0	195	1305	0	$1.79 \cdot 10^{-2}$
1	600	"	705	$1.00 \cdot 10^{-3}$	"
2	300	"	1005	$5.00 \cdot 10^{-4}$	"
3	150	"	1155	$2.50 \cdot 10^{-4}$	"
4	75	"	1230	$1.25 \cdot 10^{-4}$	"
5	37.5	"	1268	$6.25 \cdot 10^{-5}$	"
6	12	"	1294	$2.00 \cdot 10^{-5}$	"

Quantification of CGA in absorbance mode and in fluorescence mode at 700nm ([1] 3.6 mM)

A 27.6 mM **1** mother solution has been prepared dissolving 13.75 mg in 2.033 mL of carbonate buffer 180 mM, pH 9.5. A 2.0 mM CGA mother solution has been prepared dissolving 4.12 mg of CGA in 5.814 mL of the same carbonate buffer. Starting from the mother solutions and from carbonate buffer 180 mM, six different solutions have been prepared, containing **1** in excess (3.59 mM) and CGA at different concentrations ranging between 360 µM and 10 µM, keeping the volume constant at 2 mL by adding aliquots of carbonate buffer. A control solution containing only CGA at the highest tested concentration (360 µM) without lysine has also been prepared, as well as a blank solution containing lysine without CGA. (Table 7.29). After 100 minutes of reaction with vessels opened, 520 µL of each solution have been acidified with 102 µL of HCl 1M: after acidifying, a pH around 6 was measured with pH indicator paper. For each analysis, the cuvette was filled with 400µL of each acidified solution, exciting at 660 nm, with slits of excitation and emission of 15-15 nm.

*Table 7.29- Solutions to study **2** formation at different CGA concentrations in fluorescence mode ([**1**] 3.6mM)*

Solution	Mother CGA Vol. (µL)	Mother 1 Vol. (µL)	Buffer vol. (µL)	[CGA] (mol/L)	[1] (mol/L)
0 (control CGA)	360	0	1640	$3.60 \cdot 10^{-4}$	0
Blank (only lysine)	0	260	1740	0	$3.59 \cdot 10^{-3}$
1	360	"	1380	$3.60 \cdot 10^{-4}$	"
2	180	"	1560	$1.80 \cdot 10^{-4}$	"
3	90	"	1650	$9.00 \cdot 10^{-5}$	"
4	45	"	1695	$4.50 \cdot 10^{-5}$	"
5	20	"	1720	$2.00 \cdot 10^{-5}$	"
6	10	"	1730	$1.00 \cdot 10^{-5}$	"

Test in HEPPS buffer

A 138 mM **1** mother solution has been prepared dissolving 50.88 mg in 1.497 mL of HEPPS buffer 200mM, pH 9.03. A 2.5 mM CGA mother solution has been prepared dissolving 5.94 mg of CGA in 6.706 mL of the same HEPPS buffer. Starting from the mother solutions and from HEPPS buffer 200 mM, six different solutions have been prepared, containing **1** in excess (17.9 mM) and CGA at different concentrations ranging between 1 mM and 20 µM, keeping the volume constant at 1.5 mL by adding aliquots of HEPPS buffer. A blank solution containing lysine without CGA has also been prepared. (Table 7.30). After 15 minutes of reaction with vessels opened, 500 µL of each solution have been acidified with 96 µL of HCl 1 M: after acidifying, a pH around 6 was measured with pH indicator paper. For each analysis the cuvette was filled with 400 µL of each acidified solution, exciting at 620 nm, with slits of excitation and emission of 15-15 nm.

*Table 7.30 Solutions to study **2** formation at different CGA concentrations in fluorescence mode performing the reaction in HEPPS buffer.*

Solution	Mother CGA Vol.(µL)	Mother 1 Vol. (µL)	Buffer vol. (µL)	[CGA] (mol/L)	[1] (mol/L)
0 (blank)	0	195	1305	0	$1.79 \cdot 10^{-2}$
1	600	"	705	$1.00 \cdot 10^{-3}$	"
2	300	"	1005	$5.00 \cdot 10^{-4}$	"
3	150	"	1155	$2.50 \cdot 10^{-4}$	"
4	75	"	1230	$1.25 \cdot 10^{-4}$	"
5	37.5	"	1268	$6.25 \cdot 10^{-5}$	"
6	12	"	1294	$2.00 \cdot 10^{-5}$	"

7.7.1.2 P-BSA protein labeling

LOD of P-BSA in fluorescence mode

A 25 µM **P-BSA** solution has been prepared dissolving 3.2 mg of the modified protein in 2 mL of carbonate buffer 10 mM (molarity has been calculated based on BSA molecular weight, since degree of functionalization is unknown). To allow complete dissolution of P-BSA, the mixture has been left under stirring for 30 minutes, and it has been sonicated for further 15 minutes. By diluting the 25 µM P-BSA mother solution, six solutions have been prepared, at increasingly lower **P-BSA** concentrations (Table 7.31). For each solution the emission spectrum has been registered three times (λ_{ex} =346 nm), making an average of the maxima fluorescence emission values at 470 nm. In the same way, a blank spectrum of a solution containing only carbonate buffer 10 mM has been registered, repeating the measurement six times and making an average of the emission value at 470 nm. The whole experiment has been performed in triplicate, starting each time from a different **P-BSA** mother solution. A 5x5 mm cuvette has been used, setting slits at 10-20 nm.

Table 7.31- Solutions to determine P-BSA LOD in fluorescence mode

Solution	[P-BSA] (mol/L)	Average F (a.u.)	Std. Dev.	Error %
0 (Blank)	0	5.6	0.48	8.6
1	$1.0\cdot10^{-5}$	$4.5x10^2$	8.3	1.8
2	$5.0\cdot10^{-6}$	$3.0x10^2$	9.2	3.1
3	$2.5\cdot10^{-6}$	$1.6x10^2$	1.5	9.5
4	$2.0\cdot10^{-6}$	$1.0x10^2$	1.3	13
5	$1.0\cdot10^{-6}$	$1.1x10^2$	3.2	29
6	$5.0\cdot10^{-7}$	43	7.0	17

7.7.2 Boronic acids

7.7.2.1 Fluorescence titrations with 5

All the fluorescence experiments have been done using sodium phosphate buffer 0.1 M, pH 7.4.

A 6 mM mother solution has been prepared by dissolving 3.5 mg of **5** in 2 mL of DMSO (**$F5_0$**). All the measurements have been performed registering the emission spectra between 350 and 500 nm, exciting the fluorophore at 335 nm, having slits of excitation and emission at 15-20 nm, using the Perkin Elmer fluorimeter.

Catechol

A 100 mM catechol mother solution M_0 has been prepared by dissolving 22 mg in 2 mL of DMSO. Starting from M_0, mothers M_1, M_2, M_3 and M_4 have been prepared by successive dilutions with phosphate buffer, having concentrations of 30 mM, 3 mM, 300 µM and 30 µM. A first emission spectrum has been registered on a solution prepared by inserting in a 1 cm optical pathway cuvette 2500 µL of phosphate buffer and 12.5 µL of **$F5_0$**, thus obtaining an initial fluorophore concentration of 30 µM. Then, titration has been carried out by adding every 4 minutes an aliquot from M_1-M_4 solutions (Table 7.32), registering the emission spectrum after each addition.

*Table 7.32- Solutions to study **5** fluorescence changes upon addition of increasing concentrations of catechol*

Measurement	Mother solution	Added volume	[CC] final	Final volume
Only **5**	**F5$_0$** 6 mM	12.5 µL	0	2512.5 µL
1	M_4 30 µM	30 µL	350 nM	2542.5 µL
2	M_3 300 µM	30 µL	3.8 µM	2572.5 µL
3	M_2 3 mM	30 µL	38 µM	2602.5 µL
4	M_1 30 mM	30 µL	380 µM	2632.5 µL

Chlorogenic acid

A 500 mM CGA mother solution M_0 has been prepared by dissolving 265 mg in 1.5 mL of DMSO. Starting from M_0, mothers M_1, M_2, M_3, M_4 and M_5 have been prepared by successive dilutions with phosphate buffer, having concentrations of 300 mM, 30 mM, 3 mM, 300 µM and 30 µM. A first emission spectrum has been registered on a solution prepared by inserting in the cuvette 748 µL of phosphate buffer and 4 µL of **F5$_0$**, thus obtaining an initial fluorophore concentration of 32 µM. Then, titration has been carried out by adding aliquots from M_1-M_5 solutions (Table 7.33), registering the emission spectrum after each addition.

*Table 7.33 Solutions to study **5** fluorescence changes upon addition of increasing concentrations of chlorogenic acid*

Measurement	Mother solution	Added volume	[CGA] final	Final volume
Only **5**	**F5$_0$** 6 mM	4 µL	0	752 µL
1	M_5 30 µM	9.6 µL	393 nM	761.6 µL
2	M_4 300 µM	9.6 µL	4.3 µM	771.2 µL
3	M_3 3 mM	9.6 µL	43 µM	780.8 µL
4	M_2 30 mM	9.6 µL	408µM	790.4 µL
5	M_1 300 mM	9.6 µL	4 mM	800 µL

The titration with CGA has been repeated, in order to investigate in more details the range of concentrations 40-400 µM. A 100 mM CGA mother solution M_0 has been prepared by dissolving 53 mg in 1.5 mL of DMSO. Starting from M_0, mothers M_1, M_2, M_3, M_4 and M_5 have been prepared by successive dilutions with phosphate buffer, having concentrations of 30 mM, 24 mM, 12 mM, 6 mM and 3 mM. A first emission spectrum has been registered adding in the cuvette 748 µL of phosphate buffer and 4 µL of **F5$_0$**, thus obtaining an initial fluorophore concentration of 32 µM. Then, titration has been carried out by adding aliquots from M_1-M_5 solutions (Table 7.34), registering the emission spectrum after each addition.

*Table 7.34 Solutions to study **5** fluorescence changes upon addition of increasing concentrations of chlorogenic acid (intermediate concentrations).*

Measurement	Mother solution	Added volume	[CGA] final	Final volume
Only **5**	**F5$_0$** 6 mM	4 µL	0	752 µL
1	M_5 3 mM	9.6 µL	38 µM	761.6 µL
2	M_4 6 mM	9.6 µL	112 µM	771.2 µL
3	M_3 12 mM	9.6 µL	257 µM	780.8 µL
4	M_2 24 mM	9.6 µL	543 µM	790.4 µL
5	M_1 30 mM	9.6 µL	898 µM	800 µL

Caffeic acid, quinic acid, *p*-coumaric acid, hydroxytyrosol

A 500 mM mother solution M_0 of each target has been prepared by dissolving in 1.5 mL of DMSO respectively 135.1 mg of caffeic acid, 144.1 mg of quinic acid, 123.1 mg of *p*-coumaric acid and 115.6 mg of hydroxytyrosol. Starting from M_0, mothers M_1, M_2, M_3, M_4, M_5, M_6, M_7 and M_8 have been prepared by successive dilutions with phosphate buffer, having concentrations of 300 mM, 30 mM, 24 mM, 12 mM, 6 mM, 3 mM, 300 µM and 30 µM. A first emission spectrum has been registered on a solution prepared by inserting in a 0.5 cm optical pathway cuvette 715.2 µL of phosphate buffer and 8 µL of **$F5_0$**, thus obtaining an initial fluorophore concentration of 66 µM. Then, titration has been carried out by adding aliquots from M_1-M_8 solutions (Table 7.35), registering the emission spectrum after each addition.

*Table 7.35- Solutions to study **5** fluorescence changes upon addition of increasing concentrations of caffeic acid, quinic acid, p-coumaric acid and hydroxytyrosol*

Measurement	Mother solution	Added volume	[target] final	Final volume
Only **5**	**$F5_0$** 6 mM	8 µL	0	723.2 µL
1	M_8 30 µM	9.6 µL	393 nM	732.8 µL
2	M_7 300 µM	9.6 µL	4.3 µM	742.4 µL
3	M_6 3 mM	9.6 µL	43 µM	752 µL
4	M_5 6 mM	9.6 µL	118 µM	761.6 µL
5	M_4 12 mM	9.6 µL	267 µM	771.2 µL
6	M_3 24 mM*	9.6 µL	558 µM	780.8 µL
7	M_2 30 mM	9.6 µL	916 µM	790.4 µL
8	M_1 300 mM	9.6 µL	4.5 mM	800 µL

*Last tested value for quinic acid

Determination of CGA extinction coefficient

The molar extinction coefficients of CGA at the excitation and emission wavelengths of **5** have been calculated to apply the inner filter correction. A 100 mM CGA mother solution has been prepared by dissolving 3.5 mg of CGA in 100 µL of DMSO. By successive dilutions in sodium phosphate buffer 0.1 M, pH 7.4, four diluted CGA solutions have been prepared at concentrations 60 µM, 50 µM, 40 µM and 30 µM respectively, keeping constant the ratio between buffer and DMSO. For each mother solution, an absorbance spectrum has been registered between 270 and 450 nm. By using the Lambert-Beer Law, the molar extinction coefficient has been calculated to be 8380 $L \cdot M^{-1} \cdot cm^{-1}$ at **5** excitation wavelength (335 nm) and 1250 $L \cdot M^{-1} \cdot cm^{-1}$ at the emission wavelength of **5** (390 nm).

7.7.2.2 Fluorescence titrations with 20

A 4.7 mM mother solution of fluorophore **20** (**$F20_0$**) has been prepared by dissolving 4.7 mg of **20** in 2 mL of DMSO. All the measurements have been carried out registering emission spectra between 510 and 700 nm, exciting the fluorophore at 490 nm, having slits of excitation and emission respectively at 5 and 10 nm, using the Varian Cary eclipse fluorometer. Between one addition and the other 4 minutes have been waited. For all the fluorescence experiments sodium phosphate buffer 0.1 M, pH 7.4, has been used.

500 mM mother solutions of each target (M_0) have been prepared by dissolving in 100 µL of DMSO respectively 5.5 mg of catechol, 17.7 mg of chlorogenic acid, 9 mg of caffeic acid, 9.6 mg of quinic acid, 7.7 mg of hydroxytyrosol, 6.9 mg of tyrosol and 8.2 mg of *p*-coumaric acid.

Starting from each M_0 mother solution for each target, by successive dilutions with phosphate buffer 0.1 M, solutions M_1, M_2, M_3, M_4, M_5, M_6, M_7 and M_8 have been prepared at the concentrations respectively of 300 mM, 30 mM, 24 mM, 12 mM, 6 mM, 3 mM, 300 µM, 30 µM. A first emission spectrum has been registered on a solution prepared by inserting in a 0.5 cm optical pathway cuvette 715.2 µL of phosphate buffer and 8 µL of **F20$_0$**, thus obtaining an initial fluorophore concentration of 52 µM. Then, titration has been carried out by adding aliquots from M_0-M_8 solutions (Table 7.36), registering the emission spectrum after each addition. Measurements for CGA, CA, HT and CC have been performed in triplicate.

*Table 7.36- Solutions to study **20** fluorescence changes upon addition of increasing concentrations of catechol, caffeic acid, chlorogenic acid, hydroxytyrosol, tyrosol, p-coumaric acid, quinic acid.*

Measure	Mother solution	Added volume	Final [target]	Final volume
Only **20**	**F20$_0$** 4.7 mM	8 µL	0	723.2 µL
1	M_8 30 µM	9.6 µL	393 nM	732.8 µL
2	M_7 300 µM	9.6 µL	4.3 µM	742.4 µL
3	M_6 3 Mm	9.6 µL	43 µM	752 µL
4	M_5 6 mM	9.6 µL	118 µM	761.6 µL
5	M_4 12 mM	9.6 µL	267 µM	771.2 µL
6	M_3 24 mM	9.6 µL	558 µM	780.8 µL
7	M_2 30 mM	9.6 µL	916 µM	790.4 µL
8	M_1 300 mM	9.6 µL	4.5 mM	800 µL
9	M_0 500mM*	9.6 µL	10.3 mM	809.6µL

* only for CC and HT

7.7.2.3 Fluorescence titrations with P3

A 4.7 mM mother solution of peptide **P3** (**P3$_0$**) has been prepared by dissolving 0.41 mg of P3 in 100 µL of DMSO. All the measurements have been carried out registering emission spectra between 510 and 700 nm, exciting the fluorophore at 490 nm, having slits of excitation and emission respectively at 10 and 10 nm, using the Varian Cary Eclipse fluorimeter. Between one addition and the other 4 minutes have been waited.

500 mM mother solutions of each target (M_0) have been prepared by dissolving in 100 µL of DMSO respectively 5.5 mg of catechol, 17.7 mg of chlorogenic acid, 9 mg of caffeic acid and 7.7 mg of hydroxytyrosol.

Starting from each M_0 mother solution for each target, by successive dilutions with phosphate buffer 0.1 M, pH 7.4, more diluted mother solutions M_1, M_2, M_3, M_4, M_5, M_6, M_7, M_8 have been prepared at the concentrations respectively of 300 mM, 30 mM, 24 mM, 12 mM; 6 mM, 3 mM; 300 µM, 30 µM. A first emission spectrum has been registered on a solution prepared by inserting in a 5 mm optical pathway cuvette 713.2 µL of phosphate buffer and 10 µL of **P3$_0$**, thus obtaining an initial peptide concentration of 66 µM. Then, titration has been carried out by adding aliquots from M_1-M_8 solutions (Table 7.37), registering the emission spectrum after each addition. Measurement for CGA has been performed in triplicate.

*Table 7.37- Solutions to study **P3** fluorescence changes upon addition of increasing concentrations of catechol, caffeic acid, chlorogenic acid, hydroxytyrosol.*

Measurement	Mother solution	Added volume	Final [target]	Final volume
Only **P3**	**P3$_0$** 4.7 mM	10 µL	0	723.2 µL
1	M_8 30 µM	9.6 µL	393 nM	732.8 µL
2	M_7 300 µM	9.6 µL	4.3 µM	742.4 µL
3	M_6 3 Mm	9.6 µL	43 µM	752 µL
4	M_5 6 mM	9.6 µL	118 µM	761.6 µL
5	M_4 12 mM	9.6 µL	267 µM	771.2 µL
6	M_3 24 mM	9.6 µL	558 µM	780.8 µL
7	M_2 30 mM	9.6 µL	916 µM	790.4 µL
8	M_1 300 mM	9.6 µL	4.5 mM	800 µL
9*	M_1 300 mM	9.6 µL	8 mM	809.6 µL

*only for CC and HT

7.7.2.4 Fluorescence titrations with P4 and P5

4.7 mM mother solution of peptides P4 and P5 (**P4$_0$** and **P5$_0$**) have been prepared by dissolving 0.39 mg of **P4** in 100 µL of DMSO and 0.61 mg of **P5** in 120 µL of DMSO. All the measurements have been carried out registering emission spectra between 510 and 700 nm, exciting the fluorophore at 490 nm, having slits of excitation and emission respectively at 10-5 nm for **P4**, 5-10 for **P5**, using the Varian Cary Eclipse fluorimeter. For all the measurements phosphate buffer 0.1 M, pH 7.4 has been used.

500mM mother solutions of each target (M_0) have been prepared by dissolving in 200 µL of DMSO respectively 11 mg of catechol, 35.4 mg of chlorogenic acid, 18 mg of caffeic acid and 15.4 mg of hydroxytyrosol. Starting from each M_0 mother solution for each target, by successive dilutions with phosphate buffer, more diluted mother solutions M_1, M_2, M_3, M_4, M_5, M_6, M_7 and M_8 have been prepared at the concentration respectively of 300 mM, 30 mM, 24 mM, 12 mM; 6 mM, 3 mM; 300 µM, 30 µM. A first emission spectrum has been registered on a solution prepared by inserting in a 5 mm optical pathway cuvette 715.2 µL of phosphate buffer and 8 µL of **P4$_0$** or **P5$_0$**, thus obtaining an initial peptide concentration of 52 µM. Then, titration has been carried out by adding aliquots from M_0-M_8 solutions (Table 7.38), registering the emission spectrum after each addition. Measurements have been performed in triplicate.

*Table 7.38- Solutions to study **P4** and **P5** fluorescence changes upon addition of increasing concentrations of catechol, caffeic acid, chlorogenic acid, hydroxytyrosol.*

Measurement	Mother solution	Added volume	Final [target]	Final volume
Only **P4**/**P5**	**P4**$_0$/**P5**$_0$ 4.7 mM	8 µL	0	723.2 µL
1	M_8 30 µM	9.6 µL	393 nM	732.8 µL
2	M_7 300 µM	9.6 µL	4.3 µM	742.4 µL
3	M_6 3 Mm	9.6 µL	43 µM	752 µL
4	M_5 6 mM	9.6 µL	118 µM	761.6 µL
5	M_4 12 mM	9.6 µL	267 µM	771.2 µL
6	M_3 24 mM	9.6 µL	558 µM	780.8 µL
7	M_2 30 mM	9.6 µL	916 µM	790.4 µL
8	M_1 300 mM	9.6 µL	4.5 mM	800 µL
9	M_0 500 mM	9.6 µL	10.3 mM	809.6 µL

7.7.3 Diazo coupling

7.7.3.1 Non-covalent interactions of P6 with tyrosol

A 51.4 µM solution of **P6** in water/DMF (90:10) has been prepared. In three wells of a multiwell plate 74 µL of the 51.4 µM mother solution of **P6** have been inserted, together with 124 µL of a mixture of aqueous Na_2CO_3 0.1 M and DMF in a ratio 50:50, so that in the well the peptide concentration is 19 µM. In the other wells, 74 µL of the 51.4 µM mother solution of **P6** have been inserted, together with 124 µL of tyrosol solutions prepared in a mixture of aqueous Na_2CO_3 0.1 M and DMF in a ratio 50:50. Tyrosol mother solutions have been used at the concentrations of 80 µM, 32.3 µM, 16 µM, 11 µM, 6.5 µM, 3 µM, 1 µM. Final concentration of peptide in wells resulted to be 19 µM, whereas tyrosol was present at the concentrations 50 µM, 20 µM, 10 µM, 6.8 µM, 4 µM, 1.87 µM and 626 nM. Measurements have been registered in triplicate.

7.7.3.2 Non-covalent interactions of P7 with tyrosol

A 51.4 µM solution of **P7** in water/DMF (90:10) has been prepared. In three wells of a multiwell plate 74µL of the 51.4 µM mother solution of **P7** have been inserted, together with 124 µL of a mixture of aqueous Na_2CO_3 0.1 M and DMF in a ratio 50:50, so that in the well the peptide concentration is 19 µM. In the other wells, 74 µL of the 51.4 µM mother solution of **P7** have been inserted, together with 124 µL of tyrosol solutions prepared in a mixture of aqueous Na_2CO_3 0.1 M and DMF in a ratio 50:50. Tyrosol mother solutions used are respectively at the concentrations 80 µM; 32.3 µM; 16 µM; 11 µM; 9 µM; 3 µM; 1 µM. Final concentration of peptide in wells resulted to be 19 µM, whereas tyrosol was present at the concentrations of 50 µM, 20 µM, 10 µM, 6.8 µM, 5.6 µM, 1.87 µM and 626 nM. Measurements have been registered in triplicate.

7.8 BIBLIOGRAPHY

(1) Iacomino, M.; Weber, F.; Gleichenhagen, M.; Pistorio, V.; Panzella, L.; Pizzo, E.; Schieber, A.; d'Ischia, M.; Napolitano, A. Stable Benzacridine Pigments by Oxidative Coupling of Chlorogenic Acid with Amino Acids and Proteins: Toward Natural Product-Based Green Food Coloring. *J. Agric. Food Chem*., **2017**, 65 (31), 6519–6528.

(2) Yang, C., Chen, K., Chen, M., Hu, X., Huan, S. Y., Chen, L., Song, g.; Zhang, X. B. Nanoscale metal–organic framework based two-photon sensing platform for bioimaging in live tissue. *Anal. Chem.*, **2019**, 91(4), 2727-2733.

(3) Ma, C.; Zhang, F.; Wang, Y.; Zhu, X.; Liu, X.; Zhao, C.; Zhang, H. Synthesis and Application of Ratio Fluorescence Probe for Chloride. *Anal. Bioanal. Chem.,* **2018**, 410 (25), 6507–6516.

(4) Jensen, K. B.; Braxmeier, T. M.; Demarcus, M.; Frey, J. G.; Kilburn, J. D. Synthesis of Guanidinium-Derived Receptor Libraries and Screening for Selective Peptide Receptors in Water. *Chem. Eur. J.,* **2002**, 8 (6), 1300–1309.

(5) Dai, N.; Zhao, H.; Qi, R.; Chen, Y.; Lv, F.; Liu, L.; Wang, S. Fluorescent and Biocompatible Ruthenium-Coordinated Oligo(P- Phenylenevinylene) Nanocatalysts for Transfer Hydrogenation in the Mitochondria of Living Cells. *Chem. Eur. J.,* **2020**, 26 (20), 4489–4495.

(6) Chen, H.; Wang, H.; Qin, X.-J.; Chen, C.; Feng, L.; Chen, L.-Z.; Du, L.-P.; Li, M.-Y. A Bestatin-Based Fluorescent Probe for Aminopeptidase N Cell Imaging. *Chin. Chem. Lett.,* **2015**, 26 (5), 513–516.

(7) Hebel, M.; Riegger, A.; Zegota, M.M.; Kizilsavas, G.; Gačanin, J.; Pieszka, M.; Lückerath, T.; Coelho, J. A. S.; Wagner, M.; Gois, P. M. P.; Ng, D. Y. W.; Weil, T. Sequence programming with dynamic boronic acid/catechol binary codes. *J. Am. Chem. Soc.,* **2019**, 141(36), 14026-14031.

(8) Scrafton, D. K.; Taylor, J. E.; Mahon, M. F.; Fossey, J. S.; James, T. D. "Click-Fluors": Modular Fluorescent Saccharide Sensors Based on a 1,2,3-Triazole Ring. *J. Org. Chem*., **2008**, 73 (7), 2871–2874.

(9) Wang, J.; Jin, S.; Akay, S.; Wang, B. Design and Synthesis of Long-Wavelength Fluorescent Boronic Acid Reporter Compounds. *Eur. J. Org. Chem*., **2007**, 2007 (13), 2091–2099.

(10) Liu, Y.; Zhou, P.; Da, H.; Jia, H.; Bai, F.; Hu, G.; Zhang, B.; Fang, J. An Azo Coupling Strategy for Protein 3-Nitrotyrosine Derivatization. *Chem. Eur. J.,* **2019**, 25(48), 11228-11232.

(11) Vida, V.; Minisini, M.; Mardirossian, M.; Brancolini, C.; Scocchi, M.; Forzato, C.; Berti, F. Novel Synthesis of 1,2-Diaza-1,3-Dienes with Potential Biological Activity from Cinnamic Acids and Diazonium Salts of Anilines. *RSC Adv.,* **2023**, 13 (1), 456–463.

(12) Conroy, T.; Jolliffe, K. A.; Payne, R. J. Efficient Use of the Dmab Protecting Group: Applications for the Solid-Phase Synthesis of N-Linked Glycopeptides. *Org. Biomol. Chem*., **2009**, 7 (11), 2255- 2258.

(13) Engfeldt, T.; Renberg, B.; Brumer, H.; Nygren, P. Å.; Eriksson Karlström, A. Chemical Synthesis of Triple-Labelled Three-Helix Bundle Binding Proteins for Specific Fluorescent Detection of Unlabelled Protein. *ChemBioChem.,* **2005**, 6 (6), 1043–1050.

(14) Alvarez-Rivera, F.; Rey-Rico, A.; Venkatesan, J. K.; Diaz-Gomez, L.; Cucchiarini, M.; Concheiro, A.; Alvarez-Lorenzo, C. Controlled Release of RAAV Vectors from APMA-Functionalized Contact Lenses for Corneal Gene Therapy. *Pharmaceutics,* **2020**, 12 (4), 335.

8 ACKNOWLEDGEMENTS

I would like to acknowledge Regione Friuli-Venezia Giulia for having granted my PhD fellowship within the European Social Fund 2014–2020.

A very sincere acknowledgement goes to my supervisors, Prof. Federico Berti and Prof. Cristina Forzato, for all their great support and help during the PhD. In these three years I learnt a lot and I had the opportunity to work on a project I really enjoyed, stimulating my curiosity, always working in a serene environment in which to share opinions and ideas. It has been a hard-working period, but I will miss all of this.

I would also like to express my gratitude to the members of the GSOLFA group at Complutense University in Madrid, in particular to Prof. Elena Benito Peña, Prof. Guillermo Orellana Moraleda and, of course, Prof. María Cruz Moreno Bondi, even if she is not with us, for letting me be part of this group in which I had the possibility to have a very formative experience in a multidisciplinary environment, and for being always so welcoming and available to me, ready to solve problems and find new solutions.

Of course, special thanks go to Dott. Andrea Caporale, for being a fundamental reference point in the field of peptides chemistry during these three years, for sharing his knowledge with me, being always so helpful and friendly.

I would also like to acknowledge the team of engineers composed by Prof. Antonio Boscolo and Prof. Agostino Accardo of the Department of Engineering and Architecture of the University of Trieste, and Dott. Giuseppe Boscolo of the company GRUPPO TECNICHE AVANZATE, for developing the in-lab built portable devices used in this thesis, and for being always very available in adapting their technological devices to the specific analytical needs of our systems.

Last, but not least, I would really like to thank my family and friends, and Luca, for being always by my side.